



# **Application of Chemical Looping for Solar Thermal Energy Storage**

**Mahyar Silakhori**

Thesis Submitted for the degree of Doctor of philosophy

School of Mechanical Engineering

Faculty of Engineering, Computer & Mathematical Sciences

The University of Adelaide. Australia

February 2019

## **ACKNOWLEDGMENT**

I would like to acknowledge the efforts of all the people who have made a contribution towards this thesis. I would cherish memories of all of them for the rest of my life. Many thanks to my mother, father, and lovely family who have been so understanding throughout my study and always encouraged me to pursue my dreams. I am thankful to their unconditional love and support of all my undertakings, academic and otherwise.

I would also like to thank my wonderful supervisors and mentors Maziar Arjomandi, Graham ‘Gus’ Nathan, and Mehdi Jafarian for their great guidance, insightful inputs, encouragement, endless support and friendship. I could not possibly wish for a better supervisory board.

I would also like to acknowledge “Australian Government Research Training Program Scholarship” for the financial supports.

I would also like to give thanks to my friends Amin Kamyar, Nima Moradi, Mohammad Mohsen Sarafraz, Farzin Ghanadi, Nima Sedaghatizadeh, Navid Freidoonimehr, and Azadeh Jafari many more that I cannot list all of them who made my journey joyful and helped me through the dark moments of my study.

## **THESIS DECLARATION**

I certify that this work contains no material which has been accepted for the award of any other degree or diploma in my name, in any university or other tertiary institution and, to the best of my knowledge and belief, contains no material previously published or written by another person, except where due reference has been made in the text. In addition, I certify that no part of this work will, in the future, be used in a submission in my name, for any other degree or diploma in any university or other tertiary institution without the prior approval of the University of Adelaide and where applicable, any partner institution responsible for the joint-award of this degree.

I give consent to this copy of my thesis when deposited in the University Library, being made available for loan and photocopying, subject to the provisions of the Copyright Act 1968.

The author acknowledges that copyright of published works contained within this thesis resides with the copyright holder(s) of those works.

I also give permission for the digital version of my thesis to be made available on the web, via the University's digital research repository, the Library Search and also through web search engines, unless permission has been granted by the University to restrict access for a period of time.

Mahyar Silakhori

## THESIS SUMMARY

In the recent years, Thermal Energy Storage (TES) systems have received significant attention because they can offer a low-cost Concentrating Solar Power (CSP) plant. Moreover, TES systems increase the economic viability of CSP plant for dispatchable power production over other renewable energy technologies. A state-of-the-art thermal energy storage system utilises commercially available molten salt as a medium for sensible thermal energy storage. Nevertheless, the operating temperature of molten salt is limited to 600°C, which gives a thermodynamic efficiency of approximately 35% in a Steam Rankine cycle. Higher cycle temperatures would offer greater efficiency but new receivers, heat transfer fluids and storage media need to be developed for this to be achieved.

Thermochemical energy storage with multivalent metal oxides provides high operating temperatures (600°C to 1100°C) and high storage capacity, depending on the storage media, through reduction and oxidation (RedOx) reactions. The RedOx reactions of multivalent metal oxides are based on Le Chatelier's principle in which the spontaneous shift for rebalancing the reaction can be brought on by changing the temperature and/or pressure of the system. Nevertheless, both temperature and pressure swing systems have their own advantages and technical challenges.

Different metal oxides have been assessed for their potential to store thermochemical energy in solid phase by changing the temperature of storage media during RedOx reactions. The CuO/Cu<sub>2</sub>O, Co<sub>3</sub>O<sub>4</sub>/CoO, and Mn<sub>2</sub>O<sub>3</sub>/Mn<sub>3</sub>O<sub>4</sub> pairs are promising storage media for thermochemical energy. However, one of the main challenges of thermochemical energy storage is the thermal hysteresis that results from the temperature difference during RedOx reactions. This leads to a decreased energy efficiency because the charging temperature is higher than the discharging temperature. Many efforts have been made to address this issue by



preparing a porous structure, a composite structure, and a binary system. One plausible way to address this issue is to perform a chemical looping cycle with pressure swing for thermal energy storage. This study assesses the potential of suitable metal oxides for thermochemical storage by pressure swing thermodynamically and experimentally through phase diagram and Thermogravimetric Analysis (TGA), respectively. The results showed that CuO/Cu<sub>2</sub>O, Co<sub>3</sub>O<sub>4</sub>/CoO, and Mn<sub>2</sub>O<sub>3</sub>/Mn<sub>3</sub>O<sub>4</sub> pairs have a strong potential for chemical storage by pressure swing and excellent reversibility over ten successive RedOx cycles. Moreover, advantages and technical challenges of chemical storage by pressure swing have been identified.

Liquid Chemical Looping for Thermal Energy Storage (LCL-TES) has been proposed to increase the operating temperature of a TES system by liquefying the storage media. It has also been proposed to improve the storage capacity of a solar-thermal energy system by combining sensible, latent and thermochemical storages. The thermodynamic performance of a LCL-TES system has been assessed for copper oxide. However, it has not been assessed for alternative metal oxides. Hence, the present study compares the thermodynamic feasibility of alternative metal oxides in the LCL-TES system. Moreover, a thermodynamic selecting procedure for the potential liquid metal oxide needs to be developed. This procedure provides a back-to-back comparison between various metal oxides with the purpose to identify the most suitable ones for the LCL-TES.

A series of experiments at different oxygen partial pressures (0.05 bar to 0.8 bar) were performed by TGA to develop an understanding of the technical challenges of LCL-TES and to prove the thermodynamic assessment of copper oxide in a LCL-TES system. Results revealed that copper oxide has a strong potential for application in RedOx reactions in liquid state. However, a key challenge is to identify suitable combinations of metals and refractories with sufficiently low reactions to withstand multiple cycles of successive oxidation and reduction.

The performance of LCL-TES with a Gas Turbine Combined Cycle (GTCC) was assessed and resulted in a 44.9% thermal efficiency which improved to 50% when an after-burner was added to the system and the operating temperature increased to 1700°C.

The potential of chemical looping cycles by pressure swing for TES applications was demonstrated in this project. The CuO/Cu<sub>2</sub>O, Co<sub>3</sub>O<sub>4</sub>/CoO, and Mn<sub>2</sub>O<sub>3</sub>/Mn<sub>3</sub>O<sub>4</sub> pairs were found to be suitable storage media for chemical storage by pressure swing at temperatures up to 1000°C. In addition, the kinetics of the reaction were improved from two hours to fifteen minutes by pressure swing. The results show that the rate of oxidation can be increased with increasing the partial pressure of oxygen from 0.2 bar to 0.8 bar. Thermal hysteresis of metal oxides in RedOx reactions were eliminated by this cycle. The operating temperature of the thermal energy storage system was also improved by liquefying the metal oxide. The LCL- TES system can improve energy density by combining sensible, latent and chemical storage in a process. The energy density of the LCL- TES system with copper oxide was estimated to be approximately 5 GJ/m<sup>3</sup>, which is six-times higher than that of molten salt (0.83 GJ/m<sup>3</sup>). Therefore, this system can be considered as an alternative plausible storage system for future CSP technologies.

## Table of contents

<b>ACKNOWLEDGMENT .....</b>	<b>i</b>
<b>THESIS DECLARATION .....</b>	<b>ii</b>
<b>THESIS SUMMARY .....</b>	<b>iii</b>
<b>Chapter 1 Introduction.....</b>	<b>1</b>
1.1 Background .....	1
1.2 Objectives .....	5
1.3 Thesis outline .....	6
1.4 Publications.....	9
1.5 Format .....	9
1.6 References.....	10
<b>Chapter 2 Literature review .....</b>	<b>13</b>
2.1 Concentrating solar thermal (CST).....	13
2.2 Solar thermal energy storage (TES).....	17
2.2.1 Sensible TES.....	18
2.2.2 Latent heat.....	20
2.2.3 Chemical heat of reaction .....	23
2.3 General challenges of thermochemical storage with temperature and pressure swing .....	50
2.4 Bench-marking of economic assessment for thermal energy storage.....	53
2.5 Liquid Chemical Looping for Thermal Energy Storage (LCL-TES) systems.....	55

2.6 Hybrid solar power plants .....	57
2.6.1 Hybrid solar steam power plants .....	58
2.6.2 Hybrid Brayton cycles .....	60
2.6.3 Hybrid solar combined cycles .....	63
2.7 References .....	66
<b>Chapter 3 Experimental investigation of metal oxides for thermochemical storage.....</b>	<b>82</b>
3.1 Chapter preview .....	82
3.2 Abstract .....	86
3.3 Introduction .....	86
3.4 Experimental setup .....	91
3.4.1 Materials and methods .....	91
3.5 Results and discussion .....	94
3.5.1 CuO/Cu <sub>2</sub> O cycle .....	94
3.5.2 Co <sub>3</sub> O <sub>4</sub> /CoO cycle .....	97
3.5.3 Mn <sub>2</sub> O <sub>3</sub> /Mn <sub>3</sub> O <sub>4</sub> cycle .....	99
3.5.4 Pb <sub>3</sub> O <sub>4</sub> /PbO cycle .....	102
3.6 Conclusion .....	104
3.7 References .....	105
<b>Chapter 4 Thermodynamic potential of alternative metal oxides for liquid chemical looping for storage of solar thermal energy .....</b>	<b>109</b>
4.1 Chapter preview .....	109
4.2 Abstract .....	113

4.3 Introduction.....	113
4.4 Methodology.....	117
4.4.1 LCL-TES system.....	117
4.4.2 Operating temperature of the LCL-TES.....	119
4.4.3 Red-Ox reaction in a LCL-TES system.....	120
4.4.4 Vapour pressure of LCL-TES materials.....	120
4.4.5 Phase diagram of metal oxides.....	120
4.4.6 Enthalpy of LCL-TES materials.....	120
4.5 Results and discussion.....	121
4.5.1 Melting temperature.....	121
4.5.2 Ellingham diagram.....	122
4.5.3 Vapour pressure of selected metal oxides.....	123
4.5.4 Reaction temperature.....	124
4.5.5 Identifying the multiple thermal energy storage in a LCL-TES system.....	126
4.5.6 Enthalpy of the storage medium.....	128
4.6 Conclusion.....	130
4.7 References.....	131
<b>Chapter 5 Experimental assessment of copper oxide in LCL-TES.....</b>	<b>136</b>
5.1 Chapter overview.....	136
5.2 Abstract.....	140
5.3 Introduction.....	140

5.4 Experimental setup.....	143
5.4.1 Material and method .....	143
5.4.2 Crucible.....	144
5.4.3 Thermal analysis .....	145
5.5 Results.....	147
5.5.1 DSC analysis .....	147
5.5.2 Variation of partial pressure in reduction stage .....	148
5.5.3 Variation of partial pressure in oxidation stage .....	150
5.5.4 Multiple cycles of reduction and oxidation .....	151
5.5.5 SEM analysis .....	152
5.6 Conclusion .....	154
5.7 References.....	154
<b>Chapter 6 Energetic performance of liquid chemical looping cycle with solar thermal energy storage.....</b>	<b>157</b>
6.1 Chapter preview .....	157
6.2 Abstract.....	161
6.3 Introduction.....	162
6.4 LCL-TES Gas Turbine Combined Cycle (GTCC) .....	165
6.5 Methodology.....	169
6.6 Results and discussion .....	173
6.6.1 Effect of operating pressure of the air reactor .....	176
6.6.2 Influence of concentration ratio of the solar collector .....	178

6.6.3 Effect of conversion extent of $\text{Cu}_2\text{O}$ (l) to $\text{CuO}$ (l).....	181
6.6.4 Influence of after-burner on operating condition of LCL-TES cycle .....	183
6.7 Conclusions.....	184
6.8 References.....	186
<b>Chapter 7 Conclusion &amp; future works.....</b>	<b>190</b>
7.1 Conclusion .....	190
7.1.1 Application of chemical looping by pressure swing for thermal energy storage .	190
7.1.2 Suitable materials for LCL-TES .....	191
7.1.3 Advantages and technical challenges of molten metals in TES .....	192
7.1.4 Performance of LCL-TES with GTCC .....	192
7.2 Recommendations for future work .....	193
7.2.1 Solar reactor .....	193
7.2.2 Heat recovery .....	193
7.2.3 Composite materials for LCL-TES .....	193
7.2.4 Challenges of molten metals .....	194
7.3 References.....	194

## Chapter 1 Introduction

---

### 1.1 Background

The increase in greenhouse gases in the atmosphere from anthropogenic emission is the main reason that the global mean temperature is increasing (Figueroa et al. 2008; Metz 2005). Among the greenhouse gases in the atmosphere, methane (CH<sub>4</sub>) and chlorofluorocarbons (CFCs) have the most detrimental influence on the environment when compared by unit mass of carbon dioxide (CO<sub>2</sub>) (He et al. 2011). However, the significant amount of CO<sub>2</sub> in the atmosphere also makes it a major source of global warming (Yamasaki 2003). According to the US Energy Information Administration (EIA) report in 2017, world energy-related carbon dioxide emissions are projected to increase by 6% per year between 2015 and 2040 (International energy outlook 2017). This is mainly due to an increase in the world energy consumption by 28% between 2015 and 2040 (International energy outlook 2017). This trend can increase the temperature of the Earth by 4°C at the end of this century if suitable action is not taken (Lund & Mathiesen 2012). Increasing the temperature of the Earth by more than 2°C would have critical effects on areas such as agriculture, water supply, and sea levels and could lead to catastrophic changes on the earth (Adanez et al. 2012; Huaman & Jun 2014). In order to prevent these changes, the CO<sub>2</sub> concentration should not be increased by more than 15% of the today's levels (Adanez et al. 2012). Despite the fact that the CO<sub>2</sub> levels should be urgently decreased, more than 18% of the world's energy demand is provided by fossil fuels, due to their high energy density, low cost and the availability of the associated technology (Liu et al. 2009; Metz 2005). Therefore, there is a need for new energy technologies with the reduced level of CO<sub>2</sub> emissions to the atmosphere. One alternative approach is to use renewable energy resources such as solar energy, and wind energy (Yang et al. 2008).



The sun is the main source of energy in the world, with a temperature of 5800 K and solar radiation of approximately  $63 \text{ MW/m}^2$  (Blanco & Miller 2017; Romero & Steinfeld 2012). Although solar radiation is traditionally called solar constant, it varies proportionally to the square of the distance between the sun and Earth and fluctuates by about 1.6% annually (Blanco & Miller 2017). The incoming solar radiation from the sun decreases before reaching the Earth's atmosphere because of absorption and scattering by different atmospheric components. Nevertheless, the total amount of solar radiation that reaches the Earth's surface annually is around 885 TWh or  $3.06 \times 10^{24} \text{ J}$  (Philibert 2014).

An optical concentrator device with a large reflective surface area can be used to concentrate the solar radiation to a solar receiver. The advent of Concentrated Solar Thermal (CST) power plant technologies provides the potential to produce power economically, particularly in regions with abundant sunlight (Hischier et al. 2012). Furthermore, CST power plant technologies could be incorporated with Thermal Energy Storage (TES) systems (Figure 1.1), to improve the economic viability of CST technology in comparison to other renewable energy technologies (Bayon et al. 2018; Gil et al. 2010; Kuravi et al. 2013; Silakhori et al. 2017).

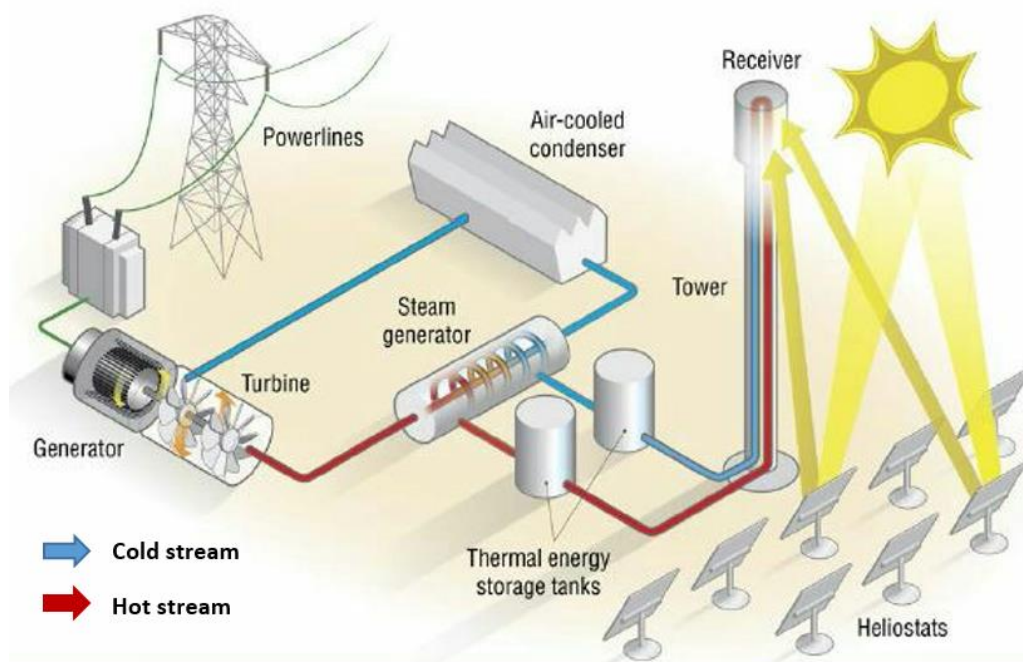


**Figure 1.1.** A schematic diagram of a concentrating solar thermal power plant connected to thermal energy storage system, adapted from Gil et al. (Gil et al. 2010).

A state-of-the-art sensible thermal energy storage system uses molten salt, with an operating temperature of up to approximately  $600^{\circ}\text{C}$ , as a storage medium which is commercially available for CST plants (Haseli et al. 2017; Kolb 1998; Robak et al. 2011). However, the main drawback of this system is its high capital cost, estimated at 10% - 20% of a solar thermal system, depending on its storage capacity (Gil et al. 2010). Moreover, the operating temperature of the molten salt is only suitable for Rankin cycles. Another disadvantage of this system is the temperature difference between storage ( $556 - 600^{\circ}\text{C}$ ) and release ( $540^{\circ}\text{C}$ ) of the molten salt, which leads to the exergy destruction (Dunham & Iverson 2014). Therefore, an alternative approach is required to increase the system's operating temperature, improve the efficiency of the power generation, and reduce the cost of the electricity generation.

Thermochemical energy storage metal oxides, has recently received a significant attention due to its high operating temperatures (up to  $1000^{\circ}\text{C}$ ), high energy density, and long-term storage capacity (Prieto et al. 2016; Silakhori et al. 2017). However, thermal hysteresis of the charging and discharging of the storage media occurs at different temperatures, which decreases the

efficiency of the system (Carrillo et al. 2015). In addition, metal oxides suffer from sintering and agglomeration during Reduction and Oxidation (RedOx) reactions (Figure 1.2), which reduces the potential of the storage media over long term operation (Agrafiotis et al. 2016; Agrafiotis et al. 2014; Jafarian et al. 2017). Furthermore, the application of the solid-phase metal oxides in thermochemical storage systems typically limits the charge/discharge temperatures to around  $1000^{\circ}\text{C}$  to avoid softening, sintering or other damages to the solid storage medium. This is significantly lower than the state-of-the-art systems in commercially available gas turbines, which are currently around  $1250^{\circ}\text{C}$  (Bhargava et al. 2007; Jafarian et al. 2017), and lowers the maximum thermodynamic efficiency of the solar thermal combined cycle power plants with this type of storage. Therefore, an alternative approach should be developed to improve the thermodynamic efficiency of a solar system.



**Figure 1.2.** (A) Top view and (B) side view of copper oxide after one RedOx cycle (C) top view and (D) inside view of copper oxide after 20 RedOx cycles, adapted from Deutsch et al. (Deutsch et al. 2017).

To address these limitations, a new concept based on chemical looping technology was proposed that uses a liquid metal oxide as the storage medium (Jafarian et al. 2017), which is referred to as Liquid Chemical Looping Thermal Energy Storage (LCL-TES). This system comprises two reactors where the changes in the temperature, state of oxidation and phase of the metal oxide occur. Hence, the system combines the benefits of sensible, latent and thermochemical TES methods. The proposed system can operate based on the pressure and temperature swings as

driving forces to reduce and oxidize a metal oxide and hence store and release heat. Use of metal oxide in solid phase has been mostly investigated using temperature swing as the driving force for the reduction and oxidation of the metal oxide. However, the LCL-TES system is still at its early stage of development so that its potential benefits and limitations are yet to be identified. Therefore, the main aim of this study is to assess the potential, kinetics and possible technical challenges of metal oxides in solid and liquid phases for thermochemical energy storage.

## 1.2 Objectives

The specific objectives of the thesis are to:

1. assess the application of a chemical looping cycle for chemical thermal energy storage by solid metal oxides using pressure swing

A chemical looping cycle, which is typically performed by changing the partial pressure of the system, has been used for different applications such as oxygen production (Moghtaderi 2009). However, the use of change in partial pressure of oxygen for thermal energy storage has not been studied well yet. Thermochemical energy storage of multivalent metal oxides is typically facilitated by the temperature difference between endothermic and exothermic reactions, in which the charging temperature is higher than discharging temperature which leads to a reduced thermodynamic efficiency of the system. For example, the  $Mn_2O_3/Mn_3O_4$  pair can be reduced and oxidised at temperatures of 940°C and 840°C, respectively, in an air atmosphere (Agrafiotis et al. 2016; Carrillo et al. 2014). A chemical looping cycle, which is performed at a constant temperature, has the potential to eliminate the temperature difference between the charging and discharging of thermochemical energy storage. Therefore, the first aim of this project is to assess the chemical energy storage potential of metal oxides via pressure swing, and explore the advantages and challenges of pressure and temperature swings for chemical energy storage.

2. identify the parameters that best describe the performance of a LCL-TES system

It has been proposed that LCL-TES has a potential to increase the operating temperature and improves the storage capacity of the system by combining sensible, latent and chemical energy storage in a process. This process has been assessed thermodynamically with copper oxide (Jafarian et al. 2017), but the criteria for selection of the suitable storage media have not yet been identified. Therefore, the second aim of this project is to identify the parameters with which the thermodynamic potential of metal oxides to be determined in a LCL-TES system, and identify their respective advantages and technical challenges.

3. assess the potential of suitable materials in a LCL-TES experimentally;

Once the thermodynamic potential of different metal oxides in a LCL-TES cycle have been identified, the suitable material must be assessed experimentally to evaluate the technical challenges of the proposed system. Moreover, the kinetics of the reduction and oxidation reactions, which are the important parameters that need to be considered in designing a reactor, must be assessed through experimental analysis. Therefore, the third aim of this project is to assess the potential of selected metal oxides by Thermogravimetric Analysis (TGA).

4. explore the performance of the proposed LCL-TES in a Gas Turbine Combined Cycle (GTCC).

After the LCL-TES system is assessed thermodynamically via modelling and experiments, the last step is to assess the performance of this system in a GTCC. Thermal efficiency, and exergy efficiency are assessed and a sensitivity study is conducted by changing the system parameters such as pressure and temperature.

### **1.3 Thesis outline**

This thesis is presented in seven chapters, the sequence of which highlights the chronology of the knowledge developed and research undertaken to meet the defined objectives. The first chapter is this introduction, which gives an overview of the subject, briefly outlines the

---

knowledge gaps and defines the principal research objectives and aim. Chapter 2 provides a comprehensive literature review and explains the gaps in knowledge as well as the importance of the research in more detail. The main body of the thesis, Chapters 3 to 6, is a collection of four manuscripts that have been published or are currently under review. These publications present the progress made in the course of this study and explain the achievements of this research. Finally, the research conclusions and some basic recommendations for future work are given in Chapter 7. The chapter contents and the alignment of the research with the specified aims are explained in the following paragraphs.

Chapter 2 provides a critical review of the literature related to CST and TES technologies. The emphasis of the chapter is on state-of-the-art system in TES, particularly thermochemical energy storage and the potential storage media for this system.

The research began by looking at the potential of the chemical looping process for chemical energy storage in CST technology. Chapter 3 holds the first of four journal publications. In this chapter, the chemical looping process was assessed for thermochemical energy storage of solid metal oxides on the basis of changing the partial pressure of oxygen at an isothermal condition. This concept was assessed thermodynamically and experimentally (through phase diagram and thermogravimetric analysis, respectively) for potential thermochemical energy storage media which were commonly utilised at a non-isothermal condition. The advantages and challenges of both isothermal and non-isothermal thermochemical storage were identified. The thermal hysteresis, fatigue and thermal stress of storage media during charging and discharging cycles observed in non-isothermal thermochemical storage can be eliminated in isothermal thermochemical storage. Energy density, reaction temperature, kinetics of the reaction, and the main criteria for thermochemical energy storage were assessed for the potential materials. This chapter also presents the configuration of the proposed system that stores chemical heat through changing the system's partial pressure.

Chapter 4 contains the second of four journal publications which compares the thermodynamic feasibility of alternative metal oxides in a Liquid Chemical Looping for a Thermal Energy Storage (LCL-TES) system. This system can operate at a high temperature (up to 1400°C) and has the potential to combine sensible, latent and thermochemical energy storage. In this study, the thermodynamic performance of different metal oxides is assessed based on their melting temperature, reaction temperature, Gibbs free energy, and phase diagrams.

Chapter 5, the third of four journal publications, presents the experimental investigation of copper oxide in a LCL-TES system. In this section, the kinetics of the copper oxide is assessed by thermogravimetric analysis. Moreover, the technical challenges related to selecting a suitable container for liquid metal at a temperature of 1250°C is studied.

Chapter 6 contains the fourth of five journal publications which aims to identify the energetic performance of the LCL-TES GTCC. The hot gas produced from the LCL-TES system is transferred to a gas turbine for power generation. The effect of different parameters, such as air reactor pressure; the concentration ratio of the solar concentrator; conversion extent; and thermal input from the after-burner, on the cycle efficiency is assessed.

This research investigation demonstrates that a chemical looping process can be used for a thermal energy storage system. It can eliminate the limitations of solid metal oxides in chemical storage and increase the operating temperature of the system, which leads to an improvement of thermal efficiency, particularly for power generation. The proposed system has been assessed experimentally by thermogravimetric analysis (TGA) and the results show the potential of these materials for chemical storage and the LCL-TES system. Finally, Chapter 7 lists the research conclusions along with recommendations for further concept development towards commercialisation.

## 1.4 Publications

The research presented in this thesis has led to the generation of four journals and one peer-reviewed conference papers. The journals in which the papers are published or have been submitted are some of the best in solar energy and engineering fields.

### *Journal papers*

- **Mahyar Silakhori**, Mehdi Jafarian, Maziar Arjomandi, Graham J. Nathan, *Thermogravimetric analysis of Cu, Mn Co and Pb oxides for thermochemical Energy storage*, Journal of Energy Storage (2018), Under review.
- **Mahyar Silakhori**, Mehdi Jafarian, Maziar Arjomandi, Graham J. Nathan, *Comparing the thermodynamic potential of alternative liquid metal oxides for the storage of solar thermal energy*, Solar Energy, vol. 157. pp. 251-258 (2017).
- **Mahyar Silakhori**, Mehdi Jafarian, Maziar Arjomandi, Graham J. Nathan, *Experimental Assessment of Copper Oxide for Thermal Energy Storage*, Journal of Energy Storage, vol. 21. pp. 216-221 (2019).
- **Mahyar Silakhori**, Mehdi Jafarian, Maziar Arjomandi, Graham J. Nathan, *The energetic performance of a liquid chemical looping solar thermal energy storage*, Energy, vol. 170. pp. 93-101 (2019).
- **Mahyar Silakhori**, Mehdi Jafarian, Maziar Arjomandi, Graham J. Nathan, *High temperature solar thermal energy storage system with copper oxide*, Asia-Pacific Solar Research Conference (5 -7 December 2017), Melbourne, Australia.

## 1.5 Format

The thesis has been submitted as a portfolio of the publications according to the formatting requirements of The University of Adelaide. The printed and online versions of this thesis are identical. The online version of the thesis is available as a PDF.



---

## 1.6 References

J. Adanez, A. Abad, F. Garcia-Labiano, P. Gayan & F. Luis 2012, 'Progress in chemical-looping combustion and reforming technologies', *Progress in energy and combustion science*, vol. **38**. 2, pp. 215-282.

C. Agrafiotis, M. Roeb & C. Sattler 2016, 'Exploitation of thermochemical cycles based on solid oxide redox systems for thermochemical storage of solar heat. Part 4: Screening of oxides for use in cascaded thermochemical storage concepts', *Solar energy*, vol. **139**. pp. 695-710.

C. Agrafiotis, M. Roeb, M. Schmücker & C. Sattler 2014, 'Exploitation of thermochemical cycles based on solid oxide redox systems for thermochemical storage of solar heat. Part 1: Testing of cobalt oxide-based powders', *Solar energy*, vol. **102**. pp. 189-211.

A. Bayon, R. Bader, M. Jafarian, L. Fedunik-Hofman, Y. Sun, J. Hinkley, S. Miller & W. Lipiński 2018, 'Techno-economic assessment of solid-gas thermochemical energy storage systems for solar thermal power applications', *Energy*, vol. **149**. pp. 473-484.

R. Bhargava, M. Bianchi, A. De Pascale, G. N. Di Montenegro & A. Peretto 2007, 'Gas turbine based power cycles-a state-of-the-art review', in *Challenges of power engineering and environment*, Springer, pp. 309-319.

M. Blanco & S. Miller 2017, 'Introduction to concentrating solar thermal (CST) technologies', in *Advances in Concentrating Solar Thermal Research and Technology*, Elsevier, pp. 3-25.

A. J. Carrillo, D. P. Serrano, P. Pizarro & J. M. Coronado 2014, 'Thermochemical heat storage based on the  $Mn_2O_3/Mn_3O_4$  redox couple: influence of the initial particle size on the morphological evolution and cyclability', *Journal of Materials Chemistry A*, vol. **2**. 45, pp. 19435-19443.

A. J. Carrillo, D. P. Serrano, P. Pizarro & J. M. Coronado 2015, 'Thermochemical Heat Storage at High Temperatures using  $Mn_2O_3/Mn_3O_4$  System: Narrowing the Redox Hysteresis by Metal Co-doping', *Energy Procedia*, vol. **73**. Supplement C, pp. 263-271.

M. Deutsch, F. Horvath, C. Knoll, D. Lager, C. Gierl-Mayer, P. Weinberger & F. Winter 2017, 'High-Temperature Energy Storage: Kinetic Investigations of the  $CuO/Cu_2O$  Reaction Cycle', *Energy & Fuels*, vol. **31**. 3, pp. 2324-2334.

M. T. Dunham & B. D. Iverson 2014, 'High-efficiency thermodynamic power cycles for concentrated solar power systems', *Renewable and Sustainable Energy Reviews*, vol. **30**. pp. 758-770.

J. D. Figueroa, T. Fout, S. Plasynski, H. McIlvried & R. D. Srivastava 2008, 'Advances in  $CO_2$  capture technology: the US Department of Energy's Carbon Sequestration Program', *International journal of greenhouse gas control*, vol. **2**. 1, pp. 9-20.

A. Gil, M. Medrano, I. Martorell, A. Lazaro, P. Dolado, B. Zalba & L. F. Cabeza 2010, 'State of the art on high temperature thermal energy storage for power generation. Part 1: Concepts, materials and modellization', *Renewable and Sustainable Energy Reviews*, vol. **14**. 1, pp. 31-55.

P. Haseli, M. Jafarian & G. J. Nathan 2017, 'High temperature solar thermochemical process for production of stored energy and oxygen based on CuO/Cu<sub>2</sub>O redox reactions', *Solar energy*, vol. **153**. pp. 1-10.

F. He, T. Han, H. Hong & H. Jin 2011, 'Solar thermochemical hybrid trigeneration system with CO<sub>2</sub> capture using dimethyl ether-fueled chemical-looping combustion', in *ASME 2011 5th International Conference on Energy Sustainability*, American Society of Mechanical Engineers, pp. 1651-1660.

I. Hischer, P. Leumann & A. Steinfeld 2012, 'Experimental and numerical analyses of a pressurized air receiver for solar-driven gas turbines', *Journal of Solar Energy Engineering*, vol. **134**. 2, p. 021003.

R. N. E. Huaman & T. X. Jun 2014, 'Energy related CO<sub>2</sub> emissions and the progress on CCS projects: a review', *Renewable and Sustainable Energy Reviews*, vol. **31**. pp. 368-385.

International energy outlook 2017, USDOE Energy Information Administration (EIA), Washington, DC (United States). Office of Energy Analysis.

M. Jafarian, M. Arjomandi & G. J. Nathan 2017, 'Thermodynamic potential of molten copper oxide for high temperature solar energy storage and oxygen production', *Applied Energy*, vol. **201**. pp. 69-83.

G. J. Kolb 1998, 'Economic evaluation of solar-only and hybrid power towers using molten-salt technology', *Solar energy*, vol. **62**. 1, pp. 51-61.

S. Kuravi, J. Trahan, D. Y. Goswami, M. M. Rahman & E. K. Stefanakos 2013, 'Thermal energy storage technologies and systems for concentrating solar power plants', *Progress in energy and combustion science*, vol. **39**. 4, pp. 285-319.

W. Liu, D. King, J. Liu, B. Johnson, Y. Wang & Z. Yang 2009, 'Critical material and process issues for CO<sub>2</sub> separation from coal-powered plants', *Jom*, vol. **61**. 4, pp. 36-44.

H. Lund & B. V. Mathiesen 2012, 'The role of carbon capture and storage in a future sustainable energy system', *Energy*, vol. **44**. 1, pp. 469-476.

B. Metz 2005, *Carbon dioxide capture and storage: special report of the intergovernmental panel on climate change*, Cambridge University Press.

B. Moghtaderi 2009, 'Application of chemical looping concept for air separation at high temperatures', *Energy & Fuels*, vol. **24**. 1, pp. 190-198.

C. Philibert 2014, 'Technology roadmap: solar thermal electricity: 2014 edition', *IEA, Paris, France*.

C. Prieto, P. Cooper, A. I. Fernández & L. F. Cabeza 2016, 'Review of technology: Thermochemical energy storage for concentrated solar power plants', *Renewable and Sustainable Energy Reviews*, vol. **60**. pp. 909-929.

C. W. Robak, T. L. Bergman & A. Faghri 2011, 'Economic evaluation of latent heat thermal energy storage using embedded thermosyphons for concentrating solar power applications', *Solar energy*, vol. **85**. 10, pp. 2461-2473.

M. Romero & A. Steinfeld 2012, 'Concentrating solar thermal power and thermochemical fuels', *Energy & Environmental Science*, vol. **5**. 11, pp. 9234-9245.

M. Silakhori, M. Jafarian, M. Arjomandi & G. J. Nathan 2017, 'Comparing the thermodynamic potential of alternative liquid metal oxides for the storage of solar thermal energy', *Solar energy*, vol. **157**. pp. 251-258.

A. Yamasaki 2003, 'An overview of CO<sub>2</sub> mitigation options for global warming: emphasizing CO<sub>2</sub> sequestration options', *Journal of Chemical Engineering of Japan*, vol. **36**. 4, pp. 361-375.

H. Yang, Z. Xu, M. Fan, R. Gupta, R. B. Slimane, A. E. Bland & I. Wright 2008, 'Progress in carbon dioxide separation and capture: A review', *Journal of Environmental Sciences*, vol. **20**. 1, pp. 14-27.

## Chapter 2 Literature review

### 2.1 Concentrating solar thermal (CST)

Solar radiation from the sun is collected and concentrated by Concentrating Solar Thermal (CST) technologies and transformed into high-temperature thermal energy. This thermal energy can be used in various applications such as heating for different processes, electricity production, material processing, domestic and industrial heating and cooling cycles, and chemical processing (Blanco & Miller 2017). The thermal energy produced with CST technologies can be stored and used when it is required (Figure 2.1). It can also be hybridised with other sources of energy such as fossil fuels or renewables (e.g. biomass). A CST consists of a collector field referred to as “concentrator”, a thermal receiver and heat transfer fluid. A thermal energy storage is an essential part of the system not only to address the intermittency of the solar energy but also to increase the solar thermal share of the process, when the system is hybridised with fossil-fuel resources. Depending on the thermal demand of the process and/or plant, size of the concentrator and collector field, the type of the receiver and the heat transfer fluid is determined.

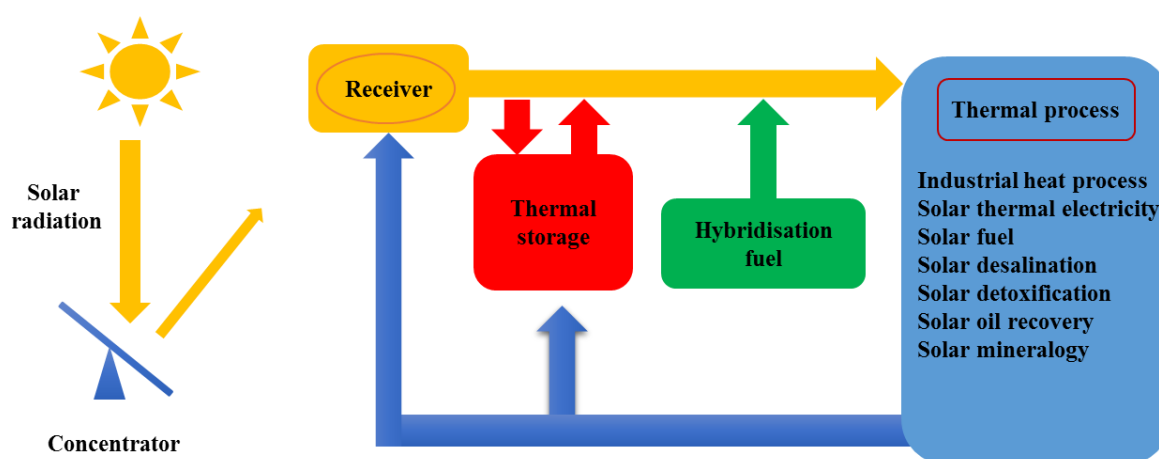


**Figure 2.1.** A schematic diagram of a CST system with thermal energy storage and hybridised fuel system (Blanco & Miller 2017).

There are four main pilot scale and commercially available CST technologies. Two are linear-focusing technologies including parabolic trough and linear Fresnel, while the other ones are point focusing technologies including parabolic dish and central receiver (Mills 2004; Rao 2011; Zhang et al. 2013). A parabolic trough is comprised of parabolic reflectors mounted in parallel rows to concentrate the solar radiation onto an absorber tube (Figure 2.2a). It is generally designed to maximise the energy output where the solar collector is aligned from north to south in order to track the sun's rays from east to west. A commercial parabolic trough achieves concentration ratios between 50 and 80 (Blanco & Miller 2017). Moreover, working fluids such as synthetic oil, water/steam, molten salt and some hydrocarbon mixtures have been demonstrated in parabolic trough concentrators (Zhang et al. 2013). These working fluids can also be used in linear Fresnel systems. A linear Fresnel solar collector consists of some reflectors that are flat or slightly parabolic (Figure 2.2b). The concentration ratio of a commercially available linear Fresnel collector ranges from 30 to 70 (Blanco & Miller 2017). The fluid temperature in both parabolic trough and linear Fresnel systems can reach to approximately 500°C and can be utilised in steam Rankine cycles (Barlev et al. 2011; Romero & Steinfeld 2012). A parabolic dish collector comprises a thermal receiver and a dish parabolic reflector (Figure 2.2c). The receiver is mounted on a reflector with a support structure to track the sun beam with both the receiver and the dish. A two-axis sun tracking system is well in-line with the parabolic trough and linear Fresnel technologies. The operating temperature of a parabolic dish can reach approximately 1500°C (Romero & Steinfeld 2012), while the concentration ratio of the commercially available parabolic dishes exceed approximately 2000. The central receiver technology (Figure 2.2d) comprises a tower and some heliostat reflectors, which are slightly parabolic. This is because the parabolic shape provides a better reflection, while collecting a wider range of sun beam. The tower is placed in a solar field which is surrounded with heliostat reflectors. The concentration ratio of this technology ranges between

500 and 2000. This system can operate with different working fluids such as molten salt, saturated steam or superheated and pressurised air, with varying operating temperatures from 500°C to 2000°C (Romero & Steinfeld 2012). This temperature range is well-matched to the operating temperature of Gas Turbine Combined Cycles (GTCC), which are more efficient than Rankine steam turbines.

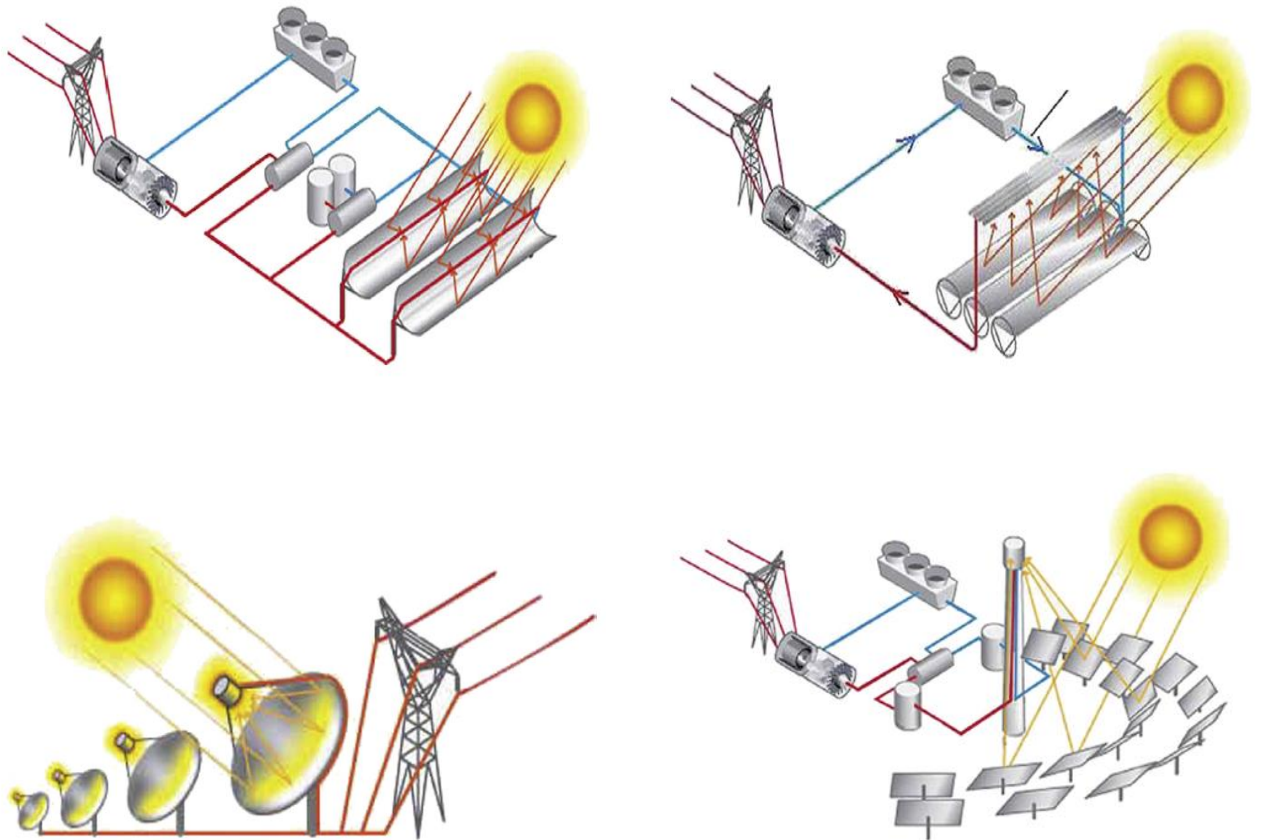


**Figure 2.2.** Schematic representation of different concentrated solar technologies adapted from Balanco and Miller 2017 (Blanco & Miller 2017), (a) Parabolic trough, (b) Linear Fresnel, (c) Parabolic dish, (d) Central receiver technologies.

Table 2.1 presents a summary of the advantages, specifications and requirements for the technologies.

**Table 2.1.** Comparison between the available concentrated solar thermal energy technologies (Villamil et al. 2013; Liu et al. 2016).

Concentrator type	Parabolic Trough	Tower	Linear Fresnel	Dish
Typical plant capacity (MW)	5-100 MW	50-90 MW	30-50 MW	3-30 kW
Operating temperature range (°C)	200-390	300-800	250-390	500-800
Collector concentration (suns)	70-80	> 1000	30-70	> 1300
Capital cost (\$/kW)	6400 with TES	11,750 with TES	N/A	N/A
LCOE (\$/kWh)	0.22 with TES	0.24-0.26 with TES	0.17-0.37 with TES	N/A
Maturity	High, commercially available	Medium, recently used commercially	Low	Low
Advantages	Technology readiness is high. Suitable for two-phase operation and steam production. Lower demand for maintenance and material. Modularity and good use of terrain. Sun tracking system is one axis and is relatively cheaper than two axis.	High-temperature operation. Concentration ratio can be as high as 2000. Various types of working fluids can be used for this technology including molten metals, molten salts, and some oils. Storage at high-temperatures.	Low production costs for the mirrors. One axis sun tracking system, which reduces the fixed costs associated with the technology.	Suitable for domestic uses and low temperature applications. Lower capital costs in comparison with other technologies. One axis tracking system, which reduces the fixed costs. Great concentration (> 1300 suns)
Disadvantages	The operating temperature has been limited to ~400°C.	Massive amount of re-radiation. Technology readiness is medium and needs further developments. Sun tracking system is two-axial which adds to the O&M cost.	Technology readiness is low. Concentration is low (~60 suns).	Recent market entry, only small operational projects, in which no phase change occurs. Technology readiness is very low.

The International Energy Agency (IEA) has predicted that CST technologies will have the potential to generate base-load power in regions with abundant sun-light by 2025-2030 (Philibert 2014). However, the economic viability of CST technologies is limited due to their intermittent nature and low solar radiation intensity. For the continuous production of energy through CST, thermal energy storage and/or backup power generation i.e. hybridisation with

established fossil fuel based power plants (used when sunlight is below a threshold) are highly recommended (Duffie & Beckman 2013). Hence, the hybrid systems have the potential to improve the efficiency of CST plants and make them more competitive with conventional fossil fuel systems. Thermal energy storage is a key thermal unit which can improve the solar share of a hybrid system while improving the economic viability of the process.

## **2.2 Solar thermal energy storage (TES)**

Solar thermal energy can be stored in the form of a sensible heat, latent heat, the heat of chemical reactions or a combination of them (Gil et al. 2010). Sensible heat storage can be achieved by raising the temperature of a storage media, while latent heat storage occurs through changing the phase of the material from solid to liquid, or liquid to gas. Chemical storage is also based on endothermic and exothermic chemical reactions (Azpiazu et al. 2003; Sharma et al. 2009; Silakhori et al. 2015; Silakhori et al. 2014).

Depending on the amount of solar thermal energy, the application of the CST and the type of the storage material, various TES systems are available. Table 2.2 represents a rough comparison between the different types of thermal energy storage systems. As shown in this table, the storage capacity of a thermochemical storage is higher than sensible and latent heat storage, which is due to the release of the heat of reaction together with entropy dissipation.



**Table 2.2.** Technical characteristics of utility-scale electricity storage technologies (Wu et al. 2018).

Storage technologies	Sensible	Latent	Thermochemical	References
Energy storage form	Thermal	Thermal	Thermochemical	(Lott et al. 2014)
Efficiency (%)	50-90 (Thermal)	75-90 (Thermal)	75-100 (Thermal)	(Lott et al. 2014)
Energy cost (USD/kWh)	0.1-13	10-56	8-100	(Kyriakopoulos & Arabatzis 2016; Lott et al. 2014)
Durability (years)	10-30+	10-30+	10-30+	(Beaudin et al. 2010)
Durability (cycles)	2000-14600	2000-14600	2000-14600	(Beaudin et al. 2010; Kyriakopoulos & Arabatzis 2016)
Energy storage density (kWh/m <sup>3</sup> )	25	100	~500	(Beaudin et al. 2010; Lott et al. 2014)
Energy storage density (kWh/tonne)	10-50	50-150	~120-250	(Wu et al. 2018)
Storage capacity (MW)	0.1-300	0.1-300	0.1-300	(Beaudin et al. 2010)

### 2.2.1 Sensible TES

Sensible heat can be stored in both solid and liquid media. This media's heat capacity and the storage operating temperature are the main parameters affecting the amount of stored energy per unit volume. A suitable storage medium for sensible thermal energy storage needs to (Cabeza 2014):

- have high mechanical and chemical stability during charging and discharging cycles;
- maintain a high heat transfer rate during charging and discharging cycles;
- have a high storage temperature and density (Cabeza 2014).

Solid materials have some advantages in energy storage in comparison with liquid materials. Solid materials represent reasonable operating temperature range from 40°C to 70°C, for concrete or rocks, to more than 160°C for metals (Tatsidjodoung et al. 2013) for some industrial applications such as chemical and food production plants. Another significant advantage of the

solid materials is their inherent potential to be employed at high temperatures with no leakage and containment issues (Hasnain 1998). For example, refractory bricks have been proved to have a promising future for thermal storage. A mixture of carbonate oxides are commercially available for high-temperature applications without any corrosions and containment issue (Laing et al. 2011; Laing et al. 2006). Also, concrete has been found as another TES material with a reasonable chemical stability without the containment issue, which can store thermal energy up to  $\sim 500^{\circ}\text{C}$  (Laing et al. 2011).

Liquid materials such as organic liquids, molten salts, or liquid metals represent a strong potential for sensible heat storage. In several studies reviewed by Kuravi et al. (Kuravi et al. 2013), the thermal capacity of storage, stability and life cycles of various liquid materials have been assessed with the view to identify the plausible ones for thermal energy storage. Also, different mixtures of nitrate-based molten salt such as  $\text{KNO}_3\text{-NaNO}_3$  (40:60) have already been assessed and are commercially available for thermal storage systems (Kuravi et al. 2013). The density of these materials varies from  $1600\text{ kg/m}^3$  to  $2000\text{ kg/m}^3$  at  $300^{\circ}\text{C}$  with a minimum operating temperature of approximately  $140^{\circ}\text{C}$  (above their freezing point) and a maximum operating temperature of  $565^{\circ}\text{C}$  (below the decomposition temperature of the storage media). The state-of-the-art molten salt technologies employ two tanks (hot and cold tanks), which can operate at a temperatures up to  $565^{\circ}\text{C}$ . However, molten salt storage technologies increase the capital cost of the system by 10% - 20% depending on the amount of storage (Kousksou et al. 2014) together with a small increment in operating cost due to the trace heating in order to prevent the solidification in pipes and joints (Mills 2004). Currently, the operating temperature of a commercially-available molten salt system is limited to  $\sim 600^{\circ}\text{C}$ , which reduces the thermodynamic efficiency of the power generation system (Silakhori et al. 2017). However, this temperature range is suitable for steam Rankine cycles. With the progress in power production systems, supercritical power blocks have been recently developed. Hence, there is

a need to fortify the storage units with the purpose to adapt the thermal storage units to such high temperature processes. Thereby, liquid metals are plausible candidates for sensible thermal energy storage at high temperatures.

Liquid metals have been identified to work at operating temperatures of more than 750°C (Pacio et al. 2013). Much effort has been made to employ liquid metals such as lead - bismuth ( $C_p = 0.143 \text{ kJkg}^{-1}\text{K}^{-1}$ ) for sensible thermal energy storage, but the low heat capacity of liquid metals when compared to molten salts ( $C_p = 1.52 \text{ kJkg}^{-1}\text{K}^{-1}$ ) is one of the challenges associated with the use of liquid metals in thermal storage systems (Pacio et al. 2013; Pacio & Wetzel 2013). Hence, it is desirable to seek alternative liquid metals to be employed for storage medium in sensible TES system.

### **2.2.2 Latent heat**

In a latent heat storage technology, energy is stored in the material through phase transition from one state to another one such as solid-to-liquid and liquid-to-gas phase changes. The solid-to-liquid phase transition is typically studied for the CST applications due to its low volumetric expansion and high volumetric energy density in comparison with liquid-to-gas phase transitions (Silakhori 2012). Phase Change Material (PCM) refers to the materials with the capability to store thermal energy in the form of latent heat.

The stored heat in latent heat is greater than sensible heat storage due to higher enthalpy through phase change than sensible heating. For example, the energy required to smelt 1 kg of  $\text{KNO}_3$  is 95 times higher than energy required to increase its temperature by 1 K. For a better understanding, the energy density of a PCM molten salt (Hoshi et al. 2005; Kenisarin 2010; KotzÃš et al. 2013; Li et al. 2011), solar salt and oil (Kearney et al. 2003; Shabgard et al. 2012) have been compared in Figure 2.3. Notably, the sensible heat storage media operate at temperatures between 300°C and 600°C, while latent heat storage can be used at higher temperatures and with a higher energy density.

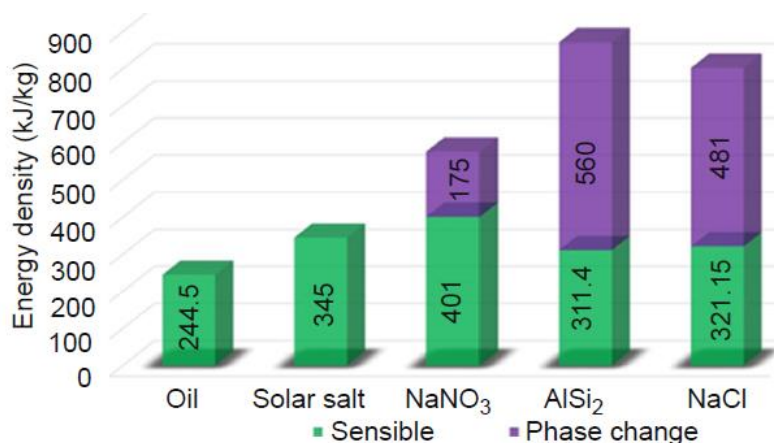


**Figure 2.3.** Comparing the storage capacity of the sensible heat storage materials and phase change materials at a temperature range between 300°C and 600°C (Nithyanandam et al. 2017).

Although molten salt is considered as a suitable material for thermal energy storage, it still has some limitations such as low thermal conductivity. Metallic materials with high thermal conductivity greater than molten salt are considered as alternative candidates for high temperature CST application because of their high heat capacity, high energy density, low vapour pressure and high thermal stability (Liu et al. 2015; Wei et al. 2018). Furthermore, the high thermal conductivity of metallic materials eliminates the need for using the fillers or other enhancement methods for improving the heat transfer in PCMs (Liu et al. 2015). Table 2.3 presents the thermo-physical properties of some potential metals and their compounds as PCMs (Liu et al. 2015; Mohamed et al. 2017). For the first time, metallic materials were first proposed for the latent thermal energy storage by Birchenall and Telkes (Birchenall & Telkes 1976). After that, the mixtures of aluminium metals with calcium, copper, manganese, silicone, and zinc were reported in 1980s (Achard 1981; Farkas & Birchenall 1985). They found that the binary and multi-component alloys of aluminium are plausible candidates for phase change materials due to their suitable operating temperature (327°C-657°C), high thermal conductivity, and thermal stability. Nevertheless, thermal cycling tests of aluminium-silicon showed that the weight of the alloy decreases by 10.5% after 720 cycles (Wei et al. 2018). Huang et al (Huang et al. 1991; ZHuang et al. 1999) assessed experimentally different alloys with the base of

Aluminium. The results depicted that high enthalpy of 553.1 kJ/kg at 552°C for aluminium-magnesium-silicon alloy, while enthalpy of 520 kJ/kg was evaluated for aluminium-copper-silicon at temperature of 365°C. These studies show that metal alloys are suitable candidates for latent heat thermal energy storage system. However, the corrosiveness of the liquid metals at high temperatures is one of the main challenges of these materials which results in poor compatibility with the container and reducing performance of these materials at high temperature applications (Wei et al. 2018).

**Table 2.3.** Thermo-physical properties of potential metals and metal alloys for phase change materials (Liu et al. 2015; Mohamed et al. 2017; Wei et al. 2018).

Metals and compounds	Melting point (°C)	Density (kg/m <sup>3</sup> )	Enthalpy of fusion (kJ/kg)	Energy Storage (GJ/m <sup>3</sup> )
Tin	232		60.5	0.439
Bismuth	271.4		53.3	0.521
Pb	328		23	0.261
Al	660		397	1.071
Cu	1083		193.4	1.73
Mg-Zn (48/52 wt %)	340		180	
Zn-Al (96/4 wt %)	381	6630	138	0.916
Al-Mg-Zn (59/33/6 wt%)	443		310	
Al-Mg-Zn ( 59/35/6 wt%)	443	2338	310	7.4
Mg-Al (34.65/65.35 wt%)	497	2300	285	0.71
Al-Cu-Mg (60.8/33.2/6 wt%)	506		365	
Al-Si-Cu (68.5/5/26.5 wt%)	525		364	
Al-Si-Cu (65/5/30 wt%)	520	2730	422	1.15
Al-Cu (66.8/33.2 wt%)	548	3424	548	1.2
Al-Si (87.76/12.24 wt%)	557		498	
Al-Si (87.5/12.5 wt%)	577	2250	515	1.16
Al-Si-Cu (65/5/30 wt%)	571		422	
Al-Si (20/80 wt%)	585		460	
Al-Si (92/8 wt%)	576		428.9	
Cu-Sb (34/1.7 wt%)	545	4000	331	1.32
Zn-Cu-Mg (49/45/6 wt%)	703		176	
Cu-Zn-P (69/17/14 wt%)	720		368	
Cu-Zn-Si (74/19/7 wt%)	765		125	
Mg-Ca (84/16 wt%)	790		272	
Mg-Si-Zn (47/38/15 wt%)	800		314	

Other PCMs such as chlorides, fluorides, nitrates, and carbonates have also been suggested for high-temperature applications between 200°C and 1000°C (Kenisarin 2010). The heat of fusion, storage cost, and thermal conductivity are the main criteria used to select the suitable PCM(s) for the latent heat thermal storage (Hoshi et al. 2005; Kenisarin 2010; KotzÃŠ et al.

2013). However, the thermal stability and the corrosive behaviour of a PCM are the main issues that need to be studied (Liu et al. 2015). This is because such behaviour reduces the life cycle and the operation time of the PCMs in thermal storage units (Liu et al. 2015).

### 2.2.3 Chemical heat of reaction

The energy density of Thermo-Chemical Energy Storage (TCES) is approximately 15 times higher than sensible heat storage and approximately 6 times higher than latent thermal energy storage (Gil et al. 2010; Pardo et al. 2014; Wu et al. 2018). This is because a lot of exergy is stored/released during the charging/discharging processes, which is attributed to the high enthalpy of chemical reactions. Since the discharge reactions in thermochemical storage occur at a high and constant temperature, a stable heat source with a constant temperature can be provided with this type of energy storage (Wu et al. 2018). Moreover, the system with chemical TES can work at higher temperatures in comparison with sensible and latent TES. The operation of a thermochemical TES is flexible due to a large number of chemical reactions. It can also be incorporated with various applications at different locations and times without a limitation in temperature. This is because the reaction products have the potential to store heat at the ambient temperature. TCES can also be used for seasonal thermal energy storage, which is one of its advantages over other thermal energy storage systems (Irwin et al. 2017). Thereby, recently, more attention has been paid to this type of thermal storage with the view to apply the technology to high temperature applications such as process heat and power generation.

The concept of the thermochemical heat storage is based on the “Le Chatelier’s” principle of chemical reactions in which the change in temperature and/or pressure causes a spontaneous shift towards rebalancing the reaction referred to as “temperature swing” and/or “pressure swing”, respectively. This principle can be explained by Equation (Eq.1):



Here, A and B are chemical compounds and C, D are the products of the chemical reactions. The change in chemical potential of the components in either side of this reaction in the system shifts the reaction in one direction. For example, supplying heat on the left side of Eq.1 leads to an increase in the production of C and D in order to balance the equilibrium. Hence, for an endothermic reaction, this can result in the storage of thermal energy in the products as a chemical energy. Conversely, extracting heat from the left side of Eq.1 leads to revert the products to reactants. This results in recovery of the stored heat in a TCES. Similarly, forward and reverse reactions can also be achieved through a change in the pressure of the gaseous component(s) involved in the reactions. A Chemical Looping Air Separation (CLAS) is an example in which the metal oxide undergoes cyclic reduction and oxidation reactions to separate oxygen from air (Moghtaderi 2009). In this process, the partial pressure of the oxygen in the gas phase determines the state of oxidation of the metal oxides. The CLAS system comprises two separate interconnected reactors shown in Figure 2.4. During the operation, a metal oxide is circulated (typically as metal oxide particles) between the reactors as the oxygen carrier (OC). Either steam or CO<sub>2</sub> is fed to the reduction reactor, to reduce the OC particles using an endothermic reaction. This occurs because the concentration of oxygen in the gas phase is lower than the equilibrium partial pressure of oxygen over the metal oxide (Moghtaderi 2009). The released oxygen can either be separated from the steam through a condensation process or to be used in an oxy-fuel firing plant (Shah et al. 2012). In the next step, the reduced OC particles are transferred to the air reactor, in which the exothermic oxidation reaction of the OC particles occurs as a result of the higher concentration of oxygen in the gas phase than the equilibrium partial pressure of oxygen over the metal oxide (Moghtaderi 2009). The heat required for the endothermic reduction of OC particles in the reduction reactor can be provided with the exothermic oxidation of metal oxides in the air reactor. Sometimes, fuel is also required to be combusted to maintain the temperature, or solar thermal energy can be employed

to hybridise the system. Note that, the heat from the oxidation reactor is transferred to the reduction reactor with hot OC particles and direct contact between the reduction and oxidation reactors (Moghtaderi 2009).

Theoretically, since both reactors operate at the same temperature, the heat released in the exothermic oxidation reaction, within the oxidation reactor, is the same as that which is consumed through the endothermic reduction reaction, within the reduction reactor (Moghtaderi 2009). However, due to heat transfer limitations and the parasitic losses associated with the system, further heat must be added to the system (Figure 2.4), which can be supplied with solar thermal energy.

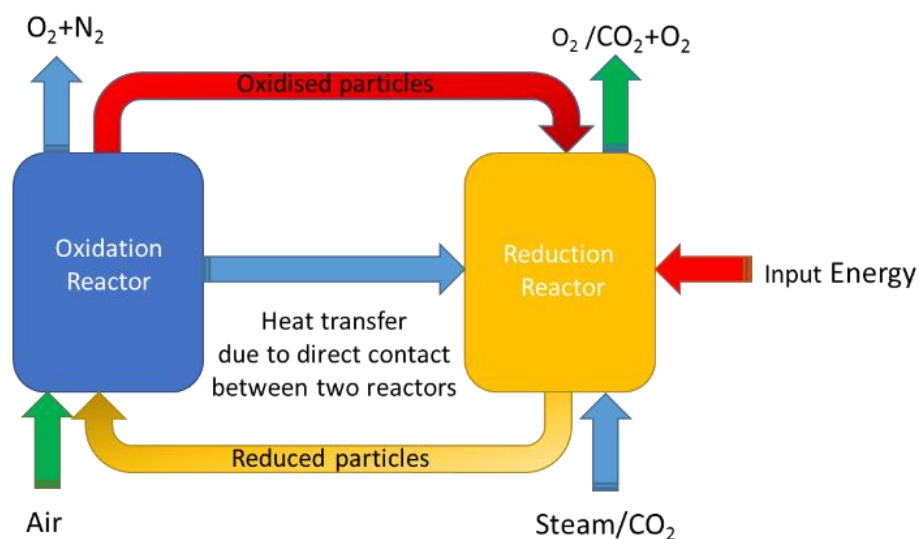


**Figure 2.4** A schematic diagram of a typical chemical looping air separation (CLAS) system, adapted from Moghtaderi (Moghtaderi 2009). The extent of the reduction and oxidation reactions is determined by the partial pressure of oxygen within the reduction and the oxidation reactors.

As can be seen, the oxygen carrier in the CLAS system is a key parameter, which not only has to tolerate the high temperature and pressure conditions, but must also have good heat transfer characteristics and compatibility with solar thermal energy and thermo-chemical energy storage. A suitable material for thermo-chemical storage needs to have a high reaction temperature to be in-line with the characteristics of a CST technology (André et al. 2016;



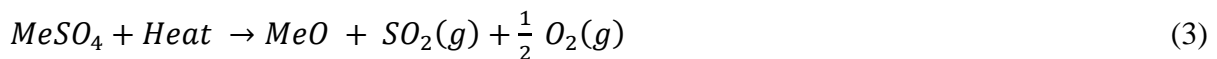
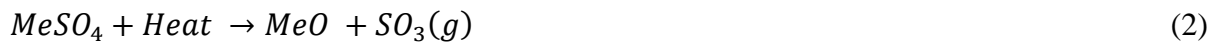
Abedin & Rosen 2011; Solé et al. 2012; Solé et al. 2015; Wentworth & Chen 1976). High energy density of the storage media is another important parameters in TCES system (Wu et al. 2018). The rate of the chemical reaction in TCES system must be high so it can optimise the design of the reactor and the conversion extent (Wu et al. 2018). Excellent reversibility of the reaction is another important parameter in TCES. It means that degradation, side reaction and undesirable by-products must not be observed after a short-term operation (André et al. 2016; Abedin & Rosen 2011; Solé et al. 2012; Solé et al. 2015; Wentworth & Chen 1976). Hence, various chemical compounds have been proposed for thermo-chemical energy storage systems in solid–gas reversible reactions, which has been expressed in Table 2.4. Metal oxides, carbonates, hydroxides, and sulfates are the main materials for thermochemical cycles.

**Table 2.4.** The strengths and weaknesses of different categories of thermochemical storage media.

TCES class	Strengths	Weakness	Future research	References
Metal oxide	High temperature Moderate cost Simple chemistry	Cyclic stability Slow kinetics Low heat transfer characteristics	Preventing sintering Improving heat transfer	(André et al. 2016; Block & Schmücker 2016; Irwin et al. 2017)
Carbonation	Moderate to high temperature Low cost	Cyclic stability Slow kinetics Low heat transfer characteristics Gas storage is required.	Preventing sintering Improving heat transfer	(Irwin et al. 2017)
Metal sulfates	Moderate to high temperature	Cyclic stability Slow kinetics Corrosion	Preventing sintering Improving heat transfer	(André et al. 2016)
Metal hybrid	Moderate temperature High reaction enthalpy High energy density Fast kinetics	Costly Low cyclic stability Chemistry affects the containment vessel Low heat transfer characteristics	Preventing sintering Improving heat transfer Reducing cost	(Irwin et al. 2017)

Each of these materials has its own advantages and disadvantages, which has been discussed in Table 2.4.

In a study conducted by Andre et al. (André et al. 2016) the potential of metallic sulphates for thermochemical energy storage was investigated and it was found that this category of metallic materials can be used for TCES due to their high reaction temperatures (900°C - 1400°C) and storage capacity. The following reactions were developed and proposed for the TCES at high temperatures:



Here, 'Me' represents the metals suitable for a reversible reaction in a thermochemical energy storage system, which include (but not limited to) aluminium, copper, cobalt, iron, manganese, nickel, and zinc (Kolta & Askar 1975; L'vov & Ugolkov 2004; Morgan et al. 1986; Siriwardane et al. 1999; Tmar et al. 1981). This chain of studies concluded that intermediate compounds can be formed during the decomposition of the metal sulfates, leading to the occurrence of two-step reactions in the process (Ibanez et al. 1984; Tagawa & Saijo 1985).

Further investigations were conducted on the mixture of CaSO<sub>4</sub> with different metal oxides (SiO<sub>2</sub>, Al<sub>2</sub>O<sub>3</sub> and Fe<sub>2</sub>O<sub>3</sub>) using thermogravimetric analysis for high temperature applications (Yan et al. 2015). The results showed that the rate of decomposition is accelerated by adding SiO<sub>2</sub>, Al<sub>2</sub>O<sub>3</sub> and Fe<sub>2</sub>O<sub>3</sub> due to the transformation in the crystal structure of CaSO<sub>4</sub>. For example, the solid-phase reaction of CaO and SiO, formed the silicate mineral, which reduced the initial decomposition temperature. Although these materials present the potential to be used in thermochemical storage, the associated corrosion effect is one of the main challenges of this system. This corrosion effect further developed a new challenge of containment, which limited their applications in thermal energy storage.

The assessment of metal carbonates for the carbon capture and thermal energy storage applications was conducted with the view to reduce the concentration of greenhouse gases in

the atmosphere. The results showed that metal carbonates can be used to store thermochemical energy since they have a high storage density and reaction temperatures (Duan et al. 2012; Abedin & Rosen 2011; Solé et al. 2012; Solé et al. 2015; Yan et al. 2015). The two-step reaction of metal carbonates for thermochemical storage is as follows:



Table 2.5 presents the reaction temperature and energy density of some carbonate materials. As shown in this Table,  $CaCO_3$ ,  $SrCO_3$ ,  $MgCO_3$ , and  $BaCO_3$  provide higher energy density in comparison with the other candidates. However, the irreversibility of the reaction is still the main drawback of these materials observed during the kinetics assessment (L'vov & Ugolkov 2004). Similar studies were conducted on the potential of carbon-based sorbents, different metal oxides and hydrotalcite-like compounds for  $CO_2$  capture applications (Feng et al. 2007; L'vov & Ugolkov 2004; Maitra et al. 2008).

**Table 2.5.** The reaction temperature and storage capacity of metal carbonates calculated by experimental assessment (André et al. 2016).

Chemical material	Temperature (°C)	Reaction enthalpy (kJ/mol)
$CaCO_3/CaO$	885	165.832
$SrCO_3/SrO$	1200	202.349
$MgCO_3/MgO$	300	98.984
$BaCO_3/BaO$	1555	165.096
$CdCO_3/CdO$	290	96.573
$ZnCO_3/ZnO$	120	68.326
$PbCO_3/PbO$	310	83.908

The potential of reversible carbonation/decomposition of  $SrO/SrCO_3$  for energy storage system has also been proposed for energy storage system (Bagherisereshki et al. 2018). The operating temperature of 1200°C in the atmospheric pressure is estimated for Carbonation/decomposition of  $SrO/SrCO_3$ . The enthalpy of this reaction is estimated at approximately 202.3 kJ/mol. Moreover, the high operating temperature of this system is suitable for high efficiency cycles

such as gas turbine combined cycles which provide the opportunity for more competitive solar electricity prices. The SrCO<sub>3</sub>/SrO system has some advantages over other thermochemical energy storage systems. This is because CO<sub>2</sub> is not corrosive or flammable, and there is no side reaction or catalyst involved in the reaction of SrCO<sub>3</sub>/SrO (Rhodes et al. 2015). The potential of Strontium carbonate for thermal energy storage has been assessed previously by thermogravimetric analysis (Charsley et al. 1993; Robbins et al. 1995). Thermal decomposition of orthorhombic ( $\alpha$ -SrCO<sub>3</sub>) and hexagonal ( $\beta$ -SrCO<sub>3</sub>) strontium carbonate polymorphs has been observed through thermal analysis. As shown in Figure 2.5, the partial pressure of the CO<sub>2</sub> affects the thermodynamics of the system (Rhodes et al. 2015). This figure shows that the carbonation and decomposition occur at temperatures between 900 °C and 1175 °C at different values of P<sub>CO<sub>2</sub>,eq</sub> (Dou et al. 2010).

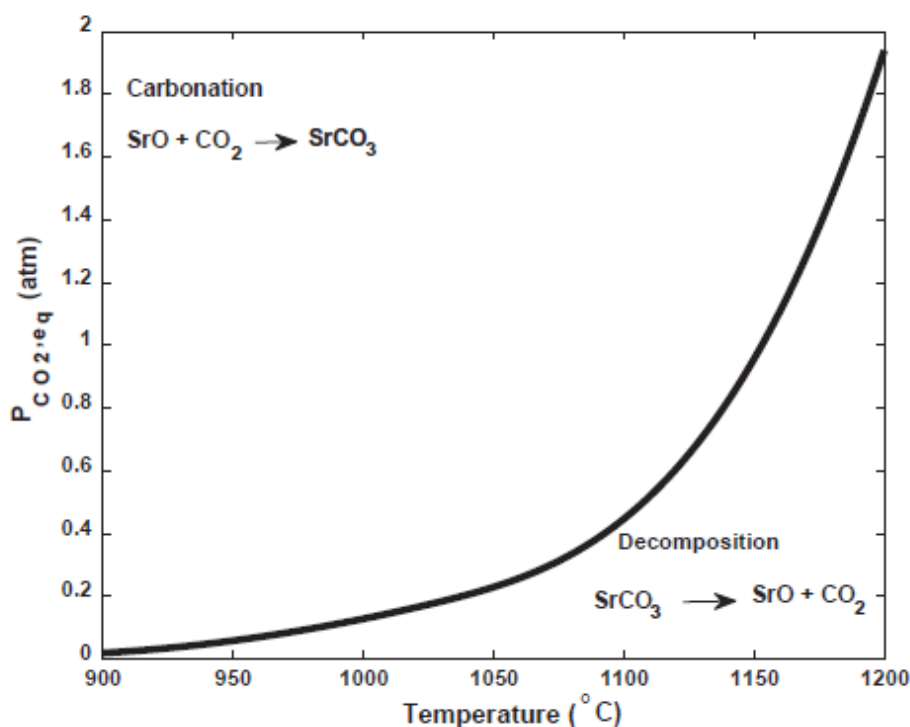


**Figure 2.5.** Equilibrium for the SrO-SrCO<sub>3</sub>-CO<sub>2</sub> system under stoichiometric conditions at various temperatures taken from Bagherisereshki et al. 2018 (Bagherisereshki et al. 2018).

The sintering issue has also been considered during carbonation and decomposition of the SrCO<sub>3</sub>/SrO which decreases its reactivity as a result of reducing its surface area. The inert

materials with high thermal stability such as polymorphic spacers are recommended for preventing the sintering problem of SrCO<sub>3</sub>/SrO during carbonation and decomposition (Bagherisereshki et al. 2018). Sintering of the material due to high operating temperatures is a common issue in such storage systems, which slows down the rate of the reaction. The effect of sintering on energy density of SrO with different supports such as strontium zirconate has been assessed by Rhodes et al. (Rhodes et al. 2015). The results showed that energy density reduces from 1500 MJ/m<sup>3</sup> to 1260 MJ/m<sup>3</sup> with an increase in the number of cycles from 10 to 45 cycles. The carbonation and decomposition temperature of this reaction occur at 1150°C and 1235°C, respectively.

Among the various compounds tested, the chemical reaction of CaO/carbon dioxide was suitable for high-temperature thermal energy storage applications. This was because of its high energy storage density of 3.26GJ/m<sup>3</sup> (Kyaw et al. 1996) together with high tolerance against high temperatures. Figure 2.6 presents the schematic diagram of carbonate loosing process for thermochemical energy storage. As shown in this figure, the CaCO<sub>3</sub> calcines through endothermic process with concentrated solar energy, which leads to production of CO<sub>2</sub> and CaO. After that, the stored energy is released through exothermic reaction as a result of CaO and Ca carbonation reaction. Then, the electricity is generated by introducing generated heat to the gas turbine.

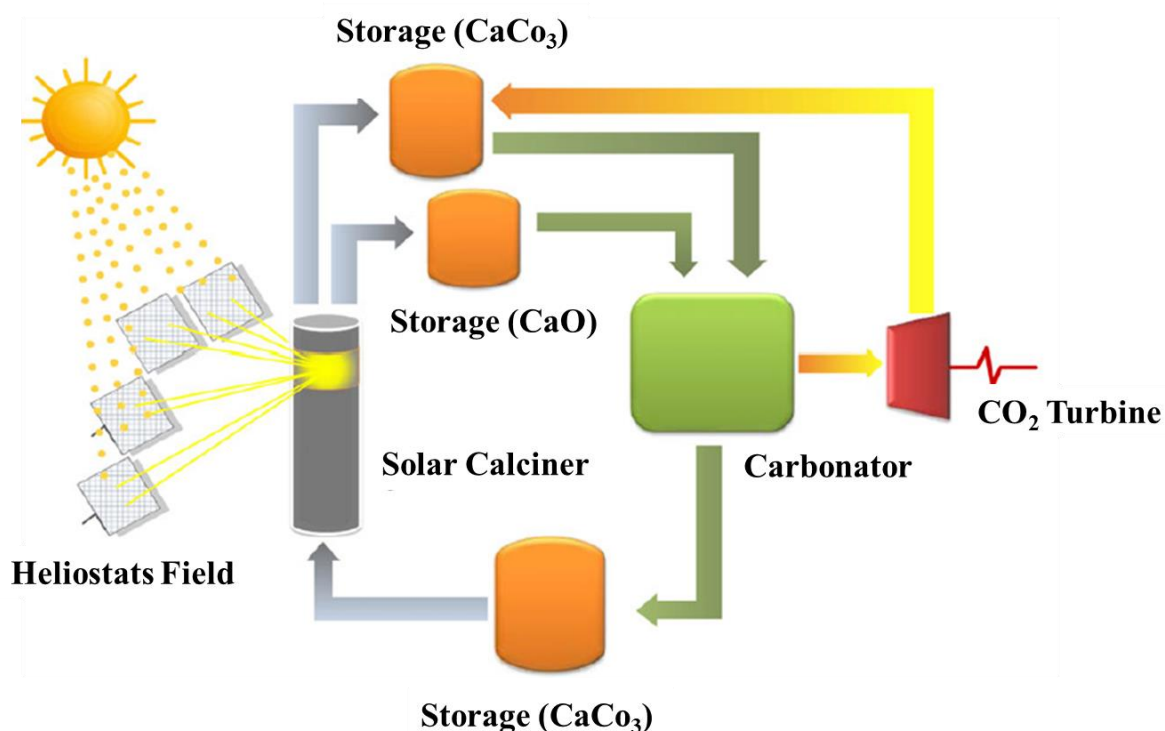


**Figure 2.6.** Schematic diagram of the calcium looping for thermochemical energy storage system adapted from Liu et al. (Liu et al. 2018)

The materials involved in the reversible reaction of CaO/carbon dioxide were not corrosive or toxic. However, the storage capacity of calcium oxide/carbon oxides reactions reduced over each cycle of carbonation and/or calcination (Feng et al. 2007; Grasa & Abanades 2006; Wang & Anthony 2005).

To address the challenge of storage capacity loss of metal carbonate during cyclic carbonation/calcination process, steam hydration (Han et al. 2009) and pre-treating of CaO sorbents with doping and synthesising were recommended (Liu et al. 2012). Among these methods, calcium hydration was a more effective technique to overcome the storage capacity loss. However, these methods are expensive and need advanced technology, which hinders these materials from commercialization.

---

The high thermal energy storage capacity of metal hydroxides in metal hybrid reaction makes these materials a suitable candidate for thermo-chemical energy storage. The two-steps reactions of metal hydroxides for thermo-chemical storage are as follows:

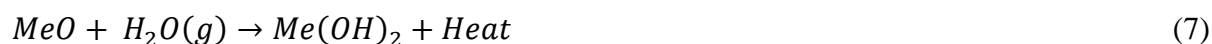
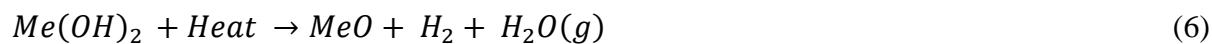


Table 2.6 represents the list of suitable materials with their reaction temperature and energy storage capacity. As shown in this table, the reaction temperature of the materials is in the range of 70°C and 1005°C. However, the reaction temperature of a large portion of these materials is significantly low and not suitable for high-temperature CSP applications.

The high reaction enthalpy and low cost of  $Ca(OH)_2/CaO$  in a reversible reaction make it a suitable candidate for thermal energy storage applications (Darkwa 1998; Fujii et al. 1985). In a similar study conducted by Schmidt et al. (Schmidt et al. 2014), the potential of  $Ca(OH)_2/CaO$  for thermal energy storage was assessed and a chemical conversion extent of 77% was achieved in a reversible chemical reaction. Likewise,  $Ca(OH)_2/CaO$  was tested in a lab-scale system for 100 cycles demonstrating that this material is highly stable (Schaube et al. 2012). The thermodynamic and kinetics of  $Ca(OH)_2/CaO$  were also assessed by Schaube et al. (Schaube et al. 2012) and the complete conversion of the reaction with a chemical enthalpy of 104.4 kJ/mol was observed.  $Mg(OH)_2/CaO$  was also considered as another suitable material for thermal energy storage due to its high enthalpy of the reaction (77.745 kJ/mol) (André et al. 2016).

**Table 2.6.** The reaction temperature and storage capacity of metal hydroxides calculated by an experimental assessment (André et al. 2016).

Chemical material	Temperature (°C)	Reaction enthalpy (kJ/mol)	Energy density (kJ/kg)
Ca(OH) <sub>2</sub> /CaO	515	100.177	1352
Mg(OH) <sub>2</sub> /MgO	265	77.745	1333
Be(OH) <sub>2</sub> /BeO	70	51.276	1191
Mn(OH) <sub>2</sub> /MnO	190	67.072	754
Sr(OH) <sub>2</sub> /SrO	755	88.581	728.3
Ba(OH) <sub>2</sub> /BaO	1005	93.462	545.47
Ni(OH) <sub>2</sub> /NiO	70	47.846	516
Zn(OH) <sub>2</sub> /ZnO	55	49.609	498.96
Cd(OH) <sub>2</sub> /CdO	125	59.952	409.4

Perovskites have been proposed as another potential material for high temperature energy storage, which is defined by ABO<sub>3</sub> where A and B refer to the different metals with the same crystal structure (Albrecht et al. 2016; André et al. 2016; Babiniec, Coker, Miller, et al. 2016; Prieto et al. 2016). One of the main advantages of the perovskites materials is high oxygen permeability, which helps absorbing and releasing oxygen during reduction and oxidation reactions (André et al. 2016). The Redox reactions of the perovskite is as follows:



where  $\delta$  and  $\Delta\delta$  are defined as equilibrium oxygen non-stoichiometry and oxygen deficiency, respectively. The potential of the perovskite for high temperature thermochemical energy storage has been proposed by Miller et al. (Miller et al. 2016) due to the high stability of perovskite at high temperatures, and good reversibility during reduction and oxidation reactions (Miller et al. 2016).

Babiniec et al. (Babiniec et al. 2015) firstly proposed the use of La<sub>x</sub>Sr<sub>1-x</sub>Co<sub>y</sub>Mn<sub>1-y</sub>O<sub>3-δ</sub> (LSCM) and La<sub>x</sub>Sr<sub>1-x</sub>Co<sub>y</sub>Fe<sub>1-y</sub>O<sub>3-δ</sub> (LSCF). La<sub>x</sub>Sr<sub>1-x</sub>Co<sub>y</sub>Mn<sub>1-y</sub>O<sub>3-δ</sub> (LSCM) and La<sub>x</sub>Sr<sub>1-x</sub>Co<sub>y</sub>Fe<sub>1-y</sub>O<sub>3-δ</sub> (LSCF) for high temperature thermochemical energy storage. Thermogravimetric analysis showed that the reduction and oxidation activity of both LSCM and LSCF reached to the highest level when the content of La reached to 0.3 (Babiniec et al. 2015; Babiniec, Coker, Miller, et al. 2016). As shown in Table 2.7, there is a relationship between  $\delta$  and enthalpy



change of the LSCF. It means that the maximum value of the  $\delta$  (0.49) leads to a maximum enthalpy change of 250 kJ/kg. This can be explained by their higher enthalpy per mole  $O_2$  at low values of  $\delta$ .

**Table 2.7.** Enthalpy values at maximum  $\delta$ s of reduction of LSCM and LSCF (Babiniec et al. 2016)

Composition	$\delta$	$\Delta H$ ( kJ/kg)
$La_{0.1}Sr_{0.9}Co_{0.9}Mn_{0.1}O_{3-\delta}$ (LSCM1991)	0.43	220
$La_{0.3}Sr_{0.7}Co_{0.9}Mn_{0.1}O_{3-\delta}$ (LSCM3791)	0.46	250
$La_{0.3}Sr_{0.7}Co_{0.8}Mn_{0.2}O_{3-\delta}$ (LSCM3782)	0.41	230
$La_{0.2}Sr_{0.8}Co_{0.8}Fe_{0.2}O_{3-\delta}$ (LSCF2882)	0.49	210
$La_{0.3}Sr_{0.7}Co_{0.9}Fe_{0.1}O_{3-\delta}$ (LSCF3791)	0.46	220
$La_{0.3}Sr_{0.7}Co_{0.7}Fe_{0.3}O_{3-\delta}$ (LSCF3773)	0.45	220

The reversibility of LSCM3791 has been assessed for up to 100 cycles at temperature ranges between 400 °C and 1050 °C in an air atmosphere. As shown in Figure 2.7, the morphology of the materials remained stable for up to 100 cycles (Babiniec, et al. 2016). Moreover, no weight loss has been observed over 100 cycles.

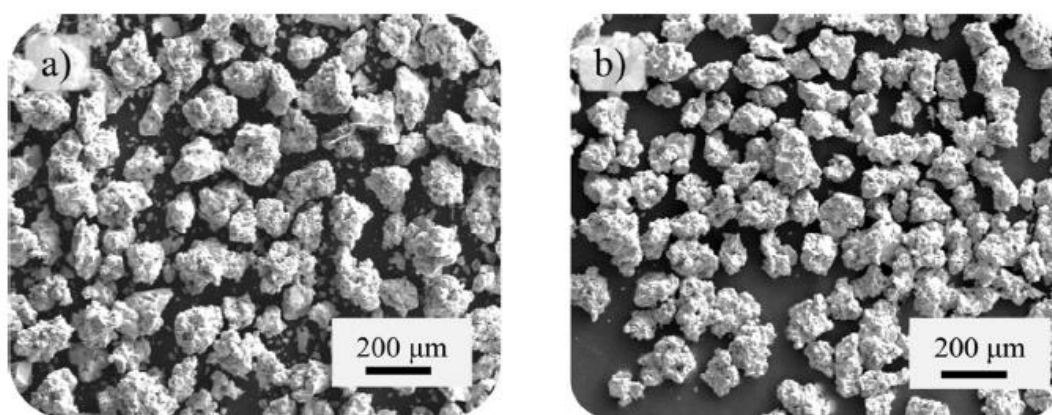


**Figure 2.7.** SEM micrograph of the LSCM3791 (a) before and (b) after 100 cycles adopted from Babiniec et al. (Babiniec et al. 2016)

Imponenti et al. (Imponenti et al. 2016; Imponenti et al. 2017) conducted a study to assess the performance of  $\text{CaCr}_y\text{Mn}_{1-y}\text{O}_{3-\delta}$  and  $\text{Ca}_{1-x}\text{Sr}_x\text{MnO}_{3-\delta}$  as perovskites materials for high-temperature energy storage. It was found that the stability of the materials can be improved through doing (Cr and Sr) on the  $\text{CaMnO}_3$ . They also compared different perovskites materials in terms of energy storage density. Among them, the highest total energy density of the 985 kJ/kg was calculated for  $\text{Ca}_{0.95}\text{Sr}_{0.05}\text{MnO}_{3-\delta}$  at temperature of  $750^\circ\text{C}$ , in which 56.3% of this energy belongs to chemical storage and 43.7% was for sensible energy storage (Imponenti et al. 2016; Imponenti et al. 2017). The stability of  $\text{Ca}_{0.9}\text{Sr}_{0.1}\text{MnO}_{3-\delta}$  has been assessed for up to 1000 cycles through fix bed reactor at temperatures of  $500^\circ\text{C}$  -  $900^\circ\text{C}$  and oxygen partial pressure of  $10^{-4}$  bar (Imponenti et al. 2016; Imponenti et al. 2017). The results show that  $\Delta\delta$  reduced by 0.02 over 1000 cycles due to aggregation of the materials. Nevertheless, the good stability of this materials for up to 1000 cycles was reported.

Figure 2.8 shows the schematic configuration of the perovskites system integrated with a concentrated solar receiver. The perovskites materials is heated and reduced by concentrated heat flux before transferring to the hot storage reservoir. Then the reduced material is introduced to an air-fluidized bed reactor for exothermic oxidation reaction. The released heat can be transferred to power cycles, such as supercritical  $\text{CO}_2$ , for power generation.

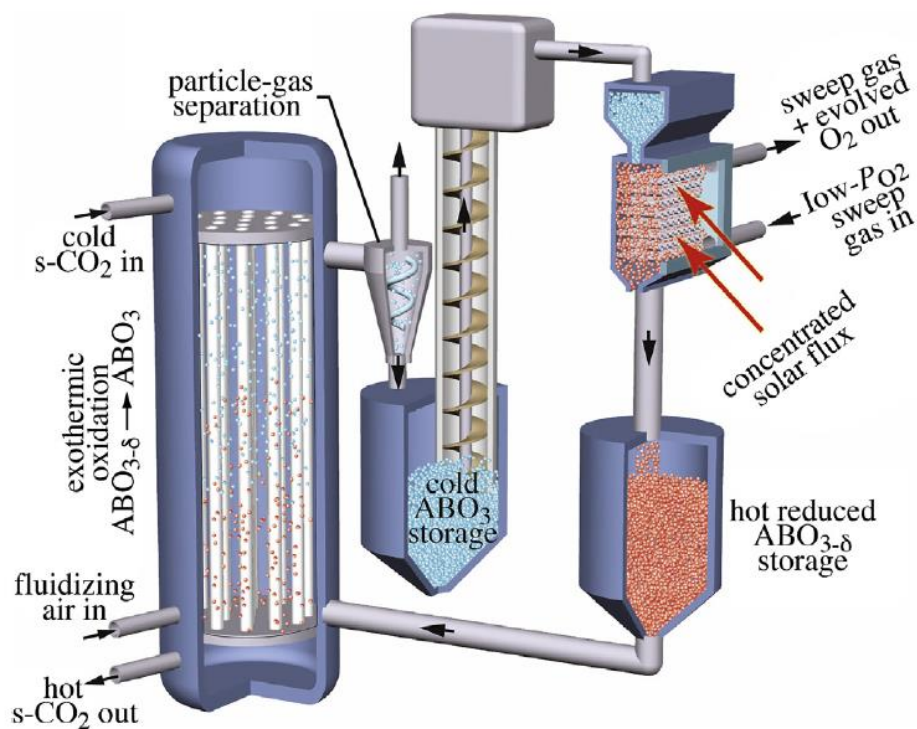


**Figure 2.8.** Schematic of a TCES sub-system using reducible perovskites and integrated with a concentrating solar receiver taken from Imponenti et al. (Imponenti et al. 2017).

Ammonia-based thermal energy storage is another suitable system for long-term storage. Shakeri et al. (Shakeri et al. 2014) found that ammonia based thermal energy storage was more efficient than other storage systems such as pumped hydroelectric, compressed air, and vanadium flow battery. Dissociation and synthesizing of ammonia-based thermochemical energy storage are defined as follows:



As shown in Figure 2.9, dissociation of ammonia ( $\text{NH}_3$ ) occurs by endothermic reaction as it absorbs the solar energy. The stored energy can be released on demand by synthesising ammonia, which happens through reaction of  $\text{H}_2$  and  $\text{N}_2$ . Electricity can be generated by the released energy.

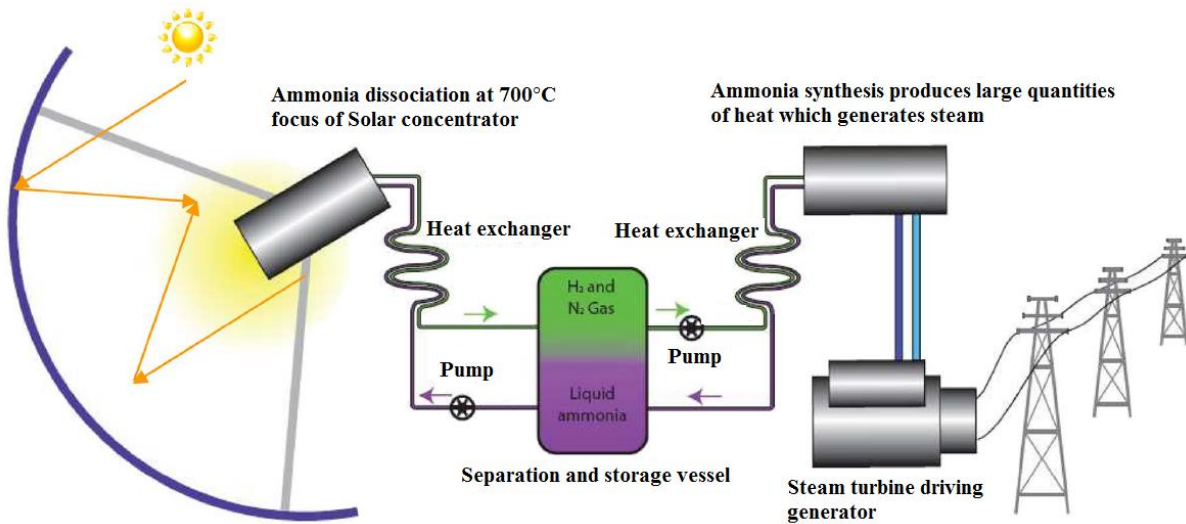


**Figure 2.9.** Schematic of the ammonia dissociation and storage system adopted from Dunn et al. (Dunn et al. 2012).

Synthesising of ammonia with hydrogen and nitrogen at high pressures and temperatures with catalyst is a mature process in industry. The application of ammonia decomposition for CSP technology has been studied since 30 years ago (Luzzi & Lovegrove 1997). Ammonia-based thermochemical energy storage has been proposed and established by the National University of Australia (ANU) for supercritical steam Rankine cycle with an operating temperature from 350°C to 650°C (Dunn et al. 2012). Decomposition and synthesizing reaction of ammonia-based thermochemical energy storage is a reversible reaction with no side reaction. Moreover, the product and reactant of ammonia-based TCES are stable in their operating temperature ranges. The ammonia-based TCES is supported by extensive industrial experience in ammonia treatment and synthesis, design guidelines and operational processes.

US department of energy has carried out a research under SunShot project to achieve a target cost of 15\$/ kWh for ammonia-based TCES process at an operating temperature of 650°C (Lavine et al. 2016). This process operates in a closed cycle, and it has the potential to frequently refill materials. It is worth mentioning that the cost of this process depends on the initial capital cost which is related to the cost of the reactor wall material. Optimizing the design based on the power generation and wall material volume is necessary for feasibility of the

ammonia-based TCES (Liu et al. 2018). Ammonia-based TCES process, integrated with a high-temperature pre-treatment system and a supercritical steam heat recovery reactor, has recently been designed and optimized by Chen et al (Chen et al. 2018). The results depict that the material required for structure of the system is relatively expensive because of necessity of using resistant materials for high operating temperature. It is worth mentioning that ammonia-based TCES system has some limitations, namely, the severe chemical reaction conditions, high pressure operation condition. Furthermore, N<sub>2</sub> and H<sub>2</sub> must be safely stored for a long time. The operating cost of the system is also relatively high (Chen et al. 2018).

Facing the aforementioned literature, among the various thermochemical thermal storage materials, metal oxides have received significant attention due to their high operating temperatures (350°C-1100°C) which leads to improving the Carnot and thermal efficiency of the CSP plants (Stekli et al. 2013; Wu et al. 2018). Moreover, metal oxides benefit from high energy density. For example, at a theoretical transition temperature in air, the energy density of Co<sub>3</sub>O<sub>4</sub>/CoO, CuO/Cu<sub>2</sub>O and Mn<sub>2</sub>O<sub>3</sub>/Mn<sub>3</sub>O<sub>4</sub> is 844 kJ/kg, 811 kJ/kg, and 204 kJ/kg, respectively (Agrafiotis et al. 2016; Deutsch et al. 2017). For such energy storage systems with metal oxides, air is used as a reactant and heat transfer medium in the system (Kodama & Gokon 2007; Yan et al. 2015). Such materials are simply available in the nature. Moreover, most metal oxides are environmentally benign and commercially available (Block & Schmücker 2016).

The two-step reduction and oxidation reactions for metal oxides in a thermo-chemical storage are as follows:



In these reactions, “Me” represents a suitable metal oxide for the reduction and oxidation reactions. The potential of various metal oxides have been extensively assessed for chemical looping methods (Zhou et al. 2015; Zhou et al. 2016; Zhou et al. 2017), in which the performance and stability of different metal oxides in RedOx reactions were studied. Different metal oxides were also assessed for the thermochemical energy storage by Wong et al. (Wong 2011; Wong et al. 2010). They found that BaO<sub>2</sub>, Co<sub>3</sub>O<sub>4</sub>, Mn<sub>2</sub>O<sub>3</sub>, CuO, Fe<sub>2</sub>O<sub>3</sub>, and Mn<sub>3</sub>O<sub>4</sub> were suitable for application of TCES (Wong 2011; Block et al. 2014; Wong et al. 2010) due to their high operating temperature, energy storage density, kinetics and cost. However, there are some challenges associated with the use of these materials requiring to be addressed before they can be utilised on a commercial scale. An overview of each type of metal oxide is presented in the following section.

Simple RedOx reactions of metal oxides have firstly been proposed for thermal energy storage by Wentworth and Chen (Wentworth & Chen 1976). The potential of Barium oxides for thermal energy storage was theoretically assessed by Simmones (Simmons 1976). Later, the experimental investigation of Barium oxide for thermal energy storage was conducted by Bowrey and Jutsen (Bowrey & Jutsen 1978) for five reduction and oxidation cycles with a maximum conversion of 93% for the oxidation reaction (Bowrey & Jutsen 1978). In this experiment, a maximum temperature of 850°C and heating rate of 8°C/min were used to prevent the crusting on the surface of the material. In another study, the kinetics of the reaction for BaO<sub>2</sub>/BaO couples was developed with thermogravimetric methods in isothermal and non-isothermal conditions by Fahim and Ford (Fahim & Ford 1983). The results revealed that the activation energy for the forward and the reverse reactions was 33.6 kcal/mol and 12.4 kcal/mol, respectively. They have also found that the RedOx reactions of BaO<sub>2</sub>/BaO pair happened at temperatures between 400°C and 1027°C (Fahim & Ford 1983). However, a mass transfer limitation and the crusting of material at different temperatures and pressures inhibits

the complete conversion. The reported reaction temperature of Barium oxide in the literature varies from 738°C to 880°C due to the different calculation methods and experimental conditions (André et al. 2016; Kubaschewski et al. 1967; Wentworth & Chen 1976). Formation of the solid solution ( $\text{BaO}_2 + \text{Ba}(\text{OH})_2$  and  $\text{BaO} + \text{Ba}(\text{OH})_2$ ) as a result of water in the system can also be another reason for different reaction temperature of Barium oxide (Till 1971). The pressure of the system can also affect the reduction temperature. For example, the reduction temperature of Barium oxide decreases from 870°C to 145°C with decreasing the pressure from 1 bar to 0.1 bar (Carrillo et al. 2016). The theoretical weight loss of the  $\text{BaO}_2/\text{BaO}$  couples is 9.45%. However, it can be increased due to some side reactions (Carrillo et al. 2016). The reported energy density for  $\text{BaO}_2/\text{BaO}$  varied from 390 kJ/kg to 526 kJ/kg (Wu et al. 2018). The difference in the energy density is because of the impurity of materials, incomplete conversion and/or heat losses (Carrillo et al. 2016). Although the  $\text{BaO}_2/\text{BaO}$  reaction is considered to be reversible and suitable for TCES, the conversion fraction decreases with an increase in the number of cycles due to sintering phenomenon in the particles after 10 cycles (Carrillo et al. 2016). Figure 2.10 presents the sintering of the  $\text{BaO}_2$  after 10 cycles of reduction and oxidation reactions. It showed that sintering increased with decreasing the cooling rate.



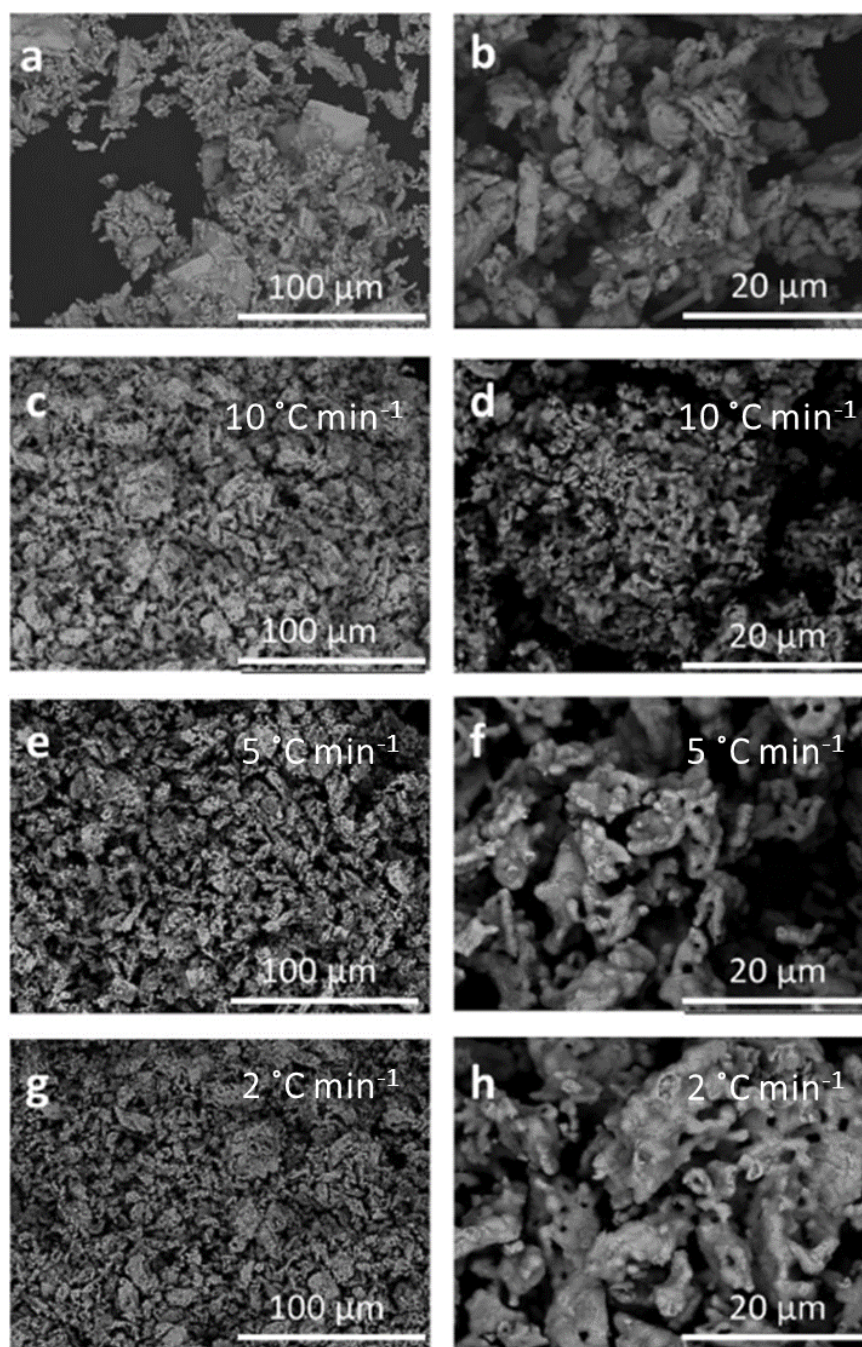


**Figure 2.10.** Surface morphology of BaO<sub>2</sub> particles before cycling (a and b) and after cycling (c to h) at different cooling rates (2, 5 and 10 °C min<sup>-1</sup>) adapted from Carrillo et al. (A. J. Carrillo et al. 2016).

Cobalt oxide is one of the promising materials for TCES systems due to its high energy storage capacity (844 kJ/kg) and excellent reversibility, but the high cost of this material is the main drawback (André et al. 2016). The practical energy storage density is different from theoretical one because of the materials properties. The reported energy storage capacity of Co<sub>3</sub>O<sub>4</sub>/CoO



couple was different in various structures such as pellets (525 kJ/kg), powder (495 kJ/kg) and honeycomb (549 kJ/kg) (Karagiannakis et al. 2014; Pagkoura et al. 2014). In another study, the energy storage capacity of 400 kJ/kg was reported for  $\text{Co}_3\text{O}_4/\text{CoO}$  powder in a rotary kiln reactor (Neises et al. 2012). The reason was explained by incomplete conversion of the material due to the either insufficient mixing within the reactor or mass transfer limitations (Neises et al. 2012). The RedOx temperature of the cobalt oxide depends on the gaseous atmosphere and experimental conditions, and occurred at 820°C (for the reduction reaction) and 900°C (for the oxidation reaction) in an air atmosphere (Neises et al. 2012). Agrafiotis et al. (Agrafiotis et al. 2014) reported that the reduction temperature occurred at a temperature range between 885 °C and 905°C under the atmospheric condition with air. A similar study was conducted by Andre et al. (André et al. 2016) to investigate the reduction temperature of 772°C in an argon atmosphere and similar results were reported.

The effect of oxygen concentration on the RedOx reaction of cobalt oxide was obtained by Müller et al. (Müller et al. 2017). They found that the RedOx reaction of  $\text{Co}_3\text{O}_4/\text{CoO}$  occurred at temperature ranges between 480°C and 630°C. Hutching et al. (Hutchings et al. 2006) found that the reaction temperature changes with the variation of the partial pressure of oxygen in the system because it changed the thermodynamic driving force in the gas phase. The temperature range for the RedOx cycle was between 885°C and 905°C, and RedOx cycles can reach ~30 cycles. Muroyama et al. (Muroyama et al. 2015) also found that the overall weight change of the cobalt oxide powder over 10 RedOx cycles remained stable. Cobalt oxide has been used with porous, foam and rigid structures to retain the performance of the stoichiometric RedOx cycles and integrity after each cycle (Agrafiotis et al. 2015). For example, the kinetics of cobalt oxide with pellet structure was assessed and good cycling stability was observed up to 10 cycles (Karagiannakis et al. 2014). The stability of the cobalt oxide in the form of honeycomb was also investigated by Pagkoura et al. (Pagkoura et al. 2015). The assessment revealed a good

---

stability of the cobalt oxide up to 10 cycles. Some cracks were observed in the cobalt oxide pellets for the number of cycles exceeding thirty and no degradation appeared in the  $\text{Co}_3\text{O}_4$ -loaded honeycomb with an increase in the number of cycles. This demonstrated the high stability of honeycomb structure (Neises et al. 2012; Tescari et al. 2014). The result revealed that the sintering and agglomeration of the  $\text{Co}_3\text{O}_4$  had no effect on degradation of the material. The thermal stability of commercial-scale  $\text{Co}_3\text{O}_4$  was also assessed with Thermogravimetric analysis (TGA) at a temperature range between 955 °C and 870 °C and the results proved the high stability of cobalt oxide over several cycles. This was because the reactivity of the material was not decreased (Hutchings et al. 2006) over the time. The morphology of the cobalt oxides after 500 RedOx cycles at a temperature range between 700°C and 900°C was studied by Wong et al. (Wong 2011). Figure 2.11 shows the surface morphology of the copper oxide after different numbers of cycles. They found that the size of the particles increased with an increase in the number of the cycles. The sintering issues of the cobalt oxide was highlighted by Block et al. (Block et al. 2014) after 3 RedOx cycles at temperature ranges between 1100°C and 1400°C. Moreover, mechanical stress and material fatigue were investigated during the RedOx cycle and sintering of the materials was identified, which was intensified over the time and with an increase in the number of cycles (Block & Schmücker 2016; Karagiannakis et al. 2016).

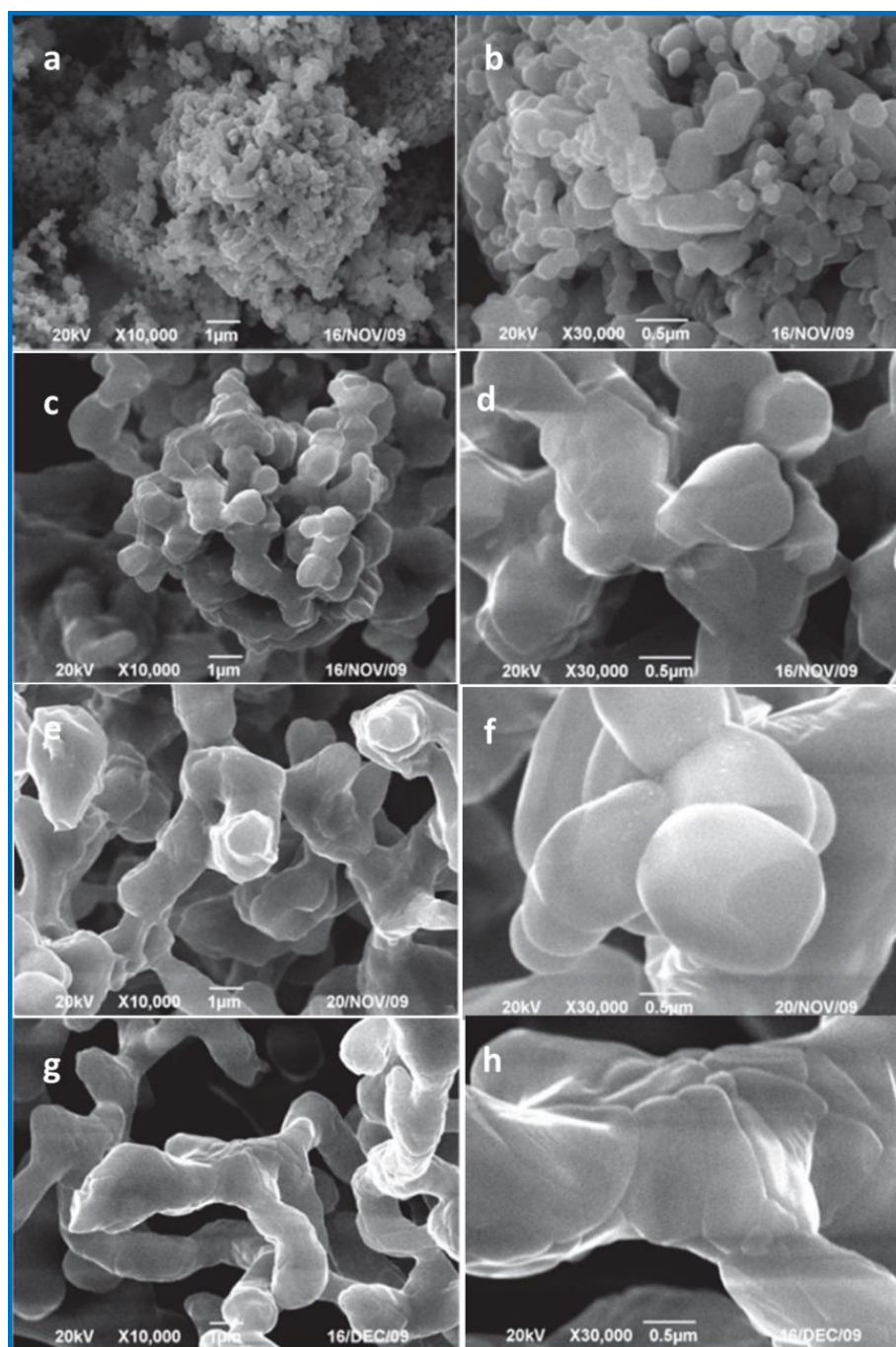


**Figure 2.11.** Surface morphology of  $\text{Co}_3\text{O}_4$  before (a and b) and after cycling test (c and d: 50 cycles, e and f: 150 cycles and g and h: 500 cycles) between  $700^\circ\text{C}$  and  $900^\circ\text{C}$  adapted from Wong (B.Wong 2011).

The kinetics assessment of the cobalt oxide showed that the oxidation fraction can be changed with the heating and cooling rates. Higher oxidation rates can be achieved by lowering the cooling rate. This was because it provided prolonged residence time. For example, the oxidation fraction of cobalt oxide decreases from 94.6% to 30% with an increase in the cooling rate from  $1^\circ\text{C}/\text{min}$  to  $30^\circ\text{C}/\text{min}$  (Wong 2011). Karagiannakis et al. (Karagiannakis et al. 2014)

mentioned that the physical form of the cobalt oxide can affect the kinetics of the reaction. The assessment of cobalt oxide in both pellets and powder showed that the oxidation of cobalt oxide in the form of the pellets is faster than cobalt oxide powder. This is because the heat transfer in pellet structure is more intensified in comparison with the other structures (Karagiannakis et al. 2014). To reduce the cost of the cobalt oxide in a real-case application, Carrillo et al. (Carrillo et al. 2014) suggested to combine cobalt oxide with low-cost and less-harmful materials. It has recently been reported that the binary cobalt oxide can improve thermal stability and reaction kinetics (Babiniec et al. 2015; Pagkoura et al. 2014).

The  $\text{Mn}_2\text{O}_3/\text{Mn}_3\text{O}_4$  pair have been considered to be promising materials for the TCES system due to their moderate energy storage capacity (202 kJ/kg), high reaction temperature (lower than  $1000^\circ\text{C}$ ), low cost and non-toxic nature (Wong 2011; Block & Schmäcker 2016; Carrillo et al. 2016). However, similar to other metal oxides, they suffer from a slow oxidation reaction, and sintering problems during RedOx cycles (Carrillo et al. 2016). The RedOx reactions of  $\text{Mn}_2\text{O}_3/\text{Mn}_3\text{O}_4$  occur at a temperature range between  $550^\circ\text{C}$  to  $1000^\circ\text{C}$ , which is suitable for high temperature applications such as CSP technologies (Karagiannakis et al. 2014; Wu et al. 2018). However, a wide temperature gap between reduction and oxidation reactions leads to a decrease in exergy efficiency of the system. Therefore, the cascade structures have been proposed to eliminate the temperature difference between reduction and oxidation (Agrafiotis et al. 2015). Experimental results showed that the reduction reaction occurs at a temperature of approximately  $950^\circ\text{C}$  and it varies slightly depending on the rate of the reaction (Carrillo et al. 2014). The  $\text{Mn}_2\text{O}_3/\text{Mn}_3\text{O}_4$  couple was also assessed experimentally at temperatures between  $500^\circ\text{C}$  and  $1000^\circ\text{C}$  with a heating rate of  $10^\circ\text{C}/\text{min}$ . A wide temperature gap occurred between the reduction ( $940^\circ\text{C}$ ) and oxidation reaction ( $840^\circ\text{C}$ ) (Agrafiotis et al. 2016; Carrillo et al. 2014) which can further increase the exergy loss in a real-case test. To address this issue, doping with Cu and Fe is suggested to both reduce the temperature difference for the reduction

---

and the oxidation (Figure 2.12), while improving the thermal stability and kinetics of the reaction (Carrillo et al. 2015).

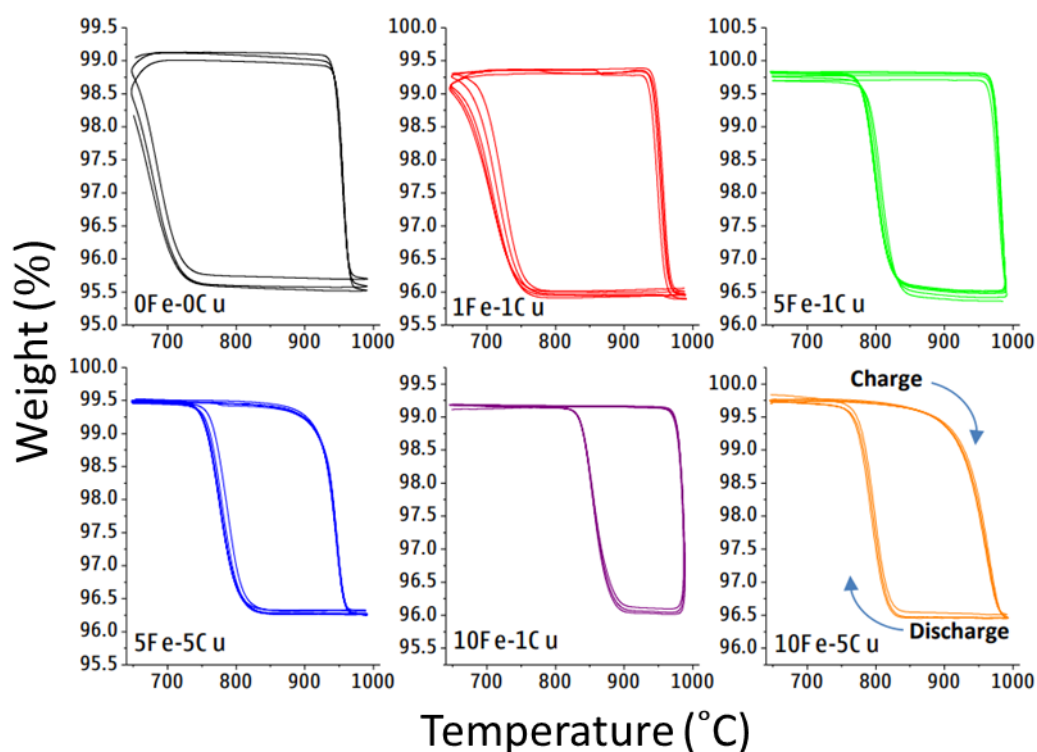


**Figure 2.12.** Weight variation versus temperature plot of four redox cycles for six Fe-Cu doped Mn oxides. The arrows indicate the cycle direction, adapted from (Carrillo et al. 2015).

The study on the conversion of  $\text{Mn}_2\text{O}_3/\text{Mn}_3\text{O}_4$  demonstrated that low cooling rate can improve the oxidation reaction (Agrafiotis et al. 2015). Karagiannakis et al. (Karagiannakis et al. 2014) studied the flow through pellets of  $\text{Mn}_2\text{O}_3/\text{Mn}_3\text{O}_4$  and the results showed that the reaction kinetics improved with using pellets because of the increase in the heat transfer through pellets. They found that the reduction occurs at a temperature range between  $920^\circ\text{C}$  and  $1000^\circ\text{C}$ , while the oxidation occurs between  $500^\circ\text{C}$  and  $850^\circ\text{C}$ . The energy density of  $110 \text{ kJ/kg}$  was calculated for  $\text{Mn}_2\text{O}_3/\text{Mn}_3\text{O}_4$  couple. Nevertheless, no obvious degradation of RedOx was identified over six RedOx cycles. Another important parameter in RedOx reactions of metal oxides is the particle size of the material. It has been found that smaller particles reduce the oxidation temperature due to the large specific area of the particles (Carrillo et al. 2014).

Copper oxide with good heat and mass transfer characteristics has also been investigated by several researchers. For example, the suitability of CuO/Cu<sub>2</sub>O RedOx cycles for oxygen separation has been assessed by Hänchen et al. (Hänchen et al. 2012), and it was suggested that this material is suitable for high-temperature CSP technology. Advantageously, the price of copper is lower than other metal oxides (Carrillo et al. 2016). Chadda et al. (Chadda et al. 1989) pioneered the application of copper oxide for thermo-chemical energy storage at a temperature range between 400°C and 910°C. The porous structure of CuO/Cu<sub>2</sub>O was observed after the 20 RedOx cycles due to the swelling of the materials (Chadda et al. 1989). The study also showed that the surface area of the material increases from approximately 0.1 to 0.79 m<sup>2</sup>/g with an increase in the number of cycles from 0 to 20 maintaining the reactivity of the material. Nevertheless, there is a conflict on the reversibility of copper oxide over various cycles. For example, Wong et al, (Wong 2011) reported that CuO/Cu<sub>2</sub>O pair cannot be reversible for even 5 cycles due to sintering problems and shrinkage of the particles. The CuO/Cu<sub>2</sub>O pair was also assessed in TGA and pack bed in which the RedOx reactions of copper oxide was tested in 20 RedOx cycles (Deutsch et al. 2017). The results demonstrated that the sintering of the copper oxide occurs after 20 cycles of reduction and oxidation. In spite of the fact that the reactive surface of the copper oxide was blocked after thermal cycling, the granular structure was observed in the core of the materials. In a similar study conducted by Deutsch et al. (Deutsch et al. 2017), it was found that the sample (after 20 cycles of thermogravimetric tests) showed good reversibility of CuO/Cu<sub>2</sub>O pair with some sintering found inside the samples. To address the sintering problem, Alonso et al. (Alonso et al. 2015) proposed that a rotary reactor could be the solution. Thereby, in their study, the sintering problem was avoided as the particles were kept rotating and mixing. This finding paves a new way for the practical use of Cu<sub>2</sub>O/CuO pair as an energy storage material.

One of the main challenges of copper oxide in thermo-chemical storage is its melting temperature, which is close to the reaction temperature of copper oxide that may result in sintering of the particles (Block & Schmücker 2016). A feasibility study of the copper oxide in rotary kiln reactor confirmed the sintering of the materials at a temperature of 1235°C, which is the melting temperature of copper oxide (Alonso et al. 2015). They also found that the grain of the material grew after thermal cycling. A reaction temperature of 1030°C has been reported for the reduction of CuO to Cu<sub>2</sub>O (Wong 2011). As shown in Figure 2.13, the RedOx cycle of CuO/Cu<sub>2</sub>O was recently assessed at two heating rates of 1°C/min and 5°C/min with no dwell time during reduction and oxidation at 1090°C and 1000°C, respectively, in an air atmosphere (Agrafiotis et al. 2016). The results showed that the reduction reaction was faster than the oxidation reaction due to sintering during the reduction reaction which led to the incomplete oxidation of the copper oxide. Narrowing the RedOx temperature range and using a dwell time of two hours for oxidation have been suggested to overcome this matter (Agrafiotis et al. 2016).

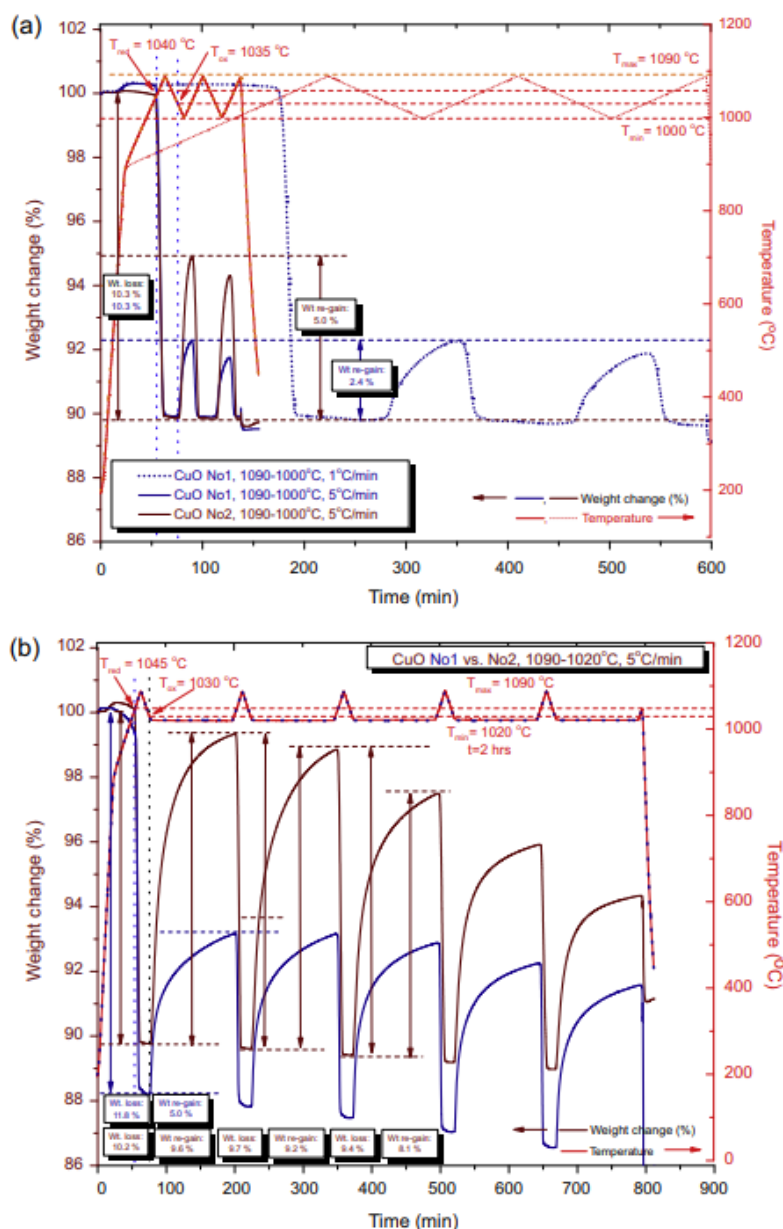


**Figure 2.13.** Weight change of CuO powder with at two different rate of 2 and 5°C/min with and without dwell time for oxidation at temperature of 1020°C, adapted from Agrafiotis et al. (Agrafiotis et al. 2016).

The RedOx cycles of CuO/Cu<sub>2</sub>O have also been assessed for the reactions under various environments of different gases such as argon and nitrogen in a rotary solar reactor (Alonso et al. 2015). The results showed that the conversion during the reduction reaction decreased from 80% to 40% for the case in which the gas changes from argon to air. However, 9% conversion was achieved during the oxidation reaction with air (Alonso et al. 2015). The material was



tested for several cycles in this condition but small weight loss due to the sintering, evaporation and volatilization was observed after each cycle (André et al. 2016).

The above review of the literature, CuO/Cu<sub>2</sub>O pair has some advantages in thermo-chemical energy storage such as high storage capacity and abundant resources. However, O<sub>2</sub> concentration of carrier gas influences the reduction and oxidation reactions where the oxidation reaction is slower than the reduction reaction (Alonso et al. 2015; André et al. 2016). In addition, the incomplete oxidation of CuO/Cu<sub>2</sub>O pair as a result of sintering and shrinkage requires further investigation to be well understood and resolved.

### **2.3 General challenges of thermochemical storage with temperature and pressure swing**

In a thermochemical energy storage with temperature swing, the reduction reaction temperature, where energy is stored, is typically higher than that of the oxidation reaction, where energy is released (Carrillo et al. 2015). This results in the discharge of the energy at a temperature lower than charging temperature, which decreases the thermal efficiency of the system (Carrillo et al. 2015). Furthermore, fatigue, thermal stress, and containment issue, are other challenges of the temperature swing system (Muhich et al. 2016).

On the contrary, the isothermal system, which is based on pressure swing, can mitigate dwell time in the heating and cooling of the materials during the reduction and oxidation reactions (Amar et al. 2015). In fact, the rate of the reactions is higher in isothermal process in comparison with the temperature swing process (Al-Shankiti et al. 2017). It is worth mentioning that despite the advantages of pressure swing technique, it has some challenges. In a pressure swing process, the reduction step requires a low pressure of O<sub>2</sub> which can be achieved by either a vacuum pump or the use of an inert sweeping gas. Moreover, oxidation reaction needs to be undertaken at high partial pressures of O<sub>2</sub>, which can be achieved through

pressurising air. This is advantageous, because it facilitates the integration of energy storage system with a GTCC which requires high pressure operating conditions. The capital and operational cost of the pressure swing system is higher than that of temperature swing system. This is because the pressure swing system not only requires the different pressure but also needs a high temperature to operate. However, the temperature swing system has lower efficiency than pressure swing due to the exergy loss, which is caused by its higher charging temperature compared to its discharge temperature. Therefore, the temperature swing system has lower capital and operating costs while the pressure swing system has higher efficiency.

One of the applications of RedOx, especially by p-swing is in the CLAS concept. This concept can be readily adapted to be incorporated with solar thermal energy. Solar thermal energy is stored and released through endothermic reduction and exothermic oxidation reactions, respectively and is also stored in OC particles as sensible heat. The application of p-swing for power generation and oxygen production has recently been proposed by Haseli et al. (Haseli et al. 2017). The so-called Sol-CLAS process offers a potential to store heat at both sensible and chemical forms (Figure 2.14). An operating temperature of 1000°C was suggested for the reduction and the oxidation reactors which reduced the exergy destruction of the process. Moreover, a cycle efficiency of 46% was achieved by the Sol-CLAS system.

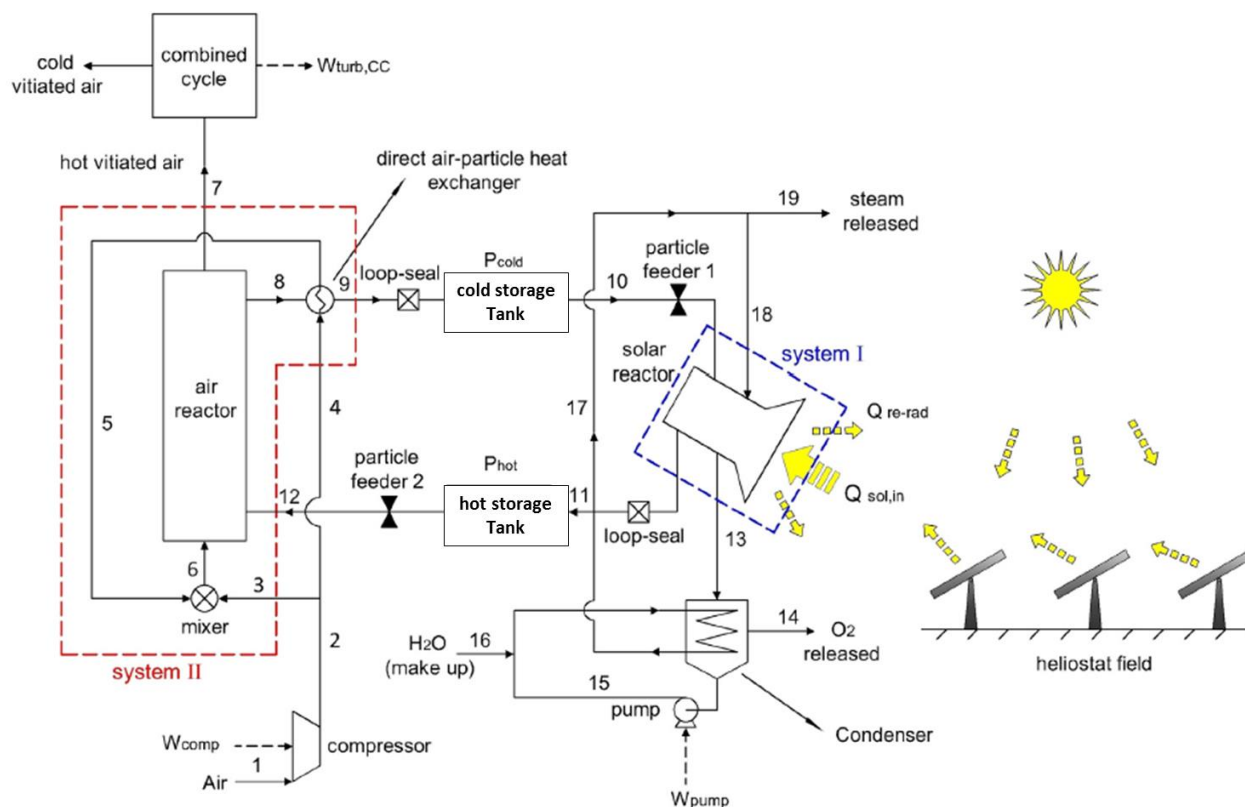


**Figure 2.14.** A schematic diagram of the Sol-CLAS process, adapted from Haseli et al. (Haseli et al. 2017).

Solid metal oxides play a major role in sol-CLAS. They are not only used as oxygen carrier, but are also the storage media. However, the application of solid metal oxides is limited due to the technical challenges associated with the use of solid metal oxides at high temperature conditions (e.g. 1000°C during charging and/or discharging process) such as sintering, softening, and agglomeration of solid metal oxide in RedOx reactions (Adanez et al. 2012; Jafarian et al. 2017). Nevertheless, a temperature of 1000°C is still lower than the temperature of the state-of-the-art gas turbine (Bhargava et al. 2007). Hence, apart from other technical and economical requirements, an advanced thermal energy storage system is required to operate at high temperatures, so liquid metal oxides are proposed as an alternative solution to the current solid metal oxide system, to address the aforementioned challenges (Pacio et al. 2013; Pacio & Wetzel 2013).

## 2.4 Bench-marking of economic assessment for thermal energy storage

The commercially available molten salt is now operating at a temperature of 565°C and it can be used for Rankine cycle with conversion efficiencies of 36%–40%. Commercial combined power cycles could offer high efficiency of 55% to 60% at an operating temperature of 1200°C. More efficient alternative power cycles exist, thus it has the potential to reduce the Levelised Cost of Electricity (LCOE) by up to 33% (Dunham & Iverson 2014). The use of metal is considered as an alternative to the conventional molten salt, which has the potential to increase the inlet temperature of the turbine and thus increasing the efficiency of the system (Silakhori et al. 2019).

Table 2.8 shows the price of the metal oxides in the scale of laboratory and Tonnage scale. As shown in this table the price of  $\text{Co}_3\text{O}_4$  is in the highest level at 250 €/kg compared to other metal oxides (Block & Schmücker 2016). This value is six times higher than the price of the  $\text{Fe}_3\text{O}_4$ . While the price in the tonnage scale is lower than laboratory scale, the purchase value of  $\text{Co}_3\text{O}_4$  is still in the highest level compared to other metal oxides.

**Table 2.8.** Comparison the price of the met oxides in different scales (Block & Schmücker 2016; Wu et al. 2018).

Metal oxides	Laboratory purchases	Tonnage scale
$\text{Co}_3\text{O}_4$	250€/kg (97% purity)	23€/kg (72% purity)
$\text{CuO}$	60€/kg (97% purity)	6€/kg (98% purity)
$\text{Fe}_3\text{O}_4$	40€/kg (97% purity)	0.8€/kg (95% purity)
$\text{MnO}_2$	100€/kg (97% purity)	2€/kg (91% purity)

The estimated cost for metal oxides in thermochemical energy storage system has also been assessed by Wong et al. (Wong 2011) The result depicts that  $\text{UO}_3$ ,  $\text{Rh}_2\text{O}_3$  and  $\text{PtO}_2$  with the price of 1000 \$/kWh are much more expensive than  $\text{CuO}$ ,  $\text{Co}_3\text{O}_4$ ,  $\text{Mn}_2\text{O}_3$ ,  $\text{Mn}_3\text{O}_4$ ,  $\text{MnO}_2$ ,  $\text{Fe}_2\text{O}_3$ ,  $\text{PbO}_2$ , and  $\text{BaO}_2$  with the price of less than 100 \$/kWh. The LCOE analysis of the thermochemical energy storage also shows that Mn oxide based materials can compete with other metal oxides. However, the performance of the Mn oxide-based material in term of

reduction and oxidation was not satisfactory in the experiments (Wong 2011). While the LCOE and cost target of the US department of Energy (DOE) for storage were reported to be under \$0.10/kWh and under \$15/kWh per cycle, respectively, only few metal oxides such as  $\text{Mn}_3\text{O}_4$   $\text{Fe}_2\text{O}_3$  may meet these targets (Wu et al. 2018).

Regarding to the cost analysis of the materials in thermochemical energy storage, there are several parameters that should be considered, such as material storage, storage system, heat exchanges, and operational and maintenance cost. The cost of a CSP plant which consists of a packed bed reactor and  $\text{Co}_3\text{O}_4+\text{Al}_2\text{O}_3$  redox couple was estimated by Wong et al. (Wong 2011). Eight fix bed reactors with the potential of  $18.75\text{MW}_t$  were designed to operate at temperature ranges between  $600^\circ\text{C}$  and  $1200^\circ\text{C}$ . The results show that the cost of the storage system can reach to \$10/kWh, which is highly related to the cost of the raw materials. It was also recommended that the moving bed reactor could improve the performance of the  $\text{Mn}_2\text{O}_3/\text{Mn}_3\text{O}_4$  redox cycles. Another economic assessment with  $\text{CaTi}_{0.2}\text{Mn}_{0.8}\text{O}_{3-\delta}$  and a plant with a capacity of  $111.7\text{MW}_e$  estimates the storage cost of \$15/kWh (Miller et al. 2016). Bayon et al. (Bayon et al. 2018) have recently proposed a techno-economic assessment of solid-gas thermochemical energy storage. Table 2.9 compares the operating temperature, energy storage capacity, thermal efficiency and capital cost of the molten salts, hydroxides, carbonates, and metal oxides. The minimum temperature of endothermic reaction and maximum temperature of exothermic reaction are listed as charging and discharging temperature, respectively. Table 2.9 also shows that the chemical reaction of the materials, such as metal oxides and carbonates, provides high energy density at high operating temperatures (over  $600^\circ\text{C}$ ), which can be used as a suitable alternative for conventional molten salt system in high temperature solar thermal plants.

**Table 2.9.** Summary of calculated techno-economic assessment of selected thermochemical energy storage system for 1176 MWh<sub>th</sub> and four house of storage (Bayon et al. 2018).

TCES concept	Operating temperature (°C)		Energy storage capacity (MJm <sup>-3</sup> )	Parasitic energy (%)	Thermal efficiency (%)	Total capital cost (\$MJ <sup>-1</sup> )
	Charging temperature	Discharging temperature				
<b>Molten salt</b>						
Salt						
Stream60/40	565	235	64.61	2.77	97.23	9.61
Salt Stream700	700	300	51.85	4.09	95.91	16.78
<b>Hydroxides</b>						
Ca(OH) <sub>2</sub> /CaO	700	505	101.97	1.49	98.51	4.78
Sr(OH) <sub>2</sub> /SrO	600	525	97.09	2.44	97.56	7.09
Ba(OH) <sub>2</sub> /BaO	700	520	77.61	3.5	96.50	8.28
<b>Carbonates</b>						
CaCO <sub>3</sub> /CaO	898	650	39.01	48.7	51.30	15.09
SrCO <sub>3</sub> /BaO	1200	1150	51.32	41.47	58.53	22.74
BaCO <sub>3</sub> /MgO	1400	1300	47.76	42.53	57.47	25.64
MgCO <sub>3</sub> /MgO	900	550	19.12	66.94	33.06	25.02
La <sub>2</sub> O <sub>2</sub> CO <sub>3</sub> /La <sub>2</sub> O <sub>3</sub>	980	550	39.39	40.23	59.77	30.29
MgCO <sub>3</sub> .CaCO <sub>3</sub>	930	600	8.05	82.48	17.52	82.19
<b>Metal oxides</b>						
Co <sub>3</sub> O <sub>4</sub> /CoO	905	885	102.45	2.86	97.14	306.84
Mn <sub>2</sub> O <sub>3</sub> /Mn <sub>3</sub> O <sub>4</sub>	989	650	32.69	8.24	91.76	126.96
BaO <sub>2</sub> /BaO	980	690	46.09	5	95	23.93
CuO/Cu <sub>2</sub> O	1100	900	113.43	2.12	97.88	55.51

## 2.5 Liquid Chemical Looping for Thermal Energy Storage (LCL-TES) systems

The use of liquid metal oxides in LCL-TES systems has recently been proposed by Jafarian et al. (Jafarian et al. 2017) to address the technical challenges, such as sintering, softening, attrition and agglomeration of solid metal oxides. They proposed a LCL-TES system (Figure 2.15). In a LCL-TES system, a liquid metal oxide is used as the storage medium. The system is designed to combine the benefits of sensible, latent, and thermochemical solar thermal energy storage to achieve high storage temperature and energy density. In a LCL-TES system, concentrated solar radiation provided by a solar collector field is captured and stored in a liquid metal oxide.

A LCL-TES system consists of two reduction and oxidation reactors, two reservoirs (for liquid and solid metals), and a heat recovery unit. The solid metal oxide particles are introduced into the solar reduction reactor (stream 1), where they are reduced due to both high temperatures

and low partial pressure of oxygen in the gas phase. This enables solar thermal energy to be stored through sensible heating of particles from the input temperature to their melting point. Then, particles are melted and reduced to a lower state of oxidation. The concentration of oxygen in the gas phase is controlled by steam injection. Then, the reduced liquid metal oxide is conveyed to the hot storage tank (stream 2). Afterward, the liquid metal oxide is introduced into the oxidation reactor (stream 3) and heat recovery unit (stream 4) to be oxidised and solidify the liquid metal oxide. The oxidation process of the heat recovery unit in LCL-TES is different from the previously proposed heat recovery system for molten slag in blast furnaces. This is because of the presence of chemical reactions occurring simultaneously with the heat transfer and granulation processes. It is worth noting that the hot air leaving the oxidation reactor is used to generate power (stream 7). Finally, the metal oxide is conveyed to the cold storage tank after releasing the thermal energy (stream 8).

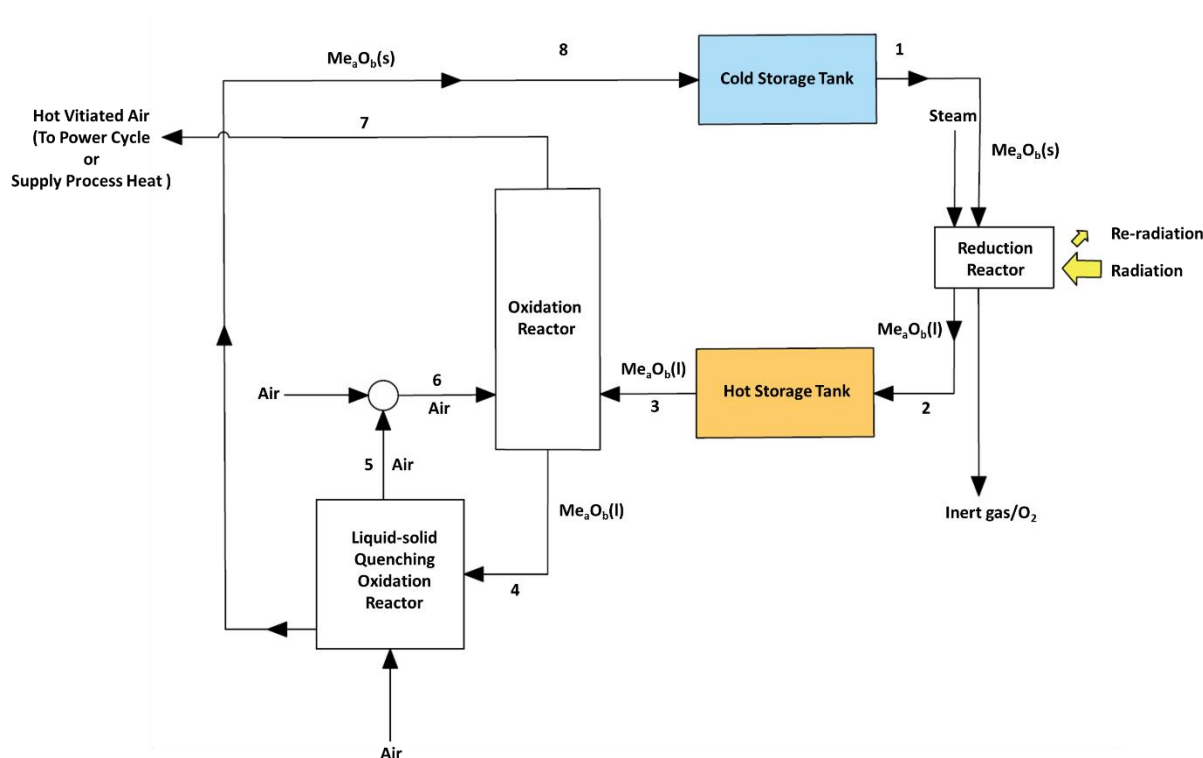


**Figure 2.15.** A schematic diagram of the key components of the LCL-TES system adapted from Silakhori et al. (Silakhori et al. 2017) and Jafarian et al. (Jafarian et al. 2017).

Although LCL-TES system has been assessed for copper oxide, the potential of different metal oxides for a LCL-TES have not been assessed and this research needs to be undertaken. Moreover, a thermodynamic selection procedure for the potential liquid metal oxide needs to be developed. This procedure provides a back-to-back comparison between various metal oxides with the purpose to identify the most suitable ones for the LCL-TES. The energetic performance of the materials suitable for use in this system have not been assessed yet and this requires further research. The use of various metals in LCL-TES can also decrease the operating temperature of the process. Hence, the thermodynamic efficiency of the process can be decreased. To overcome this challenge, one potential approach is to use an after-burner which leads to the hybridisation of the system (Jafarian et al. 2014), which is discussed in the following sub-section.

## **2.6 Hybrid solar power plants**

Combining two source of energies such as concentrating solar thermal technologies and combustion technologies in a single plant is referred to as “hybridisation” (Nathan et al. 2018). Hybridisation offers several advantages over conventional processes. These advantages include (but are not limited to) low cost power generation, reducing CO<sub>2</sub> emissions by decreasing the fuel consumption, high conversion efficiency due to smaller heliostat field and sharing infrastructure with new or existing combustion power plants (Buck et al. 2017; Kaniyal et al. 2012)

The state-of-the-art technologies for the solar hybrid power cycles include solar hybrid steam cycle, solar hybrid Brayton cycle and a solar hybrid combined cycle system. The performance of these systems can be compared based on their thermal efficiency, solar share and solar-to-electrical efficiency. The “efficiency” of a cycle can also be identified by its ratio of net generated power to the ratio of the total input power by both solar and fuel sources (Sheu et al.



2012). The contribution of solar energy into the total input energy of a cycle is known as “solar share”, which can be performed at any time (Buck et al. 2002). The “solar-to-electrical efficiency” is the ratio of power generated by a hybrid cycle compared to pure fossil-based power plant, to the input solar thermal energy of the hybrid system (Sheu et al. 2012).

### **2.6.1 Hybrid solar steam power plants**

In a Rankine cycle, the maximum temperature is 600°C, which is suitable for a molten salt TES system (Buck et al. 2006; Dersch et al. 2004). The condensation temperature in the condenser is also controlled by the cooling medium, which depends on the geographical location of the power plant. The new generation of Rankine cycles known as regeneration Rankine cycles, have been modified with several intermediate stages to heat the condensed water with outlet steam from the turbine instead of pumping it directly to the boiler. This modified cycle can improve the thermal efficiency by 37% up to 42% (Barigozzi et al. 2012; Dunham & Iverson 2014). Zoschak and Wu first proposed the solar hybridisation of steam power plants (Zoschak & Wu 1975). They applied different methods to use concentrated solar thermal energy as a heat source in a conventional steam power plant. In the proposed cycle, an absorber mounted on the tower was employed to absorb the solar radiation emitted by the flat mirrors in a collector field. The absorbed heat was considered for different purposes, such as heating feed water, superheating steam, evaporating water, combined evaporation, super heating and preheating of the air required for the combustion units. This study showed that the use of solar energy can reduce the costs of the plant, while also decreasing the complexity of the design and operation of the combined evaporation and super heating processes. The economic viability of various hybrid and solar-only configurations for a molten salt power tower was pioneered by Kolb (Kolb 1998). They found that a hybrid power tower was more beneficial than a solar-only plant of the same size. In another study, the hybridisation of a coal-fired power plant with solar energy was assessed by Pai (Pai 1991). In this study, the heat generated from a solar thermal

Rankine cycle was used to reheat the condenser water, which improved the fuel economy by 24.5%. In another study, a coal-fired steam and solar power plant with a secondary air pre-heating system was proposed by Deng (Deng 2014). A solar share and solar-to-electrical efficiency of 5% and 24.1% were estimated for this hybrid power cycle, respectively. Yang et al. (Yang et al. 2011) proposed a hybridised solar coal-fired power cycle at temperatures ranging from 100°C to 260°C. The feed water was preheated in a regenerative Rankine cycle, which led to a 36.5% solar-to-electrical efficiency at 260°C.

Recently, more attention has been paid to supercritical steam power cycles. This is because such power blocks can provide higher operating temperatures and lower exergy loss in comparison with subcritical steam power cycles. These advantages can result in a significant increase in thermal efficiency of the power block by 45% (Forsberg et al. 2007; Tsiklauri et al. 2005). However, to tolerate such high pressure and temperature steam in pipes, Inconel or high-quality nickel is required at temperatures greater than 627°C, which increases the fixed, operating and maintenance costs of the power cycle (Wheeldon 2008). To assess the supercritical power blocks, Yan et al. (Yan et al. 2011) evaluated the potential of CST systems to be hybridised with subcritical, critical and super critical coal-fired power plants. In this cycle, the feed water was re-heated by solar thermal energy and up to 20% fuel savings were achieved (Figure 2.16). They also found that the advantages of hybridisation can vary with different power plants and positions of steam. Moreover, the results of this study showed that hybridisation can be magnified by increasing the size of the power plant.

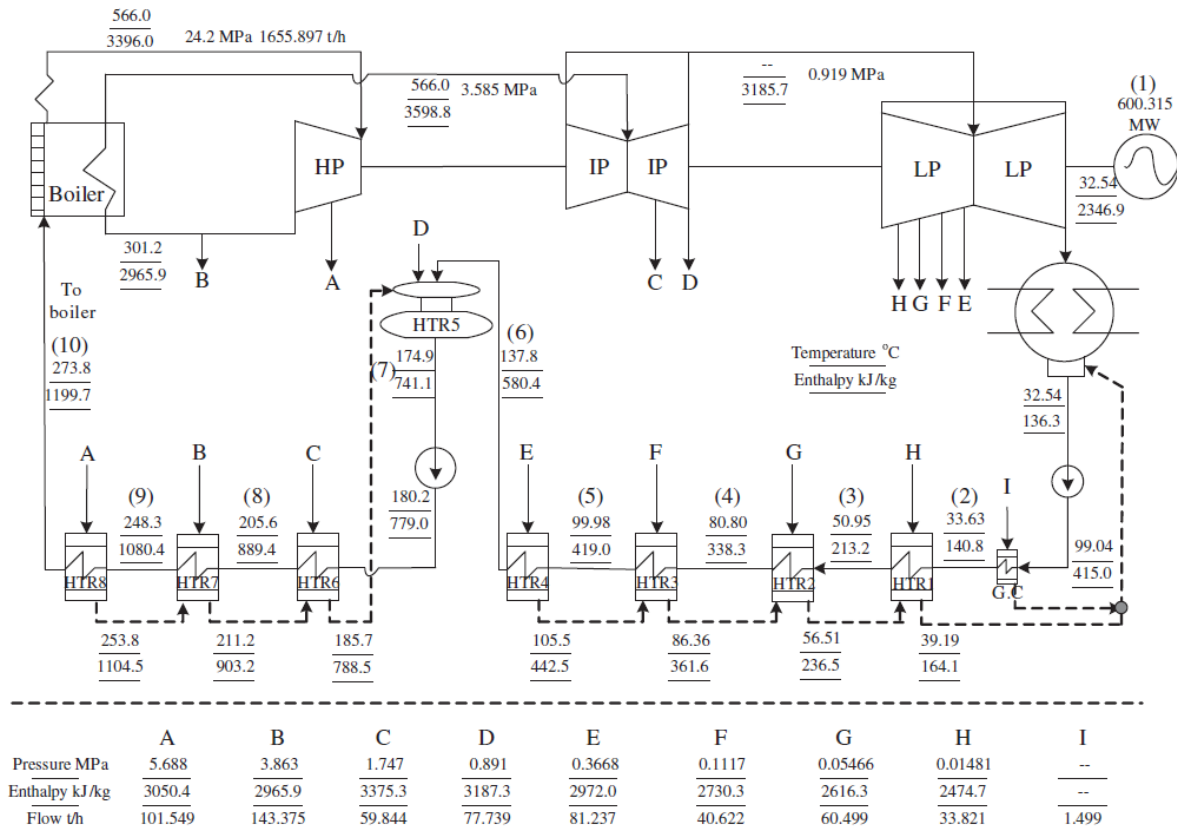


**Figure 2.16.** Schematic diagram of a thermal system with power production of 600MW for a supercritical unit adapted from Yan et al. (Yan et al. 2011)

Although hybridised Rankine cycles are commercially available, the daily solar share of these technologies is limited to maximum 15%. Furthermore, the low thermal efficiency of Rankine cycles along with other factors, such as suitable solar sources and plant characterisation, limit the opportunity to retrofit this technology to existing power plants (Meehan & Rudge 2013; Garcia et al. 2011).

### 2.6.2 Hybrid Brayton cycles

Solar gas turbine cycle system has been considered as an alternative option for improving the solar-to-electrical efficiency (Buck et al. 2017). As shown in Figure 2.17, a solar gas turbine system consists of a solar concentrator (Heliostat field), solar receiver, and gas turbine with a combustor. First, air at ambient condition is transferred to a compressor to be pressurised to 30 bar (Hischier 2011). Then, the temperature of the pressurised air is further increased with solar energy together with combusting fuel in a combustion chamber. Finally, the air at high pressure

and temperature is introduced into a gas turbine to be expanded and deliver power (Hischier 2011).

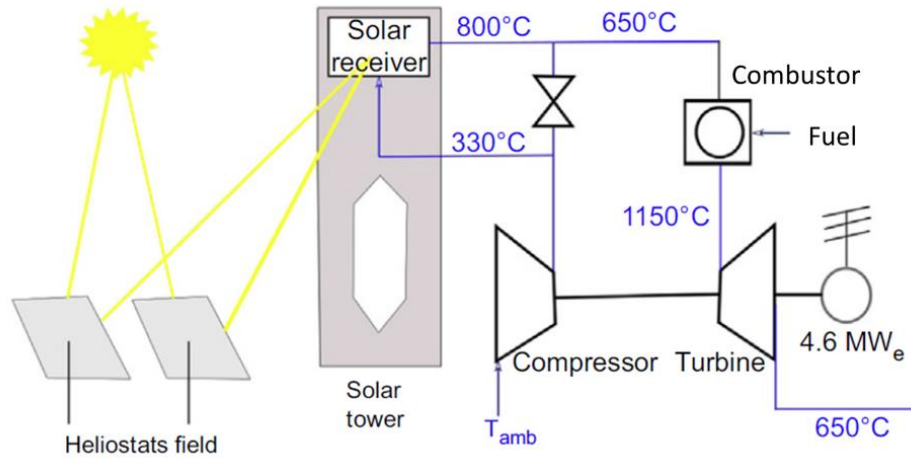


**Figure 2.17.** Schematic configuration of a solar hybrid gas turbine system adapted from Korzynietz et al. (Korzynietz et al. 2016).

The thermal efficiency of a simple Brayton cycle is higher than that of the simple Rankine cycle because a gas turbine operates at a higher temperature (1200°C) than a steam cycle (Bhargava et al. 2007). Moreover, the operating temperature of a gas turbine is predicted to reach 1700°C in the future (Chyu 2012). Thus, hybridisation of Brayton cycle with concentrated solar thermal energy is more efficient than simple Rankine cycles because a higher solar-to-electrical efficiency can be achieved.

Solar thermal energy and fuel combustion can be used to increase the temperature of pressurised air in a Brayton cycle. In a hybrid solar gas turbine cycle, the pressurised air is first preheated with concentrated solar thermal energy in a solar receiver, then the temperature of the pressurised air is further increased by an afterburner (Schwarzbözl et al. 2006). The afterburner compensates for solar energy fluctuations and maintains the power produced with power cycle during off-sun (Barigozzi et al. 2012). Solar share can be increased in a hybrid gas turbine cycle by increasing the output temperature of the pressurised air in a solar receiver (Nathan et

al. 2014). Therefore, a suitable solar receiver, which absorbs the concentrated solar radiation, plays a significant role in a hybrid gas turbine cycle.

Pressurised solar receivers have different configurations based on whether they use direct or indirect heating of working fluid. If the concentrated solar energy is absorbed by a working fluid such as a high-pressure gas, it is considered to be a direct heating configuration. For example, the fluid under pressure can be used in a pressurised volumetric receiver (Figure 2.18-a) (Heller et al. 2006; Spelling et al. 2014). In the front side of this receiver, secondary concentrator with hexagonal entry aperture is proposed to be used for complete convergence of focal spot (Figure 2.18-b). A high temperature (1300°C) can be achieved in this configuration due to direct contact between solar radiation and the working fluid and a high rate of heat transfer (Hischier et al. 2012; Karni et al. 1997; Pritzkow 1991). However, one of the technical challenges of a direct heating configuration is the transparent window of solar receivers, which is vulnerable to high-pressure particularity with an increase in the size of the window. Therefore, special structures need to be manufactured with high mechanical strength, high diurnal variable working receiver temperatures (Avila-Marin 2011; Posnansky & Pylkkänen 1991; Pritzkow 1991).

In an indirect configuration, the concentrated solar thermal is absorbed by one surface and then transferred to another surface by a conductive medium. The heat is generally transferred from the second surface to the working fluid. One of the advantages of indirect solar receivers is that they eliminate the use of windows because they use a heat transfer medium. However, the rate of heat transfer is limited by the solar absorber wall, which is related to its construction material (Jarvinen 1977; Strumpf et al. 1982). This material must have high thermal conductivity, must not react with air, and must be resistant to thermal shocks (Hischier 2011). Results of the study conducted by Hischier (Hischier 2011) showed that for an indirect receiver working at 1060°C

and pressure of five bar, solar heat flux and thermal efficiency can reach  $4360 \text{ W/m}^2$  and 36%, respectively.

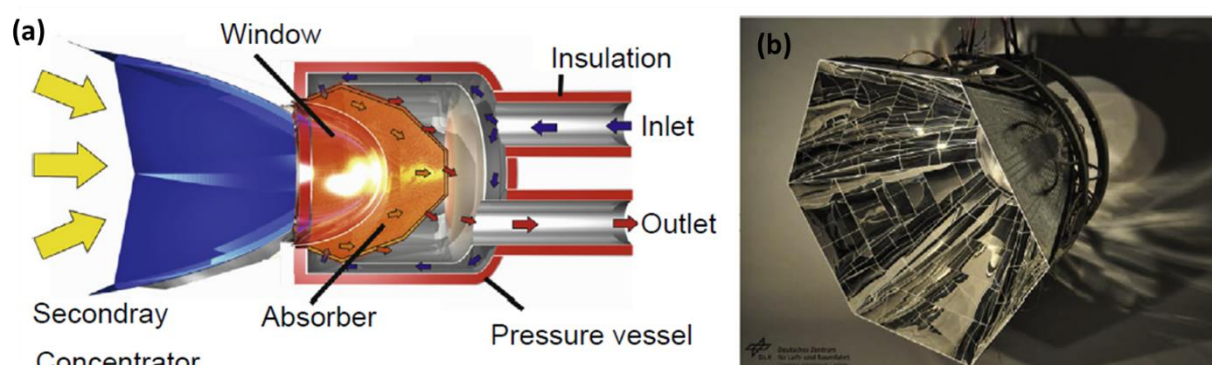


**Figure 2.18.** A schematic configuration of a) a pressurised volumetric receiver and b) a secondary concentrator adapted from Buck et al. (Buck et al. 2017).

### 2.6.3 Hybrid solar combined cycles

Much effort has been conducted to improve the efficiency of Rankine and Brayton cycles. Nevertheless, the efficiency of about 35% was achieved in the state-of-the-art molten salt solar system, which used the steam cycle (Buck et al. 2017). To improve efficiency of the system, a gas turbine combined cycle (GTCC) has been implemented to provide higher thermal efficiency than single cycles (Buck et al. 2017). A hybrid solar combined cycle is schematically shown Figure 2.19. It comprises a Brayton cycles and a Rankine cycle in which the heat released from the high temperature gas turbine is transferred to the Rankine cycles as a heat source.

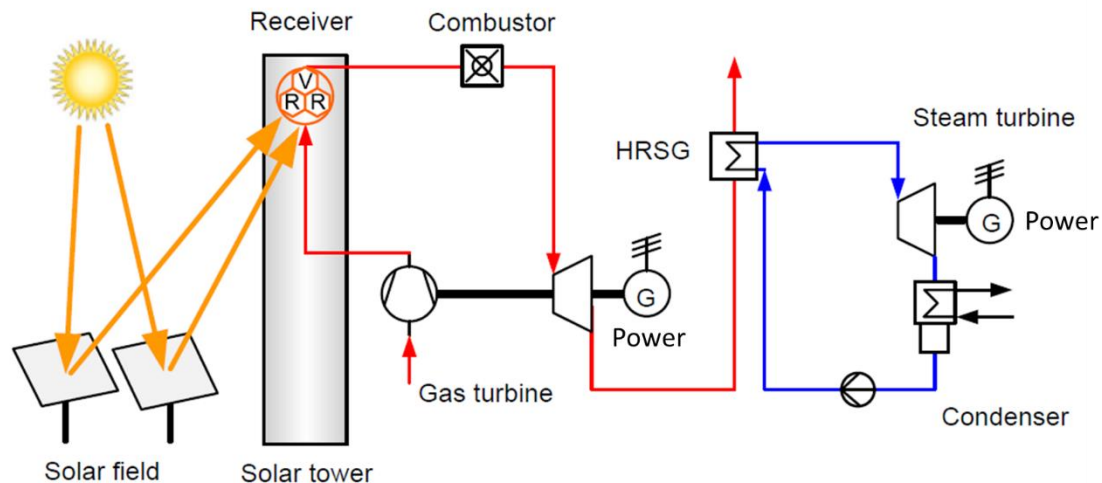


**Figure 2.19.** A schematic diagram of a solar-hybrid combined Brayton and Rankine cycle adapted from Buck et al. (Buck et al. 2017).

Solar thermal energy can also be incorporated with GTCC by preheating the pressurised air before introducing it into a Brayton cycle combustion chamber or by increasing steam generation in a Rankine cycle by power boosting and fuel saving (Rolf et al. 1999). These cycles are identified as hybrid solar GTCC or integrated solar combined cycles (ISCC).

Hybrid solar GTCC was first implemented in various configurations in which solar thermal energy was utilised to preheat the compressed air or to preheat the Rankine cycle (Oda & Hashem 1988). However, the thermal efficiency of this hybrid GTCC was limited to 30%. Another hybrid solar GTCC, with a capacity of 30 MW<sub>e</sub>, was conceptually assessed by the Sacramento Municipal Utility District (SMUD) and the National Renewable Energy Technology (NRET) (Price et al. 1997). In this cycle a nitrate-salt solar tower and a salt/air heat exchanger were used to heat the pressurised air when solar energy was available (Price et al. 1997). The estimated solar share of this cycle was 27%. In another study, the effect of a solar hybrid GTCC's main components such as heliostat field, tower, receivers and power block, on thermal efficiency was assessed (Segal & Epstein 2003). It was found that the efficiency of the hybrid system increased from 35% to 55% when the temperature of the solar receiver increased from 727°C to 1727°C (Buck et al. 2017). Kakras et al. (Kakaras et al. 2004)

proposed a hybrid combined cycle with wet gas turbine technology. In this cycle, solar thermal energy is used to evaporate the water injected into the compressed air before it goes through the combustion chamber. Although the efficiency of the cycle increased, the hybrid cycle has not been implemented because it increased the cost of the system. A solar hybrid GTCC with Direct Steam Generator (DSG) was proposed by Li and Yang (Li & Yang 2014). This cycle provides a thermal efficiency of 53% and a solar share of 27.8%. They found that using solar thermal heat to evaporate feedwater was superior to using it for sensible heating purposes. Another study assessed the annual operation of a solar hybrid GTCC cycle and identified the effects of different pressures on preheating of the generated steam in Rankine cycle (Montes et al. 2011). This simulation was conducted at two different locations: Las Vegas and Almería. Although both locations were suitable for a solar thermal power plant, the benefits of coupling the solar field–combined cycle was more evident in Las Vegas because of its hot and dry environment.

Recently, a new hybrid solar power block has been developed by Jafarian et al. (Jafarian et al. 2014). They theoretically assessed the performance of a chemical looping combustion system linked with a gas turbine power cycle. Methane was selected as fuel in this system. They used the outlet stream from the air reactor to be linked with a gas turbine and for the next stage, they considered an afterburner to increase the temperature of the gas. The estimations were conducted using Aspen software and they used a diurnal profile of normal irradiance for Port Augusta, South Australia. Their results showed that efficiency was as high as ~50% where an afterburner was used and ~ 44% without an afterburner. Noticeably, the solar share decreased from 60% to 41.4% without an afterburner.

Facing the aforementioned literature, the thermodynamic efficiency of an LCL-TES system in a power plant cannot be derived readily from previous studies due to the significant differences



in their operating conditions. Therefore, further investigation is required to assess the operation of the LCL-TES system proposed for a solar power plant.

## 2.7 References

P. Achard 1981, 'Heat Storage at 450°C in Aluminum-magnesium alloys', *Rational Utiliz. Energy*, vol. **3**, pp. 39-46.

J. Adanez, A. Abad, F. Garcia-Labiano, P. Gayan & F. Luis 2012, 'Progress in chemical-looping combustion and reforming technologies', *Progress in energy and combustion science*, vol. **38**, 2, pp. 215-282.

C. Agrafiotis, A. Becker, M. Roeb & C. Sattler 2015, 'Hybrid sensible/thermochemical storage of solar energy in cascades of redox-oxide-pair-based porous ceramics', in *ASME 2015 9th International Conference on Energy Sustainability*, American Society of Mechanical Engineers.

C. Agrafiotis, M. Roeb & C. Sattler 2016, 'Exploitation of thermochemical cycles based on solid oxide redox systems for thermochemical storage of solar heat. Part 4: Screening of oxides for use in cascaded thermochemical storage concepts', *Solar energy*, vol. **139**, pp. 695-710.

C. Agrafiotis, M. Roeb, M. Schmücker & C. Sattler 2014, 'Exploitation of thermochemical cycles based on solid oxide redox systems for thermochemical storage of solar heat. Part 1: Testing of cobalt oxide-based powders', *Solar energy*, vol. **102**, pp. 189-211.

C. Agrafiotis, M. Roeb, M. Schmücker & C. Sattler 2015, 'Exploitation of thermochemical cycles based on solid oxide redox systems for thermochemical storage of solar heat. Part 2: Redox oxide-coated porous ceramic structures as integrated thermochemical reactors/heat exchangers', *Solar energy*, vol. **114**, Supplement C, pp. 440-458.

C. Agrafiotis, S. Tescari, M. Roeb, M. Schmücker & C. Sattler 2015, 'Exploitation of thermochemical cycles based on solid oxide redox systems for thermochemical storage of solar heat. Part 3: Cobalt oxide monolithic porous structures as integrated thermochemical reactors/heat exchangers', *Solar energy*, vol. **114**, Supplement C, pp. 459-475.

I. Al-Shankiti, B. D. Ehrhart & A. W. Weimer 2017, 'Isothermal redox for H<sub>2</sub>O and CO<sub>2</sub> splitting: A review and perspective', *Solar energy*, vol. **156**, Supplement C, pp. 21-29.

A. Alarcón Villamil, J. E. Hortúa & A. López 2013, 'Comparison of thermal solar collector technologies and their applications', *Tecciencia*, vol. **8**, 15, pp. 27-35.

K. J. Albrecht, G. S. Jackson & R. J. Braun 2016, 'Thermodynamically consistent modeling of redox-stable perovskite oxides for thermochemical energy conversion and storage', *Applied Energy*, vol. **165**, pp. 285-296.

---

E. Alonso, A. Gallo, C. Pérez-Rábago & E. Fuentealba 2016, 'Thermodynamic study of CuO/Cu<sub>2</sub>O and Co<sub>3</sub>O<sub>4</sub>/CoO redox pairs for solar energy thermochemical storage', in *AIP Conference Proceedings*, AIP Publishing, vol. 1734, p. 050004.

E. Alonso, C. Pérez-Rábago, J. Licurgo, E. Fuentealba & C. A. Estrada 2015, 'First experimental studies of solar redox reactions of copper oxides for thermochemical energy storage', *Solar energy*, vol. **115**. Supplement C, pp. 297-305.

E. Alonso, C. Pérez-Rábago, J. Licurgo, E. Fuentealba & C. A. Estrada 2015, 'First experimental studies of solar redox reactions of copper oxides for thermochemical energy storage', *Solar energy*, vol. **115**. pp. 297-305.

V. Amar, J. Puszynski & R. Shende 2015, 'H<sub>2</sub> generation from thermochemical water-splitting using yttria stabilized NiFe<sub>2</sub>O<sub>4</sub> core-shell nanoparticles', *Journal of Renewable and Sustainable Energy*, vol. **7**. 2, p. 023113.

L. André, S. Abanades & G. Flamant 2016, 'Screening of thermochemical systems based on solid-gas reversible reactions for high temperature solar thermal energy storage', *Renewable and Sustainable Energy Reviews*, vol. **64**. pp. 703-715.

A. L. Avila-Marin 2011, 'Volumetric receivers in solar thermal power plants with central receiver system technology: a review', *Solar energy*, vol. **85**. 5, pp. 891-910.

M. Azpiazu, J. Morquillas & A. Vazquez 2003, 'Heat recovery from a thermal energy storage based on the Ca (OH)<sub>2</sub>/CaO cycle', *Applied thermal engineering*, vol. **23**. 6, pp. 733-741.

B. Wong 2011, *Thermochemical heat storage for concentrated solar power, final report for the U.S. Department of Energy*, Department of Energy, San Diego, CA, USA.

S. M. Babiniec, E. N. Coker, A. Ambrosini & J. E. Miller 2016, 'ABO<sub>3</sub> (A = La, Ba, Sr, K; B = Co, Mn, Fe) perovskites for thermochemical energy storage', *AIP Conference Proceedings*, vol. **1734**. 1, p. 050006.

S. M. Babiniec, E. N. Coker, J. E. Miller & A. Ambrosini 2015, 'Investigation of LaxSr<sub>1-x</sub>CoyM<sub>1-y</sub>O<sub>3-δ</sub> (M=Mn, Fe) perovskite materials as thermochemical energy storage media', *Solar energy*, vol. **118**. Supplement C, pp. 451-459.

S. M. Babiniec, E. N. Coker, J. E. Miller & A. Ambrosini 2016, 'Doped calcium manganites for advanced high-temperature thermochemical energy storage', *International Journal of Energy Research*, vol. **40**. 2, pp. 280-284.

E. Bagherisereshki, J. Tran, F. Lei & N. AuYeung 2018, 'Investigation into SrO/SrCO<sub>3</sub> for high temperature thermochemical energy storage', *Solar energy*, vol. **160**. pp. 85-93.

G. Barigozzi, G. Bonetti, G. Franchini, A. Perdichizzi & S. Ravelli 2012, 'Thermal performance prediction of a solar hybrid gas turbine', *Solar energy*, vol. **86**. 7, pp. 2116-2127.

D. Barlev, R. Vidu & P. Stroeve 2011, 'Innovation in concentrated solar power', *Solar Energy Materials and Solar Cells*, vol. **95**. 10, pp. 2703-2725.

A. Bayon, R. Bader, M. Jafarian, L. Fedunik-Hofman, Y. Sun, J. Hinkley, S. Miller & W. Lipiński 2018, 'Techno-economic assessment of solid-gas thermochemical energy storage systems for solar thermal power applications', *Energy*, vol. **149**. pp. 473-484.

M. Beaudin, H. Zareipour, A. Schellenberglobe & W. Rosehart 2010, 'Energy storage for mitigating the variability of renewable electricity sources: An updated review', *Energy for Sustainable Development*, vol. **14**. 4, pp. 302-314.

R. Bhargava, M. Bianchi, A. De Pascale, G. N. Di Montenegro & A. Peretto 2007, 'Gas turbine based power cycles-a state-of-the-art review', in *Challenges of power engineering and environment*, Springer, pp. 309-319.

C. Birchenall & M. Telkes 1976, 'Thermal storage in metals', in *Sharing the Sun: Solar Technology in the Seventies, Volume 8*, vol. 8, pp. 138-154.

M. J. Blanco & S. Miller 2017, '1 - Introduction to concentrating solar thermal (CST) technologies', in *Advances in Concentrating Solar Thermal Research and Technology*, Woodhead Publishing, pp. 3-25.

T. Block, N. Knoblauch & M. Schmücker 2014, 'The cobalt-oxide/iron-oxide binary system for use as high temperature thermochemical energy storage material', *Thermochimica Acta*, vol. **577**. pp. 25-32.

T. Block & M. Schmücker 2016, 'Metal oxides for thermochemical energy storage: A comparison of several metal oxide systems', *Solar energy*, vol. **126**. pp. 195-207.

R. G. Bowrey & J. Jutsen 1978, 'Energy storage using the reversible oxidation of barium oxide', *Solar energy*, vol. **21**. 6, pp. 523-525.

R. Buck, C. Barth, M. Eck & W. D. Steinmann 2006, 'Dual-receiver concept for solar towers', *Solar energy*, vol. **80**. 10, pp. 1249-1254.

R. Buck, T. Brauning, T. Denk, M. Pfänder, P. Schwarzbözl & F. Tellez 2002, 'Solar-hybrid gas turbine-based power tower systems (REFOS)', *Journal of Solar Energy Engineering*, vol. **124**. 1, pp. 2-9.

R. Buck, S. Giuliano & R. Uhlig 2017, '16 - Central tower systems using the Brayton cycle', in MJ Blanco & LR Santigosa (eds), *Advances in Concentrating Solar Thermal Research and Technology*, Woodhead Publishing, pp. 353-382.

---

R. Buck, S. Giuliano & R. Uhlig 2017, '16 - Central tower systems using the Brayton cycle - Blanco, Manuel J', in LR Santigosa (ed.), *Advances in Concentrating Solar Thermal Research and Technology*, Woodhead Publishing, pp. 353-382.

L. F. Cabeza 2014, *Advances in thermal energy storage systems: Methods and applications*, Elsevier.

A. J. Carrillo, J. Moya, A. Bayón, P. Jana, V. A. de la Peña O'Shea, M. Romero, J. Gonzalez-Aguilar, D. P. Serrano, P. Pizarro & J. M. Coronado 2014, 'Thermochemical energy storage at high temperature via redox cycles of Mn and Co oxides: Pure oxides versus mixed ones', *Solar Energy Materials and Solar Cells*, vol. **123**. pp. 47-57.

A. J. Carrillo, D. Sastre, D. P. Serrano, P. Pizarro & J. M. Coronado 2016, 'Revisiting the BaO<sub>2</sub>/BaO redox cycle for solar thermochemical energy storage', *Physical Chemistry Chemical Physics*, vol. **18**. 11, pp. 8039-8048.

A. J. Carrillo, D. P. Serrano, P. Pizarro & J. M. Coronado 2014, 'Thermochemical heat storage based on the Mn<sub>2</sub>O<sub>3</sub>/Mn<sub>3</sub>O<sub>4</sub> redox couple: influence of the initial particle size on the morphological evolution and cyclability', *Journal of Materials Chemistry A*, vol. **2**. 45, pp. 19435-19443.

A. J. Carrillo, D. P. Serrano, P. Pizarro & J. M. Coronado 2015, 'Thermochemical Heat Storage at High Temperatures using Mn<sub>2</sub>O<sub>3</sub>/Mn<sub>3</sub>O<sub>4</sub> System: Narrowing the Redox Hysteresis by Metal Co-doping', *Energy Procedia*, vol. **73**, pp. 263-271.

A. J. Carrillo, D. P. Serrano, P. Pizarro & J. M. Coronado 2015, 'Thermochemical Heat Storage at High

A. J. Carrillo, D. P. Serrano, P. Pizarro & J. M. Coronado 2016, 'Manganese oxide-based thermochemical energy storage: Modulating temperatures of redox cycles by Fe–Cu co-doping', *Journal of Energy Storage*, vol. **5**. pp. 169-176.

D. Chadda, J. D. Ford & M. Fahim 1989, 'Chemical energy storage by the reaction cycle CuO/Cu<sub>2</sub>O', *International Journal of Energy Research*, vol. **13**. 1, pp. 63-73.

E. L. Charsley, C. M. Earnest, P. K. Gallagher & M. J. Richardson 1993, 'Preliminary round-robin studies on the ICTAC certified reference materials for DTA', *Journal of thermal analysis*, vol. **40**. 3, pp. 1415-1422.

C. Chen, K. M. Lovegrove, A. Sepulveda & A. S. Lavine 2018, 'Design and optimization of an ammonia synthesis system for ammonia-based solar thermochemical energy storage', *Solar energy*, vol. **159**. pp. 992-1002.

M. K. Chyu 2012, 'Recent advances in turbine heat transfer with a view of transition to coal-gas based systems', *Journal of Heat Transfer*, vol. **134**. 3, p. 031006.

K. Darkwa 1998, 'Thermochemical energy storage in inorganic oxides: An experimental evaluation', *Applied thermal engineering*, vol. **18**. 6, pp. 387-400.

S. Deng 2014, 'Hybrid solar and coal-fired steam power plant based on air preheating', *Journal of Solar Energy Engineering*, vol. **136**. 2, p. 021012.

J. Dersch, M. Geyer, U. Herrmann, S. A. Jones, B. Kelly, R. Kistner, W. Ortmanns, R. Pitz-Paal & H. Price 2004, 'Trough integration into power plants: a study on the performance and economy of integrated solar combined cycle systems', *Energy*, vol. **29**. 5, pp. 947-959.

M. Deutsch, F. Horvath, C. Knoll, D. Lager, C. Gierl-Mayer, P. Weinberger & F. Winter 2017, 'High-Temperature Energy Storage: Kinetic Investigations of the CuO/Cu<sub>2</sub>O Reaction Cycle', *Energy & Fuels*, vol. **31**. 3, pp. 2324-2334.

B. Dou, Y. Song, Y. Liu & C. Feng 2010, 'High temperature CO<sub>2</sub> capture using calcium oxide sorbent in a fixed-bed reactor', *Journal of Hazardous Materials*, vol. **183**. 1, pp. 759-765.

Y. Duan, D. Luebke & H. Pennline 2012, 'Efficient theoretical screening of solid sorbents for CO<sub>2</sub> capture applications', *International Journal of Clean Coal and Energy*, vol. **1**. NETL-PUB-318.

J. A. Duffie & W. A. Beckman 2013, *Solar engineering of thermal processes*, John Wiley & Sons.

M. T. Dunham & B. D. Iverson 2014, 'High-efficiency thermodynamic power cycles for concentrated solar power systems', *Renewable and Sustainable Energy Reviews*, vol. **30**. pp. 758-770.

R. Dunn, K. Lovegrove & G. Burgess 2012, 'A review of ammonia-based thermochemical energy storage for concentrating solar power', *Proceedings of the IEEE*, vol. **100**. 2, pp. 391-400.

M. Fahim & J. Ford 1983, 'Energy storage using the BaO<sub>2</sub>/BaO reaction cycle', *The Chemical Engineering Journal*, vol. **27**. 1, pp. 21-28.

D. Farkas & C. E. Birchenall 1985, 'New eutectic alloys and their heats of transformation', *Metallurgical Transactions A*, vol. **16**. 3, pp. 323-328.

B. Feng, H. An & E. Tan 2007, 'Screening of CO<sub>2</sub> adsorbing materials for zero emission power generation systems', *Energy & Fuels*, vol. **21**. 2, pp. 426-434.

C. W. Forsberg, P. F. Peterson & H. Zhao 2007, 'High-temperature liquid-fluoride-salt closed-Brayton-cycle solar power towers', *Journal of Solar Energy Engineering*, vol. **129**. 2, pp. 141-146.

I. Fujii, K. Tsuchiya, M. Higano & J. Yamada 1985, 'Studies of an energy storage system by use of the reversible chemical reaction:  $\text{CaO} + \text{H}_2\text{O} \rightleftharpoons \text{Ca}(\text{OH})_2$ ', *Solar energy*, vol. **34**. 4-5, pp. 367-377.

A. Gil, M. Medrano, I. Martorell, A. Lázaro, P. Dolado, B. Zalba & L. F. Cabeza 2010, 'State of the art on high temperature thermal energy storage for power generation. Part 1: Concepts, materials and modellization', *Renewable and Sustainable Energy Reviews*, vol. **14**. 1, pp. 31-55.

G. S. Grasa & J. C. Abanades 2006, 'CO<sub>2</sub> capture capacity of CaO in long series of carbonation/calcination cycles', *Industrial & Engineering Chemistry Research*, vol. **45**. 26, pp. 8846-8851.

A. H Abedin & M. A Rosen 2011, 'A critical review of thermochemical energy storage systems', *The Open Renewable Energy Journal*, vol. **4**. 1.

L. Han, Q. Wang, Q. Ma, J. Guan, Z. Luo & K. Cen 2009, 'Hydration reactivation of CaO-based sorbent for cyclic calcination-carbonation reactions', in *Proceedings of the 20th international conference on fluidized bed combustion*, Springer, pp. 726-731.

M. Hänchen, A. Stiel, Z. Jovanovic & A. Steinfeld 2012, 'Thermally driven copper oxide redox cycle for the separation of oxygen from gases', *Industrial & Engineering Chemistry Research*, vol. **51**. 20, pp. 7013-7021.

P. Haseli, M. Jafarian & G. J. Nathan 2017, 'High temperature solar thermochemical process for production of stored energy and oxygen based on CuO/Cu<sub>2</sub>O redox reactions', *Solar energy*, vol. **153**. pp. 1-10.

S. Hasnain 1998, 'Review on sustainable thermal energy storage technologies, Part I: heat storage materials and techniques', *Energy Conversion and Management*, vol. **39**. 11, pp. 1127-1138.

P. Heller, M. Pfänder, T. Denk, F. Tellez, A. Valverde, J. Fernandez & A. Ring 2006, 'Test and evaluation of a solar powered gas turbine system', *Solar energy*, vol. **80**. 10, pp. 1225-1230.

I. Hischier 2011, 'Development of a pressurized receiver for solar-driven gas turbines', Diss., Eidgenössische Technische Hochschule ETH Zürich, Nr. 19723, 2011.

I. Hischier, P. Leumann & A. Steinfeld 2012, 'Experimental and numerical analyses of a pressurized air receiver for solar-driven gas turbines', *Journal of Solar Energy Engineering*, vol. **134**. 2, p. 021003.

A. Hoshi, D. R. Mills, A. Bittar & T. S. Saitoh 2005, 'Screening of high melting point phase change materials (PCM) in solar thermal concentrating technology based on CLFR', *Solar energy*, vol. **79**. 3, pp. 332-339.

---

Z. G. Huang, E. N. Xiao, G. Z. Wu & S. H. Mei 1991, 'Calorimetric research on metallic phase change heat storage material', *J. Eng. Thermophys.*, vol. **12**. 1, pp. 46-49.

Z. Q. Huang, S. T. Zhang & S. F. Xie 1999, 'Spectroellipsometric studies on electrochemistry and its application', *Dianhaoxue*, vol. **5**. 3, pp. 1-5.

K. N. Hutchings, M. Wilson, P. A. Larsen & R. A. Cutler 2006, 'Kinetic and thermodynamic considerations for oxygen absorption/desorption using cobalt oxide', *Solid State Ionics*, vol. **177**. 1, pp. 45-51.

J. Ibanez, W. Wentworth, C. Batten & E. Chen 1984, 'Kinetics of the thermal decomposition of zinc sulfate', *Revue internationale des hautes températures et des réfractaires*, vol. **21**. 2, pp. 113-124.

L. Imponenti, K. J. Albrecht, R. J. Braun & G. S. Jackson 2016, 'Measuring thermochemical energy storage capacity with redox cycles of doped-CaMnO<sub>3</sub>', *ECS Transactions*, vol. **72**. 7, pp. 11-22.

L. Imponenti, K. J. Albrecht, J. W. Wands, M. D. Sanders & G. S. Jackson 2017, 'Thermochemical energy storage in strontium-doped calcium manganites for concentrating solar power applications', *Solar energy*, vol. **151**. pp. 1-13.

L. Irwin, J. Stekli, C. Pfefferkorn & R. Pitchumani 2017, '11 - Thermochemical energy storage for concentrating solar thermal (CST) systems A2 - Blanco, Manuel J', in LR Santigosa (ed.), *Advances in Concentrating Solar Thermal Research and Technology*, Woodhead Publishing, pp. 247-267.

M. Jafarian, M. Arjomandi & G. J. Nathan 2014, 'The energetic performance of a novel hybrid solar thermal & chemical looping combustion plant', *Applied Energy*, vol. **132**. pp. 74-85.

M. Jafarian, M. Arjomandi & G. J. Nathan 2017, 'Thermodynamic potential of molten copper oxide for high temperature solar energy storage and oxygen production', *Applied Energy*, vol. **201**. pp. 69-83.

P. O. Jarvinen 1977, 'Solar-heated-air receivers', *Solar energy*, vol. **19**. 2, pp. 139-147.

E. Kakaras, A. Doukelis, R. Leithner & N. Aronis 2004, 'Combined cycle power plant with integrated low temperature heat (LOTHECO)', *Applied thermal engineering*, vol. **24**. 11, pp. 1677-1686.

A. A. Kaniyal, G. J. Nathan & J. J. Pincus 2012, 'The potential role of data-centres in enabling investment in geothermal energy', *Applied Energy*, vol. **98**. pp. 458-466.

G. Karagiannakis, C. Pagkoura, E. Halevas, P. Baltzopoulou & A. G. Konstandopoulos 2016, 'Cobalt/cobaltous oxide based honeycombs for thermochemical heat storage in future concentrated solar power installations: Multi-cyclic assessment and semi-quantitative heat effects estimations', *Solar energy*, vol. **133**. Supplement C, pp. 394-407.

---

G. Karagiannakis, C. Pagkoura, A. Zygogianni, S. Lorentzou & A. G. Konstandopoulos 2014, 'Monolithic Ceramic Redox Materials for Thermochemical Heat Storage Applications in CSP Plants', *Energy Procedia*, vol. **49**. Supplement C, pp. 820-829.

J. Karni, A. Kribus, P. Doron, R. Rubin, A. Fiterman & D. Sagie 1997, 'The DIAPR: a high-pressure, high-temperature solar receiver', *Journal of Solar Energy Engineering*, vol. **119**. 1, pp. 74-78.

D. Kearney, U. Herrmann, P. Nava, B. Kelly, R. Mahoney, J. Pacheco, R. Cable, N. Potrovitza, D. Blake & H. Price 2003, 'Assessment of a molten salt heat transfer fluid in a parabolic trough solar field', *Journal of Solar Energy Engineering*, vol. **125**. 2, pp. 170-176.

M. M. Kenisarin 2010, 'High-temperature phase change materials for thermal energy storage', *Renewable and Sustainable Energy Reviews*, vol. **14**. 3, pp. 955-970.

T. Kodama & N. Gokon 2007, 'Thermochemical Cycles for High-Temperature Solar Hydrogen Production', *Chemical Reviews*, vol. **107**. 10, pp. 4048-4077.

G. J. Kolb 1998, 'Economic evaluation of solar-only and hybrid power towers using molten-salt technology', *Solar energy*, vol. **62**. 1, pp. 51-61.

G. Kolta & M. Askar 1975, 'Thermal decomposition of some metal sulphates', *Thermochimica Acta*, vol. **11**. 1, pp. 65-72.

R. Korzynietz, J. A. Brioso, A. del Río, M. Quero, M. Gallas, R. Uhlig, M. Ebert, R. Buck & D. Teraji 2016, 'Solugas – Comprehensive analysis of the solar hybrid Brayton plant', *Solar energy*, vol. **135**. pp. 578-589.

J. P. KotzÃš, T. W. von BackstrÃ¼m & P. J. Erens 2013, 'High temperature thermal energy storage utilizing metallic phase change materials and metallic heat transfer fluids', *Journal of Solar Energy Engineering*, vol. **135**. 3, p. 035001.

T. Kousksou, P. Bruel, A. Jamil, T. El Rhafiki & Y. Zeraouli 2014, 'Energy storage: Applications and challenges', *Solar Energy Materials and Solar Cells*, vol. **120**. pp. 59-80.

O. Kubaschewski, A. Evans & C. B. Alcock 1967, 'Metallurgical thermochemistry'.

S. Kuravi, J. Trahan, D. Y. Goswami, M. M. Rahman & E. K. Stefanakos 2013, 'Thermal energy storage technologies and systems for concentrating solar power plants', *Progress in energy and combustion science*, vol. **39**. 4, pp. 285-319.

K. Kyaw, H. Matsuda & M. Hasatani 1996, 'Applicability of Carbonation/Decarbonation Reactions to High-Temperature Thermal Energy Storage and Temperature Upgrading', *Journal of Chemical Engineering of Japan*, vol. **29**. 1, pp. 119-125.



G. L. Kyriakopoulos & G. Arabatzis 2016, 'Electrical energy storage systems in electricity generation: Energy policies, innovative technologies, and regulatory regimes', *Renewable and Sustainable Energy Reviews*, vol. **56**. pp. 1044-1067.

B. V. L'vov & V. L. Ugolkov 2004, 'Kinetics of free-surface decomposition of magnesium and barium sulfates analyzed thermogravimetrically by the third-law method', *Thermochimica Acta*, vol. **411**. 1, pp. 73-79.

B. V. L'vov & V. L. Ugolkov 2004, 'Kinetics of free-surface decomposition of magnesium, strontium and barium carbonates analyzed thermogravimetrically by the third-law method', *Thermochimica Acta*, vol. **409**. 1, pp. 13-18.

B. V. L'vov & V. L. Ugolkov 2004, 'Peculiarities of  $\text{CaCO}_3$ ,  $\text{SrCO}_3$  and  $\text{BaCO}_3$  decomposition in  $\text{CO}_2$  as a proof of their primary dissociative evaporation', *Thermochimica Acta*, vol. **410**. 1-2, pp. 47-55.

N. R. E. Laboratory 2003, *Assessment of parabolic trough and power tower solar technology cost and performance forecasts*, DIANE Publishing.

D. Laing, C. Bahl, T. Bauer, D. Lehmann & W.-D. Steinmann 2011, 'Thermal energy storage for direct steam generation', *Solar energy*, vol. **85**. 4, pp. 627-633.

D. Laing, M. Eickhoff, M. Fiß, M. Hempel, M. Meyer-Grünefeldt & C. Bahl 2011, 'Test results of a combined storage system for parabolic trough power plants with direct steam generation', in *ASME 5th International Conference on Energy Sustainability, Washington DC, USA*.

D. Laing, W.-D. Steinmann, R. Tamme & C. Richter 2006, 'Solid media thermal storage for parabolic trough power plants', *Solar energy*, vol. **80**. 10, pp. 1283-1289.

A. S. Lavine, K. M. Lovegrove, J. Jordan, G. B. Anleu, C. Chen, H. Aryafar & A. Sepulveda 2016, 'Thermochemical energy storage with ammonia: Aiming for the sunshot cost target', in *AIP Conference Proceedings*, AIP Publishing, vol. 1734, p. 050028.

F. Li, Y. J. Hu & R. Y. Zhang 2011, 'The influence of heating-cooling cycles on the thermal storage performances of Al-17 wt.% Si alloy', in *Advanced Materials Research*, Trans Tech Publ, vol. 239, pp. 2248-2251.

Y. Li & Y. Yang 2014, 'Thermodynamic analysis of a novel integrated solar combined cycle', *Applied Energy*, vol. **122**. pp. 133-142.

D. Liu, L. Xin-Feng, L. Bo, Z. Si-quan & X. Yan 2018, 'Progress in thermochemical energy storage for concentrated solar power: A review', *International Journal of Energy Research*, vol. **42**. 15, pp. 4546-4561.

M. Liu, J. Gomez, C. Turchi, N. Tay, W. Saman & F. Bruno 2015, 'Determination of thermo-physical properties and stability testing of high-temperature phase-change materials for CSP applications', *Solar Energy Materials and Solar Cells*, vol. **139**. pp. 81-87.

M. Liu, N. S. Tay, S. Bell, M. Belusko, R. Jacob, G. Will, W. Saman & F. Bruno 2016, 'Review on concentrating solar power plants and new developments in high temperature thermal energy storage technologies', *Renewable and Sustainable Energy Reviews*, vol. **53**. pp. 1411-1432.

W. Liu, H. An, C. Qin, J. Yin, G. Wang, B. Feng & M. Xu 2012, 'Performance enhancement of calcium oxide sorbents for cyclic CO<sub>2</sub> capture: A review', *Energy & Fuels*, vol. **26**. 5, pp. 2751-2767.

M. C. Lott, S.-I. Kim, C. Tam, D. Houssin & J. Gagné 2014, 'Technology roadmap: energy storage', *Paris. doi*, vol. **10**.

A. Luzzi & K. Lovegrove 1997, 'A solar thermochemical power plant using ammonia as an attractive option for greenhouse-gas abatement', *Energy*, vol. **22**. 2-3, pp. 317-325.

B. S. M., C. E. N., M. J. E. & A. Andrea 2016, 'Doped calcium manganites for advanced high-temperature thermochemical energy storage', *International Journal of Energy Research*, vol. **40**. 2, pp. 280-284.

S. Maitra, N. Chakrabarty & J. Pramanik 2008, 'Decomposition kinetics of alkaline earth carbonates by integral approximation method', *Cerâmica*, vol. **54**. 331, pp. 268-272.

R. Meehan & M. Rudge 2013, 'Hybridisation of Fossil Fuel Energy Generation in Australia', *Public Report, November*, vol. **20**.

J. E. Miller, A. Ambrosini, S. M. Babiniec, E. N. Coker, C. K. Ho, H. Al-Ansary, S. M. Jeter, P. G. Loutzenhiser, N. G. Johnson & E. B. Stechel 2016, 'High performance reduction/oxidation metal oxides for thermochemical energy storage (PROMOTES)', in *ASME 2016 10th International Conference on Energy Sustainability collocated*.

D. Mills 2004, 'Advances in solar thermal electricity technology', *Solar energy*, vol. **76**. 1, pp. 19-31.

B. Moghtaderi 2009, 'Application of chemical looping concept for air separation at high temperatures', *Energy & Fuels*, vol. **24**. 1, pp. 190-198.

S. A. Mohamed, F. A. Al-Sulaiman, N. I. Ibrahim, M. H. Zahir, A. Al-Ahmed, R. Saidur, B. Yılbaş & A. Sahin 2017, 'A review on current status and challenges of inorganic phase change materials for thermal energy storage systems', *Renewable and Sustainable Energy Reviews*, vol. **70**. pp. 1072-1089.

---

M. Montes, A. Rovira, M. Muñoz & J. Martínez-Val 2011, 'Performance analysis of an integrated solar combined cycle using direct steam generation in parabolic trough collectors', *Applied Energy*, vol. **88**. 9, pp. 3228-3238.

D. Morgan, S. S. J. Warne, S. Warrington & P. Nancarrow 1986, 'Thermal decomposition reactions of caledonite and their products', *Mineralogical Magazine*, vol. **50**. 357, pp. 521-526.

C. L. Muhich, B. D. Ehrhart, I. Al-Shankiti, B. J. Ward, C. B. Musgrave & A. W. Weimer 2016, 'A review and perspective of efficient hydrogen generation via solar thermal water splitting', *Wiley Interdisciplinary Reviews: Energy and Environment*, vol. **5**. 3, pp. 261-287.

D. Müller, C. Knoll, W. Artner, M. Harasek, C. Gierl-Mayer, J. M. Welch, A. Werner & P. Weinberger 2017, 'Combining in-situ X-ray diffraction with thermogravimetry and differential scanning calorimetry : An investigation of  $\text{Co}_3\text{O}_4$ ,  $\text{MnO}_2$  and  $\text{PbO}_2$  for thermochemical energy storage', *Solar energy*, vol. **153**. pp. 11-24.

A. P. Muroyama, A. J. Schrader & P. G. Loutzenhiser 2015, 'Solar electricity via an Air Brayton cycle with an integrated two-step thermochemical cycle for heat storage based on  $\text{Co}_3\text{O}_4/\text{CoO}$  redox reactions II: Kinetic analyses', *Solar energy*, vol. **122**. pp. 409-418.

G. Nathan, D. Battye & P. Ashman 2014, 'Economic evaluation of a novel fuel-saver hybrid combining a solar receiver with a combustor for a solar power tower', *Applied Energy*, vol. **113**. pp. 1235-1243.

G. J. Nathan, M. Jafarian, B. B. Dally, W. L. Saw, P. J. Ashman, E. Hu & A. Steinfeld 2018, 'Solar thermal hybrids for combustion power plant: A growing opportunity', *Progress in energy and combustion science*, vol. **64**. pp. 4-28.

M. Neises, S. Tescari, L. de Oliveira, M. Roeb, C. Sattler & B. Wong 2012, 'Solar-heated rotary kiln for thermochemical energy storage', *Solar energy*, vol. **86**. 10, pp. 3040-3048.

K. Nithyanandam, J. Stekli & R. Pitchumani 2017, '10 - High-temperature latent heat storage for concentrating solar thermal (CST) systems A2 - Blanco, Manuel J', in LR Santigosa (ed.), *Advances in Concentrating Solar Thermal Research and Technology*, Woodhead Publishing, pp. 213-246.

S. D. Oda & H. H. Hashem 1988, 'A case study for three combined cycles of a solar-conventional power generation unit', *Solar & wind technology*, vol. **5**. 3, pp. 263-270.

G. Ordorica-Garcia, A. V. Delgado & A. F. Garcia 2011, 'Novel integration options of concentrating solar thermal technology with fossil-fuelled and  $\text{CO}_2$  capture processes', *Energy Procedia*, vol. **4**. pp. 809-816.

J. Pacio, C. Singer, T. Wetzel & R. Uhlig 2013, 'Thermodynamic evaluation of liquid metals as heat transfer fluids in concentrated solar power plants', *Applied thermal engineering*, vol. **60**. 1-2, pp. 295-302.

J. Pacio, C. Singer, T. Wetzel & R. Uhlig 2013, 'Thermodynamic evaluation of liquid metals as heat transfer fluids in concentrated solar power plants', *Applied thermal engineering*, vol. **60**. 1–2, pp. 295-302.

J. Pacio & T. Wetzel 2013, 'Assessment of liquid metal technology status and research paths for their use as efficient heat transfer fluids in solar central receiver systems', *Solar energy*, vol. **93**. pp. 11-22.

C. Pagkoura, G. Karagiannakis, A. Zygogianni, S. Lorentzou & A. G. Konstandopoulos 2015, 'Cobalt Oxide Based Honeycombs as Reactors/Heat Exchangers for Redox Thermochemical Heat Storage in Future CSP Plants', *Energy Procedia*, vol. **69**. pp. 978-987.

C. Pagkoura, G. Karagiannakis, A. Zygogianni, S. Lorentzou, M. Kostoglou, A. G. Konstandopoulos, M. Rattenburry & J. W. Woodhead 2014, 'Cobalt oxide based structured bodies as redox thermochemical heat storage medium for future CSP plants', *Solar energy*, vol. **108**. Supplement C, pp. 146-163.

B. Pai 1991, 'Augmentation of thermal power stations with solar energy', *Sadhana*, vol. **16**. 1, pp. 59-74.

P. Pardo, A. Deydier, Z. Anxionnaz-Minvielle, S. Rougé, M. Cabassud & P. Cognet 2014, 'A review on high temperature thermochemical heat energy storage', *Renewable and Sustainable Energy Reviews*, vol. **32**. pp. 591-610.

C. Philibert 2014, 'Technology roadmap: solar thermal electricity, 2014 edition', *IEA, Paris, France Google Scholar*.

M. Posnansky & T. Pylkkänen 1991, 'Development and testing of a volumetric gas receiver for high-temperature applications', *Solar energy materials*, vol. **24**. 1-4, pp. 204-209.

H. W. Price, D. D. Whitney & H. B. Beebe 1997, 'SMUD Kokhala er Tower Study'.

C. Prieto, P. Cooper, A. I. Fernández & L. F. Cabeza 2016, 'Review of technology: Thermochemical energy storage for concentrated solar power plants', *Renewable and Sustainable Energy Reviews*, vol. **60**. pp. 909-929.

W. E. Pritzkow 1991, 'Pressure loaded volumetric ceramic receiver', *Solar energy materials*, vol. **24**. 1-4, pp. 498-507.

K. Rao 2011, *Energy and power generation handbook: established and emerging technologies*, ASME.

---

N. R. Rhodes, A. Barde, K. Randhir, L. Li, D. W. Hahn, R. Mei, J. F. Klausner & N. AuYeung 2015, 'Solar Thermochemical Energy Storage Through Carbonation Cycles of SrCO<sub>3</sub>/SrO Supported on SrZrO<sub>3</sub>', *ChemSusChem*, vol. **8**. 22, pp. 3793-3798.

S. A. Robbins, R. G. Rupard, B. J. Weddle, T. R. Maull & P. K. Gallagher 1995, 'Some observations on the use of strontium carbonate as a temperature standard for DTA', *Thermochimica Acta*, vol. **269-270**. pp. 43-49.

B. Rolf, N. Henrik & W. Judy 1999, 'Combined-Cycle Gas and Steam Turbine Power Plants', Pennwell Corp.

M. Romero & A. Steinfeld 2012, 'Concentrating solar thermal power and thermochemical fuels', *Energy & Environmental Science*, vol. **5**. 11, pp. 9234-9245.

F. Schaubé, L. Koch, A. Wörner & H. Müller-Steinhagen 2012, 'A thermodynamic and kinetic study of the de- and rehydration of Ca (OH)<sub>2</sub> at high H<sub>2</sub>O partial pressures for thermo-chemical heat storage', *Thermochimica Acta*, vol. **538**. pp. 9-20.

M. Schmidt, C. Szczukowski, C. Roßkopf, M. Linder & A. Wörner 2014, 'Experimental results of a 10 kW high temperature thermochemical storage reactor based on calcium hydroxide', *Applied thermal engineering*, vol. **62**. 2, pp. 553-559.

P. Schwarzbözl, R. Buck, C. Sugarmen, A. Ring, M. J. M. Crespo, P. Altwegg & J. Enrile 2006, 'Solar gas turbine systems: design, cost and perspectives', *Solar energy*, vol. **80**. 10, pp. 1231-1240.

A. Segal & M. Epstein 2003, 'Optimized working temperatures of a solar central receiver', *Solar energy*, vol. **75**. 6, pp. 503-510.

H. Shabgard, C. W. Robak, T. L. Bergman & A. Faghri 2012, 'Heat transfer and exergy analysis of cascaded latent heat storage with gravity-assisted heat pipes for concentrating solar power applications', *Solar energy*, vol. **86**. 3, pp. 816-830.

K. Shah, B. Moghtaderi & T. Wall 2012, 'Selection of suitable oxygen carriers for chemical looping air separation: a thermodynamic approach', *Energy & Fuels*, vol. **26**. 4, pp. 2038-2045.

M. Shakeri, M. Soltanzadeh, R. E. Berson & M. K. Sharp 2014, 'Comparison of Energy Storage Methods for Solar Electric Production', in *ASME 2014 8th International Conference on Energy Sustainability collocated with the ASME 2014 12th International Conference on Fuel Cell Science, Engineering and Technology*, American Society of Mechanical Engineers, pp. V001T002A008-V001T002A008.

A. Sharma, V. V. Tyagi, C. Chen & D. Buddhi 2009, 'Review on thermal energy storage with phase change materials and applications', *Renewable and Sustainable Energy Reviews*, vol. **13**. 2, pp. 318-345.

E. J. Sheu, A. Mitsos, A. A. Eter, E. M. Mokheimer, M. A. Habib & A. Al-Qutub 2012, 'A review of hybrid solar–fossil fuel power generation systems and performance metrics', *Journal of Solar Energy Engineering*, vol. **134**. 4, p. 041006.

M. Silakhori 2012, 'Preparation and Characterization of Microencapsulated Paraffin Wax as PCM for Thermal Energy Storage', Jabatan Kejuruteraan Mekanikal, Fakulti Kejuruteraan, Universiti Malaya.

M. Silakhori, H. Fauzi, M. R. Mahmoudian, H. S. C. Metselaar, T. M. I. Mahlia & H. M. Khanlou 2015, 'Preparation and thermal properties of form-stable phase change materials composed of palmitic acid/polypyrrole/graphene nanoplatelets', *Energy and Buildings*.

M. Silakhori, M. Jafarian, M. Arjomandi & G. J. Nathan 2017, 'Comparing the thermodynamic potential of alternative liquid metal oxides for the storage of solar thermal energy', *Solar energy*, vol. **157**. pp. 251-258.

M. Silakhori, M. Jafarian, M. Arjomandi & G. J. Nathan 2019, 'Experimental assessment of copper oxide for liquid chemical looping for thermal energy storage', *Journal of Energy Storage*, vol. **21**. pp. 216-221.

M. Silakhori, H. S. C. Metselaar, T. M. I. Mahlia, H. Fauzi, S. Baradaran & M. S. Naghavi 2014, 'Palmitic acid/polypyrrole composites as form-stable phase change materials for thermal energy storage', *Energy Conversion and Management*, vol. **80**. pp. 491-497.

J. A. Simmons 1976, 'Reversible oxidation of metal oxides for thermal energy storage', in *Sharing the Sun: Solar Technology in the Seventies, Volume 8*, vol. 8, pp. 219-225.

R. V. Siriwardane, J. A. Poston Jr, E. P. Fisher, M.-S. Shen & A. L. Miltz 1999, 'Decomposition of the sulfates of copper, iron (II), iron (III), nickel, and zinc: XPS, SEM, DRIFTS, XRD, and TGA study', *Applied Surface Science*, vol. **152**. 3-4, pp. 219-236.

A. Solé, X. Fontanet, C. Barreneche, I. Martorell, A. I. Fernández & L. F. Cabeza 2012, 'Parameters to take into account when developing a new thermochemical energy storage system', *Energy Procedia*, vol. **30**. pp. 380-387.

A. Solé, I. Martorell & L. F. Cabeza 2015, 'State of the art on gas–solid thermochemical energy storage systems and reactors for building applications', *Renewable and Sustainable Energy Reviews*, vol. **47**. pp. 386-398.

J. Spelling, B. Laumert & T. Fransson 2014, 'Advanced hybrid solar tower combined-cycle power plants', *Energy Procedia*, vol. **49**. pp. 1207-1217.

---

J. Stekli, L. Irwin & R. Pitchumani 2013, 'Technical Challenges and Opportunities for Concentrating Solar Power With Thermal Energy Storage', *Journal of Thermal Science and Engineering Applications*, vol. **5**. 2, pp. 021011-021011-021012.

H. Strumpf, D. Kotchick & M. Coombs 1982, 'High-temperature ceramic heat exchanger element for a solar thermal receiver', *Journal of Solar Energy Engineering*, vol. **104**. 4, pp. 305-309.

H. Tagawa & H. Saijo 1985, 'Kinetics of the thermal decomposition of some transition metal sulfates', *Thermochimica Acta*, vol. **91**. pp. 67-77.

P. Tatsidjoudoung, N. Le Pierrès & L. Luo 2013, 'A review of potential materials for thermal energy storage in building applications', *Renewable and Sustainable Energy Reviews*, vol. **18**. pp. 327-349.

S. Tescari, C. Agrafiotis, S. Breuer, L. de Oliveira, M. N.-v. Puttkamer, M. Roeb & C. Sattler 2014, 'Thermochemical Solar Energy Storage Via Redox Oxides: Materials and Reactor/Heat Exchanger Concepts', *Energy Procedia*, vol. **49**. pp. 1034-1043.

L. Till 1971, 'Thermochemical data of barium peroxide from thermogravimetric measurements', *Journal of thermal analysis*, vol. **3**. 2, pp. 177-180.

M. Tmar, C. Bernard & M. Ducarroi 1981, 'Local storage of solar energy by reversible reactions with sulfates', *Solar energy*, vol. **26**. 6, pp. 529-536.

G. Tsiklauri, R. Talbert, B. Schmitt, G. Filippov, R. Bogoyavlensky & E. Grishanin 2005, 'Supercritical steam cycle for nuclear power plant', *Nuclear Engineering and Design*, vol. **235**. 15, pp. 1651-1664.

J. Wang & E. J. Anthony 2005, 'On the decay behavior of the CO<sub>2</sub> absorption capacity of CaO-based sorbents', *Industrial & Engineering Chemistry Research*, vol. **44**. 3, pp. 627-629.

G. Wei, G. Wang, C. Xu, X. Ju, L. Xing, X. Du & Y. Yang 2018, 'Selection principles and thermophysical properties of high temperature phase change materials for thermal energy storage: A review', *Renewable and Sustainable Energy Reviews*, vol. **81**. pp. 1771-1786.

W. E. Wentworth & E. Chen 1976, 'Simple thermal decomposition reactions for storage of solar thermal energy', *Solar energy*, vol. **18**. 3, pp. 205-214.

J. Wheeldon 2008, 'Engineering and Economic Evaluation of 1300 F Series Ultra-Supercritical Pulverized Coal Power Plants: Phase 1', *EPRI, Palo Alto, CA*, vol. **1015699**.

B. Wong, L. Brown, F. Schaube, R. Tamme & C. Sattler 2010, 'Oxide based thermochemical heat storage', in *Proceedings of the 16th SolarPACES Conference, Perpignan, France*, pp. 21-24.

S. Wu, C. Zhou, E. Doroodchi, R. Nellore & B. Moghtaderi 2018, 'A review on high-temperature thermochemical energy storage based on metal oxides redox cycle', *Energy Conversion and Management*, vol. **168**. pp. 421-453.

Q. Yan, E. Hu, Y. Yang & R. Zhai 2011, 'Evaluation of solar aided thermal power generation with various power plants', *International Journal of Energy Research*, vol. **35**. 10, pp. 909-922.

T. Yan, R. Wang, T. Li, L. Wang & I. T. Fred 2015, 'A review of promising candidate reactions for chemical heat storage', *Renewable and Sustainable Energy Reviews*, vol. **43**. pp. 13-31.

Z. Yan, Z. Wang, H. Liu, Y. Tu, W. Yang, H. Zeng & J. Qiu 2015, 'Decomposition and solid reactions of calcium sulfate doped with SiO<sub>2</sub>, Fe<sub>2</sub>O<sub>3</sub> and Al<sub>2</sub>O<sub>3</sub>', *Journal of Analytical and Applied Pyrolysis*, vol. **113**. pp. 491-498.

Y. Yang, Q. Yan, R. Zhai, A. Kouzani & E. Hu 2011, 'An efficient way to use medium-or-low temperature solar heat for power generation–integration into conventional power plant', *Applied thermal engineering*, vol. **31**. 2, pp. 157-162.

H. Zhang, J. Baeyens, J. Degrève & G. Cacères 2013, 'Concentrated solar power plants: review and design methodology', *Renewable and Sustainable Energy Reviews*, vol. **22**. pp. 466-481.

C. Zhou, K. Shah, E. Doroodchi & B. Moghtaderi 2015, 'Equilibrium thermodynamic analyses of methanol production via a novel Chemical Looping Carbon Arrestor process', *Energy Conversion and Management*, vol. **96**. pp. 392-402.

C. Zhou, K. Shah & B. Moghtaderi 2015, 'Techno-Economic Assessment of Integrated Chemical Looping Air Separation for Oxy-Fuel Combustion: An Australian Case Study', *Energy & Fuels*, vol. **29**. 4, pp. 2074-2088.

C. Zhou, K. Shah, H. Song, J. Zanganeh, E. Doroodchi & B. Moghtaderi 2016, 'Integration Options and Economic Analysis of an Integrated Chemical Looping Air Separation Process for Oxy-fuel Combustion', *Energy & Fuels*, vol. **30**. 3, pp. 1741-1755.

C. Zhou, P. Tremain, E. Doroodchi, B. Moghtaderi & K. Shah 2017, 'A novel slag carbon arrestor process for energy recovery in steelmaking industry', *Fuel Processing Technology*, vol. **155**. pp. 124-133.

R. Zoschak & S. Wu 1975, 'Studies of the direct input of solar energy to a fossil-fueled central station steam power plant', *Solar energy*, vol. **17**. 5, pp. 297-305.



## Chapter 3 Experimental investigation of metal oxides for thermochemical storage

---

### 3.1 Chapter preview

In this chapter, the potential of CuO, Co<sub>3</sub>O<sub>4</sub>, Mn<sub>2</sub>O<sub>3</sub> and Pb<sub>3</sub>O<sub>4</sub> for thermochemical energy storage with changing oxygen partial pressure of the system is studied thermodynamically and experimentally. The reduction and oxidation reactions of these materials is assessed with Thermogravimetric analysis (TGA). The rate of oxidation reaction is assessed at different partial pressures of oxygens ranging from 0.2 bar to 0.8 bar to consider its effect on the thermodynamic driving force for oxidation reaction. The reversibility of these materials is investigated over ten reduction and oxidation cycles at isothermal conditions. Moreover, the structure of these material is assessed before and after ten successive reduction and oxidation cycles with X-ray Diffraction (XRD).The results show that CuO/Cu<sub>2</sub>O, Co<sub>3</sub>O<sub>4</sub>/CoO, Mn<sub>2</sub>O<sub>3</sub>/Mn<sub>3</sub>O<sub>4</sub> pairs are suitable candidates for thermochemical energy storage with pressure swing.

The following section is presented in a paper format submitted to international journal of Applied Thermal Engineering.

# Statement of Authorship

Title of Paper	Thermogravimetric analysis of Cu, Mn, Co, and Pb oxides for thermochemical Energy storage
Publication Status	<input type="checkbox"/> Published <input type="checkbox"/> Accepted for Publication <input checked="" type="checkbox"/> Submitted for Publication Unpublished and Unsubmitted work written in manuscript style
Publication Details	Mahyar Silakhori, Mehdi Jafarian, Maziar Arjomandi, Graham J. Nathan, Thermogravimetric analysis of Cu, Mn, Co, and Pb oxides for thermochemical Energy storage, Journal of Energy Storage(2018)

## Principal Author


Name of Principal Author (Candidate)	Mahyar Silakhori		
Contribution to the Paper	- Research, collecting and analysing data from different resources - Providing the data, writing of the manuscript and production of original figures - Correspondence with editor and reviewers including the production of all cover letters and rejoinder		
Overall percentage (%)	65%		
Certification:	This paper reports on original research I conducted during the period of my Higher Degree by Research candidature and is not subject to any obligations or contractual agreements with a third party that would constrain its inclusion in this thesis. I am the		
Signature		Date	04.02.2019


## Co-Author Contributions

By signing the Statement of Authorship, each author certifies that:

- i. the candidate's stated contribution to the publication is accurate (as detailed above);
- ii. permission is granted for the candidate to include the publication in the thesis; and
- iii. the sum of all co-author contributions is equal to 100% less the candidate's stated contribution.

Name of Co-Author	Mehdi Jafarin		
Contribution to the Paper	- Supervision of the work, including the production of the manuscript - Participation in the development of the concepts and ideas presented in the manuscript - Evaluation and editing of the manuscript prior to submission		
Signature		Date	04.2.2019

Name of Co-Author	Maziar Arjomandi
Contribution to the Paper	<ul style="list-style-type: none"><li>- Supervision of the work, including the production of the manuscript</li><li>- Participation in the development of the concepts and ideas presented in the manuscript</li><li>- Evaluation and editing of the manuscript prior to submission</li></ul>
Signature	 Date 4/02/2019

Name of Co-Author	Graham 'Gus' Nathan
Contribution to the Paper	<ul style="list-style-type: none"><li>- Supervision of the work, including the production of the manuscript</li><li>- Participation in the development of the concepts and ideas presented in the manuscript</li><li>- Evaluation and editing of the manuscript prior to submission</li></ul>
Signature	 Date 4/2/19

**Thermogravimetric analysis of Cu, Mn, Co, and Pb oxides for thermochemical Energy storage**

Mahyar Silakhori <sup>\*</sup>, Mehdi Jafarian, Maziar Arjomandi, Graham J. Nathan

Revised: Journal of Energy Storage

### 3.2 Abstract

The reversible reduction and oxidation (RedOx) reactions of CuO/Cu<sub>2</sub>O, Co<sub>3</sub>O<sub>4</sub>/CoO, Mn<sub>2</sub>O<sub>3</sub>/Mn<sub>3</sub>O<sub>4</sub>, and Pb<sub>3</sub>O<sub>4</sub>/PbO have been assessed experimentally with thermogravimetric Analysis (TGA). The temperature was maintained constant during charging and discharging of the thermochemical energy storage via pressure swing for a range of oxygen partial pressures spanning from 0.05 to 0.8 bar. The rate of oxidation reactions were assessed for a range of partial pressures, while changes to the structure of the materials was assessed with X-Ray diffraction spectra (XRD) before and after 10 successive reduction and oxidation cycles. The results show that the Co<sub>3</sub>O<sub>4</sub>/CoO, Mn<sub>2</sub>O<sub>3</sub>/Mn<sub>3</sub>O<sub>4</sub>, and CuO/Cu<sub>2</sub>O pairs have a potential for chemical storage at temperatures ranges from 900°C to 1000°C, while no thermochemical reaction was observed for Pb<sub>3</sub>O<sub>4</sub> up to a temperature of 550°C.

### 3.3 Introduction

Thermal energy storage systems have received significant attention because they offer potential for low cost energy storage for Concentrating Solar Thermal (CST) energy plant (Bayon et al. 2018), in comparison to other renewable energy technologies (Gil et al. 2010; Kuravi et al. 2013). Among the different types of thermal energy storage systems, thermochemical energy storage offers potential to achieve both a high energy density and operating temperatures in the range 700°C - 1100°C (Block & Schmücker 2016), which is compatible with the more efficient power cycles such as super-critical CO<sub>2</sub> and gas turbine combined cycles. However, high temperature thermochemical energy storage systems are still at an early stage of development because of technical challenges related to temperature swing system cause to sintering of the materials and thermal hysteresis during reduction and oxidation so that more work is needed to assess the potential of suitable materials at different thermodynamic conditions.

Reduction and Oxidation (RedOx) reactions of metal oxides can be described as follows:



$\text{MeO}_{\delta_1}$  and  $\text{MeO}_{\delta_2}$  represent two states of oxidation of the metal Me. Since the reduction reaction (Eq1.) is endothermic, it offers potential to be used in the charging cycle of a thermochemical thermal energy storage (TES) system. Similarly the exothermic oxidation reaction (Eq2.) can be used to release the stored heat. Based on Le Chatelier's principle, two alternative states of oxidations of  $\text{MeO}_{\delta_1}$  and  $\text{MeO}_{\delta_2}$  can be achieved by either changing the partial pressure of oxygen (P-swing), the temperature of the reaction (T-swing) or a combination of them (Irwin et al. 2017). However, the relative advantages and disadvantages of these two alternative approaches on the rate of the reaction has not previously received much attention.

The pairs of  $\text{Co}_3\text{O}_4/\text{CoO}$  and  $\text{Mn}_2\text{O}_3/\text{Mn}_3\text{O}_4$  and  $\text{CuO}/\text{Cu}_2\text{O}$  have been selected here as potential candidate materials for thermochemical storage due to their high reaction enthalpy ( $\text{Co}_3\text{O}_4/\text{CoO} = 5.15 \text{ GJ/m}^3$ ,  $\text{CuO}/\text{Cu}_2\text{O} = 5.11 \text{ GJ/m}^3$  and  $\text{Mn}_2\text{O}_3/\text{Mn}_3\text{O}_4 = 0.918 \text{ GJ/m}^3$ ), high operating temperature of approximately  $1000^\circ\text{C}$  and reaction reversibility (Agrafiotis et al. 2016; Wong 2011; Deutsch et al. 2017). These materials has been extensively assessed for thermochemical energy storage with temperature swing (Agrafiotis et al. 2016; Wong 2011; Deutsch et al. 2017). However, gaps remain in the understanding of their performance under some relevant conditions such as RedOx reactions at isothermal condition with changing the oxygen partial pressure.

The exact temperatures for the RedOx reactions (Eqs. 1 & 2) and the conversion of multivalent metal oxides in temperature-swing system depend on the partial pressure of gaseous components involved in the reactions or experimental condition (André et al. 2016). Table 3.1

presents the operating temperature of the selected metal oxides in various environments such as N<sub>2</sub>, O<sub>2</sub>, Ar and Air. Neises et al. (Neises et al. 2012) reported a reduction temperature of 800°C for Co<sub>3</sub>O<sub>4</sub>/CoO oxides in air at ambient pressure within a rotary kiln reactor. However, the measured temperature is lower at 700°C when the reduction reaction is performed with Thermogravimetric Analysis (TGA) in an argon atmosphere (Wu et al. 2018). Muller et al. (Müller et al. 2017) reported reaction temperatures of 958°C, 897.6°C and 813.6°C at different environments of O<sub>2</sub>, air and N<sub>2</sub>, respectively. The kinetics of Co<sub>3</sub>O<sub>4</sub>/CoO oxides were also assessed in an air and nitrogen environments at temperatures range of 840°C-940°C (Hutchings et al. 2006). Kinetic data propose that cobalt oxide with particle size of 1-5 µm can be oxidised and reduced at temperatures between 840°C and 940°C in air in less than 10 min at a bed thickness of 10 mm (Hutchings et al. 2006). This Carrillo, et al. (Carrillo et al. 2014) found that the RedOx reactions of Mn<sub>2</sub>O<sub>3</sub>/Mn<sub>3</sub>O<sub>4</sub> occurred at temperature ranges between 500°C and 1000°C in an air environment. In another study, Muller et al. (Müller et al. 2017) reported that a complete oxidation of Mn<sub>3</sub>O<sub>4</sub> to Mn<sub>2</sub>O<sub>3</sub> occurs at approximately 852.1°C in pure O<sub>2</sub>, while this temperature reduces to 739.5°C in air. The assessment of CuO/Cu<sub>2</sub>O pair showed that the RedOx reactions occurred at temperature ranges between 1027°C and 1050°C in an ambient air (Deutsch et al. 2017; Hallstedt et al. 1994; Shishin & Decterov 2012). In these studies, the reaction temperature, reversibility, and kinetics of the reactions were investigated through temperature-swing system. To the best of the author's knowledge, there is no investigation on the effect partial pressure of oxygen on reversibility and rate of the reaction with pressure-swing system. Moreover, most previous investigations have been limited to oxygen partial pressures of 0 or 0.21 bar for reduction and oxidation reactions, respectively. However, it is also important to investigate the performance of RedOx reactions for oxygen partial pressures corresponding to air pressure of > 3bar (i.e. O<sub>2</sub> partial pressures > 0.63 bar), because these conditions are relevant for applications in gas turbines (3-30 bar). Therefore this paper aims in

particular to assess the effect of partial pressure of oxygen in a range of 0.05 bar to 0.8 bar on RedOx reactions and rate of the reaction of CuO/Cu<sub>2</sub>O, Co<sub>3</sub>O<sub>4</sub>/CoO, Mn<sub>2</sub>O<sub>3</sub>/Mn<sub>3</sub>O<sub>4</sub> and Pb<sub>3</sub>O<sub>4</sub>/PbO.

Table 1 also shows that there is a temperature difference between reduction and oxidation reactions of temperature-swing system that reduce the thermodynamic efficiency of the system. This is because the charging temperature is higher than discharging temperature. Pressure-swing system is one of the plausible way to address this challenge. Therefore, another aims of this study is to assess the pressure-swing for thermochemical storage of CuO/Cu<sub>2</sub>O, Co<sub>3</sub>O<sub>4</sub>/CoO, Mn<sub>2</sub>O<sub>3</sub>/Mn<sub>3</sub>O<sub>4</sub> and Pb<sub>3</sub>O<sub>4</sub>/PbO.



**Table 3.2.** Operating temperature of CuO/Cu<sub>2</sub>O, Co<sub>3</sub>O<sub>4</sub>/CoO, and Mn<sub>2</sub>O<sub>3</sub>/Mn<sub>3</sub>O<sub>4</sub> at different environment (Air, O<sub>2</sub>, N<sub>2</sub>, and Ar), in comparison with the present measurements.

Materials	Methods	Operating temperature	Atmosphere in RedOx reactions ( partial pressure of oxygen)	References
CuO/Cu <sub>2</sub> O	TGA	400-910°C (Temperature-swing)	Air (0.21 bar), O <sub>2</sub> (1 bar), N <sub>2</sub> (0 bar).	(Chadda et al. 1989)
		1100-1200°C (Temperature-swing)	Air (0.21 bar)	(Wong 2011)
		Up to 1000°C (Temperature-swing)	Air (0.21 bar), Ar (0 bar).	(Alonso et al. 2015)
		Up to 1100°C (Temperature-swing)	Air (0.21 bar), N <sub>2</sub> (0 bar).	(Deutsch et al. 2017)
		1000°C (Pressure-swing)	N <sub>2</sub> & O <sub>2</sub> (0.05 bar) ≤ P <sub>O<sub>2</sub></sub> ≤ N <sub>2</sub> & O <sub>2</sub> (0.8 bar)	Present study
Co <sub>3</sub> O <sub>4</sub> /CoO	TGA	780-960°C (Temperature-swing)	Air ( 0.21 bar), O <sub>2</sub> (1 bar).	(Hutchings et al. 2006)
	Packed bed	500-900°C (Temperature-swing)	Air (0.21 bar), N <sub>2</sub> (0 bar).	(Wong et al. 2010)
	Packed bed, TGA	700-900°C (Temperature-swing)	Air ( 0.21 bar), N <sub>2</sub> (0 bar).	(Wong 2011)
	Rotary kiln reactor	Up to 1000°C (Temperature-swing)	Air (0.21 bar), O <sub>2</sub> (1 bar), N <sub>2</sub> (0 bar).	(Alonso et al. 2015)
	TGA	600-1100°C (Temperature-swing)	Air (0.21 bar), Ar (0 bar).	(Agrafiotis et al. 2014)
		177-940°C (Temperature-swing)	O <sub>2</sub> ( 0.21 bar), Ar (0 bar)	(Muroyama et al. 2015)
		25-1250°C (Temperature-swing)	Air (0.21 bar), O <sub>2</sub> ( 1 bar), N <sub>2</sub> (0 bar).	(Müller et al. 2017)
	Packed bed, TGA	800-1100°C (Temperature-swing)	Air ( 0.21 bar), Ar (0 bar)	(Agrafiotis, Becker, et al. 2016; Agrafiotis et al. 2015)
	TGA	900°C (Pressure-swing)	N <sub>2</sub> & O <sub>2</sub> (0.05 bar) ≤ P <sub>O<sub>2</sub></sub> ≤ N <sub>2</sub> & O <sub>2</sub> (0.8 bar)	Present study
	Mn <sub>2</sub> O <sub>3</sub> /Mn <sub>3</sub> O <sub>4</sub>	TGA	300-1100°C (Temperature-swing)	Air (0.21 bar).
Packed bed		500-1100°C (Temperature-swing)	Air (0.21 bar).	(Karagiannakis et al. 2014)
TGA		500-1000°C (Temperature-swing)	Air (0.21 bar).	(Carrillo, Moya, et al. 2014)
TGA		650-1000°C (Temperature-swing)	Air (0.21 bar).	(Carrillo, Serrano, et al. 2014)
Packed bed		640-1090°C (Temperature-swing)	Air (0.21 bar).	(Agrafiotis, Becker, et al. 2016)
TGA		25-1250°C (Temperature-swing)	Air (0.21 bar), O <sub>2</sub> (1 bar), N <sub>2</sub> (0 bar).	(Müller et al. 2017)
TGA		900°C (Pressure-swing)	N <sub>2</sub> & O <sub>2</sub> (0.05 bar) ≤ P <sub>O<sub>2</sub></sub> ≤ N <sub>2</sub> & O <sub>2</sub> (0.8 bar)	Present study

### 3.4 Experimental setup

#### 3.4.1 Materials and methods

The particles of CuO, Co<sub>3</sub>O<sub>4</sub>, Mn<sub>2</sub>O<sub>3</sub>, and Pb<sub>3</sub>O<sub>4</sub> with a purity of 97.5%, 99.97%, 99.9% and 97%, respectively, were procured from Chem-Supply and used as the samples. The particle size distribution of the samples was measured by MASTERSIZER2000. The average particles size distribution of CuO, Co<sub>3</sub>O<sub>4</sub>, Mn<sub>2</sub>O<sub>3</sub>, and Pb<sub>3</sub>O<sub>4</sub> is 14.68 μm, 4.89 μm, 4.153 μm and 3.21 μm, respectively. For every test, 10 mg of the sample was placed in an alumina crucible. The sample were tested using a Netzsch STA 449 F3 Jupiter Thermogravimetric analyzer (TGA), which measures weight with an accuracy of ±2%. The crucible was used without the lid to provide direct contact (and hence to facilitate reactions) between the metal oxide and the gaseous environment. The Netzsch software Proteus was used for data analysis.

The experiment was designed based on available thermodynamic data and the phase stability diagrams shown in Figure 3.1-a-d (Chen et al. 2003; Grundy et al. 2003; Risold et al. 1998; Shishin & Dechterov 2012; Silakhori et al. 2017). The oxidation and reduction processes were performed by changing the oxygen partial pressure between 0.05 and 0.8 bar via the ratio of oxygen and nitrogen in TGA for the RedOx pairs of CuO/Cu<sub>2</sub>O, Co<sub>3</sub>O<sub>4</sub>/CoO, Mn<sub>2</sub>O<sub>3</sub>/Mn<sub>3</sub>O<sub>4</sub>, and Pb<sub>3</sub>O<sub>4</sub>/PbO. Table 3.2 presents the various conditions at which the reduction and oxidation reactions were performed. The partial pressure of oxygen (P<sub>O<sub>2</sub></sub>) in a TGA can be defined with following equation:

$$P_{O_2} = y_{O_2} P_t \quad (1)$$

In this equation, P<sub>t</sub> and y<sub>O<sub>2</sub></sub> are total pressure and mole fraction of oxygen in the system. As shown in Table 3.2, P<sub>O<sub>2</sub></sub> can be modified by variation of O<sub>2</sub> and N<sub>2</sub> in the TGA. The weight change of the materials is defined as:

$$\Delta W\% = \frac{\Delta m}{m_0} \quad (2)$$

In this equation, the difference between the final mass ( $m_f$ ) and initial mass ( $m_0$ ) is denoted by  $\Delta m$ .

At the beginning of any given cycle, the temperature was increased to 200°C and held constant for 20 min to stabilise flow rate of gases in the TGA. The temperature was then increased to the desirable value (eg, 1000°C based on phase stability diagram of CuO, Figure 3.1-a) at a constant oxygen partial pressure with a heating rate of 10°C/min (from A to B- Figure 3.1-a). The partial pressure of oxygen was then changed at a constant temperature for 10 subsequent cycles (between B and C-Figure 3.1-a) before cooling the material at a rate of 20°C/min (shown as C → D in Figure 3.1). This process was completed in a nitrogen rich environment (100ml/min) with no oxygen to enable characterization of the final reduced state of the material (Agrafiotis et al. 2016). The rate of oxidation was also assessed by changing the partial pressure during the oxidation from 0.2 to 0.8 bar for the second cycle, while the reduction was constant at 0.05 bar. A dwell time of either 15 or 30 mins was chosen for each successive reduction and oxidation step (Table 3.2) to ensure complete conversion.

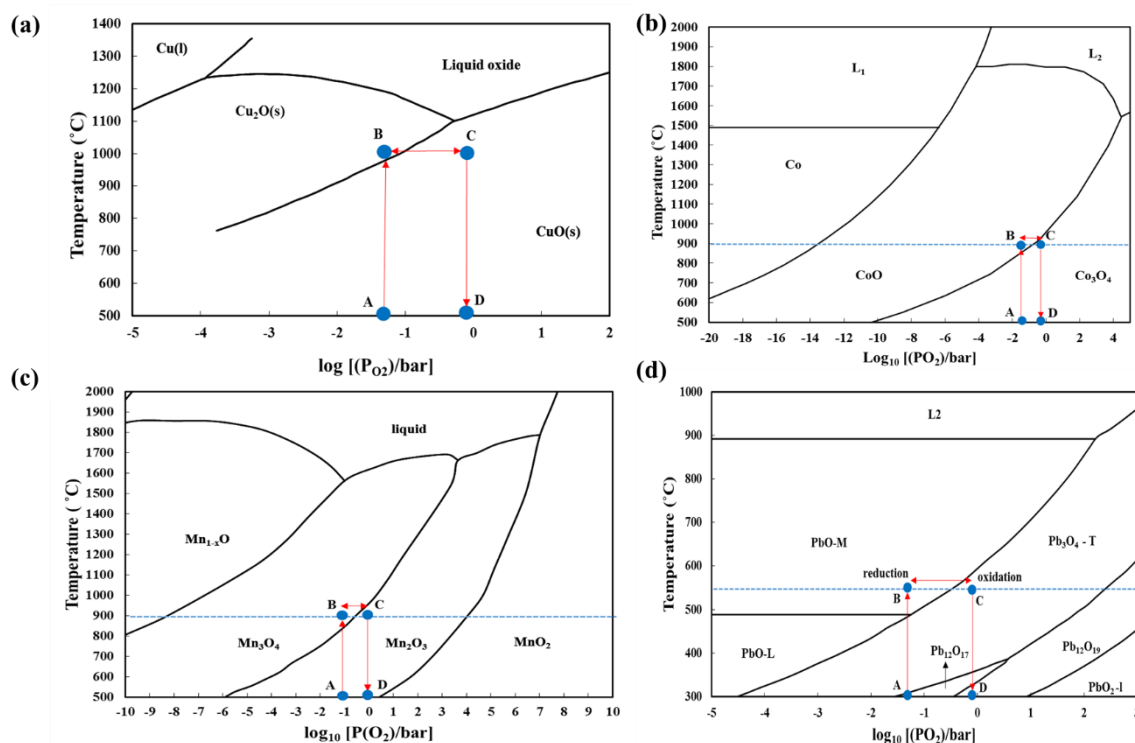


**Figure 3.1.** The condition of the experiments shown in the phase diagram for a) copper and its oxides reproduced from (Shishin & Dectero 2012; Silakhori et al. 2017) b) Cobalt and its oxides reproduced from (Chen et al. 2003) c) Manganese and its oxides reproduced from (Grundy et al. 2003) and d) Lead and its oxides reproduced from (Risold et al. 1998). The temperature was increased isobarically to the desired temperature, which is shown in the phase stability diagram for each material, over the partial pressure range from 0.05 to 0.8 bar (from A to B). The partial pressure of oxygen was then varied isothermally at partial pressure within the range from 0.05 to 0.8 bar for the reduction and oxidation reactions. At the final stage of the experiment, the temperature was decreased isobarically to low temperature (From C-D). Other details are presented in Table 3.2.

**Table 3.2.** The partial pressure of oxygen for the reduction and oxidation reactions for the redox pairs of CuO/Cu<sub>2</sub>O, Co<sub>3</sub>O<sub>4</sub>, Mn<sub>2</sub>O<sub>3</sub>, and Pb<sub>3</sub>O<sub>4</sub>.

Metal oxides	Samples	T(°C)	PO <sub>2</sub> (bar) (reduction reaction)	PO <sub>2</sub> (bar) (oxidation reaction)	Time(min) (Reduction/Oxidation)	O <sub>2</sub> /N <sub>2</sub> (ml/min)* reduction cycle	O <sub>2</sub> /N <sub>2</sub> (ml/min)* Oxidation cycle
CuO/Cu <sub>2</sub> O	S1	1000	0.05	0.2	15/15	5/95	20/80
	S2	1000	0.05	0.4	15/15	5/95	40/60
	S3	1000	0.05	0.6	15/15	5/95	60/40
	S4	1000	0.05	0.8	15/15	5/95	20/80
Co <sub>3</sub> O <sub>4</sub>	S5	900	0.05	0.2	15/15	5/95	20/80
	S6	900	0.05	0.4	15/15	5/95	40/60
	S7	900	0.05	0.6	15/15	5/95	60/40
	S8	900	0.05	0.8	15/15	5/95	80/20
Mn <sub>2</sub> O <sub>3</sub>	S9	900	0.05	0.2	30/30	5/95	20/80
	S10	900	0.05	0.4	30/30	5/95	40/60
	S11	900	0.05	0.6	30/30	5/95	60/40
	S12	900	0.05	0.8	30/30	5/95	80/20
Pb <sub>3</sub> O <sub>4</sub>	S13	500	0.05	0.8	15/15	5/95	80/20
	S14	550	0.05	0.8	15/15	5/95	80/20

---

\* The flow-rate of O<sub>2</sub> and N<sub>2</sub> through the TGA.

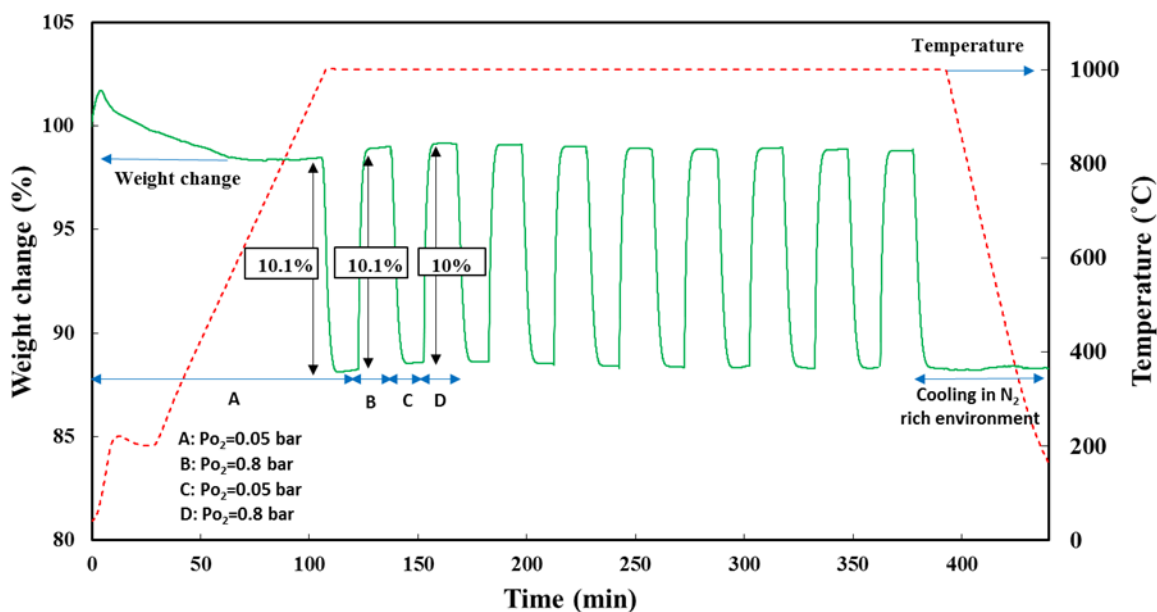
Structural characterization of the metal oxide was performed for 10 successive reduction and oxidation reactions with X-Ray Diffraction (XRD) spectra using a Rigaku MiniFlex60 in the diffraction angle (2 thetas) range of 20-80. Microstructural observations by Scanning Electron Microscopy (SEM) were performed with a Quanta 450 (ThermoFisher Scientific) instrument.

### 3.5 Results and discussion

#### 3.5.1 CuO/Cu<sub>2</sub>O cycle

Figure 3.2 presents the variations of weight with time for a CuO sample over 10 successive RedOx cycles. In this experiments the partial pressure of oxygen was 0.05 bar during reduction, while the oxidation was performed at partial pressures of oxygen of 0.8 bar at a constant temperature of 1000°C. Figure 3.2 shows that the first weight loss of 10% (the reduction reaction) occurs by temperature and pressure swing (P (O<sub>2</sub>) = 0.05 bar). Next, the same weight gain (the oxidation reaction) is induced by increasing the oxygen partial pressure (P (O<sub>2</sub>) = 0.8 bar). This cycle is repeated, with the amount of weight loss and gain in each successive cycle being almost identical at 10.1%, showing a consistent conversion extent during each of the ten cycles. That is, no significant overall weight loss was identified for up to 10 RedOx cycle in a pressure-swing system. In contrast, an overall weight loss was observed in the temperature-swing system of CuO/Cu<sub>2</sub>O pair after 5 RedOx cycles attribute to volatilization of the copper oxide (Agrafiotis et al. 2016). This is one advantageous of the pressure-swing over temperature-swing system.

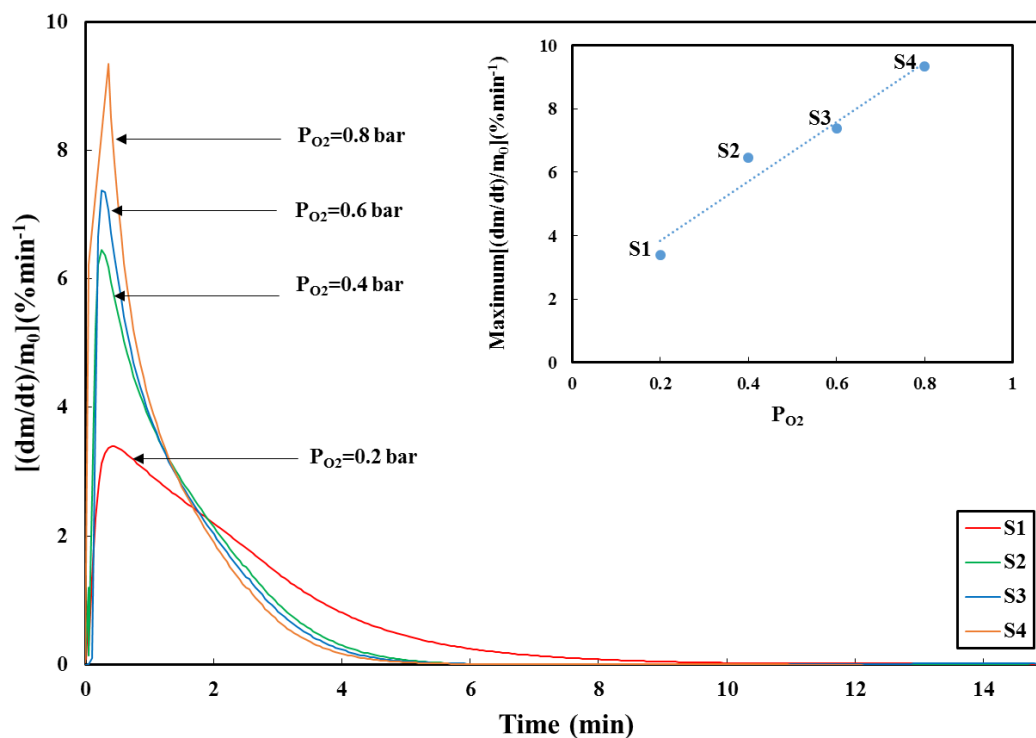
It can be seen that the time for complete reduction and oxidation is less than 15 min for copper oxide. This time for pressure swing cycle is significantly less than the 2h reported in a temperature swing system (Agrafiotis et al. 2016). This implies that the kinetics of the reactions can be improved by pressure swing process over temperature swing, which is advantageous in decreasing the size of reactors and hence capital cost.



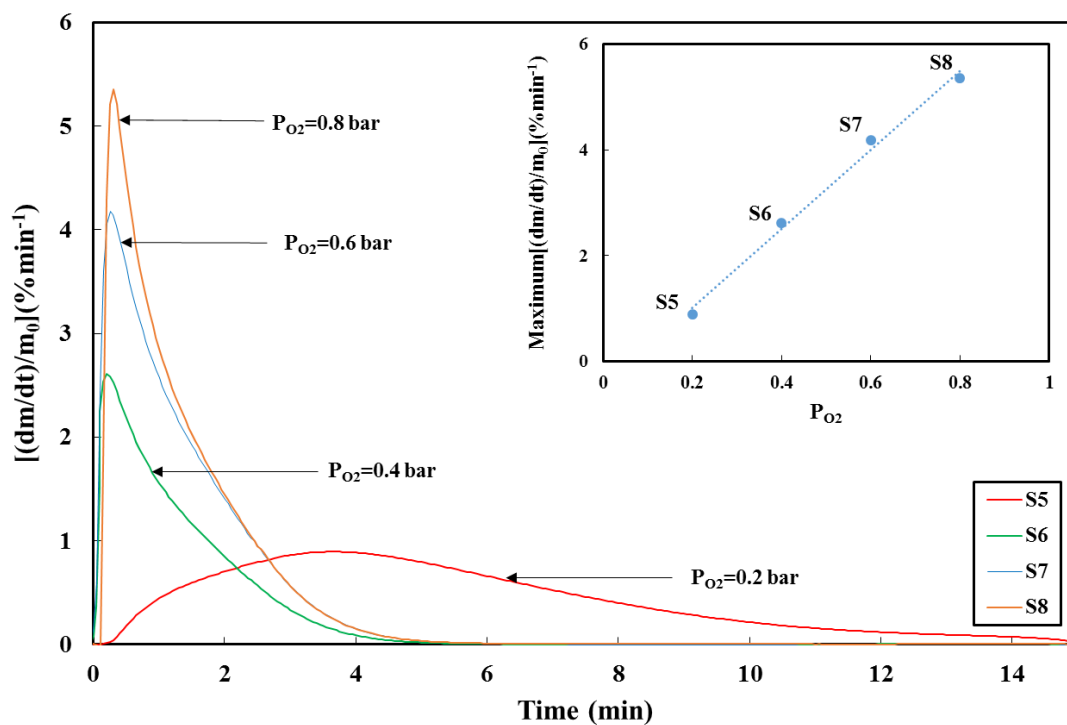
**Figure 3.2.** The weight and temperature change of copper oxide over 10 successive reduction and oxidation reactions. The partial pressure of oxygen is 0.05 bar and 0.8 bar during reduction and oxidation reactions, respectively. The red dashed line shows the temperature of the samples.

Figure 3.3-a presents the rate of oxidation as a function of time for a series of values of  $P_{O_2}$ . As shown, the rate of oxidation increases with  $P_{O_2}$  over the range 0.2 bar to 0.8 bar. The dependence of the maximum rate”  $[(dm/dt)/m_0]_{\max}$ “on  $P_{O_2}$  is plotted in the inset of the figure. It can be seen that this dependence is approximately linear and that the rate is greater for the copper than the cobalt pair (Figure 3.3-b).

(a)



(b)



**Figure 3.3.** The rate of oxidation as a function of time for a series of partial pressure of oxygen during isothermal RedOx cycling for a) copper oxide, b) cobalt oxide. Other conditions are given in Table 3.2.

Figure 3.4 presents the XRD spectra of the CuO before and after 10 cycles of reduction and oxidation at conditions for sample S4. It can be seen that the peaks associated with CuO can be observed for the sample before cycling and are matched with the crystalline monoclinic structure of CuO (JCPDS card No: 80-1916). The spectra of Cu<sub>2</sub>O appears for condition of S4 in which the CuO has a change in partial pressure ( $PO_2 = 0.8$  bar), which leads to conversion of CuO to Cu<sub>2</sub>O ( $4CuO \rightarrow 2Cu_2O + O_2$ ). The spectra of Cu<sub>2</sub>O matches with JCPDS card No: 05-0667, which is for a cubic structure of Cu<sub>2</sub>O. This confirms the final step of the cycle was the reduction reaction in a N<sub>2</sub> rich environment.

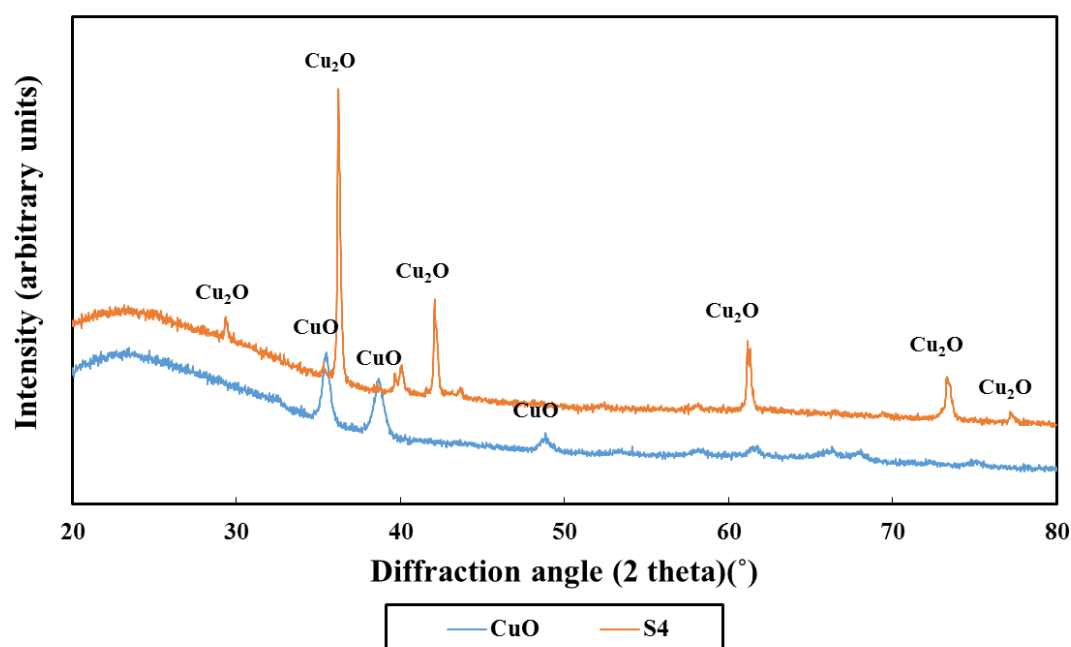


**Figure 3.4.** The XRD spectra of copper oxide before and after 10 successive RedOx cycles under conditions for S4, given in table 3.2.

### 3.5.2 Co<sub>3</sub>O<sub>4</sub>/CoO cycle

Figure 3.5 presents the corresponding time history of the weight change for Co<sub>3</sub>O<sub>4</sub>/CoO, obtained for oxygen partial pressures of 0.05 and 0.8 bar, respectively, for a constant temperature of 900°C. The weight of cobalt oxide reduces by 6.8% during the first reduction stage, while the successive weight gain is 6.65%. This difference contributes to the cumulative incorporation of oxygen into the solid phase during each cycle (Agrafiotis et al. 2014).



Consistent with the previous case, the dwell time for complete reduction and oxidation cycles was found to be 15 min, while this number was reported to be 3h in a temperature swing system (Agrafiotis et al. 2014). This provides further evidence that the kinetics of the system can be improved with pressure swing cycle. This figure also shows that the reversibility of cobalt oxide is high since no significant degradation in the weight change is observable for the 10 cycles of reduction and oxidation reactions. Therefore, the RedOx pair of  $\text{Co}_3\text{O}_4/\text{CoO}$  is worth exploring further as a potential material for thermochemical energy storage.

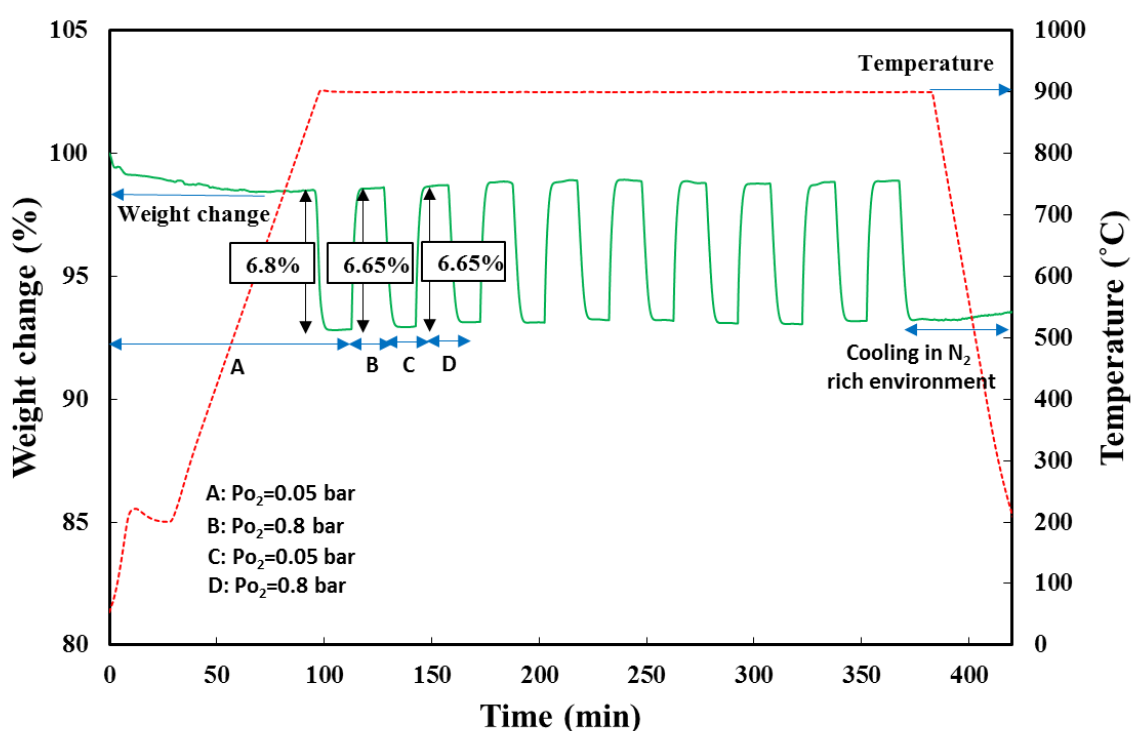


**Figure 3.5.** A time history of the weight of sample during 10 cycles of oxidation at 0.8 bar and reduction at 0.05bar, for the condition S8 shown in Table 3.2.

Figure 3.6 presents the XRD spectra of the  $\text{Co}_3\text{O}_4$  before and after 10 successive RedOx cycles, which have been matched with the available literature (Kim et al. 2014; Wu 2012). It can be seen, the  $\text{Co}_3\text{O}_4$  is fully converted to  $\text{CoO}$ , with no evidence of residual  $\text{Co}_3\text{O}_4$  after 10<sup>th</sup> reduction. This indicates that the stability of the material is high and that the  $\text{Co}_3\text{O}_4/\text{CoO}$  pair is worthy of further consideration for RedOx processes.

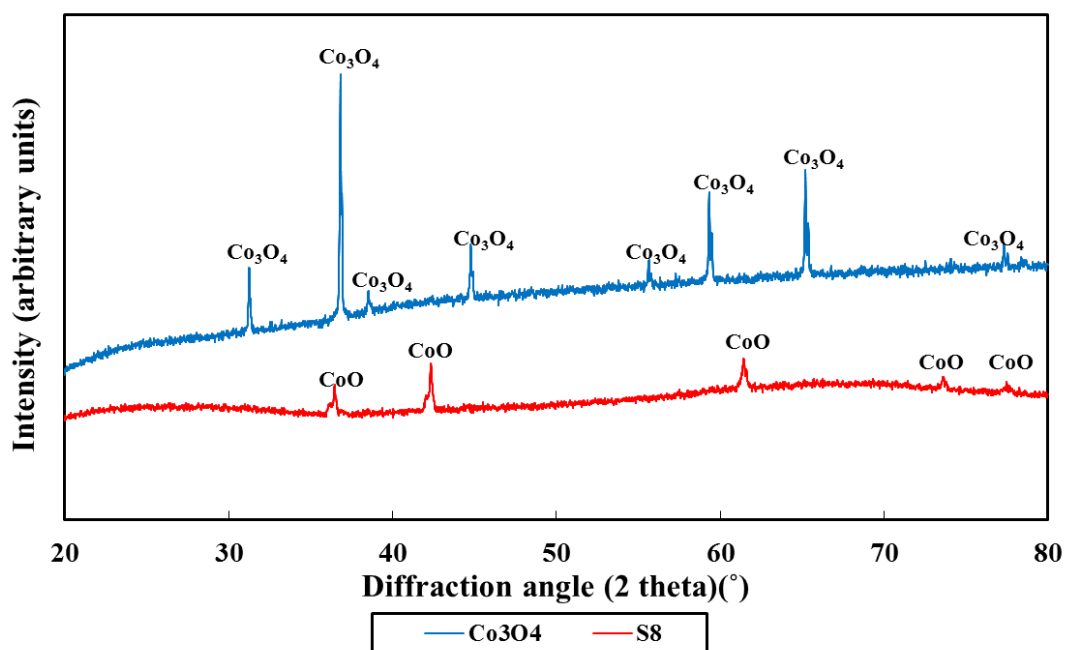


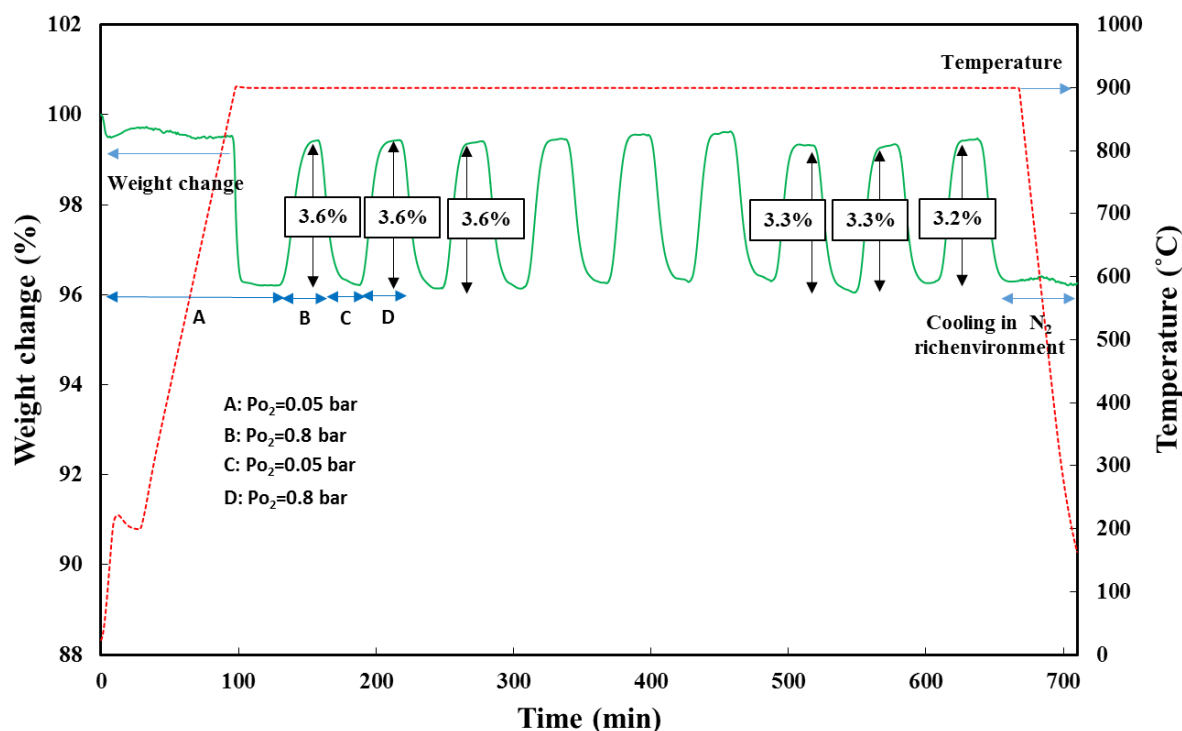
**Figure 3.6.** The XRD spectra of cobalt oxide before and after 10 successive RedOx cycles under condition of S8.

### 3.5.3 $\text{Mn}_2\text{O}_3/\text{Mn}_3\text{O}_4$ cycle

Figure 3.7 presents the time history of the weight change of  $\text{Mn}_2\text{O}_3$  samples through ten successive isothermal reduction and oxidation cycles under oxygen partial pressures of 0.05 and 0.8 bar, respectively. The dwell time has been increased to 30 min for each reduction and oxidation cycles of  $\text{Mn}_2\text{O}_3/\text{Mn}_3\text{O}_4$  pair because 15 min was not enough for complete conversion of  $\text{Mn}_2\text{O}_3$  to  $\text{Mn}_3\text{O}_4$ . As shown in Figure 3.7, the weight losses and gains from each cycle are approximately repeatable at 3.6%, although there is a slight reduction in the reversibility of the manganese oxide toward the end of the ten cycles. Consistent with other cases reported above, the dwell time for complete reduction and oxidation cycles is 30 min which is significantly less than the 2 to 3h for a temperature swing system reported previously (Agrafiotis et al. 2016), which implies an increase in the kinetics reactions.

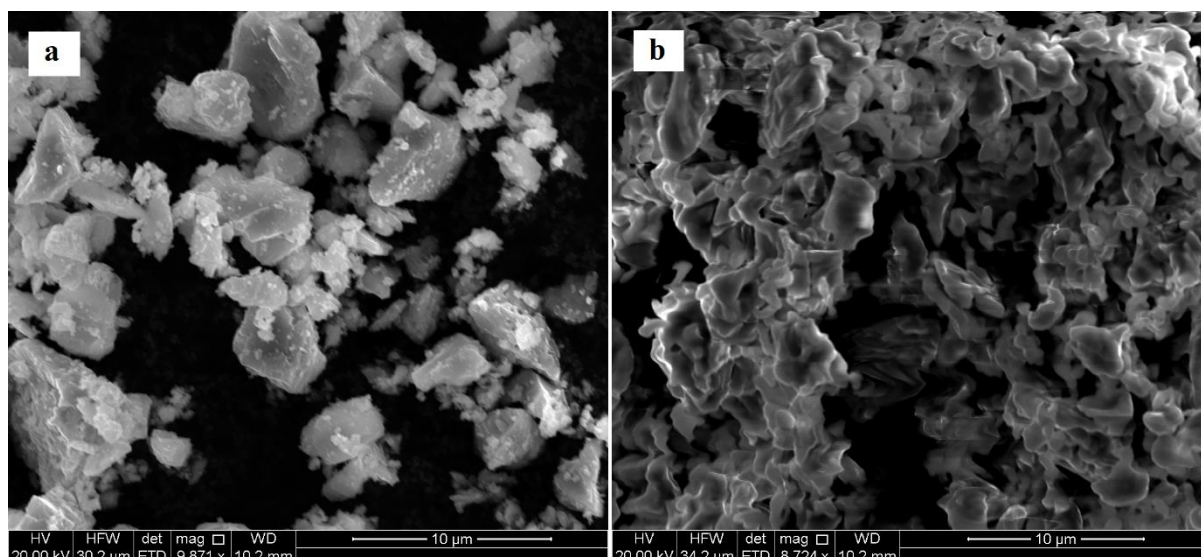
The  $\text{Mn}_2\text{O}_3/\text{Mn}_3\text{O}_4$  pair has also been reversible up 6 reduction and oxidation cycles because the weight change remained almost stable. The small reduction in the weight loss, which has

been detected after 6 cycles, implies some sintering of the material over successive reduction and oxidation cycles.



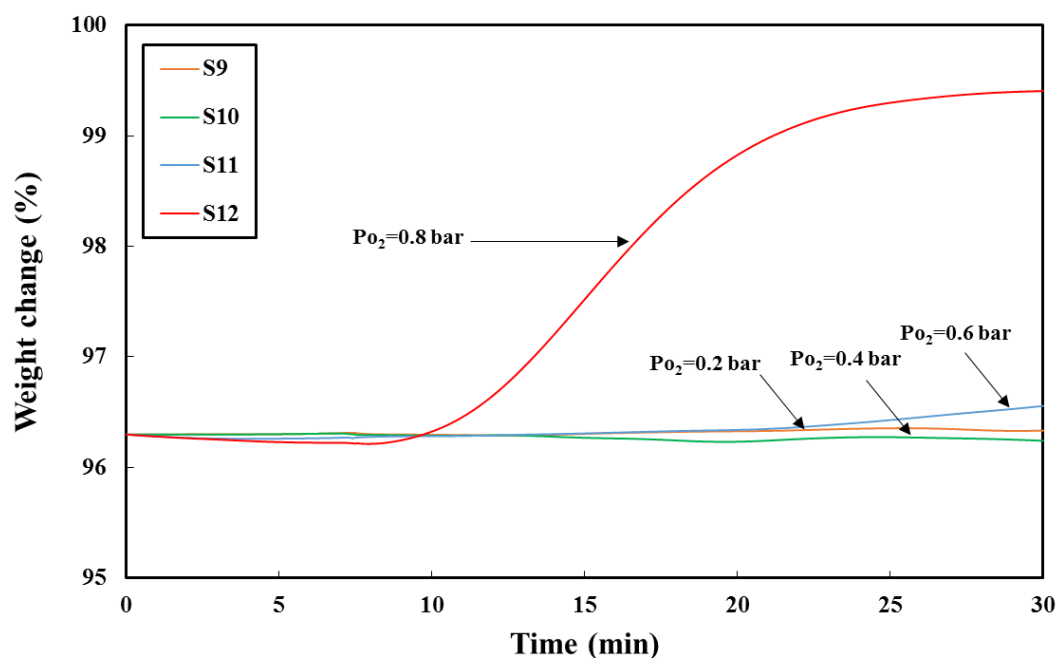
**Figure 3.7.** Weight change of  $\text{Mn}_2\text{O}_3/\text{Mn}_3\text{O}_4$  as a function of time for 10 cycles at a constant temperature of  $900^\circ\text{C}$ , under S12 condition shown in table 3.2. The dwell time for reduction and oxidation cycles was 30 minutes.

Figure 8 compares the SEM micrograph of the  $\text{Mn}_2\text{O}_3$  sample before and after 10 consecutive Redox cycles. As can be seen, the morphology of the material has been changed over RedOx reactions as a result of sintering cause by the pressure and temperature change. Commensurate with this is the slight decrease in the reactivity of the  $\text{Mn}_2\text{O}_3$  sample, especially after 6th cycle. This can be explained by the sintering effect which leads to morphology change and thermal deactivation of the materials over Redox reaction (Carrillo et al. 2014; Silakhori et al. 2019).



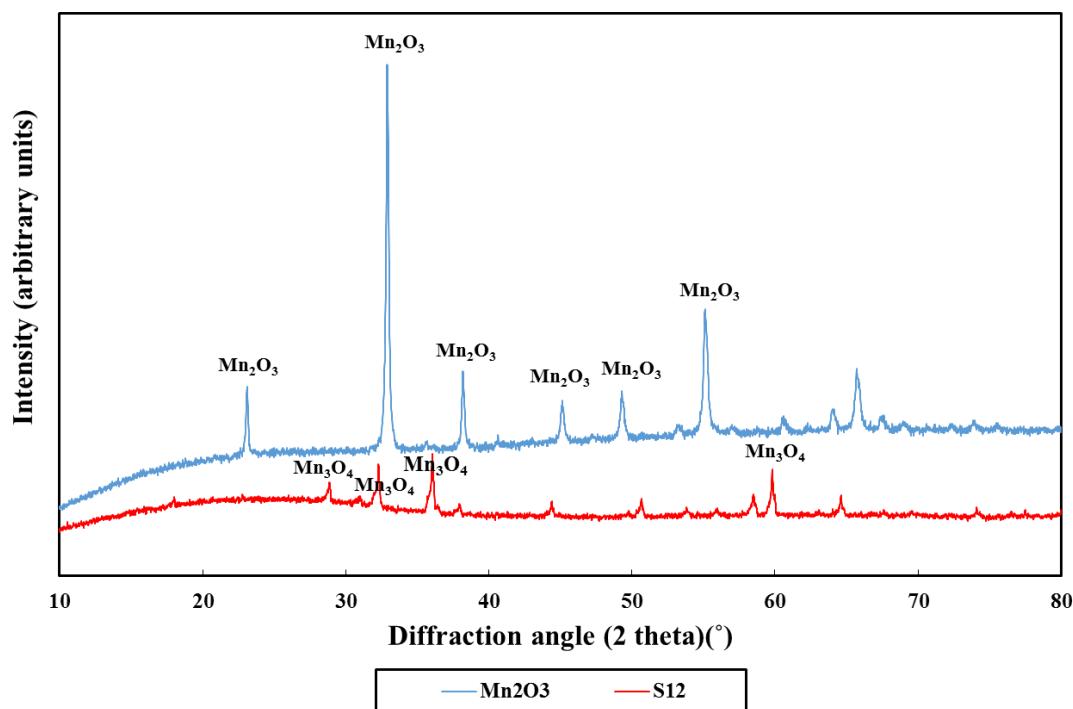
**Figure 3.8.** SEM micrograph of the Mn<sub>2</sub>O<sub>3</sub> (a) before and (b) after 10 successive RedOx cycles.

Figure 3.9 compares the oxidation of the sample at different partial pressure of oxygen for the temperature of 900°C. As shown, the rate of oxidation of the manganese oxide is only significant at this temperature for a partial pressure of 0.8 bar. This result can be matched with the phase stability of the manganese oxide reported above (Figure 3.1-c) (Grundy et al. 2003).



**Figure 3.9.** The oxidation of manganese oxide as a function time at a temperature of 900°C for different partial pressures of oxygen.

Figure 3.10 presents the XRD spectra of  $\text{Mn}_2\text{O}_3$  before and after 10 RedOx cycles. The figure confirm that the initial product was single-phase  $\text{Mn}_2\text{O}_3$  and that it was fully converted to the single-phase of  $\text{Mn}_3\text{O}_4$  during last cycle of reduction (Agrafiotis et al. 2016). This figure shows that the cycles measured with the TGA correspond to full conversion and are also consistent with the phase stability diagram.



**Figure 3.10.** The XRD spectra of  $\text{Mn}_2\text{O}_3$  before and after 10 successive RedOx cycles under conditions of S12, given in Table 3.2.

### 3.5.4 $\text{Pb}_3\text{O}_4/\text{PbO}$ cycle

Figure 3.11 presents the weight change of the  $\text{Pb}_3\text{O}_4$  at temperatures of  $500^\circ\text{C}$  and  $550^\circ\text{C}$ . In these experiments the  $P_{\text{O}_2}$  was set to 0.05 for the reduction and 0.8 bar for oxidation. As can be seen no change in the weight of samples was observed at  $500^\circ\text{C}$  even though the phase diagram (Figure 3.1-d) predicts that  $\text{Pb}_3\text{O}_4$  reduces to  $\text{PbO}$  under these conditions. This observed behavior can be plausibly explained by mass transfer limitations, although further work is needed to confirm this. For the case with a temperature of  $550^\circ\text{C}$ , it can be seen that  $\text{Pb}_3\text{O}_4$  is

partially reduced. Thus, the  $\text{Pb}_3\text{O}_4/\text{PbO}$  pair is not a suitable material for chemical storage under these conditions.

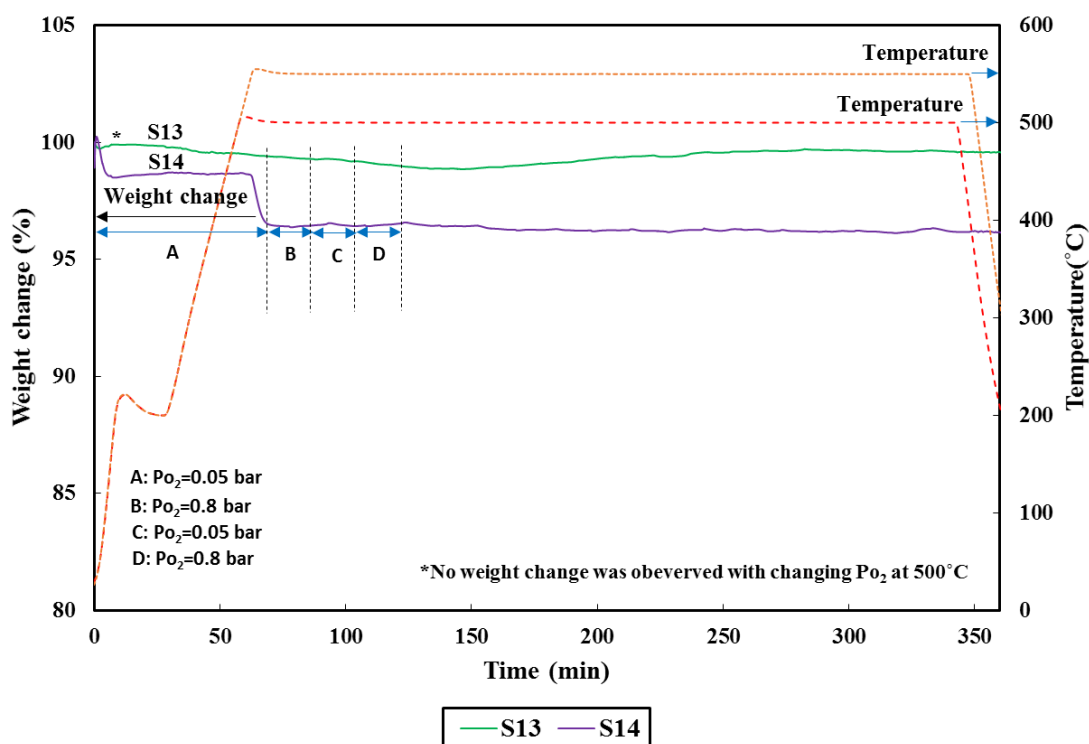


**Figure 3.11.** Weight change of  $\text{Pb}_3\text{O}_4/\text{PbO}$  as a function of time for 10 cycles at a constant temperature of 500°C and 550°C, as given in table 3.2.

Figure 3.12 presents the XRD spectra of the  $\text{Pb}_3\text{O}_4$  after 10 RedOx cycles at 500°C and 550°C. As can be seen,  $\text{Pb}_3\text{O}_4$  has not been converted to  $\text{PbO}$  at 500°C, while based on the phase diagram shown in Figure 3.1-d,  $\text{Pb}_3\text{O}_4$  has the potential to be reduced to  $\text{PbO}$  at 550°C and an oxygen partial pressure of 0.8 bar. This result confirms the TGA analysis of the  $\text{Pb}_3\text{O}_4$  at a temperature of 550°C.

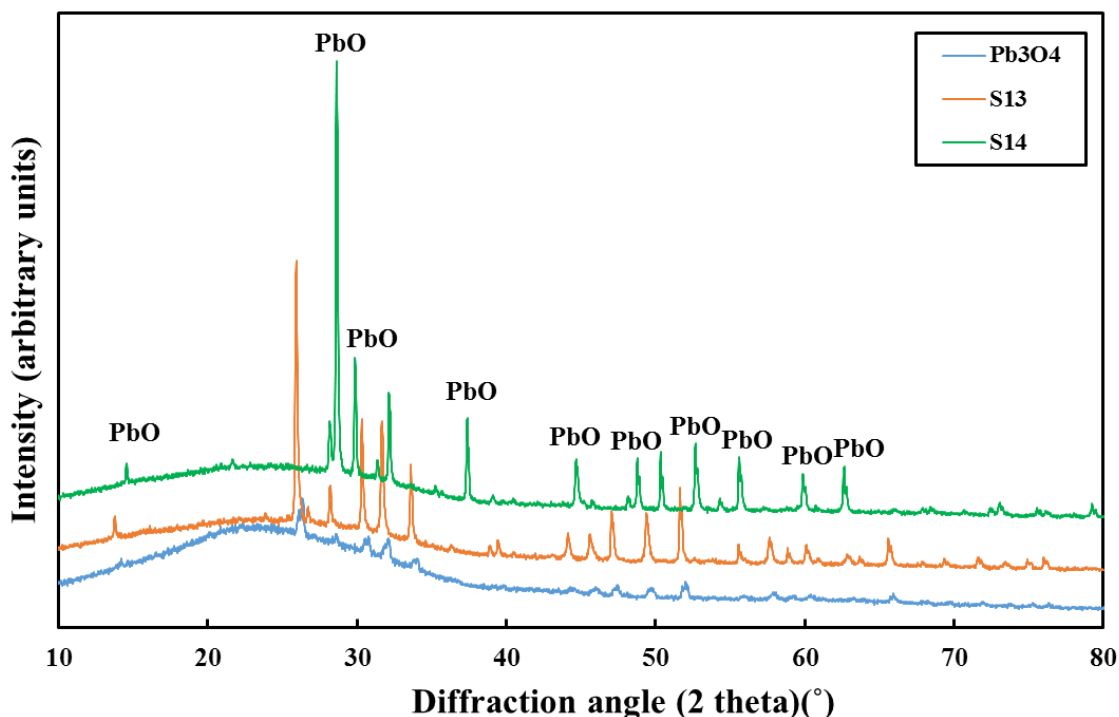


**Figure 3.12.** The XRD spectra of  $Pb_3O_4$  before and after 10 successive RedOx cycles under conditions of S13 and S14, given in table 3.2.

### 3.6 Conclusion

The potential of  $CuO/Cu_2O$ ,  $Co_3O_4/CoO$ ,  $Mn_2O_3/Mn_3O_4$ , and  $Pb_3O_4/PbO$  for reduction and oxidation reactions has been assessed with the use of a TGA. The result shows that  $CuO/Cu_2O$ ,  $Co_3O_4/CoO$  were highly reversible under isothermal pressure-swing cycles, while  $Mn_2O_3/Mn_3O_4$  exhibits slight signs of sintering. However, the pair  $Pb_3O_4/PbO$  did not show any potential for redox reaction under these conditions. The TGA result shows that complete reduction and oxidation reactions is 15 min for  $CuO/Cu_2O$ ,  $Co_3O_4/CoO$  and 30 min for  $Mn_2O_3/Mn_3O_4$ . This is significantly lower than the oxidation reaction in temperature swing system which is approximately at 3h. The result showed that the rate of oxidation increases with an increase in partial pressure of the oxygen from 0.2 bar to 0.8 bar. The maximum rate scales approximately linearly with partial pressure and can be increased from  $3.3\% \text{ min}^{-1}$  to  $9.3\% \text{ min}^{-1}$  for  $CuO/Cu_2O$  pair with an increase in partial pressure from 0.2 bar to 0.8 bar, respectively. The corresponding values for  $Co_3O_4/CoO$  are  $0.89\% \text{ min}^{-1}$  and  $5.3\% \text{ min}^{-1}$  for oxygen partial

pressures of 0.2 bar and 0.8 bar. The XRD analysis of these materials confirmed the full conversion of higher oxidation state to lower oxidation states during RedOx reaction. It can be concluded that the pair of CuO/Cu<sub>2</sub>O, Co<sub>3</sub>O<sub>4</sub>/CoO, Mn<sub>2</sub>O<sub>3</sub>/Mn<sub>3</sub>O<sub>4</sub> exhibit good potential for thermochemical energy storage through changing the partial pressure of oxygen.

### 3.7 References

C. Agrafiotis, A. Becker, M. Roeb & C. Sattler 2016, 'Exploitation of thermochemical cycles based on solid oxide redox systems for thermochemical storage of solar heat. Part 5: Testing of porous ceramic honeycomb and foam cascades based on cobalt and manganese oxides for hybrid sensible/thermochemical heat storage', *Solar energy*, vol. **139**. pp. 676-694.

C. Agrafiotis, M. Roeb & C. Sattler 2016, 'Exploitation of thermochemical cycles based on solid oxide redox systems for thermochemical storage of solar heat. Part 4: Screening of oxides for use in cascaded thermochemical storage concepts', *Solar energy*, vol. **139**. pp. 695-710.

C. Agrafiotis, M. Roeb, M. Schmücker & C. Sattler 2014, 'Exploitation of thermochemical cycles based on solid oxide redox systems for thermochemical storage of solar heat. Part 1: Testing of cobalt oxide-based powders', *Solar energy*, vol. **102**. pp. 189-211.

C. Agrafiotis, M. Roeb, M. Schmücker & C. Sattler 2015, 'Exploitation of thermochemical cycles based on solid oxide redox systems for thermochemical storage of solar heat. Part 2: Redox oxide-coated porous ceramic structures as integrated thermochemical reactors/heat exchangers', *Solar energy*, vol. **114**. Supplement C, pp. 440-458.

E. Alonso, C. Pérez-Rábago, J. Licurgo, E. Fuentealba & C. A. Estrada 2015, 'First experimental studies of solar redox reactions of copper oxides for thermochemical energy storage', *Solar energy*, vol. **115**. pp. 297-305.

L. André, S. Abanades & G. Flamant 2016, 'Screening of thermochemical systems based on solid-gas reversible reactions for high temperature solar thermal energy storage', *Renewable and Sustainable Energy Reviews*, vol. **64**. pp. 703-715.

B. Wong 2011, *Thermochemical heat storage for concentrated solar power, final report for the U.S. Department of Energy*, Department of Energy, San Diego, CA, USA.

A. Bayon, R. Bader, M. Jafarian, L. Fedunik-Hofman, Y. Sun, J. Hinkley, S. Miller & W. Lipiński 2018, 'Techno-economic assessment of solid-gas thermochemical energy storage systems for solar thermal power applications', *Energy*, vol. **149**. pp. 473-484.

T. Block & M. Schmücker 2016, 'Metal oxides for thermochemical energy storage: A comparison of several metal oxide systems', *Solar energy*, vol. **126**. pp. 195-207.



A. J. Carrillo, J. Moya, A. Bayón, P. Jana, V. A. de la Peña O'Shea, M. Romero, J. Gonzalez-Aguilar, D. P. Serrano, P. Pizarro & J. M. Coronado 2014, 'Thermochemical energy storage at high temperature via redox cycles of Mn and Co oxides: Pure oxides versus mixed ones', *Solar Energy Materials and Solar Cells*, vol. **123**. pp. 47-57.

A. J. Carrillo, D. P. Serrano, P. Pizarro & J. M. Coronado 2014, 'Thermochemical heat storage based on the  $Mn_2O_3/Mn_3O_4$  redox couple: influence of the initial particle size on the morphological evolution and cyclability', *Journal of Materials Chemistry A*, vol. **2**. 45, pp. 19435-19443.

D. Chadda, J. D. Ford & M. Fahim 1989, 'Chemical energy storage by the reaction cycle  $CuO/Cu_2O$ ', *International Journal of Energy Research*, vol. **13**. 1, pp. 63-73.

M. Chen, B. Hallstedt & L. J. Gauckler 2003, 'Thermodynamic assessment of the Co-O system', *Journal of Phase Equilibria*, vol. **24**. 3, pp. 212-227.

M. Deutsch, F. Horvath, C. Knoll, D. Lager, C. Gierl-Mayer, P. Weinberger & F. Winter 2017, 'High-Temperature Energy Storage: Kinetic Investigations of the  $CuO/Cu_2O$  Reaction Cycle', *Energy & Fuels*, vol. **31**. 3, pp. 2324-2334.

A. Gil, M. Medrano, I. Martorell, A. Lázaro, P. Dolado, B. Zalba & L. F. Cabeza 2010, 'State of the art on high temperature thermal energy storage for power generation. Part 1: Concepts, materials and modellization', *Renewable and Sustainable Energy Reviews*, vol. **14**. 1, pp. 31-55.

A. N. Grundy, B. Hallstedt & L. J. Gauckler 2003, 'Assessment of the Mn-O system', *Journal of Phase Equilibria*, vol. **24**. 1, pp. 21-39.

B. Hallstedt, D. Risold & L. J. Gauckler 1994, 'Thermodynamic assessment of the copper-oxygen system', *Journal of Phase Equilibria*, vol. **15**. 5, pp. 483-499.

K. N. Hutchings, M. Wilson, P. A. Larsen & R. A. Cutler 2006, 'Kinetic and thermodynamic considerations for oxygen absorption/desorption using cobalt oxide', *Solid State Ionics*, vol. **177**. 1, pp. 45-51.

L. Irwin, J. Stekli, C. Pfefferkorn & R. Pitchumani 2017, '11 - Thermochemical energy storage for concentrating solar thermal (CST) systems', *Advances in Concentrating Solar Thermal Research and Technology*, Woodhead Publishing, pp. 247-267.

G. Karagiannakis, C. Pagkoura, A. Zygogianni, S. Lorentzou & A. G. Konstandopoulos 2014, 'Monolithic Ceramic Redox Materials for Thermochemical Heat Storage Applications in CSP Plants', *Energy Procedia*, vol. **49**. Supplement C, pp. 820-829.

---

M. Kim, W. S. Son, K. H. Ahn, D. S. Kim, H. s. Lee & Y. W. Lee 2014, 'Hydrothermal synthesis of metal nanoparticles using glycerol as a reducing agent', *The Journal of Supercritical Fluids*, vol. **90**. Supplement C, pp. 53-59.

S. Kuravi, J. Trahan, D. Y. Goswami, M. M. Rahman & E. K. Stefanakos 2013, 'Thermal energy storage technologies and systems for concentrating solar power plants', *Progress in energy and combustion science*, vol. **39**. 4, pp. 285-319.

D. Müller, C. Knoll, W. Artner, M. Harasek, C. Gierl-Mayer, J. M. Welch, A. Werner & P. Weinberger 2017, 'Combining in-situ X-ray diffraction with thermogravimetry and differential scanning calorimetry – An investigation of Co<sub>3</sub>O<sub>4</sub>, MnO<sub>2</sub> and PbO<sub>2</sub> for thermochemical energy storage', *Solar energy*, vol. **153**. pp. 11-24.

A. P. Muroyama, A. J. Schrader & P. G. Loutzenhiser 2015, 'Solar electricity via an Air Brayton cycle with an integrated two-step thermochemical cycle for heat storage based on Co<sub>3</sub>O<sub>4</sub>/CoO redox reactions II: Kinetic analyses', *Solar energy*, vol. **122**. pp. 409-418.

M. Neises, S. Tescari, L. de Oliveira, M. Roeb, C. Sattler & B. Wong 2012, 'Solar-heated rotary kiln for thermochemical energy storage', *Solar energy*, vol. **86**. 10, pp. 3040-3048.

D. Risold, J.-I. Nagata & R. Suzuki 1998, 'Thermodynamic description of the Pb-O system', *Journal of Phase Equilibria*, vol. **19**. 3, pp. 213-233.

D. Shishin & S. A. Decterov 2012, 'Critical assessment and thermodynamic modeling of the Cu–O and Cu–O–S systems', *Calphad*, vol. **38**. pp. 59-70.

M. Silakhori, M. Jafarian, M. Arjomandi & G. J. Nathan 2017, 'Comparing the thermodynamic potential of alternative liquid metal oxides for the storage of solar thermal energy', *Solar energy*, vol. **157**. pp. 251-258.

B. Wong, L. Brown, F. Schaube, R. Tamme & C. Sattler 2010, 'Oxide based thermochemical heat storage', in *Proceedings of the 16th SolarPACES Conference, Perpignan, France*, pp. 21-24.

C. H. Wu 2012, 'Low Energy-Consumption Industrial Production of Ultra-Fine Spherical Cobalt Powders', *Energy Conservation, InTech*, Rijeka, p. Ch. 06.

S. Wu, C. Zhou, E. Doroodchi, R. Nellore & B. Moghtaderi 2018, 'A review on high-temperature thermochemical energy storage based on metal oxides redox cycle', *Energy Conversion and Management*, vol. **168**. pp. 421-453.

M. Silakhori, M. Jafarian, M. Arjomandi & G. J. Nathan 2019, 'The energetic performance of a liquid chemical looping cycle with solar thermal energy storage', *Energy*, vol. 170. pp. 93-101.

## **Chapter 4 Thermodynamic potential of alternative metal oxides for liquid chemical looping for storage of solar thermal energy**

---

### **4.1 Chapter preview**

In this chapter, thermodynamic potential of 23 metal oxides is assessed in liquid chemical looping for thermal energy storage (LCL-TES) system. The LCL-TES system has the potential to store and release sensible, latent and thermochemical heat in a cycle of heating and cooling cycle. Therefore, different thermodynamic criteria such as melting temperature, reaction temperature, Gibbs free energy, and vapour pressure of the metal oxide are important parameters for selecting suitable material in a LCL-TES system. Moreover, chemical reaction and melting temperature of metal oxide at different partial pressure can be identified by phase diagram of the material.

The details of the methodology, and supporting data for comparing different metal oxides in LCL-TES are presented and explained in the following section of this chapter. This section is published in the Journal of Solar Energy and permission to reproduce the article has been obtained from the publishing authority.

# Statement of Authorship

Title of Paper	Comparing the thermodynamic potential of alternative liquid metal oxides for the storage of solar thermal energy
Publication Status	<input checked="" type="checkbox"/> Published <input type="checkbox"/> Accepted for Publication <input type="checkbox"/> Submitted for Publication Unpublished and Unsubmitted work written in manuscript style
Publication Details	Mahyar Silakhori, Mehdi Jafarian, Maziar Arjomandi, Graham J. Nathan, Comparing the thermodynamic potential of alternative liquid metal oxides for the storage of solar thermal energy (Solar Energy, vol. 157. pp. 251-258)

## Principal Author

Name of Principal Author (Candidate)	Mahyar Silakhori		
Contribution to the Paper	<ul style="list-style-type: none"> <li>- Research, collecting and analysing data from different resources</li> <li>- Providing the data, writing of the manuscript and production of original figures</li> <li>- Correspondence with editor and reviewers including the production of all cover letters and rejoinder</li> </ul>		
Overall percentage (%)	75%		
Certification:	This paper reports on original research I conducted during the period of my Higher Degree by Research candidature and is not subject to any obligations or contractual agreements with a third party that would constrain its inclusion in this thesis. I am the		
Signature	_____	Date	04.02.2019

## Co-Author Contributions

By signing the Statement of Authorship, each author certifies that:

- iv. the candidate's stated contribution to the publication is accurate (as detailed above);
- v. permission is granted for the candidate to include the publication in the thesis; and
- vi. the sum of all co-author contributions is equal to 100% less the candidate's stated contribution.

Name of Co-Author	Mehdi Jafarin		
Contribution to the Paper	<ul style="list-style-type: none"> <li>- Supervision of the work, including the production of the manuscript</li> <li>- Participation in the development of the concepts and ideas presented in the manuscript</li> <li>- Evaluation and editing of the manuscript prior to submission</li> </ul>		
Signature	_____	Date	04/2/2019.

Name of Co-Author	Maziar Arjomandi			
Contribution to the Paper	- Supervision of the work, including the production of the manuscript - Participation in the development of the concepts and ideas presented in the manuscript - Evaluation and editing of the manuscript prior to submission			
Signature	<table border="1"><tr><td></td><td>Date</td><td>4/02/2019</td></tr></table>		Date	4/02/2019
	Date	4/02/2019		

Name of Co-Author	Graham 'Gus' Nathan			
Contribution to the Paper	- Supervision of the work, including the production of the manuscript - Participation in the development of the concepts and ideas presented in the manuscript - Evaluation and editing of the manuscript prior to submission			
Signature	<table border="1"><tr><td></td><td>Date</td><td>4/2/19.</td></tr></table>		Date	4/2/19.
	Date	4/2/19.		

**Comparing the thermodynamic potential of alternative liquid metal oxides for the storage of solar thermal energy**

**Mahyar Silakhori**, Mehdi Jafarian, Maziar Arjomandi, Graham J. Nathan

Published: Journal of Solar Energy, vol. 157. pp. 251-258.

## 4.2 Abstract

The relative potential of liquid multivalent metal oxides for the storage of thermal energy as sensible, latent and/or thermochemical storage energy in a liquid chemical looping thermal energy storage (LCL-TES) is reported. This LCL-TES cycle comprises a reduction reactor, an oxidation reactor, two reservoirs for storing the hot and cold medium and a heat recovery unit. The materials were assessed on the basis of their melting temperature, Gibbs free energy, reaction temperature and thermal storage capacity. Ellingham diagrams were used to identify regimes with a potential for application in a LCL-TES, while phase diagrams were used to identify processes which combine sensible, latent and thermochemical heat storage. Based on these criteria, the oxide of CuO/Cu<sub>2</sub>O was found to have the greatest thermodynamic potential for use in a LCL-TES system with a total enthalpy of 404.67 kJ/mol for thermal storage. However, the high temperature of ~1200°C and corrosive nature of molten copper and its oxides will make this cycle challenging to implement. Lead, on the other hand has a lower total enthalpy of 250.09 kJ/mol, but is molten at lower temperatures.

## 4.3 Introduction

Concentrated solar thermal (CST) power has received great attention due to its compatibility with thermal energy storage, which enables management of the variability of solar radiation at relatively low cost (Kuravi et al. 2013; Pacio et al. 2013; Pacio & Wetzel. 2013). Moreover, CST has many similar generation characteristics to conventional fossil and nuclear power generation, but with very low emissions of pollutants. The current state-of-the-art technology employed for the storage of solar thermal energy uses molten salt as a storage medium. However, the decomposition of molten salt limits the upper temperature of this technology to temperatures of typically below 600°C. Although this temperature is suitable for a steam Rankine cycle with a thermodynamic efficiency of approximately 35% (Wong 2011; Gil et al.

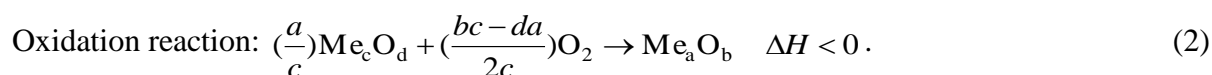
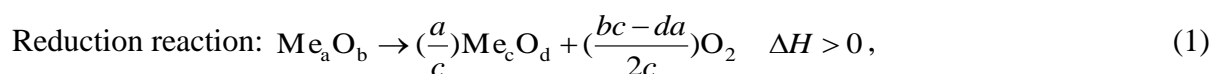


2010), it is desirable to achieve higher temperatures that offer higher efficiency. To achieve cycle temperature greater than 600°C requires the development of new receivers, heat transfer fluids and storage media. Therefore, it is important to evaluate the potential of other materials that can absorb and store energy at higher temperatures. The objective of this paper is to explore the performance of novel materials with potential to meet this need.

The three main types of thermal energy storage (TES) are sensible, latent and thermochemical heat storage (Gil et al. 2010). These are not necessarily mutually exclusive but have the potential to be combined together. At present, sensible heat storage using molten salts is the most developed storage medium (Gil et al. 2010; Kolb 1998; Kuravi et al. 2013; Price 2003; Price et al. 2002; Robak et al. 2011; Yang & Garimella 2010; Zhang et al. 2013). Molten salts operate in a broad temperature range between their melting point, which is typically around 200°C, and their stability limit of approximately 600°C. The relatively high melting temperature of molten salts results in a significant risk of solidification, which may lead to the failure of the system (Kearney et al. 2003). The need to avoid solidification is typically managed with the use of trace heating, which constitutes a significant parasitic energy loss. To avoid these challenges, liquid sodium with a melting temperature of around 98°C has been proposed as an alternative heat transfer fluid and tested for a solar thermal power plant at de Almeria (Spain) (Schiel & Geyer 1988). While sodium has excellent thermal and hydraulic performances, its implementation has been delayed at an industry scale at the de Almeria CSP plant due to its increased safety risk (Coventry et al. 2015). Nevertheless, Sodium has since been used successfully in a solar thermal plant at Jemalong in Australia (Coventry et al. 2015). There have also been some attempts to use other liquid metals such as Lead-Bismuth and molten tin for sensible heat storage (Pacio et al. 2013). However, the low heat capacity of liquid metals in comparison to molten salts is a potential disadvantage of using these materials for sensible thermal energy storage alone.

Another method to store energy is via latent TES which stores the energy within the phase change of a material. A number of materials have been proposed previously for latent TES, such as NaCl (Mehling & Cabeza 2007),  $\text{Li}_2\text{CO}_3$  (Kuravi et al. 2013),  $\text{MgCl}_2$  (Gil et al. 2010), LiF (Mehling & Cabeza 2007),  $\text{NaCO}_3\text{-BaCO}_3/\text{MgO}$  (Gil et al. 2010). These offer charge and discharge at a constant temperature and a greater energy density than sensible heat. However, the change in their volume during the charge and discharge processes, together with their low thermal conductivity have, thus far, limited their implementation. Nevertheless, a number of methods are being proposed to overcome these challenges (Naghavi et al. 2015; Silakhori et al. 2015; Silakhori et al. 2014).

Thermochemical energy storage is being investigated because it offers an energy density of up to fifteen times higher than sensible heat storage and six times higher than latent heat storage for several types of materials (Abedin & Rosen 2011). Like latent heat it also enables the heat to be stored and recovered at a similar temperature (Nagel et al. 2013), but thermochemical energy system is yet to be developed at a commercially level. The cyclic reduction and oxidation (Red-Ox) of metal oxides has been identified as a promising concept for thermochemical energy storage at a temperature range of 350-1100°C (Pardo et al. 2014; Wong et al. 2010). The general reactions for metal oxides used for thermochemical storage are:



Several metals and metal oxides have been considered for the application in thermochemical energy storage. The oxide of  $\text{BaO}_2/\text{BaO}$  was first investigated by Fahim et al. (Fahim & Ford 1983). This reaction occurs at temperatures between 400 and 1027°C for partial oxygen pressures of between 0 and 10bar. They demonstrated that complete conversion was inhibited by mass transfer limitations and crusting of the material surface (Bowrey & Jutsen 1978). A

recent study of sixteen oxides by Wong et al. (Wong et al. 2010), found that only  $\text{BaO}_2$ ,  $\text{Co}_3\text{O}_4$ ,  $\text{Mn}_2\text{O}_3$ ,  $\text{CuO}$ ,  $\text{Fe}_2\text{O}_3$ , and  $\text{Mn}_3\text{O}_4$  exhibit suitable performance as TCS materials. Of these,  $\text{Co}_3\text{O}_4$  was found to yield the best performance in terms of reversibility and energy storage density, although the consecutive cycling between the temperatures of  $850^\circ\text{C}$  and  $950^\circ\text{C}$  for oxidation and reduction, respectively, decreases the isentropic efficiency of TES process due to exergy destruction (Block et al. 2014). In addition, the application of solid metal oxides is presently limited to an operating temperature of approximately  $1000^\circ\text{C}$  (Adanez et al. 2012; Haseli et al. 2017) because of the technical challenges associated with the sintering, softening, agglomeration of solid metal oxide in RedOx reaction. This temperature is significantly lower than the state-of-the-art in commercially available gas turbines which are currently around  $1250^\circ\text{C}$  (Bhargava et al. 2007; Hunt 2010) and potentially will reach up to  $1700^\circ\text{C}$  in the future (Chyu 2012). For these reasons, considerable effort has been invested to identify materials enabling operating temperatures of more than  $1000^\circ\text{C}$ . Furthermore, liquid metal oxides have also been proposed as an alternative solution to solid metal oxide systems (Jafarian et al. 2017). Liquid chemical looping thermal energy storage (LCL-TES) system is a newly proposed technology based on the use of liquid metal oxides at a high temperature for both thermal energy storage and as a heat transfer medium to improve the overall efficiency of the system (Jafarian et al. 2017). The validity of the process as a potential storage medium has been assessed thermodynamically, but only for copper oxide. Therefore, there is a need to assess the potential of other metal oxides in a LCL-TES system. Moreover, the parameters that best describe the performance of a LCL-TES system are yet to be identified.

For the reasons outlined above, the objective of the present investigation is to compare the thermodynamic feasibility of alternative metal oxides for the application in a LCL-TES system for power generation using a gas turbine combined cycle, which requires the hot gas to be delivered at a high temperature and pressure. The LCL-TES system can alternatively be used

to supply required heat to a high temperature process such as mineral processing application. In so doing, it is recognized that the thermodynamic potential does not necessarily imply technical or economic feasibility, but is rather a necessary pre-requisite to the further work that would be required to develop and implement such a process. More specifically, the aim of this work is to compare the performance of different metal oxides in a LCL-TES system based on their melting temperature, Gibbs free energy, reaction temperature, phase diagram, and vapour pressure.

## **4.4 Methodology**

### **4.4.1 LCL-TES system**

Figure 4.1 presents a schematic diagram of the LCL-TES proposed by Jafarian et al. (Jafarian et al. 2017). The LCL-TES system consists of one reduction and one oxidation reactors, two reservoirs for the storage of hot molten metal oxide and cold particles, and a heat recovery unit. Sensible, latent and thermochemical storage occur in the reduction reactor, driven by solar radiation and changes to the partial pressure of oxygen generated by the injection of steam. The cycle is assessed for the cases in which steam is used as the inert gas in the solar reduction reactor to lower the partial pressure of  $O_2$ , and hence to lower temperature of reduction and storage. Steam is chosen because the  $O_2$  product, can be readily separated from the steam using a condensation process. One plausible configuration for the solar particle-to-liquid reduction reactor with which to achieve the sensible heating, melting and reduction reaction steps is based on a modified rotary kiln directly heated by solar energy (Funken et al. 2001), in which steam injection is used to lower the partial pressure in the reactor. Another possible device to be further developed and adapt is the solar vortex reactor of Z'Graggen et al. (Z'Graggen et al. 2006), which has already been demonstrated for heating reacting particle to  $1300^\circ\text{C}$ , to enable it to also achieve melting of the particles.

The reduced metal oxide is then conveyed to the hot storage tank (stream 2), before being transferred to the oxidation reactor as a liquid (stream 3) to generate hot vitiated air. A bubble reactor is a plausible configuration of oxidation reactor, since it can be designed to achieve high rates of both heat and mass transfer (Shah et al. 1982). Further heat recovery unit (stream 4) is thermodynamically possible through cooling and solidification of the molten metal oxide. However, to achieve this would require reliable operation of a solid quenching oxidation reactor to simultaneously oxidise and solidify the molten metal in the heat recovery system heat (Jafarian et al. 2017). This could plausibly be achieved by “atomisation” of the molten metals into droplets within a quenching air stream. While a device to achieve all of these steps is not yet available to our knowledge, closely related systems are available for heat recovery from slag metals (Barati et al. 2011; Pickering et al. 1985). These include a rotary cylinder slag atomiser, a spinning disk slag atomiser, and a rotary cup slag atomiser (Kashiwaya et al. 2010; Pickering et al. 1985), all of which recover sensible heat from the slag. To also recover latent and thermochemical heat would require sufficient residence time relative to the droplet size to solidify and oxidise the particles. However, the size of the droplets can be controlled, for example by changing the rotation speed of the rotary atomiser while the residence time can be extended by increasing the size of the reactor, or by introducing a swirl. Further development would also be required to manage the distributions of temperature and oxygen concentration within such a reactor. However, the understanding to achieve this is similar that already widely employed for the combustion of liquid fuels. Hence, while the development of a suitable quenching reactor is beyond the scope of the present investigation, it is also plausible task. Here we only assess whether such development can be justified on the basis of demonstrating sufficient thermodynamic potential from the cycle.

As shown in Figure 4.1, the hot air leaving the oxidation reactor is assessed here for the application in a power generation system (stream 7), while the cold metal oxide particles are

---

conveyed to the cold storage tank (Stream 8) (Jafarian et al. 2017). In this way the proposed system offers potential for the storage of energy in all three forms of sensible, latent and thermochemical heat.

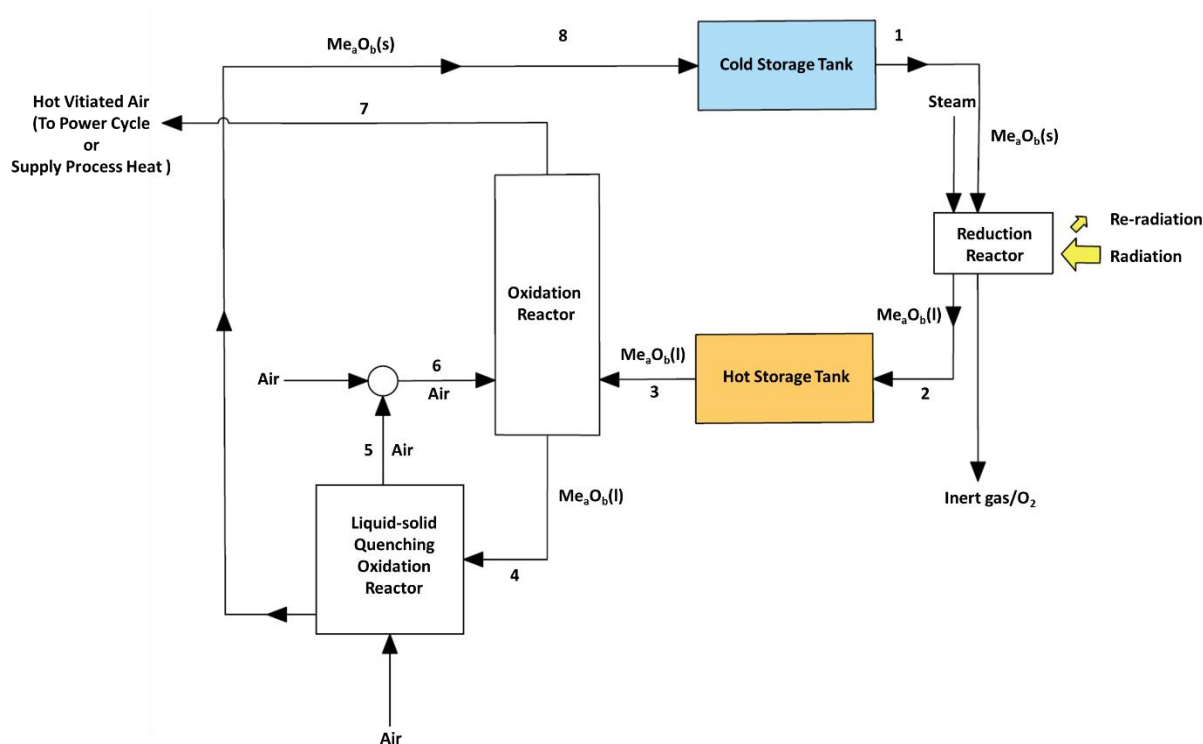


**Figure 4.1.** Schematic representation of the key components of the proposed LCL-TES system assessed here for the liquid chemical looping with thermal energy storage of solar thermal energy as sensible, latent, and thermochemical heat and for co-production of pressurized air and oxygen. A cold storage reservoir and a hot storage tank are proposed for the storage of the cold solid metal oxide particles and the hot liquid metal oxide, respectively. The hot vitiated gas can be used for a power generation at pressure of 5 to 30 bar or process heat. The figure is adopted from Jafarian et al. (Jafarian et al. 2017).

#### 4.4.2 Operating temperature of the LCL-TES

In this work the materials with a potential for application in a LCL-TES system at an operating temperature of up to 1400°C is considered, because this temperature is close to the temperature that has been achieved in the directly irradiated vortex reactor reported by Z'Graggen et al. (Z'Graggen et al. 2006), and also it matches the state-of-the art of the inlet temperature of a gas turbine. In addition, a special attention is paid to the materials that can operate at a temperature below 1000°C, since these enable the possibility of indirect heat transfer using commercially available steel tubes (Tian & Zhao 2013), and offer lower re-radiation losses.

#### 4.4.3 Red-Ox reaction in a LCL-TES system

The Gibbs free energy of the chemical reactions in a LCL-TES system is required to be negative for Red-Ox reaction to be spontaneous (Moghtaderi 2009). The Gibbs free energy ( $\Delta G$ ) for the endothermic reduction reaction of  $Me_aO_b$  to  $M_eO_d$  (Eq.1) is described by equation 3:

$$\Delta G( Me_aO_b ) = \left( \frac{bc-da}{2c} \right) \cdot \Delta G_{products} - \left( \frac{a}{c} \right) \cdot \Delta G_{reactants} \quad (3)$$

The value of  $\Delta G$  was calculated here with HSC chemistry software (Roine 2002) and presented as an Ellingham diagram, which plots  $\Delta G$  as a function of temperature. The slope of the line in Ellingham diagram changes with variation in material phases.

#### 4.4.4 Vapour pressure of LCL-TES materials

The vapour pressure of the metal oxides at high temperatures was also assessed because the effect of volatility of the metal oxides on the lifetimes of components such as valves and turbine blades. This was also calculated using the HSC chemistry database (Roine 2002).

#### 4.4.5 Phase diagram of metal oxides

Phase diagrams of the selected metal oxides were used to identify the potential of the materials for sensible, latent and thermochemical heat storage. This revealed the temperature and partial pressure at which a change in material state occurs, together with the mole fraction of oxygen.

#### 4.4.6 Enthalpy of LCL-TES materials

The enthalpies of sensible, latent and thermochemical heat were calculated with Eq. 4, 5 and 6, respectively. Here,  $\Delta H_i^f(T)$  is the formation enthalpy of component  $i$  in the product and reaction at a temperature of  $T$  (Ihsan 1995). The positive and negative values of  $\Delta H_{red,r}$  correspond to the endothermic and exothermic reactions, respectively.

$$\Delta H_{sen} = \rho C_p \Delta T , \quad (4)$$

$$\Delta H_{lat} = mL , \quad (5)$$

$$\Delta H_{chem} = \sum_{Product} \Delta H_i^f(T) - \sum_{Reactant} \Delta H_i^f(T) = \left( \frac{a}{c} \Delta H_{Me_c O_d}^f(T) + \frac{bc-da}{2c} \Delta H_{O_2}^f(T) \right) - (\Delta H_{Me_a O_b}^f(T)), \quad (6)$$

The total enthalpy of the system can be calculated with Eq. (7)

$$\Delta H_{total} = \Delta H_{sen} + \Delta H_{lat} + \Delta H_{chem}. \quad (7)$$

The chemical energy density of metal oxides can be calculated by Eq.(8) where,  $X_{red}$ ,  $\rho_{Me_a O_b}$ ,  $M_{Me_a O_b}$  and  $\Delta H_{red,r}$  are the conversion fraction, density, molecular weight and the enthalpy of the chemical reaction of the metal oxide, respectively.

$$\rho_{chem} = \frac{X_{red} \rho_{Me_a O_b} \Delta H_{red,r}}{M_{w, Me_a O_b}} \quad (8)$$

It is worth mentioning that the extent of oxidation can be controlled by changing the partial pressure of the oxygen in system. Decreasing the partial pressure of oxygen increases the extent of conversion of the chemical reaction ( $X_{red}$ ) and increases the chemical energy density.

## 4.5 Results and discussion

### 4.5.1 Melting temperature

The melting temperature of twenty-two metals and their oxides is presented in Figure 4.2. It can be seen that the melting temperature of the higher oxidation state of Sb, Pb, Mn, Ba and Cu oxides is less than 1400°C, which is within the range of interest. However, the oxides of Pb, Sb and Ba are more favourable for thermal energy storage than Cu and Mn oxides because of their lower melting temperature. Figure 4.2, also shows that the oxides of Pb, Ba and Sb have melting temperatures lower than 1000°C, which is within the operating temperature range of indirect solar receivers and the oxides of Cu and Mn have potential application if a direct solar receiver made of material with higher melting temperature than 1000°C is used. Hence, the oxides of Pb, Ba, Sb, Cu and Mn were selected for further assessment.



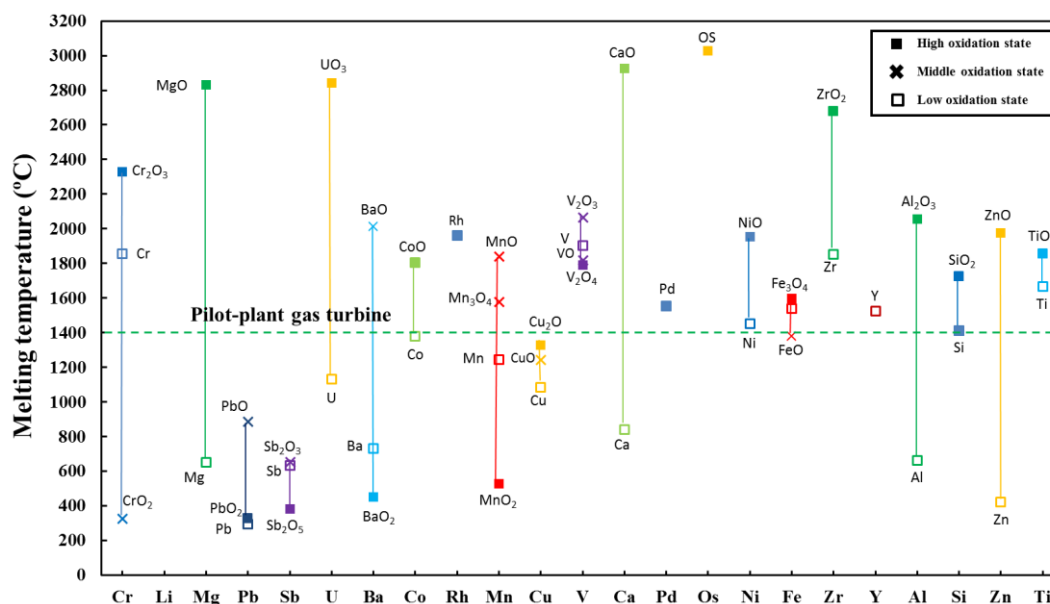


**Figure 4.2.** Comparison of the melting temperature of different metal oxides with their various oxidation states; also shown is the reference temperature is 1400°C which is the inlet temperature of current gas turbines.

#### 4.5.2 Ellingham diagram

The Ellingham diagram of the selected metal oxides is shown in Figure 4.3 as a function of temperature at an oxygen partial pressure of 0.21 bar. It can be seen that the oxides of Cu, Mn, Pb, Ba and Sb have a tendency for  $\Delta G$  to decrease with an increase in temperature. It can also be seen that the value of  $\Delta G$  at the range of temperatures considered for the LCL- TES system is positive for the reactions of PbO/Pb, MnO<sub>2</sub>/Mn, and BaO<sub>2</sub>/Ba, which means that these reactions are not suitable for a LCL- TES system even at higher temperatures of up to 1400°C. Therefore, these metals are not considered in further assessment process. The figure also reveals the reaction temperatures at which the value of  $\Delta G$  is equal to zero. This temperature is approximately 1200°C and 460°C for CuO to Cu<sub>2</sub>O and Pb<sub>3</sub>O<sub>4</sub> to PbO, respectively. The slope of the Ellingham diagram can also be used to identify the melting temperature of the metal oxides. For example, PbO, exhibits a change in slope at around 900°C, which is in agreement with the melting temperature of the PbO in Figure 4.2. The Ellingham diagram also reveals whether a given metal oxide system is reduced or oxidized when the temperature increases (Shah et al. 2012), although it does not include any information about the rate of the

reaction. Also, the extent of the reaction scales with the magnitude of  $\Delta G$ , both negative (for reduction) and positive (for oxidation) (Moghtaderi 2009). Therefore, the oxides of Pb ( $\text{Pb}_3\text{O}_4/\text{PbO}$ ) and Sb ( $\text{Sb}_2\text{O}_5/\text{Sb}_2\text{O}_3$ ) are more likely to reduce fully than the oxides of Cu ( $\text{CuO}/\text{Cu}_2\text{O}$ ). For this reason, the oxides of Pb, Sb and Cu oxides are selected for further analysis of the potential application in a LCL-TES system based on the Gibb free energy.

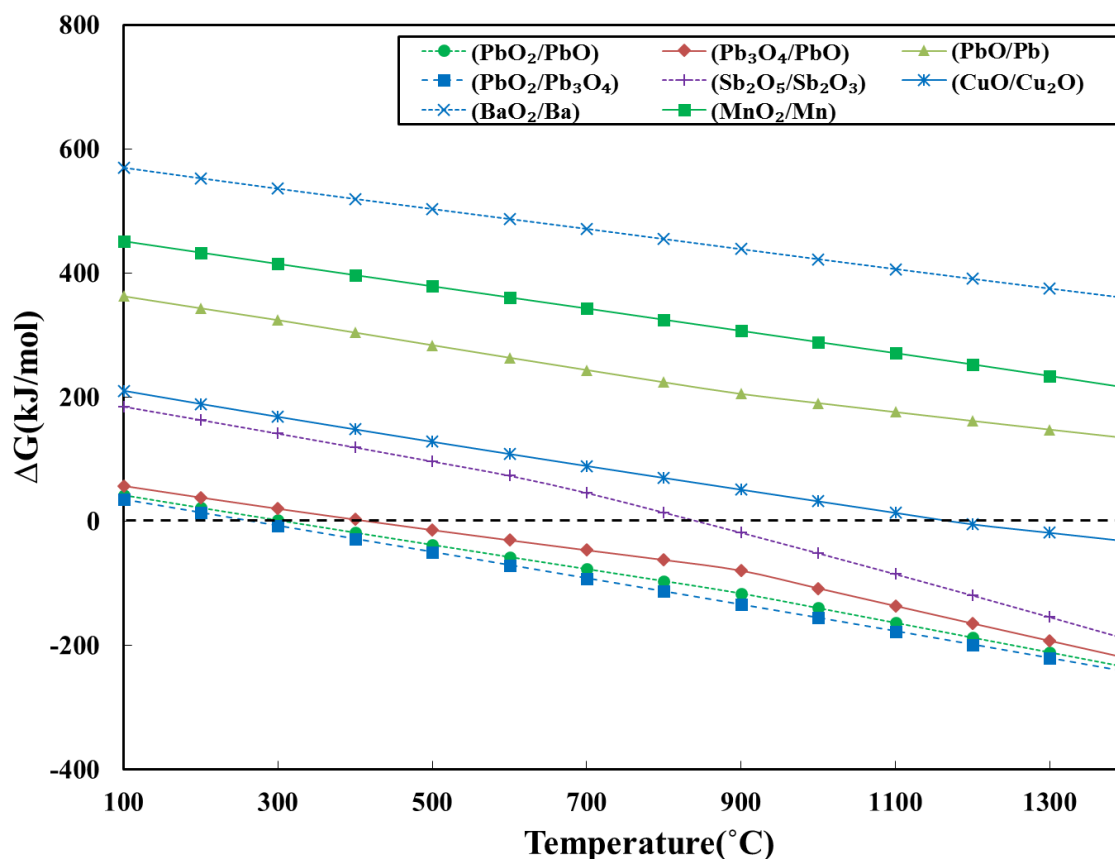


**Figure 4.3.** Ellingham diagram of the selected reactants on the basis of one mole of diatomic oxygen ( $\text{O}_2$ ) as a function of temperature at an atmospheric pressure. A negative value of  $\Delta G$  means that the reaction is spontaneous, while a change in slope implies a phase change.

#### 4.5.3 Vapour pressure of selected metal oxides

Figure 4.4 presents the vapour pressure of the selected metals as a function of temperature. It can be seen that the vapour pressure of Cu and Sb is lower than that of Pb oxides. This is beneficial not only reduce the need for make-up pressure due to the loss in vapour phase, but also to minimise the potential of deposition onto the turbine blades. Also of relevance, the boiling temperature for Cu and CuO at an atmospheric pressure is high at  $2570^\circ\text{C}$  and  $2760^\circ\text{C}$ ,

respectively (Lamoreaux & Hildenbrand 1984; Lide & Kehiaian 1994). It is still reasonably high at 1750°C and 1740°C for Pb and PbO, respectively, while it is 2000°C for Sb. This suggest that these materials are unlikely to generate a significant risk of vapour deposition onto the turbine blades at a temperature below 1400°C; however, further investigation is required both to identify the mechanism of deposition of metal vapours onto the turbine blades and to assess the effect of this deposition on turbine performance.

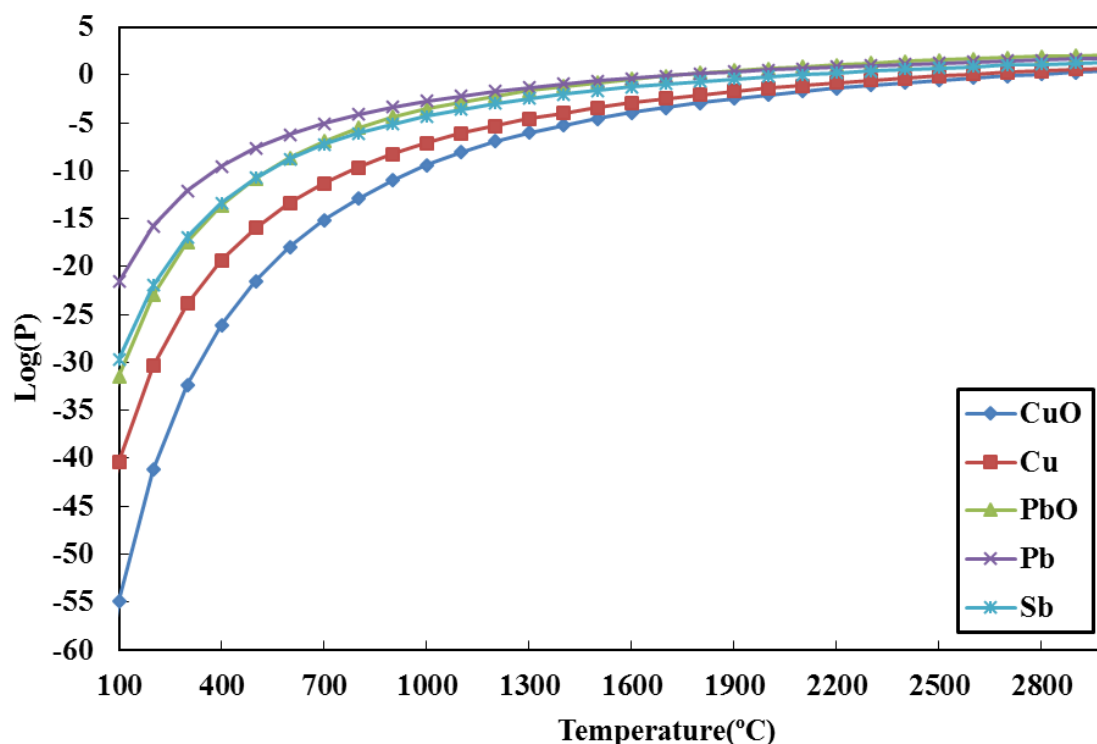


**Figure 4.4.** Variations of the vapour pressure of CuO, Cu, PbO, Pb, and Sb with temperature.

#### 4.5.4 Reaction temperature

Figures 4.5 and 4.6 present the stability phase diagrams for the Cu-O and Pb-O systems. As can be seen, the conversion of  $Pb_3O_4(s)$  and  $Cu_2O(s)$  to the liquid state occurs within a suitable temperature range for the LCL-TES system, while the concentration of oxygen varies between  $\text{Log } P_{O_2} = -2$  and 2 bar which corresponds to a suitable range for a LCL-TES system. In this range of oxygen concentration, the oxides of  $Pb_3O_4$  and CuO melt to the liquid phase at a temperature of around 900°C and 1200°C, respectively. In addition, the phase stability diagram

of the antimony oxides is not available in the literature, although phase diagram of the Sb-O system confirms that  $\text{Sb}_2\text{O}_5$  can be converted to  $\text{Sb}_2\text{O}_4$  and  $\text{Sb}_2\text{O}_3$  (Okamoto 2013; Predel 1998). The transitions between  $\text{Sb}_2\text{O}_3$ ,  $\text{Sb}_2\text{O}_4$  and  $\text{Sb}_2\text{O}_5$  are relatively complicated due to thermal instability of  $\text{Sb}_2\text{O}_5$  and volatility of  $\text{Sb}_2\text{O}_3$ . Therefore, antimony is not a suitable material for the application in a LCL-TES system. Based on these results, the oxides of Pb, Cu selected for further consideration for application in a LCL-TES system.

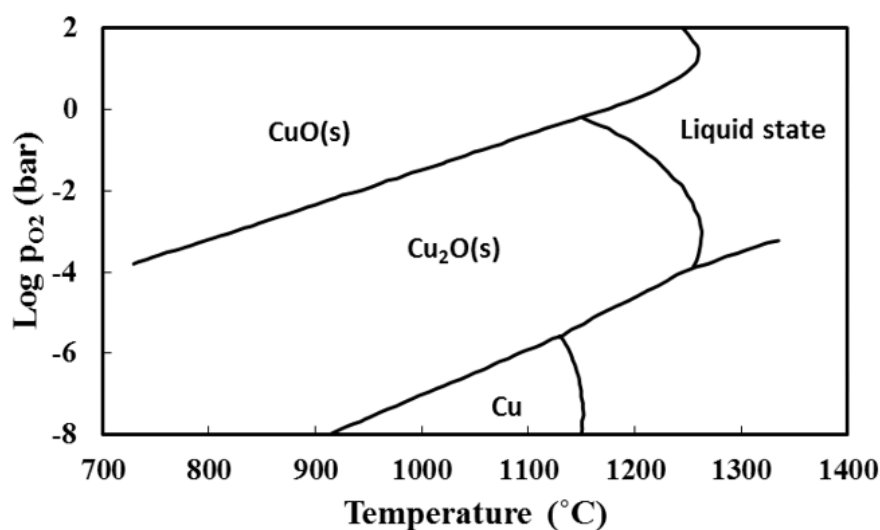


**Figure 4.5.** The equilibrium oxygen pressure for the reactions of Cu as a function of temperature. Reproduced from (Neumann et al. 1984).

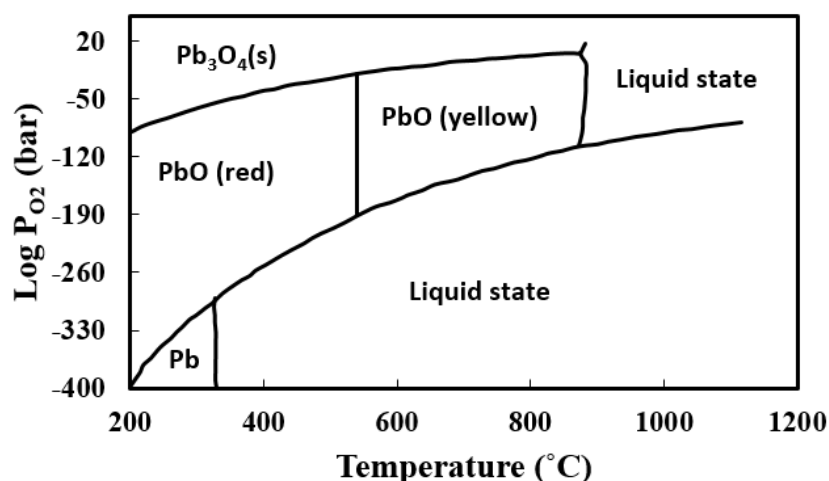


**Figure 4.6.** The equilibrium oxygen pressure for the reactions of Pb as a function of temperature (Ricci et al. 1994).

#### 4.5.5 Identifying the multiple thermal energy storage in a LCL-TES system

Figure 4.7 presents the process of the LCL-TES system in the phase diagram of the Copper-Oxygen (line A-B-C-D-E-F-G). Three types of thermal energy storage can be identified. As can be seen, the sensible heat is stored from line A to B with an increase in temperature, followed by a decomposition of  $\text{CuO(s)}$  to  $\text{Cu}_2\text{O(s)}$  as chemical energy (Line B-C). Further heating at a constant pressure results in  $\text{Cu}_2\text{O(s)}$  to store sensible energy (Line C-D), followed by a phase change from  $\text{Cu}_2\text{O(s)}$  to  $\text{Cu}_2\text{O(l)}$  at a constant temperature (Line D-E). Still more heating at an atmospheric pressure leads to more sensible heat being stored in  $\text{Cu}_2\text{O(l)}$  (Line E-F), followed by a reduction reaction, which results in a change in the concentration of the oxygen (Line F-G) as a result of changing the partial pressure of oxygen as thermochemical storage. It is worth mentioning that copper oxide has the capability to store sensible and thermochemical heat in the liquid state, which increase the total energy storage capacity of the system.

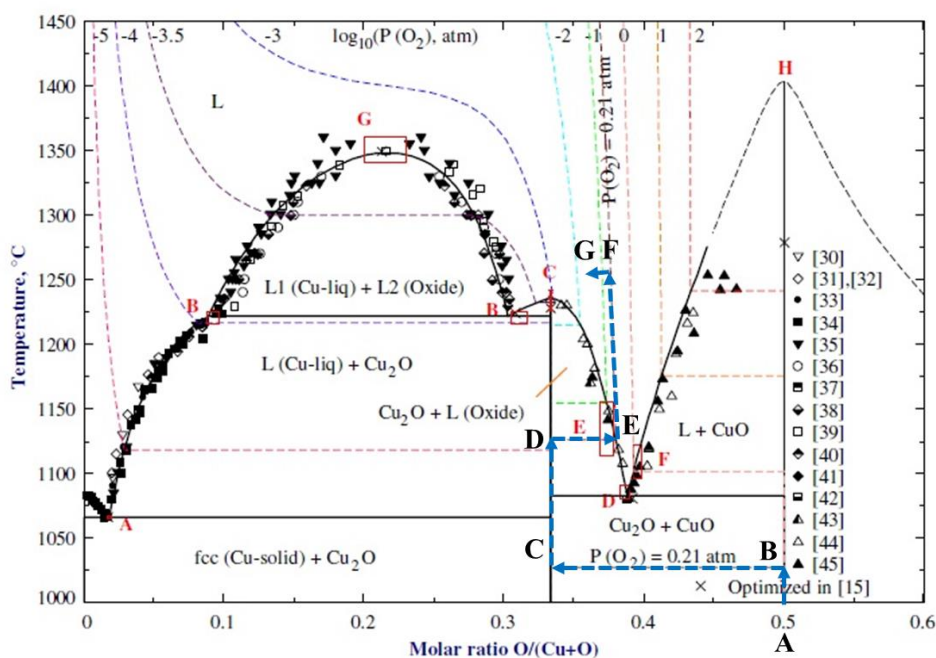


**Figure 4.7.** Copper- oxygen phase diagram (Shishin & Decterov. 2012). The process of the LCL-TES system in the phase diagram of the Copper-Oxygen (line A-B-C-D-E-F-G) is shown.

Figure 4.8 presents the process of a LCL-TES system on the phase diagram for lead and oxygen at atmospheric pressure. As shown in this figure, the first stage of heating from an ambient temperature causes the  $\text{Pb}_3\text{O}_4$  to store sensible heat up to a temperature of  $489^\circ\text{C}$  (Line A-B). With further heating, it decomposes to  $\text{PbO}(\text{s})$ , causing a change in the concentration of oxygen and leading to thermochemical storage (Line B-C). A further input of heat energy generates more sensible storage by increasing the temperature (Line C-D). In the next step, the  $\text{PbO}(\text{s})$  is melted to form  $\text{PbO}(\text{l})$  at a constant temperature, generating latent heat storage. The behaviour of the  $\text{PbO}(\text{l})$  in the liquid state cannot be predicted without the information of partial pressure of oxygen, which is not presently available for the lead-oxygen phase diagram. However, a review of literature revealed that the change in the concentration of oxygen in the liquid state for the lead-oxygen system is not significant (Risold et al. 1998). This implies that there is a limited potential to use lead oxide for thermochemical energy storage in the liquid state, in which case lead oxide is not suitable for a LCL-TES. Nevertheless, thermochemical energy storage is possible in the solid state of the lead-oxygen system.

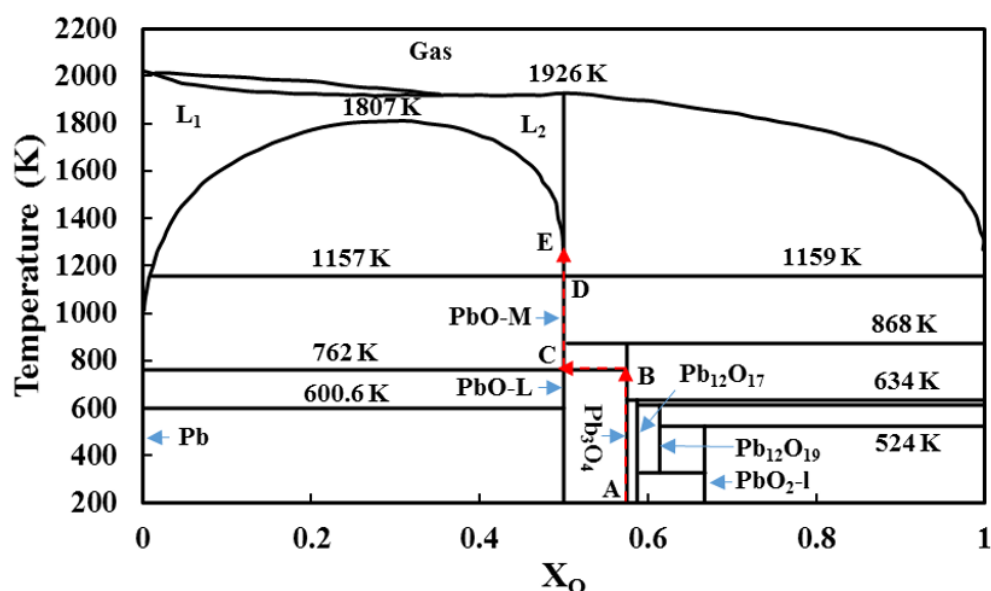
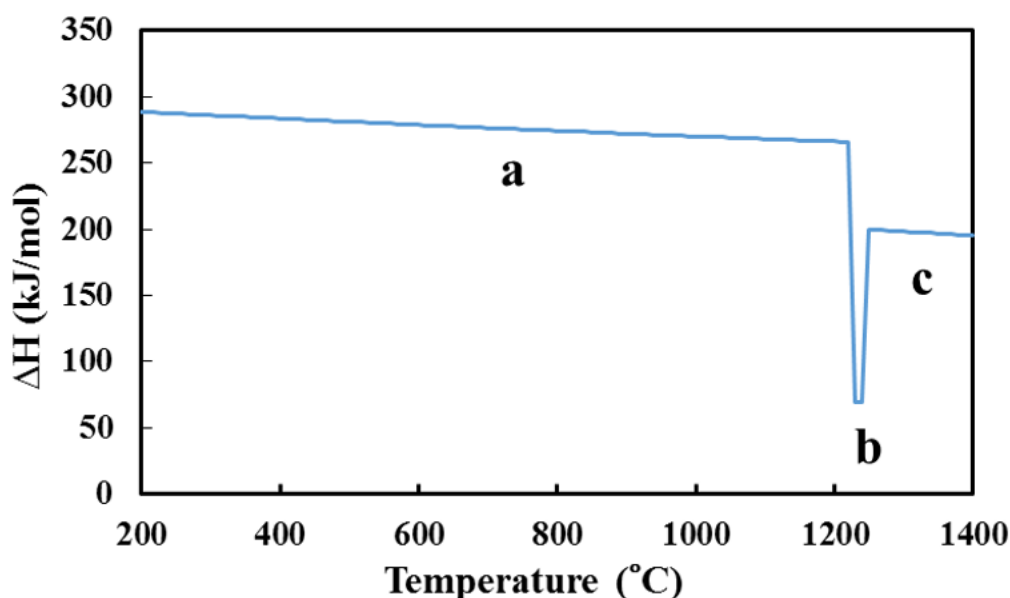


Figure 4.8. Lead-oxygen phase diagram (Risold et al. 1998).

#### 4.5.6 Enthalpy of the storage medium

Figure 4.9 presents the calculated total enthalpy of the selected metal oxides below a temperature of 1400°C. The reduction reactions of CuO to Cu<sub>2</sub>O are endothermic at the assessed temperatures. The calculated enthalpy for the reduction reaction of CuO/Cu<sub>2</sub>O begins from 288kJ/mol at ≈ 200°C. The value of  $\Delta H$  decreases gradually from 266kJ/mol with an initial increase in temperature, then more sharply between the temperatures of 1200°C and 1300°C, where  $\Delta H = 198$  kJ/mol. The Cu<sub>2</sub>O(s) melts to Cu<sub>2</sub>O (l) at this temperature range. A further increase in temperature causes the energy to be stored as sensible heat in liquid metal.



**Figure 4.9.** Calculated total enthalpy of copper oxide in a LCL-TES system. a) Before melting b) phase change c) after melting.

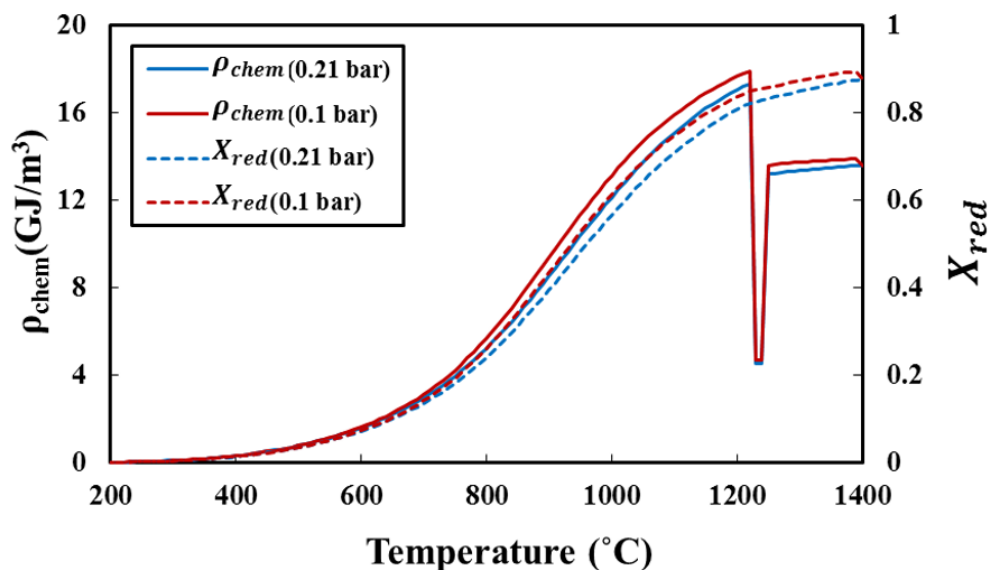


**Figure 4.10.** Calculated chemical energy density and conversion extent for CuO/Cu<sub>2</sub>O at the oxygen partial pressures of 0.21 and 0.1 bar as a function of temperature.

Figure 4.10 presents the calculated sensitivity to variations in the temperature of the chemical energy density for copper oxide at the oxygen partial pressures of 0.1 and 0.21 bar. As can be seen, the chemical energy density of the CuO/Cu<sub>2</sub>O pairs increases with a decrease in the equilibrium partial pressure of oxygen in the gas phase. For example, the chemical energy density of CuO/Cu<sub>2</sub>O increases to 16.32 GJ/m<sup>3</sup> with a decrease in the partial pressure of oxygen to 0.1 bar at 1200 °C before dropping to 13.31 GJ/m<sup>3</sup> at 1400 °C. It is also worth noting that the partial pressure of the oxygen in the system, and hence the conversion of the reactions, can be changed using an inert purge gas (Jafarian et al. 2014; Moghtaderi 2011). It can be concluded that the chemical energy density can be increased by decreasing the partial pressure of the system.

Table 4.2 provides a comparison between the calculated values of different types of energy storage for copper oxide and lead oxide in solid and liquid states. As discussed above, copper oxide offers the possibility of stored energy in the forms of sensible, latent and chemical energy. The enthalpy of chemical storage in the solid state for copper oxide is around 258.72 kJ/mol, which is some four times that of the sensible and latent heat of 69 kJ/mol and 64.7



kJ/mol, respectively. It is also much greater than both the sensible and chemical enthalpy in the liquid state of 8.32kJ/mol and 3.87kJ/mol, respectively. Nevertheless, these relatively low values of energy density in liquid state contribute to the total enthalpy of the system and enable the structure of the solid oxide to be regenerated. The heat stored by lead oxide in solid state is lower, but still significant with values of 107 kJ/mol, 25.52 kJ/mol and 114.97 kJ/mol, for sensible, latent and chemical storage, respectively. Based on Figure 4.8, lead oxide can only store sensible heat in liquid state, with an enthalpy of 2.6 kJ/mol. It is clear that copper oxide has the advantages over lead of a higher total enthalpy and the potential to store thermal energy as thermochemical storage in liquid state, which can be controlled by changing the partial pressure of the oxygen in the system.

**Table 4.2.** Comparison of the different types of energy storage in solid and liquid state for copper oxide and lead oxide.

Metal	$T_R$ (°C)	Solid state			Liquid state			$\Delta H^{**total}$ (kJ/mol)
		$\Delta H_{sen}$ (kJ/mol)	$\Delta H_{lat}$ (kJ/mol)	$\Delta H_{chem}$ (kJ/mol)	$\Delta H_{sen}$ (kJ/mol)	$\Delta H_{lat}$ (kJ/mol)	$\Delta H_{chem}$ (kJ/mol)	
Cu	1170	69	64.76	258.72	8.32	-	3.87 *	404.67
Pb	410	107	25.52	114.97	2.6	-	-	250.09

\*Thermochemical energy storage from point F to G in Figure 4.7.

\*\* Calculated enthalpy based on the process shown in Figure 4.7 and 4.8.

## 4.6 Conclusion

The thermodynamic potential of different multivalent metal oxides for application in a LCL- TES system was assessed based on their melting temperature, Ellingham diagram, reaction temperature, vapour pressure and, phase stability diagram. The oxides of Pb, Ba, Sb, Cu and Mn were found to exhibit the potential for application in a LCL- TES system based on their melting temperature at the operating temperature of the system. However, the Ellingham diagram of these materials revealed that the values of  $\Delta G$  are positive for the reactions of PbO/Pb, MnO<sub>2</sub>/Mn, and BaO<sub>2</sub>/Ba, which means that these reactions are not suitable for a LCL-

TES system within the range of temperature studied here. The negative value of the Gibbs free energy for the reactions of  $\text{PbO}_2/\text{PbO}$ ,  $\text{PbO}_2/\text{Pb}_3\text{O}_4$ ,  $\text{Pb}_3\text{O}_4/\text{PbO}$ ,  $\text{CuO}/\text{Cu}_2\text{O}$  and  $\text{Sb}_2\text{O}_5/\text{Sb}_2\text{O}_3$  imply that these materials have some potential for application in a LCL-TES system; however, the phase stability diagram analysis revealed that antimony oxide is not a suitable material for a LCL-TES system because of complicated phase transitions of various oxides. The phase diagram of copper oxide and lead oxide revealed that only copper oxide has a potential to store thermal energy in the form of sensible, and thermochemical heat in both the solid and liquid states, while also offering latent heat in the phase change process. Although lead oxide can be used to store thermal energy in the form of sensible, latent, and thermochemical in the solid state, it can only store sensible heat in the liquid state. The total calculated enthalpy for copper oxide and lead oxide showed that copper oxide can approximately store heat energy two times more than lead oxide.

Notwithstanding the strong thermochemical energy storage potential for copper in a LCL-TES system, it should be noted that there exist significant technical challenges that need to be overcome to enable the proposed system to become available at a commercial scale, given the requirement to reduce the metal oxides at a temperature well above the maximum temperature of high temperature steels. It is also anticipated that the technical challenges associated with the Pb oxides are less than these for Cu oxides because the reduction occurs at a temperature below  $1000^\circ\text{C}$ . It is worth noting that the economic feasibility assessment of the LCL-TES system requires further investigation of the performance of process components and material compatibility. In summary the challenges associated with working with liquid metals need to be overcome before the components of a LCL-TES system can be designed and tested.

## 4.7 References

A. H. Abedin & M. A. Rosen 2011, 'A critical review of thermochemical energy storage systems', *Open Renewable Energy J*, vol. 4. pp. 42-46.

J. Adanez, A. Abad, F. Garcia-Labiano, P. Gayan & L. F. de Diego 2012, 'Progress in Chemical-Looping Combustion and Reforming technologies', *Progress in energy and combustion science*, vol. **38**. 2, pp. 215-282.

B. Wong 2011, *Thermochemical heat storage for concentrated solar power*, Department of Energy.

M. Barati, S. Esfahani & T. Utigard 2011, 'Energy recovery from high temperature slags', *Energy*, vol. **36**. 9, pp. 5440-5449.

R. K. Bhargava, M. Bianchi, A. Pascale, G. Negri di Montenegro & A. Peretto 2007, 'Gas Turbine Based Power Cycles - A State-of-the-Art Review', *Challenges of Power Engineering and Environment: Proceedings of the International Conference on Power Engineering 2007*, Springer Berlin Heidelberg, Berlin, Heidelberg, pp. 309-319.

T. Block, N. Knoblauch & M. Schmücker 2014, 'The cobalt-oxide/iron-oxide binary system for use as high temperature thermochemical energy storage material', *Thermochimica Acta*, vol. **577**. pp. 25-32.

R. Bowrey & J. Jutsen 1978, 'Energy storage using the reversible oxidation of barium oxide', *Solar energy*, vol. **21**. 6, pp. 523-525.

M. K. Chyu 2012, 'Recent advances in turbine Heat Transfer: with a view of transition to coal-gas based systems', *Journal of Heat Transfer*, vol. **134**. 3, pp. 031006-031006.

J. Coventry, C. Andraka, J. Pye, M. Blanco & J. Fisher 2015, 'A review of sodium receiver technologies for central receiver solar power plants', *Solar energy*, vol. **122**. pp. 749-762.

M. Fahim & J. Ford 1983, 'Energy storage using the BaO<sub>2</sub>/BaO reaction cycle', *The Chemical Engineering Journal*, vol. **27**. 1, pp. 21-28.

K.-H. Funken, M. Roeb, P. Schwarzboezl & H. Warnecke 2001, 'Aluminum remelting using directly solar-heated rotary kilns', *Journal of Solar Energy Engineering*, vol. **123**. 2, pp. 117-124.

A. Gil, M. Medrano, I. Martorell, A. Lázaro, P. Dolado, B. Zalba & L. F. Cabeza 2010, 'State of the art on high temperature thermal energy storage for power generation. Part 1: Concepts, materials and modellization', *Renewable and Sustainable Energy Reviews*, vol. **14**. 1, pp. 31-55.

P. Haseli, M. Jafarian & G. J. Nathan 2017, 'High temperature solar thermochemical process for production of stored energy and oxygen based on CuO/Cu<sub>2</sub>O redox reactions', *Solar energy*, vol. **153**. pp. 1-10.

A. J. Hunt 2010, 'Liquid metal thermal storage system', Google Patents.

B. Ihsan 1995, 'Thermochemical data of pure substances', vol. **934**. p. 587.

M. Jafarian, M. Arjomandi & G. J. Nathan 2014, 'Influence of the Type of Oxygen Carriers on the Performance of a Hybrid Solar Chemical Looping Combustion System', *Energy & Fuels*, vol. **28**. 5, pp. 2914-2924.

M. Jafarian, M. Arjomandi & G. J. Nathan 2017, 'Thermodynamic potential of molten copper oxide for high temperature solar energy storage and oxygen production', *Applied Energy*, vol. **201**. pp. 69-83.

Y. Kashiwaya, Y. In-Nami & T. Akiyama 2010, 'Development of a rotary cylinder atomizing method of slag for the production of amorphous slag particles', *ISIJ international*, vol. **50**. 9, pp. 1245-1251.

D. Kearney, U. Herrmann, P. Nava, B. Kelly, R. Mahoney, J. Pacheco, R. Cable, N. Potrovitza, D. Blake & H. Price 2003, 'Assessment of a molten salt heat transfer fluid in a parabolic trough solar field', *Journal of Solar Energy Engineering*, vol. **125**. 2, pp. 170-176.

G. J. Kolb 1998, 'Economic evaluation of solar-only and hybrid power towers using molten-salt technology', *Solar energy*, vol. **62**. 1, pp. 51-61.

S. Kuravi, J. Trahan, D. Y. Goswami, M. M. Rahman & E. K. Stefanakos 2013, 'Thermal energy storage technologies and systems for concentrating solar power plants', *Progress in Energy and Combustion Science*, vol. **39**. 4, pp. 285-319.

R. Lamoreaux & D. Hildenbrand 1984, 'High temperature vaporization behavior of oxides. I. Alkali metal binary oxides', *Journal of physical and chemical reference data*, vol. **13**. 1, pp. 151-173.

D. R. Lide & H. V. Kehiaian 1994, *CRC handbook of thermophysical and thermochemical data*, vol. 1, Crc Press.

H. Mehling & L. F. Cabeza 2007, 'Phase change materials and their basic properties', in *Thermal energy storage for sustainable energy consumption*, Springer, pp. 257-277.

B. Moghtaderi 2009, 'Application of Chemical Looping Concept for Air Separation at High Temperatures†', *Energy & Fuels*, vol. **24**. 1, pp. 190-198.

B. Moghtaderi 2011, 'Review of the recent chemical looping process developments for novel energy and fuel applications', *Energy & Fuels*, vol. **26**. 1, pp. 15-40.

T. Nagel, H. Shao, A. Singh, N. Watanabe, C. Roßkopf, M. Linder, A. Wörner & O. Kolditz 2013, 'Non-equilibrium thermochemical heat storage in porous media: Part 1: Conceptual model', *Energy*, vol. **60**. pp. 254-270.

M. Naghavi, K. Ong, I. Badruddin, M. Mehrali, M. Silakhori & H. Metselaar 2015, 'Theoretical model of an evacuated tube heat pipe solar collector integrated with phase change material', *Energy*, vol. **91**. pp. 911-924.

J. Neumann, T. Zhong & Y. Chang 1984, 'The Cu-O (Copper-Oxygen) system', *Journal of Phase Equilibria*, vol. **5**. 2, pp. 136-140.

H. Okamoto 2013, 'Supplemental Literature Review of Binary Phase Diagrams: Cs-In, Cs-K, Cs-Rb, Eu-In, Ho-Mn, K-Rb, Li-Mg, Mg-Nd, Mg-Zn, Mn-Sm, O-Sb, and Si-Sr', *Journal of Phase Equilibria and Diffusion*, vol. **34**. 3, pp. 251-263.

J. Pacio, C. Singer, T. Wetzel & R. Uhlig 2013, 'Thermodynamic evaluation of liquid metals as heat transfer fluids in concentrated solar power plants', *Applied Thermal Engineering*, vol. **60**. 1–2, pp. 295-302.

J. Pacio & T. Wetzel 2013, 'Assessment of liquid metal technology status and research paths for their use as efficient heat transfer fluids in solar central receiver systems', *Solar energy*, vol. **93**. pp. 11-22.

P. Pardo, A. Deydier, Z. Anxionnaz-Minvielle, S. Rougé, M. Cabassud & P. Cognet 2014, 'A review on high temperature thermochemical heat energy storage', *Renewable and Sustainable Energy Reviews*, vol. **32**. pp. 591-610.

S. Pickering, N. Hay, T. Roylance & G. Thomas 1985, 'New process for dry granulation and heat recovery from molten blast-furnace slag', *Ironmaking and steelmaking*, vol. **12**. 1, pp. 14-21.

B. Predel 1998, 'O-Sb (Oxygen-Antimony)', in Ni-Np – Pt-Zr, Springer Berlin Heidelberg, Berlin, Heidelberg, pp. 1-2.

H. Price 2003, 'Assessment of parabolic trough and power tower solar technology cost and performance forecasts', *National Renewable Energy Laboratory, Golden, CO*.

H. Price, E. Lupfert, D. Kearney, E. Zarza, G. Cohen, R. Gee & R. Mahoney 2002, 'Advances in parabolic trough solar power technology', *Journal of Solar Energy Engineering*, vol. **124**. 2, pp. 109-125.

E. Ricci, A. Passerone, P. Castello & P. Costa 1994, 'Surface reactivity of liquid metal with oxygen and its relationship with surface tension measurements: a kinetic-fluodynamic model', *Journal of materials science*, vol. **29**. 7, pp. 1833-1846.

D. Risold, J.-I. Nagata & R. Suzuki 1998, 'Thermodynamic description of the Pb-O system', *Journal of Phase Equilibria*, vol. **19**. 3, pp. 213-233.

---

C. W. Robak, T. L. Bergman & A. Faghri 2011, 'Economic evaluation of latent heat thermal energy storage using embedded thermosyphons for concentrating solar power applications', *Solar energy*, vol. **85**. 10, pp. 2461-2473.

A. Roine 2002, 'Outokumpu HSC chemistry for windows: chemical reaction and equilibrium software with extensive thermochemical database'.

W. J. Schiel & M. A. Geyer 1988, 'Testing an external sodium receiver up to heat fluxes of 2.5 MW/m<sup>2</sup>: Results and conclusions from the IEA-SSPS high flux experiment conducted at the central receiver system of the Plataforma Solar de Almeria (Spain)', *Solar energy*, vol. **41**. 3, pp. 255-265.

K. Shah, B. Moghtaderi & T. Wall 2012, 'Selection of suitable oxygen carriers for chemical looping air separation: a thermodynamic approach', *Energy & Fuels*, vol. **26**. 4, pp. 2038-2045.

Y. Shah, B. G. Kelkar, S. Godbole & W. D. Deckwer 1982, 'Design parameters estimations for bubble column reactors', *AIChE journal*, vol. **28**. 3, pp. 353-379.

D. Shishin & S. A. Deckerov 2012, 'Critical assessment and thermodynamic modeling of the Cu-O and Cu-O-S systems', *Calphad*, vol. **38**. pp. 59-70.

M. Silakhori, H. Fauzi, M. R. Mahmoudian, H. S. C. Metselaar, T. M. I. Mahlia & H. M. Khanlou 2015, 'Preparation and thermal properties of form-stable phase change materials composed of palmitic acid/polypyrrole/graphene nanoplatelets', *Energy and Buildings*, vol. **99**. pp. 189-195.

M. Silakhori, H. S. C. Metselaar, T. M. I. Mahlia, H. Fauzi, S. Baradaran & M. S. Naghavi 2014, 'Palmitic acid/polypyrrole composites as form-stable phase change materials for thermal energy storage', *Energy Conversion and Management*, vol. **80**. pp. 491-497.

Y. Tian & C. Y. Zhao 2013, 'A review of solar collectors and thermal energy storage in solar thermal applications', *Applied Energy*, vol. **104**. pp. 538-553.

B. Wong, L. Brown, F. Schaube, R. Tamme & C. Sattler 2010, 'Oxide based thermochemical heat storage', in *Proceedings of the 16th SolarPACES Conference, Perpignan, France*, pp. 21-24.

Z. Yang & S. V. Garimella 2010, 'Thermal analysis of solar thermal energy storage in a molten-salt thermocline', *Solar energy*, vol. **84**. 6, pp. 974-985.

A. Z'Graggen, P. Haueter, D. Trommer, M. Romero, J. C. de Jesus & A. Steinfeld 2006, 'Hydrogen production by steam-gasification of petroleum coke using concentrated solar power—II Reactor design, testing, and modeling', *International Journal of Hydrogen Energy*, vol. **31**. 6, pp. 797-811.

H. Zhang, J. Baeyens, J. Degève & G. Cacères 2013, 'Concentrated solar power plants: review and design methodology', *Renewable and Sustainable Energy Reviews*, vol. **22**. pp. 466-481.

## Chapter 5 Experimental assessment of copper oxide in LCL-TES

---

### 5.1 Chapter overview

In this chapter, the suitable metal oxide (copper oxide), which is selected in chapter 4 for LCL- TES system, is experimentally assessed by Thermogravimetric Analysis (TGA). In this experiment, the reduction and oxidation reactions can be identified by weight loss and gain, respectively. This experiment proves that copper oxide has the potential to reduce and oxides in its liquid phase. Then, the thermal reversibility of metal oxide over 10 cycles of reduction and oxidation reactions in liquid phase is investigated. In the following section, the benefits and technical challenges of liquid metal oxides for thermal energy storage is also identified.

The details of the experiment and the characterization of the materials before and after chemical storage in liquid state are presented in the following section. This section is presented in the paper format submitted to Journal of Energy Storage.

# Statement of Authorship

Title of Paper	Experimental Assessment of Copper Oxide in Liquid Chemical Looping for Thermal Energy Storage
Publication Status	<input checked="" type="checkbox"/> Published <input type="checkbox"/> Accepted for Publication <input type="checkbox"/> Submitted for Publication Unpublished and Unsubmitted work written in manuscript style
Publication Details	Mahyar Silakhori, Mehdi Jafarian, Maziar Arjomandi, Graham J. Nathan, Experimental Assessment of Copper Oxide in Liquid Chemical Looping for Thermal Energy Storage, Journal of Energy Storage (2018)

## Principal Author

Name of Principal Author (Candidate)	Mahyar Silakhori		
Contribution to the Paper	<ul style="list-style-type: none"> <li>- Research, collecting and analysing data from different resources</li> <li>- Providing the data, writing of the manuscript and production of original figures</li> <li>- Correspondence with editor and reviewers including the production of all cover letters and rejoinder</li> </ul>		
Overall percentage (%)	70%		
Certification:	This paper reports on original research I conducted during the period of my Higher Degree by Research candidature and is not subject to any obligations or contractual agreements with a third party that would constrain its inclusion in this thesis. I am the		
Signature		Date	04.02.2019

## Co-Author Contributions

By signing the Statement of Authorship, each author certifies that:

- vii. the candidate's stated contribution to the publication is accurate (as detailed above);
- viii. permission is granted for the candidate to include the publication in the thesis; and
- ix. the sum of all co-author contributions is equal to 100% less the candidate's stated contribution.

Name of Co-Author	Mehdi Jafarin		
Contribution to the Paper	<ul style="list-style-type: none"> <li>- Supervision of the work, including the production of the manuscript</li> <li>- Participation in the development of the concepts and ideas presented in the manuscript</li> <li>- Evaluation and editing of the manuscript prior to submission</li> </ul>		
Signature		Date	4/02/2019



Name of Co-Author	Maziar Arjomandi			
Contribution to the Paper	<ul style="list-style-type: none"><li>- Supervision of the work, including the production of the manuscript</li><li>- Participation in the development of the concepts and ideas presented in the manuscript</li><li>- Evaluation and editing of the manuscript prior to submission</li></ul>			
Signature	<table border="1" style="width: 100%;"><tr><td style="width: 60%;"></td><td style="width: 10%; text-align: center;">Date</td><td style="width: 30%; text-align: center;">4/02/2019</td></tr></table>		Date	4/02/2019
	Date	4/02/2019		

Name of Co-Author	Graham 'Gus' Nathan			
Contribution to the Paper	<ul style="list-style-type: none"><li>- Supervision of the work, including the production of the manuscript</li><li>- Participation in the development of the concepts and ideas presented in the manuscript</li><li>- Evaluation and editing of the manuscript prior to submission</li></ul>			
Signature	<table border="1" style="width: 100%;"><tr><td style="width: 60%;"></td><td style="width: 10%; text-align: center;">Date</td><td style="width: 30%; text-align: center;">4/2/19.</td></tr></table>		Date	4/2/19.
	Date	4/2/19.		

**Experimental Assessment of Copper Oxide in Liquid Chemical Looping for  
Thermal Energy Storage**

Mahyar Silakhori\*, Mehdi Jafarian, Maziar Arjomandi, Graham J. Nathan

Published: Journal of Energy Storage, vol. **21**, pp. 216-221.

## 5.2 Abstract

The potential of copper oxide for both thermal energy storage and oxygen production in a liquid chemical looping thermal energy storage system has been assessed with thermogravimetric analysis. Liquid chemical looping thermal energy storage is a recently proposed system with potential to enable both the storage of thermal energy (through sensible heating, phase change and thermochemical reactions) and oxygen production. The process of isothermal reduction and oxidation of molten copper oxide was verified experimentally by heating the material isobarically, reducing or oxidising it isothermally, and then cooling it again isobarically. The isothermal reduction and oxidation reactions were achieved by varying the partial pressure of oxygen through the change in the concentrations of nitrogen and oxygen. This confirmed that copper oxide can be reduced in the liquid state by changing the partial pressure of oxygen in the system. Nevertheless, the extent of reduction in the assessed range of oxygen partial pressure in the liquid phase is approximately 2%, while this value in solid phase is approximately 10%, which implies that the thermochemical storage is mainly occurred in the solid phase. The reduction and oxidation cycles were repeated for 10 cycles. Superimposed on the cyclical weight change was an additional weight loss that was attribute to a side reaction between the copper oxide and alumina crucible.

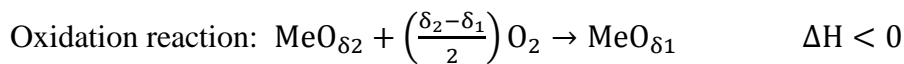
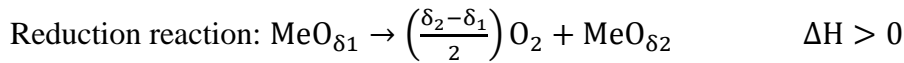
## 5.3 Introduction

Concentrated Solar Thermal (CST) technologies make use of the entire solar spectrum to provide a source of high-temperature in the range of 500-2000°C (Nathan et al. 2018). So that CST has received ongoing attention due to its compatibility with both thermal power systems, e.g. steam Rankine cycles and gas turbine combined cycles (Nathan et al. 2018), and thermal energy storage (TES), which is low cost compared with electrical energy storage (Kuravi et al. 2013). However, to date CST system are limited to the lower end of this range for power

generation, such that the state-of-the-art concentrated solar thermal power plants are limited to steam Rankine cycles with a relatively low efficiency of about 35-40%, at a temperature of approximately 550°C (Nathan et al. 2018). This is despite the viability could be increased even further if it was possible to utilise more efficient power cycles than the present steam Rankine cycles. To do so it is required to develop new technologies enabling higher storage and operating temperature because the efficiency of a thermal power cycle increases with temperature. This has motivated research activity to develop higher temperature TES systems. One of the target power cycles is gas turbine combined cycles, which operate with a turbine inlet temperature of up to 1250 °C (Bhargava et al. 2007), although the optimal temperature for a solar power plant will be lower due to the trade-off of increased radiation losses with temperature (Nathan et al. 2018). Hence, new TES technologies are required to achieve temperatures greater than that of state-of-the-art of molten salts. Thermochemical energy storage system based on endothermic reduction and exothermic oxidation of multivalent metals offers a high energy density at a temperature of around 1000 °C. However, the use of these materials in solid state leads to technical challenges, which are mainly associated with the change in the structure of the solid-state storage medium e.g. sintering, softening and agglomeration in a successive reduction and oxidation (RedOx) cycles (Haseli et al. 2017; Wu et al. 2018). These, in turn, mitigate the reactivity of the materials for reactions after a limited number of RedOx cycles. One potential option with which to address this limitation is the Liquid Chemical Looping for Thermal Energy Storage (LCL-TES) system proposed recently by Jafarian et al. (Jafarian et al. 2017). A thermodynamic assessment identified potential to store thermal energy at 1250°C with an energy density of 5 GJ/m<sup>3</sup>, which is approximately 6 times more than the 0.83 GJ/m<sup>3</sup> of molten salt, using three modes of sensible, latent and thermochemical storage (Jafarian et al. 2017; Silakhori et al. 2017). However, this assessment relied on published data of copper and oxygen phase diagram (Shishin & Decterov 2012), so

that the realistic potential of the system has yet to be assessed experimentally. Therefore the overall aim of this work is to investigate viability of the potential benefits and limitations of the LCL-TES system.

The reduction and oxidation reactions of metal oxides can be described as follows:



Here  $\text{MeO}_{\delta_1}$  and  $\text{MeO}_{\delta_2}$  are two states of oxidation of the metal 'Me'. This is sometimes also referred to as a chemical looping process, in which the state of oxidation of the metal oxide ( $\text{MeO}_{\delta}$ ) can be changed by the temperature of the system or the partial pressure of oxygen or a combination of them. For example, the equilibrium temperature for the pair  $\text{CuO(s)}$  and  $\text{Cu}_2\text{O(s)}$  is  $1042^\circ\text{C}$  at an oxygen partial pressure of 0.21 bar (Neumann et al. 1984). Therefore, increasing the temperatures more than approximately  $1042^\circ\text{C}$  in an oxygen pressure of 0.21 bar leads to the endothermic reduction of  $\text{CuO(s)}$  to  $\text{Cu}_2\text{O(s)}$ , while decreasing the temperature than  $1042^\circ\text{C}$  results in the exothermic oxidation of  $\text{Cu}_2\text{O(s)}$  to  $\text{CuO(s)}$ . Nevertheless, the use of this system under these conditions for thermochemical energy storage leads to exergy loss, because the charging temperature (for endothermic reduction) is higher than that at which the energy is released (for exothermic oxidation).

The potential of different metal oxides for thermochemical energy storage has been assessed extensively (Agrafiotis et al. 2014, 2015; Wong 2011; Fahim & Ford 1983). Among different potential materials for thermochemical energy storage in solid phase,  $\text{Co}_3\text{O}_4/\text{CoO}$ ,  $\text{Mn}_2\text{O}_3/\text{Mn}_3\text{O}_4$  and  $\text{CuO}/\text{Cu}_2\text{O}$  have been selected due their high storage capacity, high reaction temperature and reversibility (Alonso et al. 2015; Deutsch et al. 2017; Roine 2002). Silakhori et al. (Silakhori et al. 2017) have recently assessed the thermodynamic potential twenty three

metal oxides in liquid chemical looping thermal energy storage. They have found that copper oxide has high potential to store sensible, latent and thermochemical heat in a LCL-TES cycle. So that the reduction temperature of CuO to Cu<sub>2</sub>O pairs, approximately 1042°C for P<sub>O<sub>2</sub></sub>=0.21 atm, is in the range of the melting point of copper oxides, 1077°C for P<sub>O<sub>2</sub></sub>=0.21 atm, that enable the use of copper oxide in Liquid chemical looping for thermal energy storage (LCL-TES) (Jafarian et al. 2017; Silakhori et al. 2017). Silakhori et al. (Silakhori et al. 2017) have also estimated that an LCL-TES system using copper oxide can store thermal energy at approximately 77.3 kJ/mol, 64.7 kJ/mol and 267 kJ/mol through sensible, latent and chemical heat, respectively. However, the development of the system is contingent on the availability of the process components and appropriate construction materials. The postulated system has two reactors one for reduction and the other for oxidation, together with two storage tanks for the molten metal and cold particles, respectively. The cycle employs both temperature and pressure swing driving forces to reduce the exergy destruction associated with reduction and oxidation reactions of metal oxides. Therefore, the aim of this paper is to assess the performance of copper oxide in liquid chemical looping with consideration of its use for thermal energy storage. Moreover, the technical challenges of copper oxide in LCL-TES system will be investigated through experimental assessment with TGA.

## **5.4 Experimental setup**

### **5.4.1 Material and method**

Copper oxide (CuO) powder with a purity of 97.5% procured from Chem-Supply Pty Ltd, was used as sample. The experiments started with 20 mg of CuO samples, placed in a 70 ml alumina crucible supported by an alumina rod. The procedure of the experiment is presented in the phase diagram of copper and oxygen, shown in Figure 5.1. During the experiments, the samples were heated from 50°C to a temperature of 1250°C isobarically under an oxygen partial pressure of 0.05 bar (Figure 5.1 - from A to B). The partial pressure in the system was then systemically

changed to reduce and oxidise (Figure 5.1- from point B to C). Finally, the sample was cooled (Figure 5.1- from C to D) at a constant partial pressure of oxygen. The TGA experiments were performed using a Netzsch STA 449 F3 Jupiter Thermogravimetric analyser (TGA). As shown in Figure 5.1, oxidation and reduction were performed by changing the partial pressure of oxygen from 0.05 bar to 0.8 bar (Figure 5.1- from B to C), achieved by changing the ratio of inlet nitrogen and oxygen into the TGA, which was set in accordance with the limitation of experimental facilities.

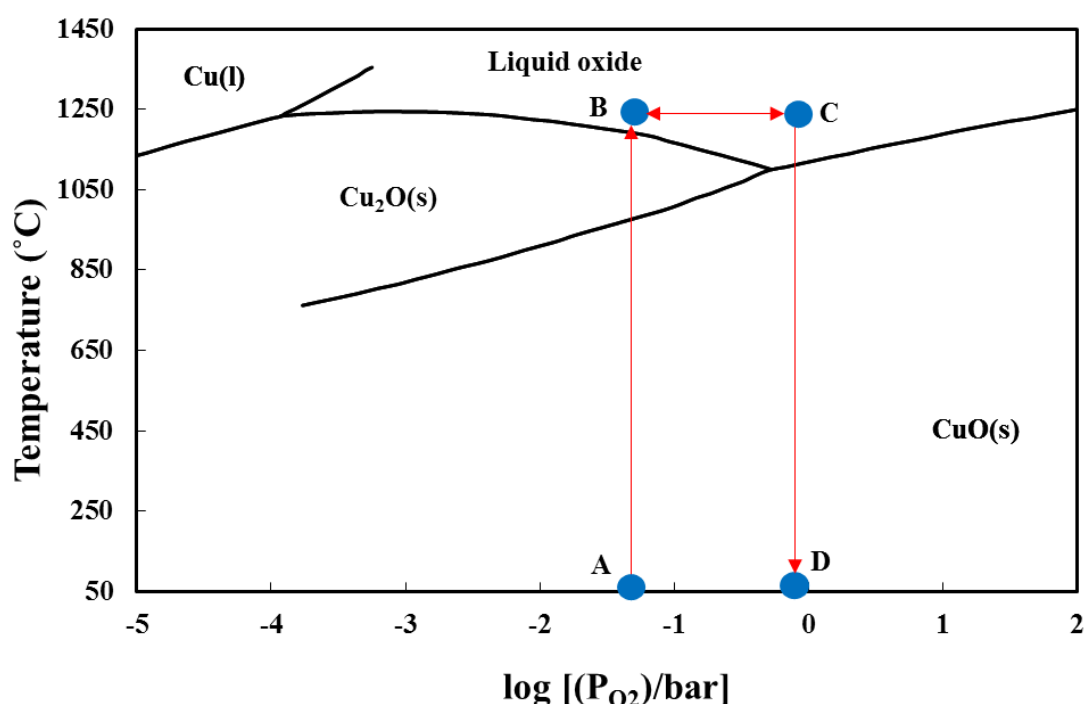


**Figure 5.1.** The phase diagram of the copper and oxygen together with the conditions of the experiments. The temperature was increased isobarically from 50°C to 1250°C (From A to B). The partial pressure was then increased isothermally from 0.05 bar to 0.8 bar (point B to C). The temperature was then decreased isobarically to 500°C. Other details are presented in Table 5.2.

#### 5.4.2 Crucible

Table 5.1 presents the different types of crucibles commercially available for high temperature application namely Al<sub>2</sub>O<sub>3</sub>, Platinum (Pt), Tungsten (W) and Boron Nitride (BN) and Yttrium (Y<sub>2</sub>O<sub>3</sub>). The potential of W, BN and Y<sub>2</sub>O<sub>3</sub> crucibles have been assessed previously with inert gases e.g. N<sub>2</sub> and Ar at high temperatures of 2400°C, 1650°C, and 1700°C, respectively

(Kurushima & Ishizaki 1992; NETZSCH 2017). However, W and BN crucibles are known to oxidize in atmospheric air at temperature of 1250°C. The reaction of Y<sub>2</sub>O<sub>3</sub> with molten copper oxide at temperature above 1000°C in atmosphere air hinder the authors to use this crucible for the experiments (Kurushima & Ishizaki 1992). The potential of Al<sub>2</sub>O<sub>3</sub> and Pt have been previously used for copper oxide with an inert gas for thermochemical energy storage (Agrafiotis et al. 2016; Block & Schmücker 2016). However, Pt reacts with molten copper oxide at temperature of 1250°C. In this study, Al<sub>2</sub>O<sub>3</sub> was selected as a suitable container for the assessment of copper oxide in liquid phase even though CuO reacts slightly with Al<sub>2</sub>O<sub>3</sub> depending on partial pressure of oxygen (Hu et al. 2016; Karni et al. 1997).

**Table 5.1.** Comparing different types of the crucible for high temperature applications.

Crucible	Advantages	Weakness	References
Al <sub>2</sub> O <sub>3</sub>	High thermal stability up to 1700°C with inert gas, compatible with solid metal oxides, Low cost.	Potential reactions with molten metal oxides.	(Agrafiotis et al. 2016; Block & Schmücker 2016; NETZSCH 2017)
Pt	High thermal stability up to 1650°C with inert gas, Compatible with solid metal oxides.	Potential reactions with molten metal oxides, High cost.	(Agrafiotis et al. 2016; Block & Schmücker 2016; NETZSCH 2017)
W	High thermal stability up to 2400°C with inert gas	High rate of oxidation at high temperatures in an atmospheric condition.	(Habainy & Nilsson 2013; NETZSCH 2017)
Y <sub>2</sub> O <sub>3</sub>	High thermal stability up to 1700°C with inert gas.	Potential reaction with copper oxide	(NETZSCH 2017)
BN	High thermal stability up to 1600°C with inert gas.	Oxidising in an atmospheric air, reaction with copper oxide	(NETZSCH 2017)

### 5.4.3 Thermal analysis

Thermogravimetric analysis (TGA) and Differential Scanning Calorimetry (DSC) was performed using a Netzsch STA 449 F3 Jupiter instrument with an accuracy of  $\pm 2\%$ . The alumina crucible was used without the lid to facilitate the reactions between the metal oxide



and the gaseous environment. The software Proteus, developed by Netzsch was used for data analysis.

As shown in Table 5.2, two types of experiments were carried out for six different conditions of reduction and oxidation cycles. For the reduction cycle, the temperature of copper oxide was increased from 50°C to 1250°C for constant oxygen partial pressures of 0.05, 0.1, and 0.2 bar. This process results in storage of sensible, latent and chemical thermal energy. To stabilise the flow rate of different gases in the system at the beginning of the experiment the temperature was increased to 200°C and held constant for 20 minutes (Block & Schmücker 2016). The oxidation was performed at an oxygen partial pressure of 0.8 bar, which is equivalent to an absolute air pressure of 3.8 bar. For the second series of experiments, the partial pressure of oxygen during the reduction cycle was held constant at 0.1 bar, while a series of partial pressures were assessed for the oxidation cycle, namely 0.2 bar, 0.4 bar and 0.6 bar. The heating and cooling cycles were carried out between 50°C and 1250°C for the pair of CuO/Cu<sub>2</sub>O along with one reduction and oxidation cycles in liquid state (at constant temperature of 1250°C) with dwell time of 30min for each of the reduction and oxidation reactions. The heating and cooling rates were each selected to be 5°C/min for preventing thermal shock during each cycle.

**Table 5.2.** The partial pressure of oxygen in the reduction and oxidation reactors through which the sample was cycled. The reduction and oxidation were performed isothermally at a temperature of 1250°C. S2 is used for assessing SEM analysis of the copper oxide in LCL-  
TES system.

Partial pressure of oxygen (bar) in the reduction and oxidation reactors						
Samples	S1	S2*	S3	S4	S5	S6
<b>Reduction cycle</b>	0.05	0.1	0.2	0.1	0.1	0.1
<b>Oxidation cycle</b>	0.8	0.8	0.8	0.2	0.4	0.6

\*the reference case for assessing the thermal reliability of copper oxide over 10 cycles

Reversibility of the copper oxide in proposed system has been assessed by ten reduction and oxidation cycles in liquid state, for condition S2 shown in Table 5.2. Before the final step of

cooling process the oxygen flow was stopped and the flow rate of nitrogen was increased to 100ml/min for preventing the re-oxidation of the metal oxides.

Microstructural observations by Scanning Electron Microscopy (SEM) were performed with a Quanta 450 (ThermoFisher Scientific) instrument coupled with an INCA Pentafet x3 Energy Dispersive X-Ray Spectroscopy (EDS) microanalysis system from Oxford Instruments.

## **5.5 Results**

### **5.5.1 DSC analysis**

Figure 5.2 presents the DSC analysis of the copper oxide (CuO) under an atmosphere of 0.21 oxygen and 0.79 nitrogen. As can be seen, CuO has two successive thermal events, beginning with the reduction of CuO to Cu<sub>2</sub>O, followed by the melting of Cu<sub>2</sub>O. As shown in Figure 5.2, the reduction reaction of CuO takes place at 1035.9°C, while the melting of Cu<sub>2</sub>O occurs at 1137.1°C. These temperatures are in agreement with the data reported in literature (Agrafiotis et al. 2016; Shishin & Decterov 2012). The enthalpy of reaction was calculated from the area above the sharp trough at 1035.9°C to be 529.16J/g, while the enthalpy of the phase change was calculated to be 175.66J/g. The reaction and melting temperatures of the copper oxide are within 102°C of each other, which represents only a slight comprise from the desirable scenario of the thermochemical and latent heats being stored at the same temperature to minimise exergy loss.

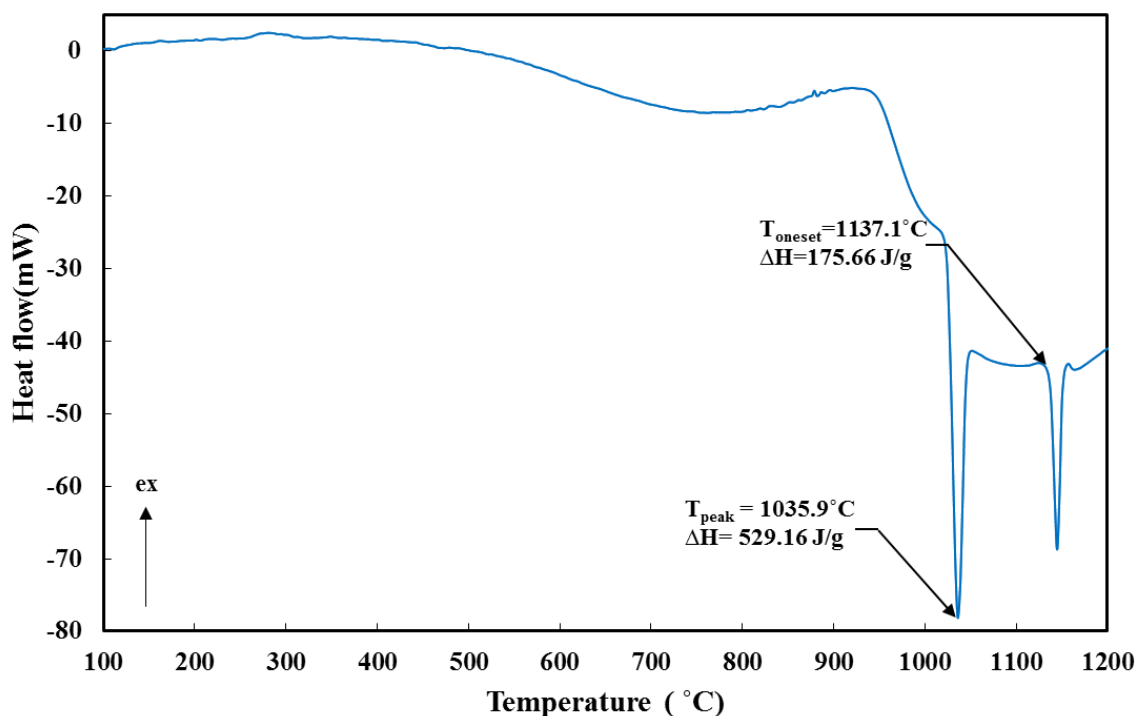


**Figure 5.2.** Temperature history for heating copper oxide in the crucible from ambient conditions, showing the reduction of CuO to Cu<sub>2</sub>O and melting temperature of Cu<sub>2</sub>O. The areas above the sharp troughs correspond to the enthalpies of latent and chemical heat.

### 5.5.2 Variation of partial pressure in reduction stage

Figure 5.3 presents a time history of the weight of three samples obtained using the TGA for a LCL-TES cycle for a series of constant oxygen partial pressures in the reduction reactor ( $P_{\text{O}_2} = 0.05, 0.1, 0.2$  bar) and for a single partial pressure in the oxidation reactor ( $P_{\text{O}_2} = 0.8$  bar). As can be seen, the copper oxide has undergone a complete heating and cooling cycle, together with one cycle of reduction and oxidation in the liquid state. The first reduction reaction occurs in solid state with a weight loss of the approximately 10% ( $4\text{CuO} \rightarrow 2\text{Cu}_2\text{O} + \text{O}_2$ ), which is similar for different partial pressures. It is clear that the reduction temperature can be increased from approximately 1130°C to 1210°C by increasing the partial pressure from 0.05 bar (S1) bar to 0.2 bar (S3). This shows the effect of pressure on reduction temperature. Returning to Figure 5.1 and comparison with Figure 5.2 shows that after the first reduction reaction the sample melts. Nevertheless, its mass also increases, which is attributed to the dissolution of oxygen into the sample at phase change point. This is in agreement with data previously reported in

the phase diagram of the Cu-O (Shishin & Decterov 2012). The second small weight loss related to the reduction reaction in liquid state followed by an oxidation reaction with increasing the weight of the sample. The reduction and oxidation reactions in the liquid state are derived by the change in the partial pressure of oxygen in the system. As can be seen in Figure 5.3, the oxidation of the material leads to approximately 5% increase in the mass of the sample, which means that the material could not reach to its initial weight in solid state. This is attribute to the limiting rate of diffusion of oxygen into the liquid sample through the liquid surface. In another word, the significance gradient of oxygen from the sample through to the depth of the liquid leads to oxidation of the sample mainly on the sample, while the liquid under the surface remains unreacted. This implies that, one should make provisions in the design of the oxidation reactor of the LCL-TES system to ensure that adequate dispersion or contact area between the liquefied reduced oxide and oxygen is achieved. This can be considered as one of the technical challenges of the proposed LCL-TES system at high temperature. This implies that thermochemical energy storage is possible in the liquid phase using copper oxide. Nevertheless, the storage in the solid phase is significantly higher. This is also in agreement with previous research by Silakhori et al. who found that 258.72 kJ/mol of the energy is stored through thermochemical reaction in the solid phase, while only 3.87 kJ/mol of energy is stored in the liquid phase.

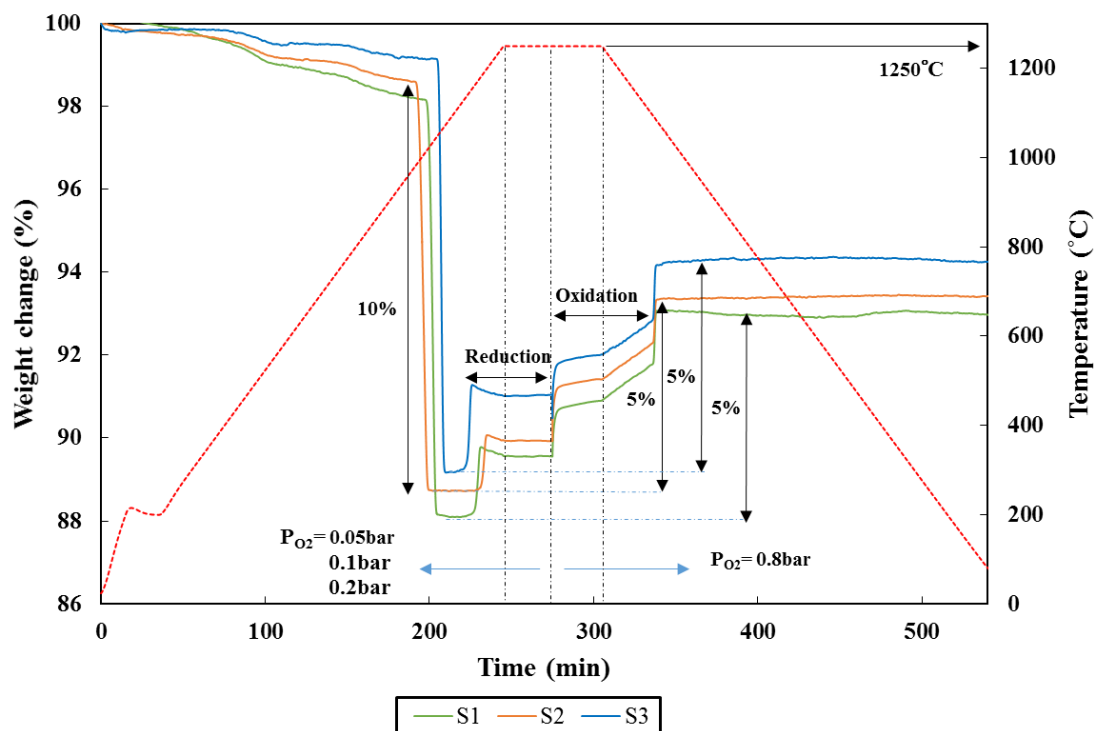


**Figure 5.3.** A time history of the weight of samples S1, S2, and S3 during one cycle of reduction and oxidation in the liquid phase, for the conditions shown in Table 5.2. The red dashed line shows the temperature of the system, while the pressure is changed at 280 minutes.

### 5.5.3 Variation of partial pressure in oxidation stage

Figure 5.4 presents a time history of one cycle of reduction and oxidation of copper oxide with the partial pressure of oxygen in the reduction cycles fixed at 0.1 bar and set to either 0.2, 0.4, or 0.6 bar for the oxidation cycles. The overall trends in Figure 5.4 are similar to those in Figure 5.3. However, the weight change in solid and liquid states during reduction are almost equal for the condition of S4, S5 and S6. This is because the partial pressure of oxygen is constant at 0.1 bar. As shown in Figure 5.4, the conversion of the oxidation reaction is lower for S4 (2%) than those of S5 and S6 (5%), which is consistent with the dependence of conversion on the partial pressure. In other words, at lower partial pressure of oxygen, the lower driving force of mass transfer limits the conversion of molten sample.

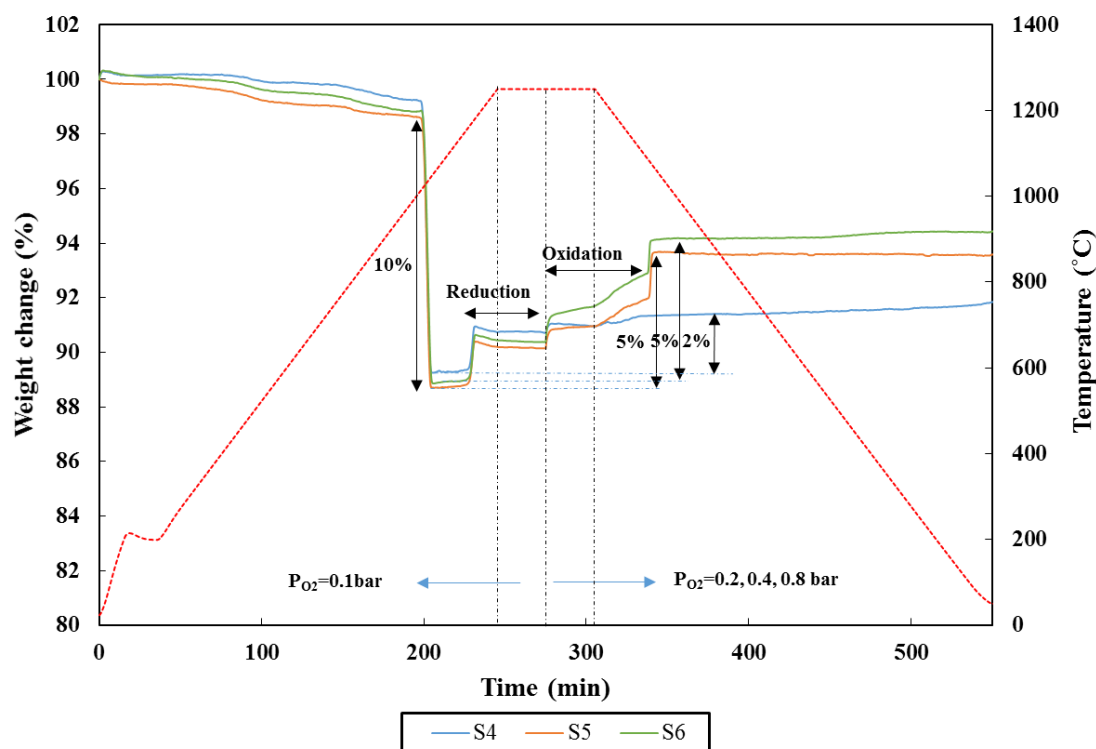
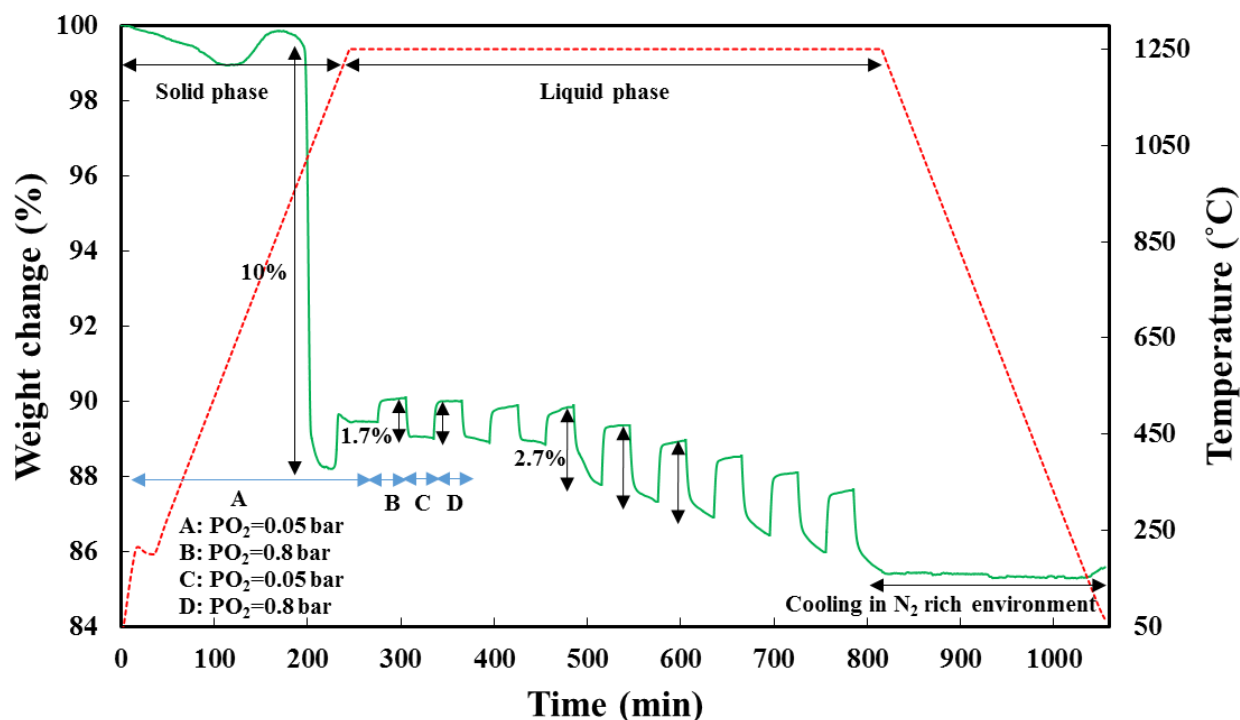


**Figure 5.4.** A time history of the weight of sample S4, S5, and S6 during one cycles of oxidation and reduction in the liquid phase, for the conditions shown in Table 5.1. The red dashed line shows the temperature of the system, while the pressure is changed at 280 minutes.

#### 5.5.4 Multiple cycles of reduction and oxidation

Figure 5.5 presents the time-weight history for ten successive cycles of reduction and oxidation of copper oxide in the liquid state at a temperature of 1250°C. The weigh change in the solid state is approximately 10% while this value is 1.7% in liquid state which supports the previous research by Silakhori et al. [6] that explains the small amount of thermochemical storage in liquid state. The same trends can be seen as those presented in Figure 5.3 and Figure 5.4. However, it can also be seen that the cycles are not identical over the ten cycles, with a gradual trend of increasing in the percentage weight change and ongoing weight loss. The change in the weight of copper oxide sample at the end of each successive cycle is consistent with previous finding that the copper reacts with alumina to form  $\text{CuAl}_2\text{O}_4$  (Karni et al. 1997; San Pio et al. 2018). This decreases the content of Cu in the molten slag and hence the activity of the copper oxide. That is,  $\text{Cu}_2\text{O}$  is consumed by reaction with  $\text{Al}_2\text{O}_3$  so that the mass of active  $\text{Cu}_2\text{O}$  decreases through the experiments. Decreasing the weight of the sample after four cycle

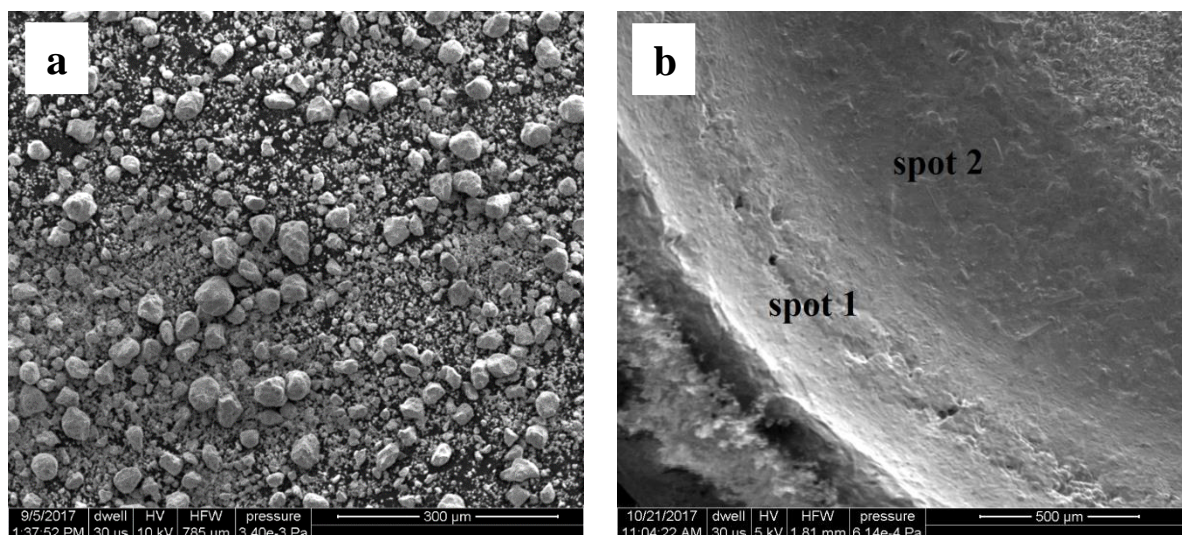
can be defined by reaction of the container with the sample at high temperature. This overall deduction in weight also highlights one of the challenges of the liquid chemical looping, which is the need to select combinations of metal oxides and refractories with low reactivity.



**Figure 5.5.** The time, temperature and weight history of reduction of solid copper oxide, followed by ten successive cycles of oxidation and reduction in liquid state. The red dashed line shows the variation of temperature in the system.

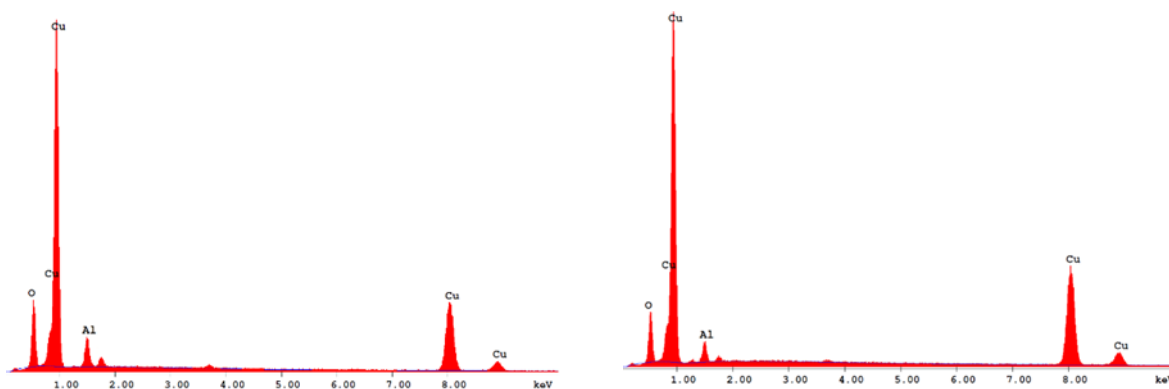
### 5.5.5 SEM analysis

Figure 5.6 presents SEM micrographs of the copper oxide powder before and after the cycling tests for the case S2. Figure 5.6-a shows the powdered form of the raw copper oxide before melting. Figure 5.6-b shows that the microstructure of copper oxides has changed after melting, and after successive stages of reduction and oxidation in the liquid state.



**Figure 5.6.** SEM micrographs of copper oxide a) in the raw form (before cycling), and b) after 10 cycles of oxidation and reduction for the conditions of S2 in table1.

Figure 5.7 also identifies the two “spots” that were selected for EDS analysis. The EDS analysis of the copper oxide for the condition of S2 after 10 cycles shows that aluminium is presented in both spots as shown on the SEM micrograph. The percentage of aluminium is approximately 7.6% near the crucible wall, while this value decreases to 4.5% in the middle of the crucible, which is attribute to the reaction of the sample with crucible.



<i>Spot 1</i>		
<i>Element</i>	<i>Wt %</i>	<i>At %</i>
<i>O</i>	<i>14.58</i>	<i>37.05</i>
<i>Al</i>	<i>7.68</i>	<i>11.57</i>
<i>Cu</i>	<i>76.74</i>	<i>51.37</i>
<i>Total</i>	<i>100</i>	<i>100</i>

<i>Spot2</i>		
<i>Element</i>	<i>Wt %</i>	<i>At %</i>
<i>O</i>	<i>9.18</i>	<i>27.33</i>
<i>Al</i>	<i>4.58</i>	<i>8.07</i>
<i>Cu</i>	<i>86.24</i>	<i>64.60</i>
<i>Total</i>	<i>100</i>	<i>100</i>

**Figure 5.7.** EDS analysis of the copper oxide in different spots shown in Figure 5.6.



## 5.6 Conclusion

In this study, the potential of copper oxide in proposed Liquid Chemical Looping for Thermal Energy Storage (LCL-TES) cycle has been assessed experimentally by TGA. More specifically, the results of the TGA showed that copper oxide can be reduced and oxides in the liquid state by changing the oxygen partial pressure from 0.05 to 0.8 bar at isothermal condition for chemical storage. However, the weight gain was lower than that weight loss in oxidation and reduction, respectively, which explained one of the technical challenges of this system due to diffusion effects. An additional experiment demonstrated the reversibility of copper oxide and the potential reaction between copper oxide and alumina crucible over 10 successive reduction and oxidation cycles. The SEM micrographs and EDS analysis of S2 after 10 cycle confirm the reaction between copper oxide and alumina during reduction and oxidation cycles. That is, we have found that the sample has partly reacts with the container materials and where major parts of have been agglomerated to a big chunk. It is worth noting that the implementation of the LCL-TES system requires further work to develop a suitable solar particle-to-liquid reduction reactor with which to achieve the process of sensible heating, melting and reduction at these temperatures. This includes the need to identify appropriate means to contain and handle the molten metals, which are aggressive. In summary, the key challenge of this cycle will require the identification of suitable combinations of metals and refractories with sufficiently low reactions to withstand multiple cycle of successive oxidation and reduction.

## 5.7 References

C. Agrafiotis, M. Roeb & C. Sattler 2016, 'Exploitation of thermochemical cycles based on solid oxide redox systems for thermochemical storage of solar heat. Part 4: Screening of oxides for use in cascaded thermochemical storage concepts', *Solar energy*, vol. **139**. pp. 695-710.

C. Agrafiotis, M. Roeb, M. Schmücker & C. Sattler 2014, 'Exploitation of thermochemical cycles based on solid oxide redox systems for thermochemical storage of solar heat. Part 1: Testing of cobalt oxide-based powders', *Solar energy*, vol. **102**, pp. 189-211.

C. Agrafiotis, M. Roeb, M. Schmücker & C. Sattler 2015, 'Exploitation of thermochemical cycles based on solid oxide redox systems for thermochemical storage of solar heat. Part 2: Redox oxide-coated porous ceramic structures as integrated thermochemical reactors/heat exchangers', *Solar energy*, vol. **114**, Supplement C, pp. 440-458.

E. Alonso, C. Pérez-Rábago, J. Licurgo, E. Fuentealba & C. A. Estrada 2015, 'First experimental studies of solar redox reactions of copper oxides for thermochemical energy storage', *Solar energy*, vol. **115**, pp. 297-305.

B. Wong 2011, Thermochemical heat storage for concentrated solar power, final report for the U.S. Department of Energy, Department of Energy, San Diego, CA, USA.

R. K. Bhargava, M. Bianchi, A. De Pascale, G. Negri di Montenegro & A. Peretto 2007, 'Gas Turbine Based Power Cycles - A State-of-the-Art Review', in Springer Berlin Heidelberg, Berlin, Heidelberg, pp. 309-319.

T. Block & M. Schmücker 2016, 'Metal oxides for thermochemical energy storage: A comparison of several metal oxide systems', *Solar energy*, vol. **126**, pp. 195-207.

M. Deutsch, F. Horvath, C. Knoll, D. Lager, C. Gierl-Mayer, P. Weinberger & F. Winter 2017, 'High-Temperature Energy Storage: Kinetic Investigations of the CuO/Cu<sub>2</sub>O Reaction Cycle', *Energy & Fuels*, vol. **31**, 3, pp. 2324-2334.

M. Fahim & J. Ford 1983, 'Energy storage using the BaO<sub>2</sub>/BaO reaction cycle', *The Chemical Engineering Journal*, vol. **27**, 1, pp. 21-28.

J. Habainy & C. Nilsson 2013, 'Oxidation of pure tungsten in the temperature interval 400°C to 900°C', *Lund University, department of mechanical engineering*.

P. Haseli, M. Jafarian & G. J. Nathan 2017, 'High temperature solar thermochemical process for production of stored energy and oxygen based on CuO/Cu<sub>2</sub>O redox reactions', *Solar energy*, vol. **153**, pp. 1-10.

W. Hu, F. Donat, S. A. Scott & J. S. Dennis 2016, 'The interaction between CuO and Al<sub>2</sub>O<sub>3</sub> and the reactivity of copper aluminates below 1000°C and their implication on the use of the Cu-Al-O system for oxygen storage and production', *RSC Advances*, vol. **6**, 114, pp. 113016-113024.

M. Jafarian, M. Arjomandi & G. J. Nathan 2017, 'Thermodynamic potential of molten copper oxide for high temperature solar energy storage and oxygen production', *Applied Energy*, vol. **201**, pp. 69-83.

J. Karni, A. Kribus, P. Doron, R. Rubin, A. Fiterman & D. Sagie 1997, 'The DIAPR: a high-pressure, high-temperature solar receiver', *Journal of Solar Energy Engineering*, vol. **119**. 1, pp. 74-78.

S. Kuravi, J. Trahan, D. Y. Goswami, M. M. Rahman & E. K. Stefanakos 2013, 'Thermal energy storage technologies and systems for concentrating solar power plants', *Progress in energy and combustion science*, vol. **39**. 4, pp. 285-319.

T. Kurushima & K. Ishizaki 1992, 'Reactions of Copper and Copper Oxides with Nitride Ceramics (AlN, SiAlON, Si<sub>3</sub>N<sub>4</sub>) and Their Oxide Additives', *Journal of the Ceramic Society of Japan*, vol. **100**. 1163, pp. 955-959.

G. J. Nathan, M. Jafarian, B. B. Dally, W. L. Saw, P. J. Ashman, E. Hu & A. Steinfeld 2018, 'Solar thermal hybrids for combustion power plant: A growing opportunity', *Progress in energy and combustion science*, vol. **64**. pp. 4-28.

NETZSCH 2017, 'Accessories for Differential Scanning Calorimeters and Thermobalances (Crucibles, Sensors, Sample Carriers, Calibration Kits for DSC, TGA and STA Systems)', NETZSCH.

J. P. Neumann, T. Zhong & Y. A. Chang 1984, 'The Cu-O (Copper-Oxygen) system', *Bulletin of Alloy Phase Diagrams*, vol. **5**. 2, pp. 136-140.

A. Roine 2002, 'Outokumpu HSC chemistry for windows: Chemical Reaction and Equilibrium Software with Extensive Thermochemical database'.

M. A. San Pio, M. Martini, F. Gallucci, I. Roghair & M. van Sint Annaland 2018, 'Kinetics of CuO/SiO<sub>2</sub> and CuO/Al<sub>2</sub>O<sub>3</sub> oxygen carriers for chemical looping combustion', *Chemical Engineering Science*, vol. **175**. pp. 56-71.

D. Shishin & S. A. Decterov 2012, 'Critical assessment and thermodynamic modeling of the Cu-O and Cu-O-S systems', *Calphad*, vol. **38**. pp. 59-70.

M. Silakhori, M. Jafarian, M. Arjomandi & G. J. Nathan 2017, 'Comparing the thermodynamic potential of alternative liquid metal oxides for the storage of solar thermal energy', *Solar energy*, vol. **157**. pp. 251-258.

S. Wu, C. Zhou, E. Doroodchi, R. Nellore & B. Moghtaderi 2018, 'A review on high-temperature thermochemical energy storage based on metal oxides redox cycle', *Energy Conversion and Management*, vol. **168**. pp. 421-453.

## **Chapter 6 Energetic performance of liquid chemical looping cycle with solar thermal energy storage**

---

### **6.1 Chapter preview**

In this chapter, the performance of copper oxide in a liquid chemical looping thermal energy storage (LCL-TES) gas turbine combined cycle is presented. The LCL-TES system that was described in chapter 4, is modelled with HSC chemistry and Matlab software in this section. Aspen plus software is used to provide a model for a gas turbine combined cycle. The effect of different parameters such as pressure and temperature of air reactor, concentration ratio of the solar reactor and the effect of the after burner on the efficiency and exergy of the system is presented in this section.

The details of the method, and results are presented in the following section. This section is presented in the paper format submitted for publication in journal of Energy.



---

Name of Co-Author	Maziar Arjomandi		
Contribution to the Paper	- Supervision of the work, including the production of the manuscript - Participation in the development of the concepts and ideas presented in the manuscript - Evaluation and editing of the manuscript prior to submission		
Signature		Date	4/02/2019

Name of Co-Author	Graham 'Gus' Nathan		
Contribution to the Paper	- Supervision of the work, including the production of the manuscript - Participation in the development of the concepts and ideas presented in the manuscript - Evaluation and editing of the manuscript prior to submission		
Signature		Date	4/2/19

**The energetic performance of a liquid chemical looping cycle with solar thermal energy storage**

**Mahyar Silakhori**, Mehdi Jafarian, Maziar Arjomandi, Graham J. Nathan

Published: Journal of Energy, vol. **21**. pp. 216-221.

## 6.2 Abstract

A Liquid Chemical Looping cycle Thermal Energy Storage (LCL-TES) with a gas turbine combined cycle is assessed for two different configurations. In the first configuration, the hot gas from the LCL-TES system is transferred directly to the gas turbine, while in the second one the hot gas is heated further by an after- burner. Aspen plus software was used together with MATLAB codes to simulate the cycle for an average diurnal normal irradiance profile of Port-Augusta in South Australia, using copper oxide as the chemical looping medium. The effect of air reactor pressure, concentration ratio of the solar concentrator, conversion extent and thermal input from the after-burner on the cycle efficiency was assessed. Also reported are the solar absorption, solar to electrical efficiency, solar share, and exergy efficiency, together with their sensitivities to relevant input parameters. On this basis, the first law efficiency was estimated to be 44.9% and 50% for the cycle without and with the after-burner, with corresponding temperatures of 1200°C and 1700°C, respectively.



## Nomenclature

$A_{coll}$	Solar collector area ( $m^2$ )	<b>subscripts</b>	
$CR$	Mean flux concentration ratio	<i>ads</i>	adsorption
$DNI$	Direct normal insolation ( $W/m^2$ )	<i>AB</i>	After-Burner
$E_{elec,LCL-TES}$	Power produced by the LCL-TES system (W)	<i>AR</i>	Air Reactor
$n_i$	Molar flow rate of the stream $i$ (mol/min)	<i>coll</i>	collector
$\dot{Q}_{coll}$	Incoming power from solar collector field (W)	<i>Sol</i>	Solar
$\dot{Q}_{re-rad}$	Re-radiated thermal power (W)	<i>RR</i>	Reduction Reactor
$\dot{Q}_{s,in}$	Input solar thermal power (W)	<i>GT</i>	Gas Turbine
$\dot{Q}_{s,abs}$	Absorbed solar thermal power (W)	<i>GTCC</i>	Gas Turbine Combined Cycle
$\dot{Q}_{s,in,max}$	Maximum input solar thermal power (W)	<i>Gen</i>	Generator
$T_{RR}$	Temperature of reduction reactor (K)	<i>in</i>	input
$T_i$	Temperature of the stream $i$ (K)	<i>OC</i>	Oxygen Carrier
$\dot{W}_{AR,ST}$	Power generated by the air reactor steam turbine(W)	<i>out</i>	output
$\dot{W}_{c,Air}$	Power generated by the air compression(W)		
$\dot{W}_{GT}$	Power generated by the Gas turbine (W)		
$\dot{W}_{pump}$	Power consumed by the pump (W)		
<b>Greek letters</b>			
$\alpha_{eff}$	Effective adsorptance		
$\Delta H_i$	Enthalpy change of stream $i$ (kJ/mol)		
$\Delta \eta_{con-sol,elec}$	Incremental efficiency of concentrated solar to electrical efficiency		
$\epsilon_{eff}$	Effective absoptancce		
$\eta$	First law efficiency		
$\eta_{abs,tot}$	Absortion efficiency		
$\eta_{coll}$	Average collector system optical efficiency		
$\sigma$	Stephan-Boltzmann constant ( $W/m^2 K^{-4}$ )		
$X_{sol,total}$	Solar share		
$X_{boost,av}$	Average fractional power boost		
$X_{boost,Pk}$	Peak fractional power boost		

## 6.3 Introduction

The interest in Thermal Energy Storage (TES) is increasing because of its potential to provide low-cost schedulable output from a variable solar resource, in particular for high temperature

application such as concentrated solar power (CSP) plants (Kuravi et al. 2013). The most common working medium chosen to date for commercial TES system is a molten salt, which can be used at a maximum operating temperature of below 600°C. This limits the maximum temperature, and hence cycle efficiency, of the plant. One of the approaches recently proposed to enable higher temperatures and efficiencies of CSP plants is through the use of liquid metal oxides as a TES medium (Jafarian et al. 2017; Silakhori et al. 2017). However, the thermodynamic efficiency of a full power cycle utilising molten metal oxide has yet to be evaluated. Therefore, the aim of the present study is to meet this need.

Thermal energy can potentially be stored in the forms of sensible, latent and/or thermochemical heat. Sensible heat storage such as the commercially available molten salt systems used in CSP plant is typically operated in the temperature range of 400-500°C (Gil et al. 2010; Kolb 1998; Kuravi et al. 2013; H Price 2003; Hank Price et al. 2002; Robak et al. 2011; Yang & Garimella 2010; Zhang et al. 2013). To achieve TES for CSP plant at higher temperature e.g. 900°C, liquid metals such as sodium, tin and Lead-Bismuth (LBE) have been recently proposed (J. Pacio et al. 2013; J Pacio & Wetzel 2013). If successful, the higher temperature would increase efficiency over commercial systems. One of the major drawbacks of the application of liquid metals, particularly at high temperatures, is their corrosiveness (Kim et al. 2015). Hence, it is necessary to identify the potential benefits that could be obtained to justify further research to meet this challenge.

Latent heat storage, which is achieved through a phase change, offers the potential for higher energy density than their sensible energy counterpart. Nevertheless, the change in volume associated with phase change as well as a low thermal conductivity are some of the barriers to their commercial implementation (Fauzi et al. 2014; Silakhori et al. 2015; Silakhori et al. 2014). The application of metal oxides as a phase change storage media with high thermal stability

and conductivity could be a measure to eliminate these limitations (Liu et al. 2015; Mohamed et al. 2017).

Thermo-chemical energy storage, which employs reversible chemical reactions, provides a high energy density of approximately fifteen times greater than that of sensible heat storage. It can also achieve six times greater energy density than that of latent heat storage (Abedin & Rosen 2011), together with energy transfer at a relatively constant temperature (Nagel et al. 2013). From the different types of thermo-chemical energy storage systems, the reduction and oxidation (redox) of metal oxides have received most attention due to their capability to provide high values of both temperature and energy density. Most metal oxide pairs investigated and proposed previously are both in the solid phase so that they suffer from attrition, agglomeration, and sintering during successive redox cycles (B.Wong 2011). One potential approach to address these challenges is the system proposed by Jafarian et al. (Jafarian et al. 2017) in which changes to the phase occur together with that of oxidation state, so that the material is “remade” with each cycle. Jafarian et al. (Jafarian et al. 2017) estimated that the normalised mass of stored solid particles in the cold storage reservoir and molten metal in hot storage reservoir is  $50.85 \text{ mol/MW}_{\text{sol,max}}$  and  $36.64 \text{ mol/MW}_{\text{sol,max}}$ , respectively. These values are based on the maximum Direct Normal Insolation (DNI) of Port Augusta, South Australia which occurs at solar noon (*Analysis of 10 years record Port Augusta australia, South Australia* 2010). Nevertheless, this concept introduces some technical challenges of its own because molten copper is a highly reactive material. Nevertheless, it also offers some significant additional potential benefits including the combined use of sensible, latent, and thermo-chemical TES at a high temperature, which leads to the generation of hot air for power generation (Silakhori et al. 2017). Furthermore, since this concept is new a wide range of alternative configuration and materials are also possible. However, to justify further work on the cycle, it is desirable to better evaluate the thermodynamic potential of the proposed LCL-TES power cycle. Hence,

---

the main objective of the preset study is to assess the performance of a LCL-TES system in a combined power cycle.

The operating temperature of the oxidation reactor in a copper-based LCL-TES system was estimated to be 1200°C (Jafarian et al. 2017), which is less than operating temperature of a commercially available gas turbine of approximately 1250°C (Jafarian et al. 2017). However, technologies to enable the inlet temperature of a gas turbine reach to 1700°C are anticipated in the foreseeable future (Jafarian et al. 2017). Application of After-burners is a well-established method to boost the temperature of pressurised air before it is introduced to the gas turbine. Therefore, this work further aims to investigate the potential of an after-burner fuelled with methane which is the main component of natural gas to further heat the pressurised air. Since such an increase in efficiency would be attained at the cost of a lower solar share, it is desirable to assess this trade-off. The paper also aims to meet this need.

#### **6.4 LCL-TES Gas Turbine Combined Cycle (GTCC)**

The key components of the proposed LCL-TES GTCC are shown in Figure 6.1. The process features a hot gas generator, shown as Section I in Figure 6.1, and a gas turbine combined cycle, shown as Section II of Figure 6.1. The hot gas generator section comprises a solid to liquid solar receiver, two storage tanks and a liquid to solid heat exchanger. This system has been explained in detail by Jafarian et al. (Jafarian et al. 2017), who provide a phase diagram and experimental data, so that only a brief explanation is provided here.

When solar thermal radiation is available at sufficient flux to overcome the re-radiation losses, it is used to heat, melt and reduce the solid CuO particles that are introduced into the solid to liquid solar receiver from Tank 1. Furthermore, it is proposed to inject steam into the solar receiver to decrease the oxygen partial pressure in the gas phase and to further reduce CuO(s) to CuO<sub>8</sub>(l). As a plausible configuration, the solid to liquid solar receiver can be a modified

version of the direct solar rotary kiln, proposed and tested at Deutsches Zentrum für Luft- und Raumfahrt e.V. (DLR) (Funken et al. 2001), in which the steam can be injected to reduce the partial pressure of reactor. Developed configuration of vortex reactor, which is demonstrated by Z'Graggen et al. (Z'Graggen et al. 2006) can be another plausible configuration. This reactor has the potential to successfully increase the temperature of the particle to 1300°C, which is a sufficient temperature to melt the particles. The system also comprises a Hot Storage Reservoir (HSR) to store the reduced copper oxide.

The molten copper oxide is proposed to be introduced to the air reactor (stream 2) for oxidation, which also generates hot air for the gas turbine for power generation through stream 16. One plausible configuration for oxidation reaction is a bubble reactor, which offers high mass and heat transfer rates (Shah et al. 1982). It is worth noting that the inlet of liquid metals to the oxidation bubble reactor can be pressurised using the difference in the elevation of the hot tank and the oxidation reactor considering the high density of liquid metal oxides. A stream of air (Stream 5), is also introduced to enable control of the operating temperature of the oxidation reactor [7]. A Heat Recovery (HR) unit is required for solidification and cooling of the liquid metal oxide (stream 4). Such a unit would need the development of a reliable oxidation reactor to consecutively solidify and oxidise the liquid metal, while also recovering heat (Jafarian et al. 2017). This can be performed in a quenching air stream by “atomisation” of the liquid copper oxide (Silakhori et al. 2017). The cold particles from HR unit transfer to Cold Storage Reservoir (CSR) and then to the RR for repeating the cycle (stream 6 and 7). In addition, a number of mechanism are available to transfer the cold particles from CSR to the reduction reactor, including a screw particle conveyer.

The inlet air is proposed to be pressurised using an air compressor. Valve V1 is used as a means to control the flow rate of the liquid metal oxide to the air reactor. A heat exchanger has been demonstrated to recover heat from the O<sub>2</sub> stream outlet from the reactor (stream 8) to produce

---

steam. The steam flow rate into the reduction reactor can be adjusted by valve V3. This energy source is intermitted, since it will only be available, when the solar radiation is available.

The power generation section, shown as Section II in Figure 6.1, comprises a gas turbine together with a two-stage steam turbine as the bottoming cycle. The hot pressurised gases from either the air reactor (stream 16) or from the after-burner (stream 19) are introduced to the gas turbine. The outlet gas leaving the gas turbine is then transferred to steam in a Heat Recovery Steam Generator (HRSG) (stream 21) to produce additional power with a two-stage steam turbine. The concept of HRSG and steam turbines are based on the previous analysis of Naqvi et al. (Naqvi et al. 2007) and Jafarian et al. (Jafarian et al. 2014). The after-burner (AB) is employed to boost the temperature of the pressurised hot gas leaving the air reactor (stream 18 in Figure. 1), prior to being introduced to the gas turbine (stream 20). The cycle can be operated with or without the after-burner, by adjusting valves V4 and V5.

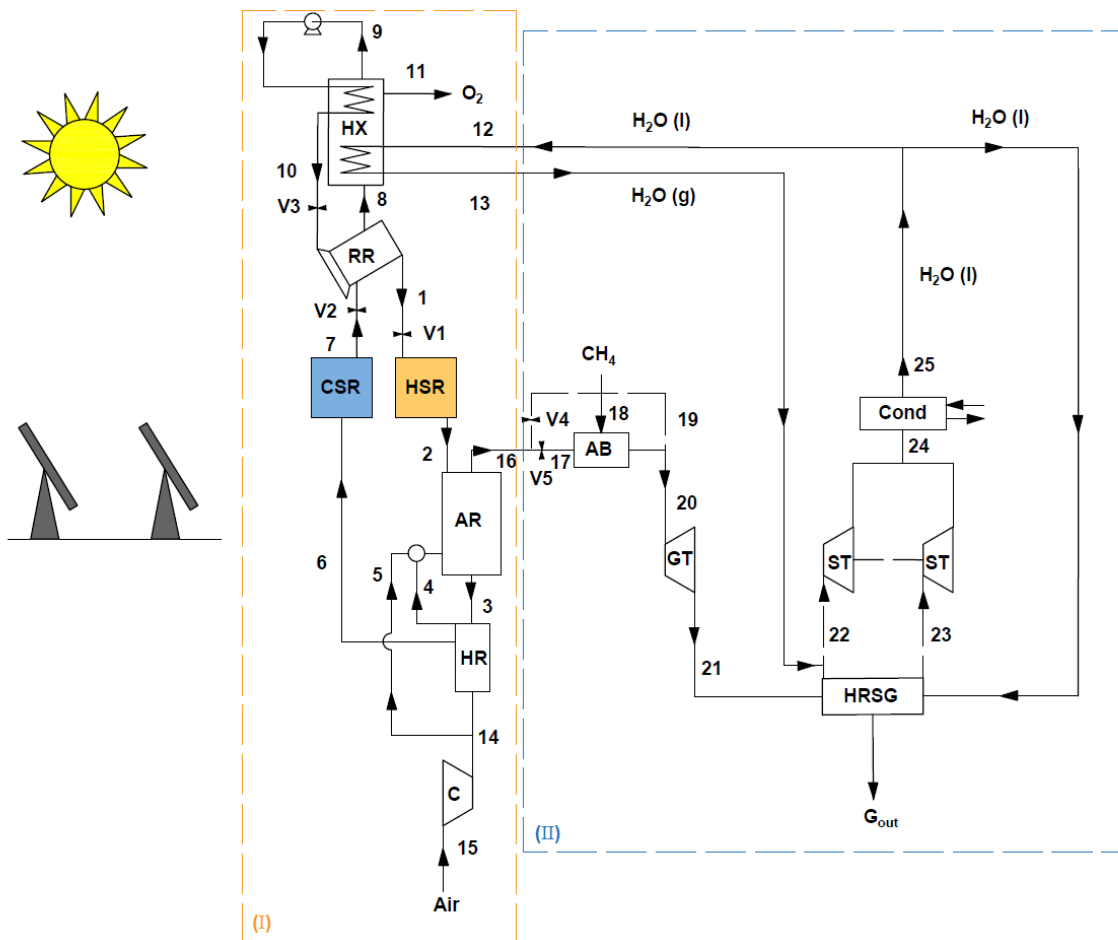


**Figure 6.1.** The LCL-TES combined cycle comprising a Cold Storage Reservoir (CSR) and a Hot Storage Reservoir (HSR) to store cold particles and hot molten metal oxide, respectively.

Figure 6.2 presents a reference case, which is used to compare of the LCL-TES system equipped with an AB. This conventional gas turbine combined cycle (GTCC) consists of a gas turbine that uses the same amount of fuel consumed by LCL-TES with an AB, together with a two-stage steam turbine. The inlet temperature and pressure of the gas turbine were chosen to be 15 bar and 1250°C, respectively.

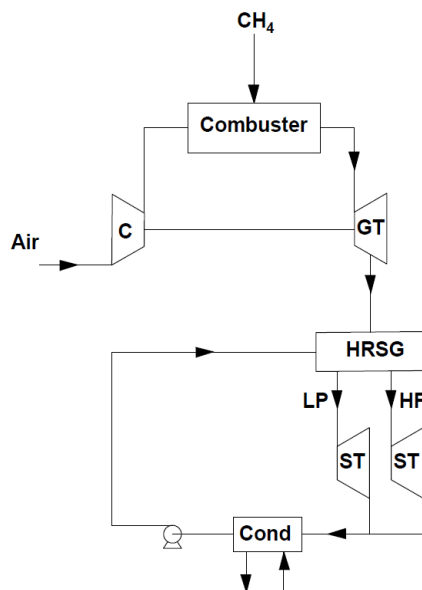


**Figure 6.2.** A schematic diagram of the reference combined cycle, comprising a gas turbine and a two-stage steam turbine (Jafarian et al. 2014).

## 6.5 Methodology

The concentrated solar heat flux from the solar collector ( $\dot{Q}_{coll}$ ) was calculated using Eq.1, where the  $\eta_{coll}$  and  $DNI$  are the mean optical efficiency of the field and the direct normal insolation, respectively. The mean optical efficiency was assumed to be 65.0% based on the literature (Hong & Jin 2005).

$$\dot{Q}_{coll} = \eta_{coll} A_{coll} DNI \quad (1).$$

To simplify the calculation, it is assumed that the aperture receives all the incoming concentrated solar thermal power from the solar collector field such that there are no spillage losses. That is, we assume,  $\dot{Q}_{coll} = \dot{Q}_{s,in}$  following earlier work (Steinfeld et al. 1996).

The total solar energy absorption efficiency,  $\eta_{abs,tot}$ , is then calculated with Eq. 2.

$$\eta_{abs,tot} = \frac{\int_{day\ time} \dot{Q}_{s,abs} dt}{\int_{day\ time} (\dot{Q}_{s,abs} + \dot{Q}_{re-rad}) dt} \quad (2),$$



where  $\dot{Q}_{s,abs}$  is the concentrated solar thermal energy that is absorbed by the solar reactor, while  $\dot{Q}_{re-rad}$  is the re-radiated power loss from the aperture of the solar reactor. The absorbed and re-radiated power are calculated with Eq.3 and 4, respectively, as:

$$\dot{Q}_{s,abs} = \dot{Q}_{s,in} \left( 1 - \frac{\varepsilon_{eff} \sigma T_{RR}^4}{\alpha_{eff} CR DNI} \right) \quad (3),$$

$$\dot{Q}_{re-rad} = \dot{Q}_{s,in} \frac{\varepsilon_{eff} \sigma T_{RR}^4}{\alpha_{eff} CR DNI} \quad (4).$$

In these equations,  $\dot{Q}_{s,in}$ ,  $\alpha_{eff}$  and  $\varepsilon_{eff}$  are the solar power input to the solar receiver, the effective adsorptance and the effective emittance of the cavity receiver, respectively.  $\sigma$  is as Stephan-Boltzmann constant. The parameters,  $T_{RR}$  and CR are the temperature of the reduction reactor and the mean flux concentration ratio, respectively.

The first law efficiency,  $\eta$ , of the LCL-TES system is as follows:

$$\eta = \frac{\int_{24 \text{ hours}} ((\dot{W}_{GT} - \dot{W}_{comp}) + (\dot{W}_{AR,ST} - \dot{W}_{pump})) dt + \int_{day \text{ time}} (\dot{W}_{RR} - \dot{W}_{pump}) dt}{\int_{day \text{ time}} (\dot{Q}_{s,abs} + \dot{Q}_{re-rad}) + \int_{24 \text{ hours}} (\dot{m}_{F,AB} LHV_{CH_4})} \quad (5).$$

The storage capacity is assumed to be sufficient for the Steam turbine and gas turbine to operate continually, so that start-up and shutdown losses are ignored. Although this is reasonable for the average solar day assessed here, it is not accurate for more general operation, since the storage capacity required truly continuous operation is likely to be prohibitive (Kueh et al. 2015). In contrast, the energy from the reduction reactor required to drive the steam turbine is available once the solar reduction reactor is working (Jafarian et al. 2014, 2014). This condition can be thought of as a ‘‘power boost’’ mode of operation over the ‘‘base load’’ element of the output generated by the hot gas generated in air reactor, adopting the terminology of Kolb (Kolb 1998) for an analogous configuration. The peak and average fractional power boost values are defined by  $X_{boost,pk}$  and  $X_{boost,av}$ , which are the ratios of excess power from the

RR-Steam turbine to the net power from AR-Steam turbines and the gas turbine. Importantly, the intermittent nature of this heat recovery can be readily accommodated without additional start-up losses since the recovery utilises the steam turbine from the combined cycle that is already operating.

$$X_{boost,av} = \frac{\int_{day\ time} (\dot{W}_{RR} - \dot{W}_{pump}) dt}{\int_{24\ hours} ((\dot{W}_{GT} - \dot{W}_{comp}) + (\dot{W}_{AR,ST} - \dot{W}_{pump})) dt + \int_{day\ time} (\dot{W}_{RR} - \dot{W}_{pump}) dt} \quad (6),$$

$$X_{boost,pk} = \frac{(\dot{W}_{RR} - \dot{W}_{pump})_{at\ solar\ noon}}{((\dot{W}_{GT} - \dot{W}_{comp}) + (\dot{W}_{AR,ST} - \dot{W}_{pump}))_{at\ solar\ noon}} \quad (7),$$

For case in which the AB is used, the total solar share,  $\chi_{sol,tot}$  can be calculated as follows:

$$\chi_{sol,tot} = \frac{\int_{day\ times} (\dot{Q}_{s,abs} + \dot{Q}_{re-rad}) dt}{\int_{day\ time} (\dot{Q}_{s,abs} + \dot{Q}_{re-rad}) + \int_{24\ hours} (\dot{n}_{F,AB} LHV_{CH_4})} \quad (8).$$

The incremental concentrated solar radiation to electrical efficiency,  $\Delta\eta_{con-sol,elec}$ , is estimated from earlier work (Buck et al. 2002; Hong et al. 2005) as follows:

$$\Delta\eta_{con-sol,elec} = \frac{\int_{24\ hours} (\dot{E}_{elec,LCL-TES} - \eta_{ref} \cdot \dot{E}_{fuel,hybrid}) dt}{\int_{day\ time} \dot{Q}_{s,in} dt} \quad (9),$$

The first law efficiency of the reference cycle ( $\eta_{ref}$ ) and its fuel consumption ( $\dot{E}_{fuel,ref}$ ) along with the power produced from the LCL-TES cycle are estimated by Eq.9.

The ratio of net output exergy to the total input exergy corresponds to the exergy efficiency and it is calculated as follows (Dincer & Rosen 2012):

$$\eta_{ex} = \frac{\int_{24\ hours} \dot{W}_t dt}{\int_{day\ time} ((\dot{Q}_{s,abs} + \dot{Q}_{re-rad}) \left(1 - \frac{T_0}{T_{RR}}\right) dt + \int_{24\ hours} \dot{n}_{F,AB} EX_F dt} \quad (10).$$

Table 1 lists the operating conditions used for assessment of the cycles here. Furthermore, the solar Direct Normal Insolation (DNI) data of Port Augusta, South Australia, has been used for the assessment.

The net power produced from each cycle (with and without AB) was calculated as follows:

$$\dot{W}_{n,l} = \sum \dot{W}_{turb} - \sum \dot{W}_{comp/pump} \quad (11).$$

In Eq. 11, the subscripts, “*comp/pump*” and “*turb*” represent the power used by the pumps and compressors and/or pumps and the power generated by the turbines, respectively.

The sensitivity to variations in the parameters listed in Table 6.1, of both the cycles with and without the use of an AB is also assessed to identify those variable with the most significant influence on the performance of the cycles.

**Table 6.1.** The input conditions for the cycle, chosen or assumed, for both the cases with and without the AB.

	Operating conditions of the reference cycle	Rang of variation	References
<b>Solar collector field</b>			
Optical efficiency (%)	65		(Hong & Jin 2005)
Mean flux concentration ratio	2000	From 500 to 8000	(Steinfeld et al. 1996)
<b>Solar reduction reactor</b>			
Effective adsorptance	1		(Steinfeld et al. 1996)
Effective emittance	1		(Steinfeld et al. 1996)
Temperature (°C)	1200	-	
Pressure (bar)	1	-	
<b>Air reactor</b>			
temperature (°C)	1200		
Pressure (bar)	15	From 10 to 15	
<b>Reservoir and heat exchanger's temperatures</b>			
Reservoir R1 temperature	450	From 100 to 600	
Reservoir R2 temperature	1200		
<b>Power cycles</b>			
Gas turbine isentropic efficiency	0.91		(Hong et al. 2010)
steam turbine isentropic efficiency	0.90		(Gou et al. 2007)
Air compressor isentropic efficiency	0.88		(Hong et al. 2010)

---

Pump isentropic efficiency	0.75	(Gou et al. 2007)
Steam pressure (HP/LP)(bar/bar)	60/5	(Naqvi et al. 2007)
Steam temperature (HP/LP) (°C/°C)	467/258	(Naqvi et al. 2007)
Generators mechanical efficiency	0.99	(Gou et al. 2007)
Efficiency of generator	0.99	(Consonni et al. 2006)

---

## 6.6 Results and discussion

The calculated solar power absorbed within the solar reactor ( $\dot{Q}_{s,abs}$ ), the re-radiation heat lost from the aperture of the solar reactor ( $\dot{Q}_{re-rad}$ ) and provided power by the fuel to AB ( $\dot{Q}_{AB}$ ) are shown in Figure 3 for the hourly solar day, calculated across the whole year. Maximum solar power input to the solar reactor ( $\dot{Q}_{s,in,max}$ ) is used to normalized these parameters. This case is chosen as reference scenario, although it is recognised that this greatly underestimates the variability in the solar resource, so that an order of magnitude increase to the capacity of storage would be needed to maintain continues output throughout the year, depending on the solar resource (Kueh et al. 2015).

As can be seen from figure 3, the output power continues for the entire 24 hours, for this time average solar resources, increasing slightly during the solar hours due to the contribution from the steam turbine (Stream 13 in Figure 6.1). This is because heat is recovered from the flow of hot O<sub>2</sub> (Stream 8 in Figure 6.1) from the output of the reduction reactor when the solar resource is available. As expected, the solar resource provides an input between t=7:30 and 18:30, with a maximum heat flux at solar noon (t=12:30pm). The maximum amount of  $\dot{Q}_{s,abs}/\dot{Q}_{s,in,max}$  at solar noon is  $79.0 \times 10^{-2}$ , while  $\dot{Q}_{re-rad}/\dot{Q}_{s,in,max}$  is  $21.0 \times 10^{-2}$  when the solar reactor is operating, since it operates at a constant temperature.

Figure 3 also presents both the estimated net power generated by LCL-TES for the cases with,  $\dot{W}_{n,AB}/\dot{Q}_{s,in,max}$ ; and without the AB,  $\dot{W}_n/\dot{Q}_{s,in,max}$ . These values are normalised by the

maximum input solar heat to the solar reactor. A small increase in  $\dot{W}_{n,AB}/\dot{Q}_{s,in,max}$  and  $\dot{W}_n/\dot{Q}_{s,in,max}$  during daylight hours can also be seen here.

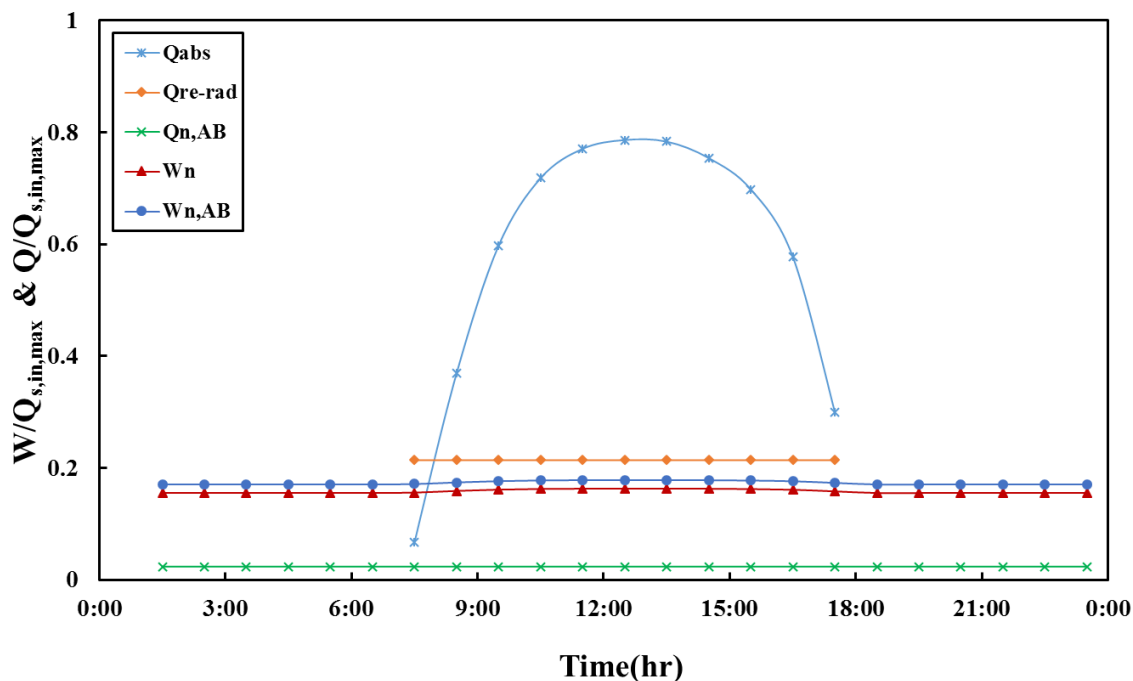


**Figure 6.3.** The calculated temporal variation in the re-radiated heat losses from aperture of the reduction reactor, the power of fuel into the AB, the total power produced by the LCL- TES GTCC, both with and without the AB.

The total solar absorption efficiency,  $\eta_{abs,tot}$  is presented in Table 6.2. This has a constant value of 73% for both the cycles with and without AB because the temperature of the reactor is the same for both cases. As shown in this table, the first law efficiency of the reference cycle,  $\eta_{ref}$ , is predicted to be about 58%. The First law efficiency of the LCL- TES system with and without the AB is estimated to be approximately 45.4% and 44.9%, respectively. The difference is mainly attributed to the higher re-radiation heat losses from the solar reactor aperture for the cycle without the AB than that of the cycle with it.

Table 6.2 also presents the average and fractional boosts of energy recovered from the reduction reactor,  $X_{boost,av}$ ,  $X_{boost,pk}$ , which are 1.6% and 4.8%, respectively, for the cycle

without an AB and 1.4% and 4.4%, respectively, for the cycle with AB. Although relatively small, the energy is recovered without requiring an additional turbine, so is relatively easy to capture. That the values of  $X_{boost,av}$  and  $X_{boost,pk}$  are lower for the cycle with an AB than that without an AB is consistent with the AB acting to reduce the relative significance of energy recovery from the reduction reactor by increasing work from the gas turbine. An exergy efficiency of 74.5% is estimated for the cycle with the after burner in comparison to 76.9% for the cycle without it. That is, the AB decreases exergy of the cycle slightly (by 3.1%) due to the exergy destruction from burning the fuel, although it increases the first law efficiency (noted above) by increasing the temperature at the turbine inlet from 1200 °C to 1250°C.

Table 6.2 also compares the value of  $\eta$ ,  $\eta_{abs,tot}$ ,  $\eta_{ref}$ ,  $X_{boost,pk}$ ,  $X_{boost,av}$  for the proposed LCL- TES cycle and with the previous Hybrid Solar Chemical Looping Combustion (Hy-Sol-CLC) cycle, which was calculated by Jafarian *et al* [26]. Their cycle uses fuel in the solar reduction reactor, in contrast to the present cycle, but is otherwise configured similarly. It can be seen that the first law efficiency of the Hy-Sol-CLC cycle is within one percentage point of the present the LCL- TES cycle. Nevertheless, the exergy efficiency of the Hy-Sol-CLC at 54% is much lower than the present 76.9% due to its consumption of fuel. The use of AB only reduces exergy efficiency slightly for the LCL- TES to 74.5% owing to the relatively small temperature rise of 50°C. Noticeably,  $X_{boost,av}$ , and  $X_{boost,pk}$  for the Hy-Sol-CLC cycle are higher than the corresponding values for LCL- TES system due to the greater enthalpy flow in the gas stream from the reduction reactor. On the other hand, the radiation heat losses from Hy-Sol-CLC are significantly lower than the present system due to its lower temperature.

**Table 6.2.** Calculated solar absorption efficiency, total solar share, first law efficiency, exergy efficiency, and both the peak and average fractional power boost of the present LCL- TES and the previous Hy-Sol-CLC (Jafarian et al. 2014) for the cases with and without the use of an AB under the operating condition provided in Table 1.

Parameters	LCL- TES		Hy-Sol-CLC (Jafarian et al. 2014)	
	Cycle with AB	Cycle without AB	Cycle with AB	Cycle without AB
$\eta_{abs,tot}$ (%)	73	73	92.5	92.5
$\eta_{ref}$ (%)	57.9	57.9	57.9	57.9
$\eta$ (%)	45.4	44.9	50	44
$X_{boost,av}$ (%)	1.4	1.6	4.2	6.9
$X_{boost,pk}$ (%)	4.4	4.8	10.6	16.8
$X_{sol,tot}$ (%)	91.6	100	41.4	60.0
$\Delta X_{con-sol,elec}$ (%)	44.6	-	39.4	35.4
$\eta_{ex}$ (%)	74.5	76.9	57.2	54.9

### 6.6.1 Effect of operating pressure of the air reactor

The sensitivity of the value of  $\eta$ ,  $\eta_{ex,AB}$ ,  $\Delta\eta_{con-sol-elec}$ ,  $X_{sol,tot}$ ,  $X_{boost,pk}$  and  $X_{boost,av}$  to variations in the air reactor operating pressure from 10 bar to 20 bar is presented in Figure 6.4, for the cycle with the AB. As shown,  $\eta$  increases from 43.2% to 46.6% when the air reactor pressure is increased from ten to twenty bar. This is because the flow rate of output air from the air reactor increases with the pressure as the result of the increase to the outlet air temperature from the air reactor. In this way, the work generated by the gas turbine increases, which thus increases the total efficiency of the system. With an increase in the air reactor pressure from ten bar to twenty bar the values of  $\eta_{ex,AB}$  and  $\Delta\eta_{con-sol-elec}$  increase by 7% and 7.1%, respectively. This can be explained by the increase in the flowrate of air with the increased pressure, which also increases the required flowrate of fuel to the AB to maintain the outlet temperature constant. The value of  $X_{boost,pk}$  and  $X_{boost,av}$  both decrease with an increase in the pressure. It is worth mentioning that the temperature of the cold storage tank and compressor outlet air temperature also change with a change in the pressure. This means that the temperature difference between these two is always maintained near to 50°C to drive the heat exchange in the heat recovery system. The flowrate of O<sub>2</sub> production can also be varied by changing the

cold storage tank temperature, which leads to a change in the generation of steam in the solar reactor. As expected, the value of  $\eta_{abs, total}$  and  $X_{sol, tot}$  remains stable because the pressure in the air reactor does not influence these parameters.

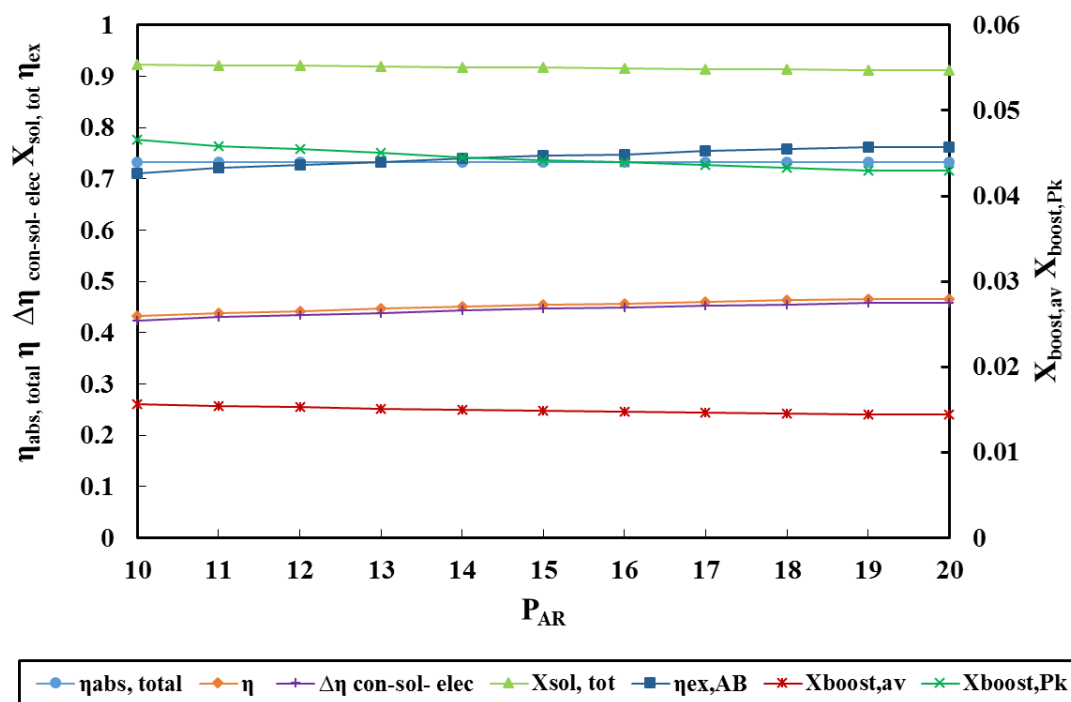


**Figure 6.4.** Calculated sensitivity analysis of the air reactor operating pressure of the solar absorption efficiency, first law efficiency, exergy efficiency, incremental concentrated solar to electrical efficiency, total solar share, peak and average fractional power boost for the cycle with the AB based on the assumption provided in Table 1.

Figure 6.5 presents the calculated sensitivity of  $\eta$ ,  $\eta_{ex, AB}$ ,  $X_{boost, Pk}$ ,  $X_{boost, av}$  to variations in the air reactor pressure between 10bar and 20bar for the cycle without an AB. As shown in this figure, that the first law efficiency of the cycle increases from 43.1% to 46.9% as the pressure of the air reactor is increased from 10 bar to 20 bar. This can be explained by the increase in the gas turbine work with the increased pressure. The value  $\eta_{ex}$ , increases by 9.5% with the increased pressure. This quantified the influence of pressure in the air reactor on energy and exergy efficiency of the LCL- TES system, which will be limited in practice by materials issues.



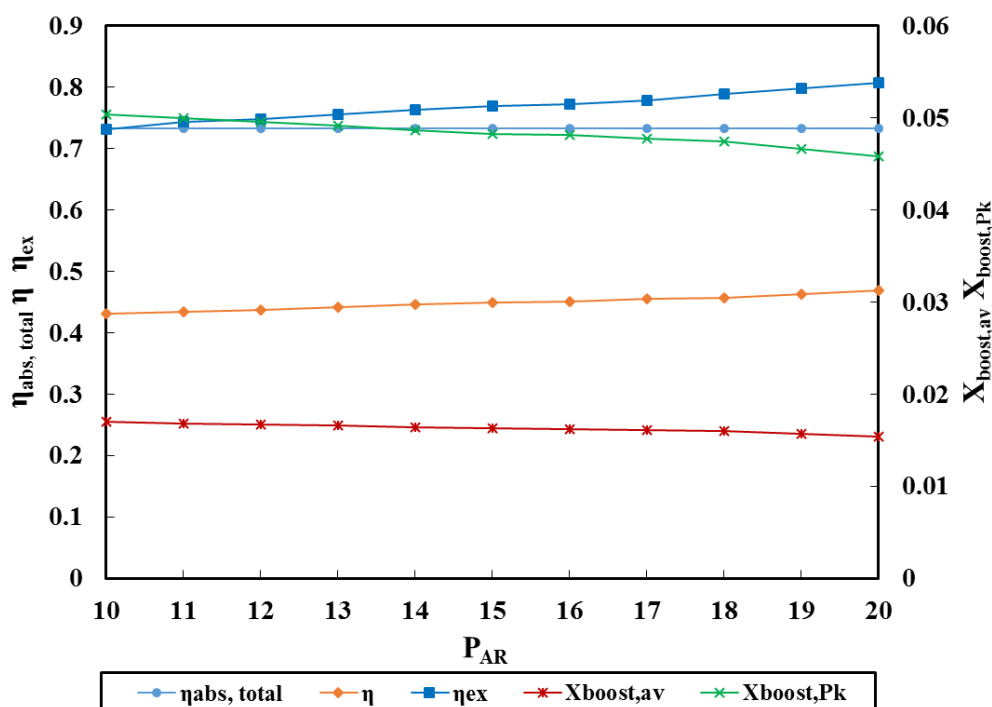


**Figure 6.5.** Calculated sensitivity to variations in air reactor operating pressure of the solar absorption efficiency, first law efficiency, exergy efficiency and both the average and peak fractional power boost for the cycle without the AB based on the assumption provided in Table 1.

### 6.6.2 Influence of concentration ratio of the solar collector

Figure 6.6 presents the sensitivity of  $\eta_{abs, tot}$ ,  $\eta$ ,  $\eta_{ex}$ ,  $\Delta\eta_{con-sol- elec}$ ,  $X_{boost, Pk}$ ,  $X_{boost, av}$  and  $X_{sol, tot}$  to different concentration ratios (CR) of the solar collector field, for the cycle using the AB. As shown in this figure, the value of  $\eta$ ,  $\eta_{abs, tot}$  and  $\Delta\eta_{con-sol- elec}$  increase significantly when the concentration ratio is increased from 500 to 8000. This is because the re-radiation heat loss decreases through the solar reactor aperture with an increase in CR. Furthermore, these parameters are more sensitive to variations in CR for low values of CR than the high ones. For instance, the value of  $\eta$ ,  $\eta_{abs, tot}$  and  $\Delta\eta_{con-sol- elec}$  increases from 7.6%, 11.5%, 7.2% to 31.7%, 49.6%, 30.2% when the ratio of CR changes from 500 to 1000, respectively. However, these values increase from 53.7%, 86% and 53.4% to 57.5%, 93.3%, and 57.5% when CR doubles from 4000 to 8000. As shown in figure 7, the value of the others parameters such as  $X_{boost, av}$ , and  $\eta_{ex}$  are not sensitive to the variations in CR. The value of the  $X_{boost, Pk}$  decreases from 7.8%

to 4.2% with increasing the concentration ratio of solar collector from 500 to 8000. Since an increase in concentration ratio increases the cost of the heliostat field, these data can guide evaluations in the trade-off between capital cost and performance.

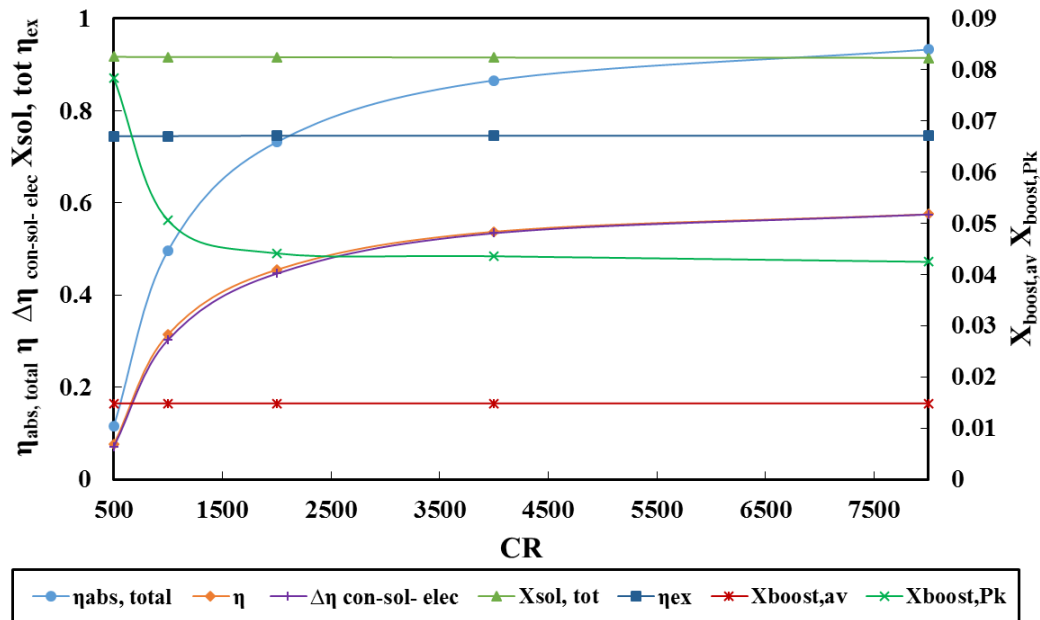


**Figure 6.6.** Calculated sensitivity analysis of concentration ratio of the solar collector for the, first law efficiency, solar absorption efficiency, exergy efficiency, incremental concentrated solar to electrical efficiency, total solar share, peak and average fractional power boost for the cycle with the AB based on the assumption provided in Table 1.

As shown in Figure 6.7, the flow rate of  $\text{O}_2$  from the reduction reactor also increases with the value of CR, which leads to an increase in the power production in steam turbine and also contributes to the increase in efficiency of the cycle.

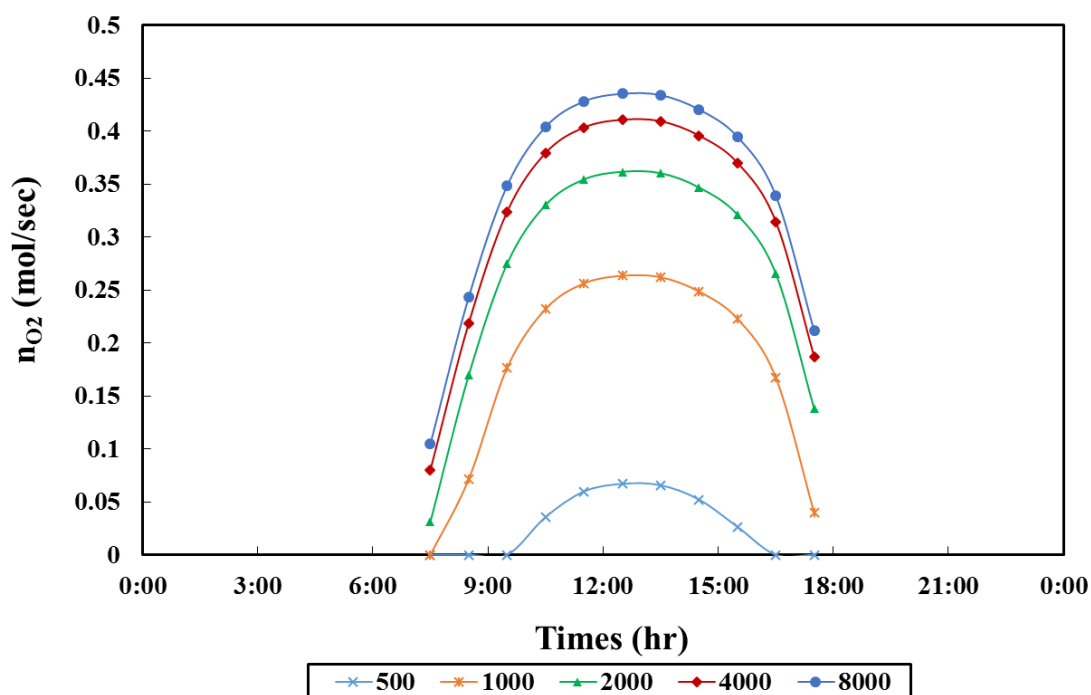


**Figure 6.7.** The dependence of O<sub>2</sub> molar flow rate on diurnal time for the various value of concentration ratio (500, 1000, 2000, 4000, and 8000).

The estimated sensitivity of the value of  $\eta_{abs,tot}$ ,  $\eta$ ,  $\eta_{ex}$ ,  $X_{boost,Pk}$  and  $X_{boost,av}$ , to variations in CR, for the cycle without AB is shown in Figure 6.8. The first law efficiency increases from 7.1% to 57.8% with an increase in CR from 500 to 8000 as the result of increased inlet flow to the air reactor, which increases the gas turbine work output. As expected the value of  $\eta_{abs,tot}$ , and  $\eta$  are found to increase significantly from 11% and 7% to 49.6% and 30% with an increase in the CR from 500 to 1000, respectively. These variations rise slightly at high ratio of CR (2000-800). The value of  $X_{boost,Pk}$  decreases from 8.5% to 4.6% with an increase in CR from 500 to 8000. However, the values of  $\eta_{ex}$ , and  $X_{boost,av}$  are not sensitive to variations in CR.

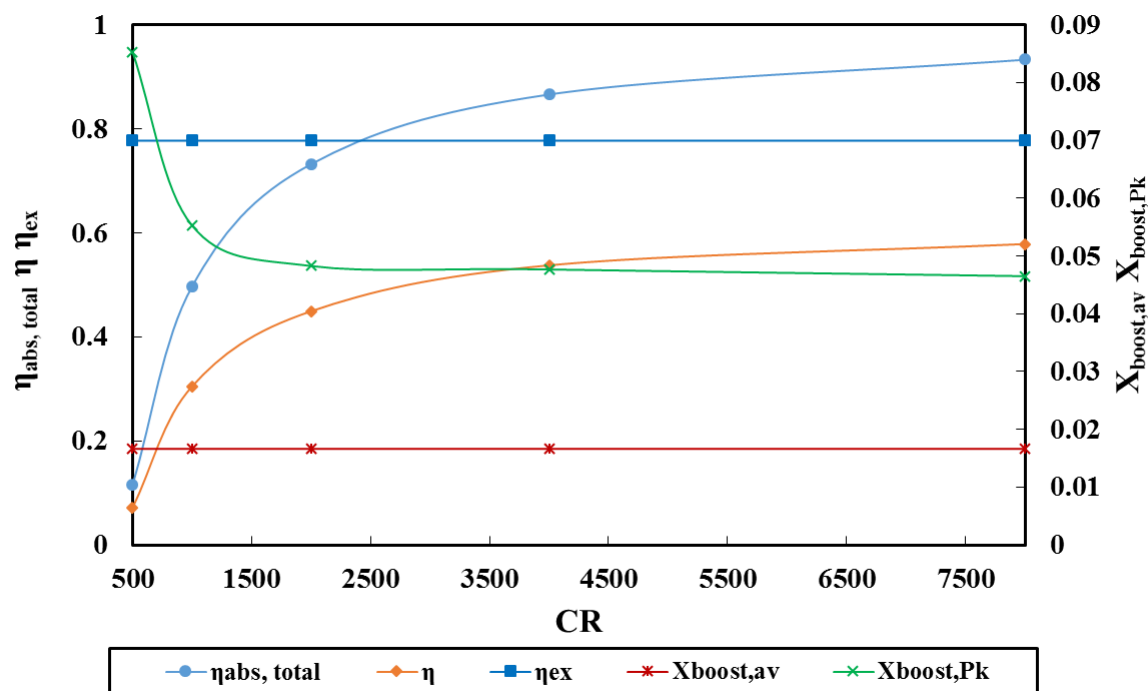


**Figure 6.8.** Calculated sensitivity the concentration ratio of the solar reduction reactor of the solar absorption efficiency, first law efficiency, exergy efficiency, peak and average fractional power boosts for the cycle without AB based on the assumption provided in Table1.

### 6.6.3 Effect of conversion extent of $\text{Cu}_2\text{O}$ (I) to $\text{CuO}$ (I)

Figure 6.9 presents the calculated dependence of  $\eta_{abs, tot}$ ,  $\eta$ ,  $\Delta\eta_{con-sol-elec}$ ,  $X_{boost, Pk}$ ,  $X_{boost, av}$ ,  $X_{sol, tot}$ ,  $\eta_{ex}$  on the conversion extent for the cycle with the AB. As shown in Figure 6.9, the values of  $\eta$ ,  $\eta_{ex}$ ,  $\Delta\eta_{con-sol-elec}$  decrease from 48.1%, 78.5%, and 47.3% to 43.9%, 72.1% and 43%, respectively with an increase in the conversion extent from 0 to 1. This can be explained by the decrease in the inlet flowrate to the air reactor and of the fuel in the system. The value of the,  $X_{boost, av}$ ,  $X_{boost, Pk}$ ,  $X_{sol, tot}$  increases from 0.5%, 1.6%, 91% to 2.1%, 6.4% and 91.8%, respectively. This is because of rising the flowrate of  $\text{O}_2$  production from the reduction reactor increases the power production from the steam turbine. It is clear that the value of  $\eta_{abs, tot}$  is independent from the conversion extent of the material.

The calculated sensitivities of  $\eta_{abs, tot}$ ,  $\eta$ ,  $\eta_{ex}$ ,  $X_{boost, av}$ ,  $X_{boost, Pk}$  to conversion extent is shown in Figure 6.10 for the cycle without AB. The variation of these parameters is the same as for the

cycle with AB. The values of  $\eta$  and  $\eta_{ex}$  decrease from 47.3% and 81% to 43.6% and 74.7% with increasing the conversion extent of the material from 0 to 1, respectively.

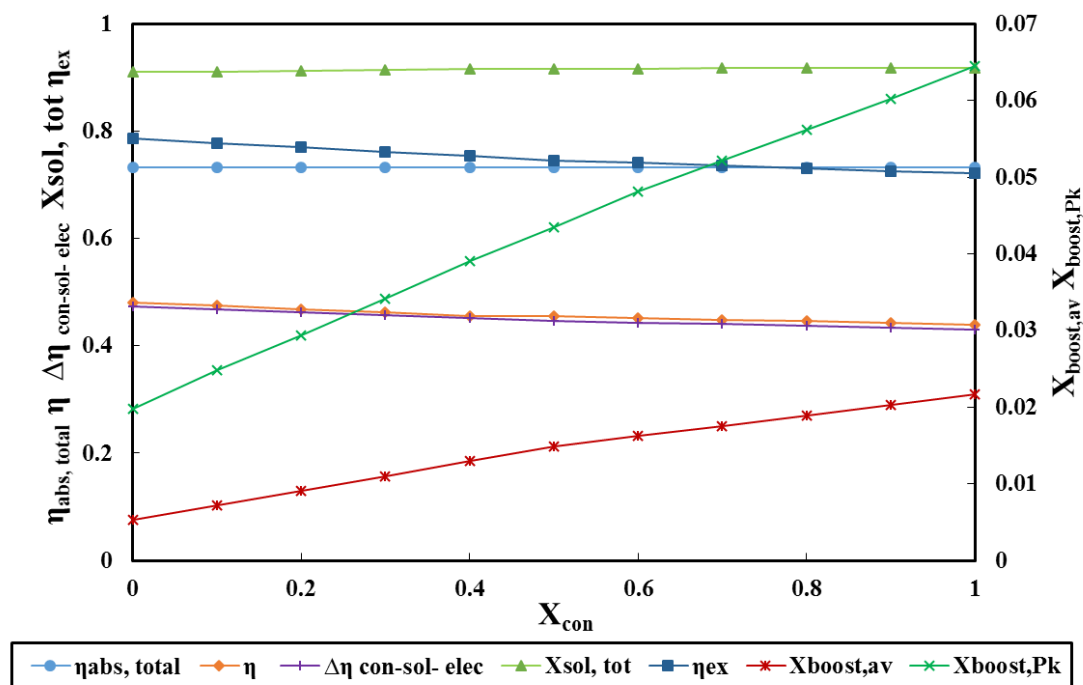


**Figure 6.9.** Calculated sensitivity of the first law efficiency, exergy efficiency, incremental concentrated solar to electrical efficiency, total solar share, peak and average fractional power boost to variation in conversion extents of the material for the cycle with an AB based on the assumption given in Table 1.

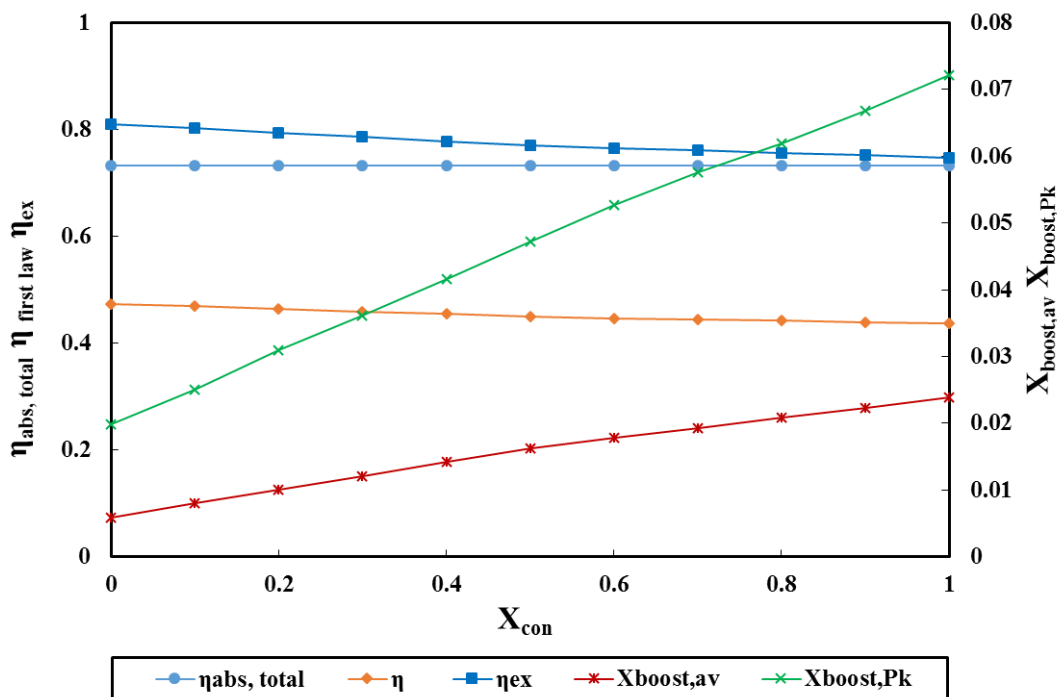


**Figure 6.10.** Sensitivity analysis of the first law efficiency, exergy efficiency, peak and average fractional power boost in different conversion extents of material for the cycle without an AB using the reference conditions provided in Table 1.

#### 6.6.4 Influence of after-burner on operating condition of LCL-TEES cycle

The estimated sensitivity of  $\eta_{abs, total}$ ,  $\eta$ ,  $\Delta\eta_{con-sol-elec}$ ,  $X_{boost, Pk}$ ,  $X_{boost, av}$ ,  $\eta_{ex}$ ,  $X_{sol, tot}$  to the variations in AB temperature,  $T_{AB}$  is presented in Figure 6.11. As can be seen, the first law efficiency of the cycle increases with the temperature boost of the AB. For example,  $\eta$  increases from 45.4% to 50% when the AB temperature is increased from 1250°C to 1700°C. The effect of the AB is also shown in Table 6.2. However, an increase in  $T_{AB}$  reduces the exergy efficiency of the cycle. This is because fuel is consumed to increase the temperature of the gas. The calculation shows that the system's exergy decreases by up to 66% for a turbine inlet temperature of 1700°C. The solar share also decreases significantly from 91% to 50% once the AB temperature is increased from 1250°C to 1700°C.

This explains the consumption of more fuel at higher temperatures (1700°C) than at lower temperatures (1250°C). The sensitivity of  $\Delta\eta_{con-sol-elec}$  to  $T_{AB}$  shows that there is a slight decrease from 44.6% to 44.4% for the temperature of 1250°C and 1700°C, respectively. The

calculations estimate that  $X_{\text{boost,av}}$  is less sensitive to the temperature of the AB than all other parameters. For example,  $X_{\text{boost,av}}$  decreases from 1.4% to 0.8% as the temperature increases from 1250°C to 1700°C.

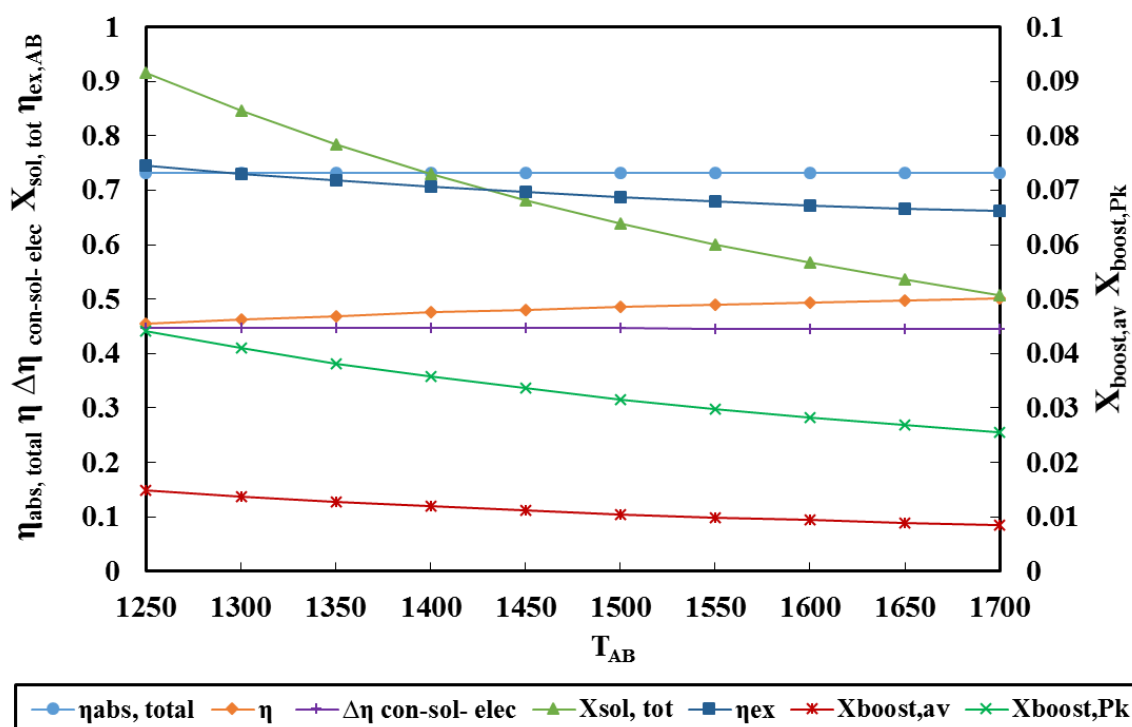


**Figure 6.11.** Calculated sensitivity of the first law efficiency, exergy efficiency, peak and average fractional power boost, incremental concentrated solar to electrical efficiency to the operating temperature of the AB for the assumptions provided in Table 1.

## 6.7 Conclusions

The first law efficiency of a LCL-TEs system without any additional heating from the AB is calculated to be 44.9%. The addition of the AB to the cycle boosts the first law efficiency from 45.4% to 50%, but at the cost of reducing the solar share from 100% to 91.6%. Given that this efficiency is compatible with an open cycle gas turbine, the main potential benefit of the boost is a reduction in number of components, and hence capital cost. The assessment also indicate that the cycle exergy efficiency decreases from 74.5% to 66.1% by using an AB. More specifically, the assessment also showed that:

- For both cycles; the calculated value for energy and exergy efficiency increases with an increase in the pressure of the system due to increased thermodynamic gas turbine's efficiency. The value of  $X_{\text{boost,Pk}}$ ,  $X_{\text{boost,av}}$  decreases with rising the pressure to the air reactor. These value can be used to estimate the added value of increase pressure ratio, which comes with a corresponding increase in cost associated with the use of more expensive materials.
- For both cycles; the first law efficiency, exergy efficiency and total absorption efficiency increase with an increase in the CR of solar collector field. However, the, average fractional power boost is not sensitive to the variation of concentration ration of the solar collector, while for the cycle with an AB, the values of peak fractional power boost and incremental solar to electrical efficiency decrease by increasing the CR of solar collector field. These values can be used to estimate the added value of an increased concentration ratio, which comes with a corresponding increase in cost of the heliostat field.
- For both cycles, the value of first law efficiency, exergy efficiency and incremental solar to electrical efficiency decrease with an increased extent of conversion from 0 to 1. However, the extent of the increase is relatively small over the ranges assessed here.
- An increase in the operating temperature of the LCL-TES system from 1250°C to 1700°C with an AB leads to an increase the first law efficiency of the LCL-TES cycle by 50% at a temperature of 1700°C. However, the exergy of the cycle decreases by 10.8% when the temperature of the AB increases from 1250°C to 1700°C, due to exergy destruction from burning a fuel.



---

## 6.8 References

A. H. Abedin & M. A. Rosen 2011, 'A critical review of thermochemical energy storage systems', *Open Renewable Energy J*, vol. **4**. pp. 42-46.

*Analysis of 10 years record Port Augusta australia, South Australia*, 2010, RenewablesSA.

B.Wong 2011, *Thermochemical heat storage for concentrated solar power, final report for the U.S. Department of Energy*, Department of Energy, San Diego, CA,USA.

R. Buck, T. Brauning, T. Denk, M. Pfänder, P. Schwarzbözl & F. Tellez 2002, 'Solar-hybrid gas turbine-based power tower systems (REFOS)', *Journal of Solar Energy Engineering*, vol. **124**. 1, pp. 2-9.

S. Consonni, G. Lozza, G. Pelliccia, S. Rossini & F. Saviano 2006, 'Chemical-Looping Combustion for Combined Cycles With CO<sub>2</sub> Capture', *Journal of Engineering for Gas Turbines and Power*, vol. **128**. 3, pp. 525-534.

I. Dincer & M. A. Rosen 2012, *Exergy: energy, environment and sustainable development*, Newnes.

H. Fauzi, H. S. Metselaar, T. Mahlia & M. Silakhori 2014, 'Sodium laurate enhancements the thermal properties and thermal conductivity of eutectic fatty acid as phase change material (PCM)', *Solar energy*, vol. **102**. pp. 333-337.

K. H. Funken, M. Roeb, P. Schwarzboezl & H. Warnecke 2001, 'Aluminum remelting using directly solar-heated rotary kilns', *Journal of Solar Energy Engineering*, vol. **123**. 2, pp. 117-124.

A. Gil, M. Medrano, I. Martorell, A. Lázaro, P. Dolado, B. Zalba & L. F. Cabeza 2010, 'State of the art on high temperature thermal energy storage for power generation. Part 1: Concepts, materials and modellization', *Renewable and Sustainable Energy Reviews*, vol. **14**. 1, pp. 31-55.

C. Gou, R. Cai & H. Hong 2007, 'A novel hybrid oxy-fuel power cycle utilizing solar thermal energy', *Energy*, vol. **32**. 9, pp. 1707-1714.

H. Hong, T. Han & H. Jin 2010, 'A Low Temperature Solar Thermochemical Power Plant With CO<sub>2</sub> Recovery Using Methanol-Fueled Chemical Looping Combustion', *Journal of Solar Energy Engineering*, vol. **132**. 3, pp. 031002-031002.

H. Hong & H. Jin 2005, 'A Novel Solar Thermal Cycle with Chemical Looping Combustion', *International Journal of Green Energy*, vol. **2**. 4, pp. 397-407.

H. Hong, H. Jin, J. Ji, Z. Wang & R. Cai 2005, 'Solar thermal power cycle with integration of methanol decomposition and middle-temperature solar thermal energy', *Solar energy*, vol. **78**. 1, pp. 49-58.

M. Jafarian, M. Arjomandi & G. J. Nathan 2014, 'The energetic performance of a novel hybrid solar thermal & chemical looping combustion plant', *Applied Energy*, vol. **132**. pp. 74-85.

M. Jafarian, M. Arjomandi & G. J. Nathan 2014, 'A hybrid solar chemical looping combustion system with a high solar share', *Applied Energy*, vol. **126**. pp. 69-77.

M. Jafarian, M. Arjomandi & G. J. Nathan 2017, 'Thermodynamic potential of molten copper oxide for high temperature solar energy storage and oxygen production', *Applied Energy*, vol. **201**. pp. 69-83.

J. S. Kim, A. Dawson, R. Wilson, K. Venkatesan & W. Stein 2015, 'High-Temperature Heat Transport and Storage Using LBE Alloy for Concentrated Solar Power System', in *ASME 2015 9th International Conference on Energy Sustainability*.

G. J. Kolb 1998, 'Economic evaluation of solar-only and hybrid power towers using molten-salt technology', *Solar energy*, vol. **62**. 1, pp. 51-61.

K. C. Y. Kueh, G. J. Nathan & W. L. Saw 2015, 'Storage capacities required for a solar thermal plant to avoid unscheduled reductions in output', *Solar energy*, vol. **118**. pp. 209-221.

S. Kuravi, J. Trahan, D. Y. Goswami, M. M. Rahman & E. K. Stefanakos 2013, 'Thermal energy storage technologies and systems for concentrating solar power plants', *Progress in energy and combustion science*, vol. **39**. 4, pp. 285-319.

M. Liu, J. Gomez, C. Turchi, N. Tay, W. Saman & F. Bruno 2015, 'Determination of thermo-physical properties and stability testing of high-temperature phase-change materials for CSP applications', *Solar Energy Materials and Solar Cells*, vol. **139**. pp. 81-87.

S. A. Mohamed, F. A. Al-Sulaiman, N. I. Ibrahim, M. H. Zahir, A. Al-Ahmed, R. Saidur, B. Yılbaş & A. Sahin 2017, 'A review on current status and challenges of inorganic phase change materials for thermal energy storage systems', *Renewable and Sustainable Energy Reviews*, vol. **70**. pp. 1072-1089.

T. Nagel, H. Shao, A. Singh, N. Watanabe, C. Roßkopf, M. Linder, A. Wörner & O. Kolditz 2013, 'Non-equilibrium thermochemical heat storage in porous media: Part 1: Conceptual model', *Energy*, vol. **60**. pp. 254-270.

R. Naqvi, J. Wolf & O. Bolland 2007, 'Part-load analysis of a chemical looping combustion (CLC) combined cycle with CO<sub>2</sub> capture', *Energy*, vol. **32**. 4, pp. 360-370.

J. Pacio, C. Singer, T. Wetzel & R. Uhlig 2013, 'Thermodynamic evaluation of liquid metals as heat transfer fluids in concentrated solar power plants', *Applied Thermal Engineering*, vol. **60**. 1–2, pp. 295-302.

J. Pacio & T. Wetzel 2013, 'Assessment of liquid metal technology status and research paths for their use as efficient heat transfer fluids in solar central receiver systems', *Solar energy*, vol. **93**. pp. 11-22.

H. Price 2003, 'Assessment of parabolic trough and power tower solar technology cost and performance forecasts', *National Renewable Energy Laboratory, Golden, CO*.

H. Price, E. Lufert, D. Kearney, E. Zarza, G. Cohen, R. Gee & R. Mahoney 2002, 'Advances in parabolic trough solar power technology', *Journal of Solar Energy Engineering*, vol. **124**. 2, pp. 109-125.

C. W. Robak, T. L. Bergman & A. Faghri 2011, 'Economic evaluation of latent heat thermal energy storage using embedded thermosyphons for concentrating solar power applications', *Solar energy*, vol. **85**. 10, pp. 2461-2473.

Y. Shah, B. G. Kelkar, S. Godbole & W. D. Deckwer 1982, 'Design parameters estimations for bubble column reactors', *AIChE journal*, vol. **28**. 3, pp. 353-379.

M. Silakhori, H. Fauzi, M. R. Mahmoudian, H. S. C. Metselaar, T. M. I. Mahlia & H. M. Khanlou 2015, 'Preparation and thermal properties of form-stable phase change materials composed of palmitic acid/polypyrrole/graphene nanoplatelets', *Energy and Buildings*.

M. Silakhori, M. Jafarian, M. Arjomandi & G. J. Nathan 2017, 'Comparing the thermodynamic potential of alternative liquid metal oxides for the storage of solar thermal energy', *Solar energy*, vol. **157**. pp. 251-258.

M. Silakhori, H. S. C. Metselaar, T. M. I. Mahlia, H. Fauzi, S. Baradaran & M. S. Naghavi 2014, 'Palmitic acid/polypyrrole composites as form-stable phase change materials for thermal energy storage', *Energy Conversion and Management*, vol. **80**. pp. 491-497.

A. Steinfeld, C. Larson, R. Palumbo & M. Foley 1996, 'Thermodynamic analysis of the co-production of zinc and synthesis gas using solar process heat', *Energy*, vol. **21**. 3, pp. 205-222.

Z. Yang & S. V. Garimella 2010, 'Thermal analysis of solar thermal energy storage in a molten-salt thermocline', *Solar energy*, vol. **84**. 6, pp. 974-985.

A. Z'Graggen, P. Haueter, D. Trommer, M. Romero, J. C. de Jesus & A. Steinfeld 2006, 'Hydrogen production by steam-gasification of petroleum coke using concentrated solar power:

---

Reactor design, testing, and modeling', *International Journal of Hydrogen Energy*, vol. **31**. 6, pp. 797-811.

H. Zhang, J. Baeyens, J. Degève & G. Cacères 2013, 'Concentrated solar power plants: review and design methodology', *Renewable and Sustainable Energy Reviews*, vol. **22**. pp. 466-481.

**Appendix A:** Direct Normal Insolation (DNI) for Port Augusta, South Australia.

Hour of day	DNI (W/m <sup>2</sup> )
7:30	175.7
8:30	364.2
9:30	506.9
10:30	582.3
11:30	615.1
12:30	624.9
13:30	623.1
14:30	604.7
15:30	569.8
16:30	494.3
17:30	321

---

## Chapter 7 Conclusion & future works

---

### 7.1 Conclusion

Reduction and Oxidation (RedOx) reactions of metal oxides such as  $\text{CuO}/\text{Cu}_2\text{O}$ ,  $\text{Co}_3\text{O}_4/\text{CoO}$ , and  $\text{Mn}_2\text{O}_3/\text{Mn}_3\text{O}_4$ , which occur through changing the temperature of the system, show a great potential for thermochemical storage. Nevertheless, the temperature difference between charging and discharging reduces the thermal efficiency of the system because the discharging temperature is lower than charging temperature. To address this challenge, one potential option is to use pressure-swing with change in the oxygen partial pressure of system as the driver of the reactions. This in turn offers the potential to store and release heat at a relatively constant temperature. However, the use of pressure-swing for thermochemical storage is not well studied. Therefore, the potential benefits and limitations are yet to be identified. Hence, this research aims to assess the potential benefits and limitations of pressure-swing system. The following sections outline the specific conclusions drawn from various parts of the study.

#### 7.1.1 Application of chemical looping by pressure swing for thermal energy storage

The primary contribution of this thesis was to assess the potential of solid metal oxides for RedOx reactions thermodynamically and experimentally. The  $\text{CuO}/\text{Cu}_2\text{O}$ ,  $\text{Co}_3\text{O}_4/\text{CoO}$ ,  $\text{Pb}_3\text{O}_4/\text{PbO}$  and  $\text{Mn}_2\text{O}_3/\text{Mn}_3\text{O}_4$  pairs were assessed thermodynamically through their phase diagrams. The thermodynamic assessment showed that these materials store and release heat with change in partial pressure of the oxygen. The experimental investigations were performed by thermogravimetric analysis and X-ray diffraction to assess the behaviour, kinetics and reversibility of these material for thermochemical storage with changing the partial pressure of the system from 0.05 to 0.8 bar. The results showed that  $\text{CuO}/\text{Cu}_2\text{O}$ ,  $\text{Co}_3\text{O}_4/\text{CoO}$ , and  $\text{Mn}_2\text{O}_3/\text{Mn}_3\text{O}_4$  pairs were suitable storage media for thermochemical storage with pressure-swing due to high storage capacity, high operating temperature (up to  $1000^\circ\text{C}$ ) and excellent reversibility up to ten reduction and oxidation cycles. In spite of the fact that  $\text{Pb}_3\text{O}_4/\text{PbO}$  pair

are considered to be a potential candidate for thermochemical storage through phase diagram, the experimental investigation showed that these materials were not able to store and release heat in an oxygen partial pressure of 0.05 bar and 0.8 bar.

In addition, the experimental assessment showed that the rate of the reactions improved significantly, which means that the required time for complete reduction and oxidation reached upto 30 min for copper oxide and cobalt oxide. This period was 1 hr for manganese oxide. Nevertheless, this value depends of the particles' size. The rate of oxidation can be increased with an increase in the partial pressure of oxygen from 0.2 bar to 0.8 bar as a result of rising the thermodynamic driving force for oxidation reaction.

### **7.1.2 Suitable materials for LCL-TES**

The reduction and oxidation reactions have been extended for liquid metals with increasing the operating temperature of the system. This process, which utilises the liquid metals as storage media, is called Liquid Chemical Looping for Thermal Energy Storage (LCL-TES). The thermodynamic potential of 23 metal oxides has been assessed through comparison of melting temperature, Gibbs minimization, reaction temperature, phase diagram and vapour pressure. The assessment showed that CuO/Cu<sub>2</sub>O and Pb<sub>3</sub>O<sub>4</sub>/PbO pairs were plausible storage media in LCL-TES system. Both CuO/Cu<sub>2</sub>O and Pb<sub>3</sub>O<sub>4</sub>/PbO pairs can store thermal energy in the form of sensible, latent and chemical heat in a heating and cooling cycle. The sensible and chemical heat storage is observed in liquid state of CuO/Cu<sub>2</sub>O, while the Pb<sub>3</sub>O<sub>4</sub>/PbO pair can only store sensible heat in liquid state. The total enthalpies of CuO/Cu<sub>2</sub>O and Pb<sub>3</sub>O<sub>4</sub>/PbO were 404.67 kJ/mol and 250.09 kJ/mol, respectively. The high storage capacity is because of the combination of sensible, latent and chemical heat in a heating and cooling cycle.

### **7.1.3 Advantages and technical challenges of molten metals in TES**

The experimental assessment of suitable materials confirmed that CuO/Cu<sub>2</sub>O can be used in the LCL-TES. The CuO/Cu<sub>2</sub>O pair was assessed at different partial pressures from 0.05 to 0.8 bar by TGA. Although, this material has the potential to store thermal heat in the forms of sensible, latent and chemical heat in solid and liquid's phase, there are some technical challenges related to reactions of molten copper oxide with the containers which affected the potential of this material over a long RedOx cycles. The reaction between copper oxides and alumina crucible was shown with XRD spectra of copper oxide after 10 RedOx reactions. Moreover, SEM and EDX results depicted the presence of alumina on the surface of the materials after 10 cycles.

### **7.1.4 Performance of LCL-TES with GTCC**

The performance of LCL-TES system incorporated with GTCC cycle was assessed for an average diurnal normal irradiance profile of Port-Augusta in South Australia. Copper oxide was used as a storage medium in this cycle due to its high operating temperature (1200°C) and high storage capacity through LCL-TES system. The performance of this system with and without an after-burner was studied. The after-burner was proposed to further heat the pressurised hot gas generated by the LCL-TES system, prior to being introduced into the gas turbine. The efficiency of 44.9% was achieved without an additional heating from an after burner. This value was increased to 50% when an after-burner was applied to the output gas from LCL-TES. However, the exergy of the system decreased from 74.5% to 66.1% by increasing the temperature of output gas from 1250°C to 1700°C. In addition, the effect of different parameters such as pressure, temperature, concentration ratio (CR) and conversion extent on the output energy from solar reactor and air reactor was studied. The results showed that energy and exergy increased with an increase in pressure, and CR. However, energy and exergy decreased with increasing the conversion extent from 0 to 1.

## **7.2 Recommendations for future work**

### **7.2.1 Solar reactor**

One of the main components of the LCL-TES system is solar reactor, which needs to work at high temperatures of up to 1200°C with the potential to melt metal oxides. However, the state-of-the-art solar receivers are limited to gas, liquid or solid particles (Buck et al. 2017; Funken et al. 2001; Z'Graggen et al. 2006), such that there is no specific configurations of a solar receiver enabling the melting of a material at high temperatures under conditions of relevance to LCL-TES system. Hence, further investigation is required on the design and operation of a suitable solar reactor for LCL-TES. The fundamental knowledge of this study provides the opportunity to perform the LCL-TES system in pilot plant and commercial scale.

### **7.2.2 Heat recovery**

The heat recovery unit is another important part of LCL-TES system that needs to be further studied. The heat recovery unit in the LCL-TES system is responsible to solidify and oxidise molten metal oxides. Although, the concept of heat recovery from slag such as a rotary cylinder slag atomiser, a spinning disk slag atomiser, and a rotary cup slag atomiser (Kashiwaya et al. 2010; Pickering et al. 1985) can plausibly be used for LCL-TES, all of which recover only sensible heat from the slag. To also recover latent and chemical heat would require sufficient residence time relative to the droplet size to solidify and oxidise the particles. Therefore, further investigation is required to develop a suitable heat recovery unit for the LCL-TES system.

### **7.2.3 Composite materials for LCL-TES**

As mentioned in chapter 2, composite materials (alloy, binary, eutectic mixture) can improve the reliability and stability of the storage media in a thermal energy storage system. Therefore, it is beneficial to develop these materials for the LCL-TES system to utilise the benefits of pressure and temperature swing system.



### 7.2.4 Challenges of molten metals

The application of liquid metals at high temperatures and pressures have some challenges such as corrosion and high reactivity with the different parts of the system e.g., solar reactor, heat exchanger, storage reservoir and oxidation reactor. Moreover, the container that stores molten metal oxides in LCL-TES system should have the potential to remain stable at a high temperature for a long period of time. Therefore, the key challenge of LCL-TES cycle requires the identification of suitable combinations of metals and refractories with sufficiently low reactions to withstand multiple cycles of successive oxidation and reduction.

### 7.3 References

R. Buck, S. Giuliano & R. Uhlig 2017, '16 - Central tower systems using the Brayton cycle', *Advances in Concentrating Solar Thermal Research and Technology*, Woodhead Publishing, pp. 353-382.

K. H. Funken, M. Roeb, P. Schwarzboezl & H. Warnecke 2001, 'Aluminum remelting using directly solar-heated rotary kilns', *Journal of Solar Energy Engineering*, vol. **123**. 2, pp. 117-124.

Y. Kashiwaya, Y. In-Nami & T. Akiyama 2010, 'Development of a rotary cylinder atomizing method of slag for the production of amorphous slag particles', *ISIJ international*, vol. **50**. 9, pp. 1245-1251.

S. Pickering, N. Hay, T. Roylance & G. Thomas 1985, 'New process for dry granulation and heat recovery from molten blast-furnace slag', *Ironmaking and steelmaking*, vol. **12**. 1, pp. 14-21.

A. Z'Graggen, P. Haueter, D. Trommer, M. Romero, J. C. de Jesus & A. Steinfeld 2006, 'Hydrogen production by steam-gasification of petroleum coke using concentrated solar power: Reactor design, testing, and modeling', *International Journal of Hydrogen Energy*, vol. **31**. 6, pp. 797-811.